frontiers | Research Topics

Ecosystem services and sustainable restoration interlinking soil, geological, and vegetation interactions for sustainable development

Edited by
Tianjiao Feng, Pengcheng Hu, Qiang Li and Huoxing Zhu

Published in
Frontiers in Environmental Science

ISSN 1664-8714
ISBN 978-2-8325-7299-3
DOI 10.3389/978-2-8325-7299-3

Generative AI statement
Any alternative text (Alt text) provided alongside figures in the articles in this ebook has been generated by Frontiers with the support of artificial intelligence and reasonable efforts have been made to ensure accuracy, including review by the authors wherever possible. If you identify any issues, please contact us.

About Frontiers

Frontiers is more than just an open access publisher of scholarly articles: it is a pioneering approach to the world of academia, radically improving the way scholarly research is managed. The grand vision of Frontiers is a world where all people have an equal opportunity to seek, share and generate knowledge. Frontiers provides immediate and permanent online open access to all its publications, but this alone is not enough to realize our grand goals.

Frontiers journal series

The Frontiers journal series is a multi-tier and interdisciplinary set of open-access, online journals, promising a paradigm shift from the current review, selection and dissemination processes in academic publishing. All Frontiers journals are driven by researchers for researchers; therefore, they constitute a service to the scholarly community. At the same time, the *Frontiers journal series* operates on a revolutionary invention, the tiered publishing system, initially addressing specific communities of scholars, and gradually climbing up to broader public understanding, thus serving the interests of the lay society, too.

Dedication to quality

Each Frontiers article is a landmark of the highest quality, thanks to genuinely collaborative interactions between authors and review editors, who include some of the world's best academicians. Research must be certified by peers before entering a stream of knowledge that may eventually reach the public - and shape society; therefore, Frontiers only applies the most rigorous and unbiased reviews. Frontiers revolutionizes research publishing by freely delivering the most outstanding research, evaluated with no bias from both the academic and social point of view. By applying the most advanced information technologies, Frontiers is catapulting scholarly publishing into a new generation.

What are Frontiers Research Topics?

Frontiers Research Topics are very popular trademarks of the *Frontiers journals series*: they are collections of at least ten articles, all centered on a particular subject. With their unique mix of varied contributions from Original Research to Review Articles, Frontiers Research Topics unify the most influential researchers, the latest key findings and historical advances in a hot research area.

Find out more on how to host your own Frontiers Research Topic or contribute to one as an author by contacting the Frontiers editorial office: frontiersin.org/about/contact

Ecosystem services and sustainable restoration interlinking soil, geological, and vegetation interactions for sustainable development

Topic editors

Tianjiao Feng — Beijing Forestry University, China

Pengcheng Hu — Department of Agriculture and Food, Commonwealth Scientific and Industrial Research Organisation (CSIRO), Australia

Qiang Li — University of Houston–Downtown, United States

Huoxing Zhu — South China Botanical Garden, Chinese Academy of Sciences (CAS), China

Citation

Feng, T., Hu, P., Li, Q., Zhu, H., eds. (2026). *Ecosystem services and sustainable restoration interlinking soil, geological, and vegetation interactions for sustainable development*. Lausanne: Frontiers Media SA. doi: 10.3389/978-2-8325-7299-3

Table of contents

05 Editorial: Ecosystem services and sustainable restoration interlinking soil, geological, and vegetation interactions for sustainable development
Tianjiao Feng, Pengcheng Hu and Huoxing Zhu

08 Ecological restoration in high-altitude mining areas: evaluation soil reconstruction and vegetation recovery in the Jiangcang coal mining area on the Qinghai-Tibet Plateau
Shaohua Feng, Zhiwei Li, Ce Zhang, Ran Qi and Liya Yang

23 Critical evaluation on the ecosystem service levels of provincial capital cities along the Yellow River Basin
Haifa Jia, Tianyou Wang, Pengyu Liang, Jianxun Zhang and Runhao Zhang

36 Identifying key elements of ecological restoration in shallow-buried high-intensity mining area based on obstacle degree model a case study in Huojitu mine
Hebing Zhang, Zhiyong Zhu, Shidong Wang, Youfeng Zou, Zhichao Chen, Yanling Zhao, Qiuji Chen, Yiheng Jiao, Yifu Li and Haoyang Du

52 Multiscale effects of climate change and anthropogenic activity on vegetation dynamics in Guangdong-Hong Kong-Macao greater bay area
Yun Tang, Yuanyuan Wang and Quanming Yang

77 Responses of alpine grassland plant communities on Sejila Mountain in the Qinghai-Tibet Plateau to phosphorus addition
Xizhe Zhang, Yanhui Ye, Jiang Tao, Ziyou Niu, Zhipan Cui, Jianlin Li and Yanying Han

90 Soil carbon and nitrogen changes due to soil particles redistribution caused by photovoltaic array
Feiyan Zhao, Zhongju Meng, Yang Liu, Peng Li and Guodong Tang

101 Analysis of changes in soil chemical stoichiometric ratios under different cultivation durations of *Pennisetum giganteum* in inner Mongolia, China
Yazhou Shao, Yunxia Ma, Gangtie Li and Xiaolu Ma

115 Research on the driving mechanisms of ecosystem services in the alpine canyon areas of Southwest China
Jiahui Jiang, Jian Hou, Chen Zeng, Haobo Feng and Yufan Zhu

128 A review of research progress on the application of bryophytes in the ecological restoration of mining areas of China
Zhanrui Qiao, Xiaoai Lin, Tao Zhang, Shuigen Luo, Cunbao Wang, Wei Zhou and Longzao Luo

139 Impacts of grazing on species diversity among different plant communities on the Qinghai–Tibet Plateau
Yu-Qi Ma, Chun-Jing Wang, De-Chao Chen, Dong-Zhou Deng, Wu-Xian Yan, Jing-Yu Yang and Ji-Zhong Wan

147 Spatial variability characteristics of soil physicochemical properties in fixed-axis and tracking tilted single-axis photovoltaic panels in qinghai desert areas
Shengjuan Yue, Mengjing Guo, Bo Yuan, Deli Ye, Hongyuan Ma and Wenwen Bai

frontiers | Frontiers in Environmental Science

TYPE Editorial
PUBLISHED 09 December 2025
DOI 10.3389/fenvs.2025.1743208

OPEN ACCESS

EDITED AND REVIEWED BY
Lalisa A. Duguma,
Global Evergreening Alliance, Australia

*CORRESPONDENCE
Tianjiao Feng,
fengtianjiaobest@sina.cn

RECEIVED 10 November 2025
REVISED 24 November 2025
ACCEPTED 27 November 2025
PUBLISHED 09 December 2025

CITATION
Feng T, Hu P and Zhu H (2025) Editorial: Ecosystem services and sustainable restoration interlinking soil, geological, and vegetation interactions for sustainable development. *Front. Environ. Sci.* 13:1743208. doi: 10.3389/fenvs.2025.1743208

Editorial: Ecosystem services and sustainable restoration interlinking soil, geological, and vegetation interactions for sustainable development

Tianjiao Feng[1,2]*, Pengcheng Hu[3] and Huoxing Zhu[4]

[1]Key Laboratory of Mine Ecological Effects and Systematic Restoration, Ministry of Natural Resources, Beijing, China, [2]School of Soil and Water Conservation, Beijing Forestry University, Beijing, China, [3]Department of Agriculture and Food, Commonwealth Scientific and Industrial Research Organisation (CSIRO), Canberra, ACT, Australia, [4]Guangdong Provincial Key Laboratory of Applied Botany, South China Botanical Garden, Chinese Academy of Sciences, Guangzhou, China

KEYWORDS

environmental science, ecosystem services (ES), soil hydrology, geological attribute, sustainable development goals-SDGs

Editorial on the Research Topic
Ecosystem services and sustainable restoration interlinking soil, geological, and vegetation interactions for sustainable development

1 Introduction

The restoration of ecosystems is increasingly critical in the context of global environmental and ecological challenges. As the world faces the growing impacts of climate change and land degradation, restoring ecosystems to enhance their services—such as water regulation, carbon sequestration, and biodiversity—is paramount. This Research Topic explores the interrelations between geological attributes, soil properties, and vegetation in ecosystem restoration, focusing on how these interactions influence ecosystem services and contribute to sustainable development goals (SDGs). Specifically, SDG 6 (Clean Water and Sanitation), SDG 13 (Climate Action), and SDG 15 (Life on Land) are particularly relevant as they align with the goals of enhancing water management, mitigating climate change, and restoring terrestrial ecosystems. Through examining empirical research and integrating findings from diverse geomorphological conditions, the articles in this Research Topic offer novel insights into enhancing ecosystem resilience and advancing ecosystem-based solutions for water and land management.

Ecosystem restoration offers a pathway to address multiple environmental issues simultaneously, particularly in regions affected by overexploitation, desertification, and deforestation. By understanding how soil, geology, and vegetation interact, researchers can design more effective restoration strategies that improve ecosystem functions and contribute to climate adaptation and the achievement of SDGs. The studies included in

this Research Topic emphasize the need for interdisciplinary approaches that combine ecological, hydrological, and geological knowledge. They provide critical insights into how restoration practices can enhance ecosystem services, improve land and water management, and ultimately support the achievement of sustainable development goals in the face of global environmental stressors.

2 Soil-plant interactions in ecosystem restoration

Soil-plant interactions are fundamental to ecosystem restoration, as they influence nutrient cycling, water retention, and plant growth. Soil properties such as texture, organic matter content, and moisture availability directly impact vegetation health, which in turn affects ecosystem functions. Feng et al. analyzed how long-term vegetation restoration in the Loess Plateau influenced soil hydrological functions and highlighted the role of soil moisture in sustaining restored vegetation. Similarly, Shao et al. found that different restoration methods in arid regions significantly enhanced soil water retention, which improved vegetation growth and ecosystem stability. These studies underscore the importance of soil-plant interactions in ecosystem restoration and their broader implications for land and water management.

3 Technological advances in ecosystem monitoring

Advances in monitoring technology have revolutionized our ability to assess and manage ecosystems. Remote sensing, GIS, and hydrological modeling tools enable more precise tracking of vegetation dynamics, soil moisture, and overall ecosystem health. Yue et al. used advanced spatial analysis to measure the impact of photovoltaic panels on soil properties in desert ecosystems, providing critical data for ecological restoration efforts. Cheng et al. also utilized remote sensing technology to study the influence of vegetation characteristics and soil properties on ecosystem dynamics in tropical forests. These innovations not only improve our understanding of ecosystem processes but also enhance the effectiveness of restoration strategies.

4 Biogeochemical processes and carbon sequestration

Biogeochemical processes are essential for understanding how ecosystems recover and enhance their ability to sequester carbon. This is particularly important in the context of climate change, as restored ecosystems can contribute to mitigating carbon emissions. Zhang et al. found that soil carbon and nitrogen changes due to soil particle redistribution in photovoltaic arrays influenced soil fertility and carbon sequestration potential. In a similar study, Zhang et al. investigated the role of vegetation restoration in improving soil organic carbon storage in degraded landscapes. These studies highlight the significant role of biogeochemical processes in carbon cycling and their potential for enhancing ecosystem services related to climate change mitigation.

5 Ecosystem services and water management

Effective water management is a critical aspect of ecosystem restoration, particularly in regions affected by droughts and water scarcity. Restoration practices that enhance water regulation, such as reforestation and wetland restoration, can help restore the hydrological cycle and mitigate the impacts of climate change. Ma et al. demonstrated that moderate grazing promotes plant diversity and increases grassland water retention in the Qinghai-Tibet Plateau, which is crucial for sustainable water management. Similarly, Ma et al. assessed the role of vegetation restoration in improving water yield in China's arid regions. Collectively, these studies underscore the importance of integrating ecosystem-based water management strategies in restoration efforts.

6 Conclusion

The research presented in this special issue collection highlights the critical connections between soil, geology, and vegetation in the restoration of ecosystems and the enhancement of their services. From improving water retention and carbon sequestration to advancing ecosystem monitoring and management strategies, these research findings offer valuable insights into how ecological restoration can contribute to sustainable development goals. Restoration is a complex and multifaceted process, and a one-size-fits-all approach is unlikely to be effective. Ecosystem restoration requires a holistic approach that incorporates local geological, soil, and vegetation conditions, as well as socio-economic factors, to ensure long-term success. These studies reinforce the need for interdisciplinary strategies to tackle the diverse challenges of ecosystem restoration and to achieve lasting improvements in ecosystem services.

Author contributions

TF: Writing – original draft, Writing – review and editing. PH: Writing – review and editing. HZ: Writing – review and editing.

Funding

The authors declare that financial support was received for the research and/or publication of this article. This study was funded by the open Fund of Key Laboratory of Mine Ecological Effects and Systematic Restoration, Ministry of Natural Resources (No. MEER-2025-08), the National Natural Science Foundation of China (No. 42371114), the Fundamental Research Funds for the Central Universities (QNTD202508).

Conflict of interest

The author declares that the research was conducted in the absence of any commercial or financial relationships that could be construed as a potential conflict of interest.

Generative AI statement

The authors declare that no Generative AI was used in the creation of this manuscript.

Any alternative text (alt text) provided alongside figures in this article has been generated by Frontiers with the support of artificial intelligence and reasonable efforts have been made to ensure accuracy, including review by the authors wherever possible. If you identify any issues, please contact us.

Publisher's note

frontiers | Frontiers in Environmental Science

TYPE Original Research
PUBLISHED 10 January 2025
DOI 10.3389/fenvs.2024.1538243

OPEN ACCESS

EDITED BY
Tianjiao Feng,
Beijing Forestry University, China

REVIEWED BY
Chenxing Wang,
Chinese Academy of Sciences (CAS), China
Yajun Li,
China University of Geosciences, China
Yongda Wang,
University of Jinan, China
Wenxiang Wang,
Weifang University, China

*CORRESPONDENCE
Liya Yang,
yangliya@mail.cgs.gov.cn

RECEIVED 02 December 2024
ACCEPTED 20 December 2024
PUBLISHED 10 January 2025

CITATION
Feng S, Li Z, Zhang C, Qi R and Yang L (2025) Ecological restoration in high-altitude mining areas: evaluation soil reconstruction and vegetation recovery in the Jiangcang coal mining area on the Qinghai-Tibet Plateau. *Front. Environ. Sci.* 12:1538243. doi: 10.3389/fenvs.2024.1538243

Ecological restoration in high-altitude mining areas: evaluation soil reconstruction and vegetation recovery in the Jiangcang coal mining area on the Qinghai-Tibet Plateau

Shaohua Feng[1,2,3], Zhiwei Li[3], Ce Zhang[3], Ran Qi[3] and Liya Yang[4,5]*

[1]State Key Laboratory of Lithospheric and Environmental Coevolution, Institute of Geology and Geophysics, Chinese Academy of Sciences, Beijing, China, [2]University of Chinese Academy of Sciences, Beijing, China, [3]China Geo-Engineering Corporation, Beijing, China, [4]Key Laboratory of Mine Ecological Effects and System Restoration, China Institute of Geo-Environment Monitoring, Ministry of Natural Resources, Beijing, China, [5]China Institute of Geo-Environment Monitoring, Beijing, China

Introduction: This study evaluates the effectiveness of soil reconstruction and restoration in the Jiangcang coal mining area on the Qinghai-Tibet Plateau, where harsh environmental conditions pose significant challenges to ecological restoration.

Methods: Two phases of ecological restoration were implemented, with outcomes assessed based on vegetation coverage, species diversity, biomass, soil properties, and community similarity.

Results: The results demonstrate that soil reconstruction significantly improved soil fertility, vegetation coverage, and community stability without noticeable degradation over time. The use of sheep manure increased species diversity by introducing native seeds, addressing the shortage of suitable grass species in alpine areas. Comparatively, the second phase of restoration, which included soil reconstruction, has elevated the vegetation coverage to 80%, matching natural background levels, and has also demonstrated superior outcomes in terms of soil stability, nutrient content, and other aspects compared to traditional methods. While aboveground biomass showed rapid recovery, belowground biomass lagged, indicating a need for longer-term restoration. Restored slopes exhibited higher similarity to natural alpine meadows compared to platforms, suggesting the dominance of the artificially seeded species on the platform areas hinders the reproduction of other species, which is unfavorable for the evolution of vegetation diversity.

Discussion: This study emphasizes the effectiveness of soil reconstruction, organic amendment, and other restoration measures, providing important experience and reference for mine ecological restoration in similar high-altitude mining areas.

KEYWORDS

Qinghai-Tibet plateau, soil reconstruction, ecological restoration, open-pit coal mining area, high-altitude vegetation recovery

1 Introduction

The Qinghai-Tibet Plateau is known for its harsh climatic conditions, high altitudes, and fragile ecosystems, which make ecological restoration efforts particularly challenging (Carabassa et al., 2020; Cheng et al., 2022). Mining activities in this region have caused severe ecological damage, particularly in high-altitude areas where permafrost and alpine meadow ecosystems are widespread (Zhang et al., 2023; Hu et al., 2018). The Muli coal mine, located at the northeastern edge of the Qinghai-Tibet Plateau, is the largest coal mine in Qinghai Province and a significant coking coal resource in northwest China (He et al., 2024). Decades of open-pit mining have led to substantial environmental degradation, including the destruction of water, soil, and vegetation resources, as well as the thawing of permafrost, which has further contributed to the degradation of alpine meadows and increased soil erosion (Reid and Naeth, 2005a; Misebo et al., 2022). The permafrost degradation not only reduces the stability of the soil but also negatively impacts the region's hydrological balance, making effective ecological restoration a critical need (Rocha and Martins, 2021; Scotton, 2021).

In recent years, the Chinese government has increased its emphasis on ecological restoration and environmental protection, with specific policies targeting mining areas in the Qinghai-Tibet Plateau. As part of this effort, numerous projects have been launched to restore vegetation and improve soil quality in these degraded regions (Wong, 2003; Yang et al., 2019). The unique climatic conditions, such as short growing seasons, low temperatures, and limited precipitation, further complicate restoration efforts, necessitating the development of adaptive restoration techniques tailored to these extreme environments (Yang et al., 2019; Zhang et al., 2023). High-altitude mining areas face severe soil degradation, loss of vegetation, and destabilized ecosystems, which exacerbate ecological fragility in regions like the Qinghai-Tibet Plateau (Zheng et al., 2023; Lu et al., 2024). Recent studies have highlighted the importance of integrating soil amendments, particularly organic inputs, to facilitate vegetation establishment and improve soil quality. For example, soil organic amendments, such as sheep manure and compost, can significantly enhance soil structure, fertility, and microbial biomass, providing essential support for plant growth (Worlanyo and Jiangfeng, 2021; Liu et al., 2022). Research on alpine mining areas in regions with similar conditions, such as the Andes and parts of Central Asia, has demonstrated the importance of selecting site-specific strategies for soil and vegetation restoration (Lim et al., 2022). Techniques like hydroseeding, the use of erosion control mats, and mixed seeding of native grass and shrub species have shown positive results in improving vegetation coverage and biodiversity (Wang et al., 2018; Penalver-Alcala et al., 2021). However, much of the research in China has focused on the Juhugeng mining area (Zhong et al., 2021; Feng et al., 2023), while restoration studies specifically targeting the Jiangcang mining area remain limited.

Over the past decade, there has been significant progress in understanding the effects of mining activities on fragile ecosystems and developing restoration techniques. Studies have shown that soil reconstruction and the use of native plant species can enhance the recovery of disturbed ecosystems in high-altitude regions (Feng et al., 2024). Soil reconstruction involving the amendment of soil with organic materials, such as sheep manure, has been shown to significantly improve soil fertility and aid in the establishment of vegetation in degraded mining areas (Cross and Lambers, 2017). Research in other regions with similar climatic conditions has highlighted the effectiveness of organic amendments in enhancing soil microbial activity and improving soil structure, which are critical for successful restoration (Luna et al., 2018; Figueiredo et al., 2024). However, most research has focused on the Juhugeng mining area, while studies on the Jiangcang mining area remain limited (Naeth and Wikinson, 2014).

Additionally, the use of remote sensing and GIS technologies has advanced the monitoring of vegetation recovery in mining areas, allowing researchers to assess changes in vegetation coverage and landscape patterns over time (Courtney et al., 2011; Pardo et al., 2014). These technological advancements have enabled more accurate assessments of restoration effectiveness and have highlighted the importance of long-term monitoring to understand the dynamics of ecosystem recovery (He et al., 2024). Despite these advancements, there remains a lack of comprehensive studies that integrate both aboveground and belowground ecological indicators to evaluate restoration success in the Qinghai-Tibet Plateau's mining areas (Heiskanen et al., 2022; Kim et al., 2020).

Although some progress has been made in relevant research, significant gaps still exist in current studies. Many studies have primarily concentrated on the short-term effects of ecological restoration, with limited focus on the long-term sustainability of restored ecosystems (Kim et al., 2020). In particular, the underground biomass recovery, which is crucial for long-term ecosystem stability, has not been adequately addressed (Jambhulkar and Kumar, 2019). The recovery of belowground biomass plays a key role in maintaining soil structure, enhancing nutrient cycling, and supporting long-term vegetation stability (Reid and Naeth, 2005b; Lupton et al., 2013). Moreover, few studies have explored the effects of different restoration techniques in the specific context of the Qinghai-Tibet Plateau, where permafrost and high-altitude conditions pose unique challenges (Zhou et al., 2015; Rothman et al., 2021). There is also a need for research that evaluates the impact of different types of organic amendments and their effectiveness under varying environmental conditions in high-altitude ecosystems (Yang et al., 2016).

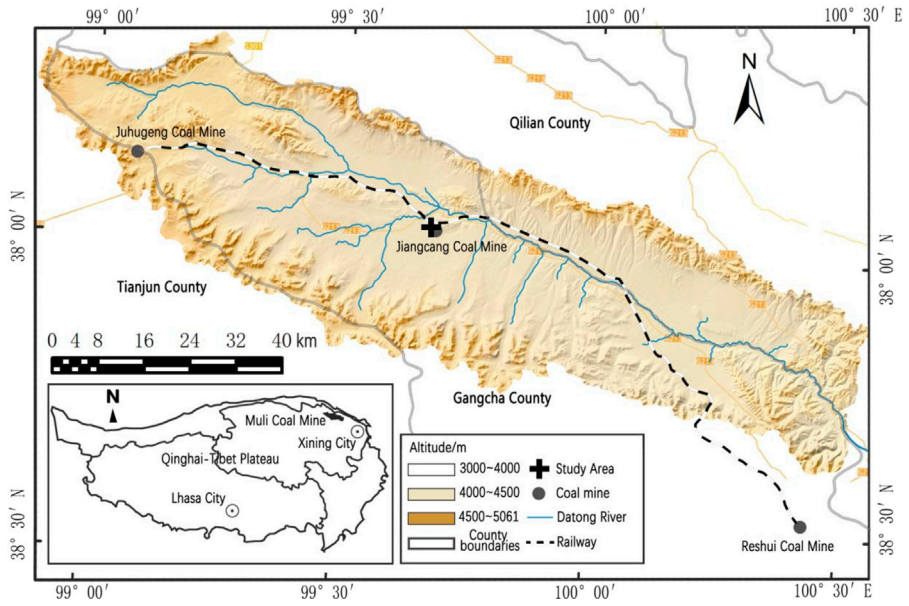

FIGURE 1
Study area location.

In this study, we address these gaps by evaluating the long-term effectiveness of soil reconstruction and ecological restoration techniques in the Jiangcang mining area of the Muli coal mine. Our research focuses on comparing two phases of ecological restoration, assessing parameters such as vegetation coverage, species diversity, biomass, and soil stability. Our hypotheses are that soil reconstruction techniques using organic amendments can significantly enhance soil fertility and vegetation recovery in high-altitude mining areas, and that the use of native plant species will lead to greater ecosystem stability and resilience compared to traditional restoration methods. We utilized organic amendments, including sheep manure, and a mixed seeding approach using native species to facilitate the restoration process. By monitoring changes over time, we aim to provide insights into the effectiveness of these restoration techniques in enhancing ecosystem resilience under harsh environmental conditions. Our approach also integrates both aboveground and belowground ecological indicators to provide a comprehensive understanding of restoration success (Williams and Thomas, 2023). The Objectives of this study is (1) to evaluate the effectiveness of soil reconstruction techniques in improving soil fertility and vegetation recovery in the Jiangcang mining area, (2) to compare the restoration outcomes of different ecological restoration approaches, including aboveground and belowground ecological indicators, and (3) to assess the long-term sustainability of restored ecosystems under high-altitude, harsh environmental conditions. The significance of this study lies in its contribution to understanding the long-term dynamics of ecological restoration in high-altitude mining areas. Our findings highlight the importance of soil reconstruction and the use of native species for successful restoration outcomes. This research also provides valuable insights into the challenges and potential solutions for restoring ecosystems in regions characterized by permafrost and alpine climates, which are particularly vulnerable to environmental degradation (Gao et al., 2019). The results of this study can inform future restoration projects in similar environments, contributing to the broader goal of achieving sustainable ecological management in high-altitude, fragile ecosystems.

2 Materials and methods

2.1 Study area

The study area is located in the Jiangcang mining area of the Muli coal mine, situated in Tianjun County, Haixi Mongolian and Tibetan Autonomous Prefecture, Qinghai Province, China. The region lies between approximately 97°30′to 100°00′E longitude and 37°30′to 39°00′N latitude, covering a total area of 17,800 ha. It is bounded approximately 110 km southeast of Gangcha County, 45 km west of the Juhugeng mining area, and 150 km southwest of Tianjun County (Figure 1). The study area includes multiple mining sites, such as Jiangcang No. 1, No. 2, No. 4, and No. 5 pits, as well as several waste rock dumps. The region is characterized by extensive permafrost, with permafrost thickness ranging from 62.5 to 174 m (Table 1) and the active layer typically less than 2 m. Permafrost begins to thaw in April and refreezes by September, while average temperatures in June through August reach above 9°C, providing a short growing season of approximately 90 days that supports revegetation efforts. The annual average precipitation exceeds 450 mm, with 80% of the rainfall occurring between May and September, which is sufficient to meet the water requirements for plant growth and establishment.

The Jiangcang mining area features a typical cold alpine ecosystem, representing the broader Qinghai-Tibet Plateau's environmental characteristics. The topography is marked by

TABLE 1 Depth statistics of the permafrost bottom boundary from near-steady-state logging at boreholes in jiangcang mining area.

Exploration area	Borehole number	Coordinate position	24-Hour permafrost bottom depth (m)	72-Hour permafrost bottom depth (m)	Depth change (m)
Jiangcang No. 4 and No. 5 Pits	ZK12-2	N38.041283° E99.519,140°	62.5	70	7.5
	ZK5-3	N38.035918° E99.479,485°	70	81	11
	ZK3-1	N38.037849° E99.468,027°	174	183	9
	ZK2-2	N38.048364° E99.465,495°	126	134	8

high-altitude ranges, with an elevation between 3,500 m and 4,500 m, averaging at 3,900 m above sea level, making it particularly sensitive to external disturbances like mining, with two main vegetation types: alpine meadow and alpine marsh meadow. These vegetation types are closely linked to the region's hydrogeological conditions, which control the distribution of plant communities. Alpine marsh meadow dominates areas with permafrost, while alpine meadow is more common in the foreland slopes and thawing regions. Alpine marsh meadow vegetation is typically low-growing and structurally simple, with dominant species including *Kobresia tibetica* and *Carex orbicularis*. Associated species include *Carex moorcroftii*, *Carex atrata*, *Allium przewalskianum*, *Polygonum viviparum*, and other perennial herbs that thrive in cold, moist conditions. Alpine meadow vegetation, in contrast, is dominated by Artemisia species, which are characterized by their low, dense growth habit and their ability to withstand harsh conditions, with species such as *Artemisia nanschanica*, *Pedicularis kansuensis Maxim*., and *Elymus nutans* being prevalent.

The mining activities have created six large excavation pits that have severely disturbed the original landscape and surface vegetation. Open-pit mining has generated significant amounts of waste rock and spoil, which are deposited in layers around the pits, forming extensive waste rock dumps with heights ranging from several meters to over 50 m. This has caused severe damage to the landscape and vegetation, particularly affecting alpine meadows in the vicinity of pits, dumps, roads, and industrial sites, leading to extensive degradation of meadow habitats. Additionally, mining activities have disrupted the permafrost, resulting in the formation of groundwater "windows" that allow groundwater to flow into the pits, leading to extensive ponding and altering the freeze-thaw dynamics. Given the area's high-altitude conditions and short growing season, ecological restoration in this region is particularly challenging, requiring careful management to ensure successful revegetation and ecosystem recovery.

2.2 Mining activities and ecological restoration

The Jiangcang mining area was discovered in the 1950s, with initial exploration activities conducted in 1956. The coal deposits are characterized by shallow burial with thin Quaternary unconsolidated sediments overlying or directly exposed at the surface, forming a partially concealed coalfield. Following the increased demand for energy and the prosperity of the coal market after 2002, several coal enterprises, including Qinghai Qinghua, Qinghai Aokai, Qinghai Jiangcang Energy, and Qinghai Coking Coal, began mining activities in the Jiangcang area. Mining commenced in 2003, with Pits No. 1, No. 2, No. 4, and No. 5 brought into production, while Pit No. 3 remained undeveloped. Open-pit mining was the primary extraction method used, and peak mining activity occurred between 2008 and 2019. Overburden and coal gangue were disposed of in stepped layers around the excavation pits, causing significant topographic changes and extensive land occupation.

Two major ecological restoration initiatives have been undertaken in the study area to date. The first large-scale restoration effort took place from 2014 to 2016, focusing on reshaping 19 waste rock dumps formed by open-pit mining and establishing vegetation. The restoration techniques included slope reshaping, organic fertilizer application, mixed seeding of grass species, and covering with non-woven fabric. These methods were relatively traditional and showed limited success in restoring meadow vegetation.

The second large-scale restoration was conducted from 2020 to 2021, building on the lessons learned from the earlier efforts. This phase aimed at improving restoration outcomes by reconstructing the soil profile, using the native soil as a reference. Restoration measures for Pits No. 4 and No. 5 included slope reshaping, screening of waste rock to separate usable soil, mixing of screened soil with sheep manure and slow-release fertilizers, mixed seeding of grass species, and covering with coir fiber blankets. This combination was designed to improve soil fertility and enhance vegetation establishment.

In the study area, specific steps in the second restoration included.

(1) Slope Reshaping: Mechanical reshaping of the terrain to a slope gradient of less than 25°, with larger stones placed at the bottom and finer particles at the top. Utilize the self-weight of machinery for compaction to prevent large-scale settlement of the landform after shaping.
(2) Soil Screening: The waste rock underwent on-site screening, where gravel was crushed by excavators. Subsequently, the soil was double-turned to guarantee uniformity of particles, and any rocks exceeding 5 cm in size were removed using a

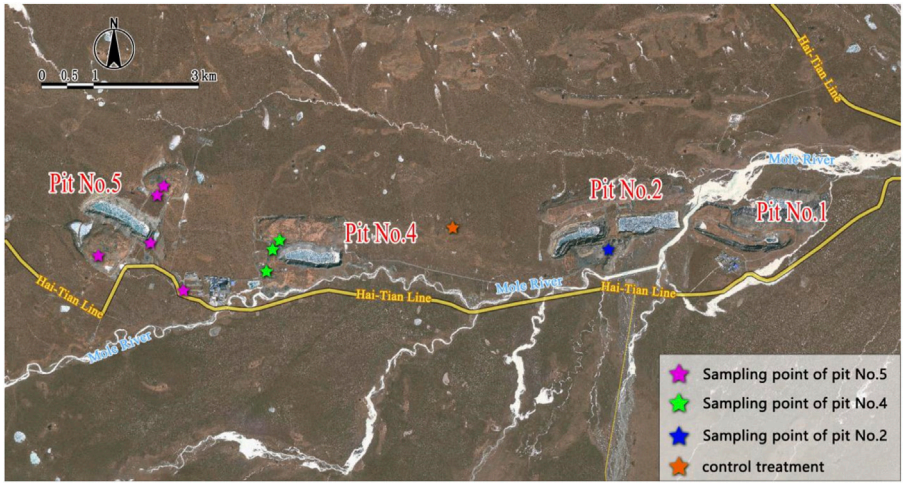

FIGURE 2
Distribution of sampling plots in the study area.

stone picker. This screened soil was then utilized as the foundation for the reconstructed soils.

(3) Soil Amendment with Sheep Manure and Slow-Release Fertilizer: The soil was evenly mixed with 495 m^3 of sheep manure and 22.5 tons of slow-release fertilizer per hectare. Given that plant roots primarily occupy the top 20 cm of soil, and accounting for an anticipated 5–10 cm of natural subsidence, the final soil layer thickness was set at 25 cm.

(4) Mixed Seeding of Grass Species:Obtaining wild grass seeds in plateau and high-altitude areas is challenging. After conducting an analysis of the market supply capacity of grass seeds and ensuring no exotic species were introduced, *E. nutans*, *Poa pratensis* var. *Qinghaiensis*, *Festuca sinensis*, and *Kentucky bluegrass* were ultimately chosen as the grass species for sowing. These species were mixed at a ratio of 1:1:1:1, with a total seeding rate of 180 kg per hectare.

(5) Coir Fiber Blanket Covering: The surface was covered with coir fiber blankets to retain moisture, prevent surface runoff, and reduce nutrient loss, ultimately promoting successful revegetation.

2.3 Ecological landscape changes

According to remote sensing interpretation results from 2002 to 2022, the area of land used for mining activities in the study area increased annually from 2003 to 2019, reaching a peak of 3,085.74 ha in 2019. This expansion came at the cost of reducing surrounding grasslands and bare land, with losses amounting to 11,183.26 ha and 3,667.88 ha, respectively, approximately five times the increase in mining land. Since the initiation of the second ecological restoration action in 2020, the area used for mining activities has gradually decreased to 1,911.78 ha, with a total restoration area of approximately 1,000 ha. Concurrently, the area of low-coverage grassland has recovered by 2,184.3 ha compared to 2015.

2.4 Sampling point distribution

This study focuses on the Jiangcang mining area to evaluate the effectiveness of soil reconstruction and revegetation. Currently, the area has undergone complete revegetation and supplementary improvements in treated zones. Areas that could fully reflect the plant species and growth conditions under different restoration measures were selected as sampling plots. In total, 10 sampling points were set up, distributed across the waste rock platforms and slopes of Pits No. 4 and No. 5 (from the second restoration phase), the south waste dump platform of Pit No. 2 (from the first restoration phase), and the natural background area. The specific distribution of vegetation survey sampling points is shown in Figure 2.

2.5 Vegetation plot survey

The plot size for herbaceous vegetation was preliminarily set to 1 m × 1 m, considering the growth status of the vegetation and terrain. The sample size was selected to adequately represent the characteristics of the vegetation while ensuring ease of observation and sampling. The survey data collected from vegetation plots included weather, elevation, coordinates, plant species, dominant species, abundance, biomass, average height, average coverage, average crown width, and growth status for each sampling point. These data were used for a comprehensive assessment of the vegetation ecosystem in the study area. The main survey indicators are detailed in Table 2.

2.6 Indicator calculations methods

2.6.1 Species diversity

Species diversity reflects the complexity of species composition within a community. In this study, we employed the Shannon

TABLE 2 Main vegetation survey indicators and descriptions.

Monitoring indicator	Description
Aboveground Biomass	Dry weight of each plant species within the unit area (g/m^2)
Coverage	Ratio of the vertical projection of aboveground plant parts to the ground area (%)
Dominant Species	Species with significant influence on the community and minimal effect from other species
Height	Distance of vegetation from the ground (cm)
Crown Width	Diameter of the vegetation's coverage range (cm)
Abundance	Number of plants (individuals or clumps)
Growth Status	Condition of plant growth, including health, withering, and pest conditions

diversity index, Pielou's evenness index, and Margalef's richness index to quantify and assess this diversity. The specific calculation formulas for these indices are as follows:

$$\text{Shannon Diversity Index: } D = 1 - \sum_{i=1}^{s} (P_i)^2$$

$$\text{Pielou's Evenness Index: } Jp = \frac{\sum_{i=1}^{s} (P_i \times ln\, P_i)}{\ln (S)}$$

$$\text{Margalef's Richness Index: } Ma = \frac{S - 1}{\ln (N)}$$

Where *Pi* represents the percentage of the number of species *i* in the entire sample plot; *S* denotes the total number of species; and *N* stands for the total number of individuals of all species.

2.6.2 Community similarity coefficient

The Sorensen community similarity coefficient represents the degree of similarity between different community structures, indicating the extent of species overlap between sampling areas. It is utilized to assess the differences among communities and is calculated using the following formula:

$$SC = 2C/(S1 + S2)$$

Where *C* is the number of species shared between communities *S1* and *S2*, and *SC* is the similarity coefficient between the communities.

2.6.3 Vegetation coverage

Vegetation coverage in the mining area from 2020 to August 2024 was calculated using Sentinel data and the mixed pixel decomposition method. In remote sensing imagery, each pixel generally comprises multiple components, each contributing to the composite signal observed. To estimate vegetation coverage, a pixel decomposition model was applied. The specific calculation formula for this model is as follows:

$$FVC = (NDVI - NDVI_{soil}) / (NDVI - NDVI_{veg})$$

Where: *FVC* is Fractional Vegetation Coverage; *NDVI* is NDVI value of the mixed pixel; $NDVI_{soil}$ is NDVI value of a pure bare soil pixel; $NDVI_{veg}$ is NDVI value of a pure vegetation pixel.

2.7 Statistical methods

Statistical analyses were performed using SPSS 26.0 and R 4.2.1. Descriptive statistics were calculated to summarize soil properties and vegetation attributes. Differences among treatments (restored pits No. 4, No. 5, No. 2, and control) were analyzed using one-way ANOVA, with *post hoc* tests (Tukey's HSD) for pairwise comparisons. t-tests were used to compare specific groups (e.g., restored vs control). Pearson correlation analysis was conducted to examine relationships between soil physicochemical properties and vegetation parameters. Network correlation analysis was employed to visualize the interactions among soil and vegetation variables. Statistical significance was set at $p < 0.05$.

3 Results

3.1 Vegetation species characteristics and coverage changes

An analysis of plant community species surveys in the alpine grassland of the study area revealed that vegetation in mining pits and waste rock dumps was almost entirely destroyed following mining activities. After the restoration and revegetation efforts, approximately 20 plant species were identified in the sampling plots. Besides the four artificially planted species—*E. nutans*, *P. pratensis* var. *Qinghaiensis*, *F. sinensis*, and *K. bluegrass*—the natural accompanying vegetation included species such as *P. kansuensis Maxim.*, *Astragalus polycladus Bur. Et Franch.*, *Oxytropis ochrocephala Bunge*, *Elsholtzia densa Benth.*, *Androsace umbellata*, *Polygonum sibiricum*, *Microula sikkimensis (C. B. Clarke) Hemsl.*, *Capsella bursa-pastoris*, etc., showing relatively rich vegetation diversity. The untreated areas within the mining zone were largely devoid of vegetation. The primary dominant species in the rehabilitated areas were the four artificially planted species. Other natural species present in the area likely germinated from seeds carried by sheep manure used in the restoration, indicating that the use of sheep manure played a significant role in the natural regeneration and establishment of wild species that are otherwise difficult to obtain.

Based on Sentinel data from 2020 to August 2024, the vegetation coverage (Fractional Vegetation Cover, FVC) of Jiangcang mining area, specifically Pits No. 4, No. 5, and the south waste dump of Pit No. 2, along with surrounding reference areas, was analyzed, and the

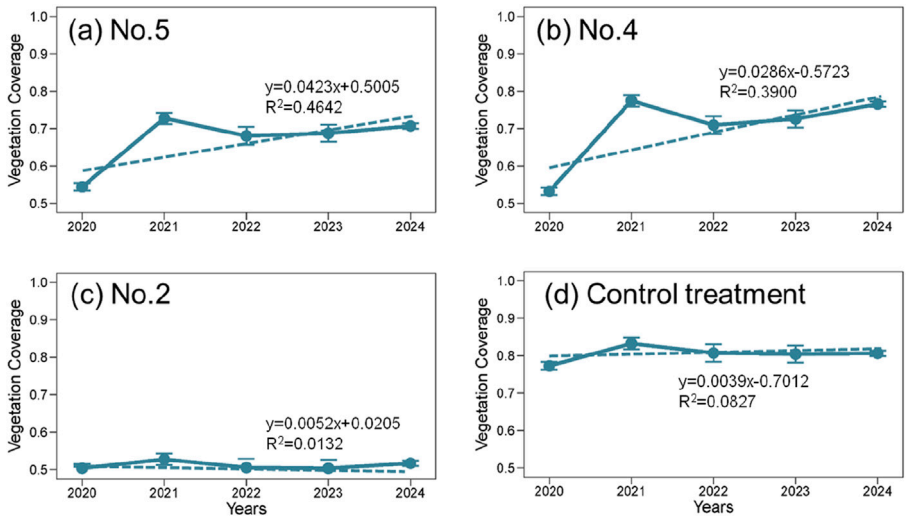

FIGURE 3
Changes in average vegetation coverage from 2020 to 2024. **(A)** No.5. **(B)** No.4. **(C)** No.2. **(D)** Control treatment.

average changes in vegetation coverage in these four regions were recorded (Figure 3). The results show that the vegetation coverage in Jiangcang Pit No. 4 initially increased, then decreased, followed by another increase, with a peak in 2021 at 77.45%. In 2020, the vegetation coverage of Pit No. 4 was 53.21%. After the second round of restoration and revegetation efforts, the coverage remained above 70% from 2021 to 2024, indicating that the restoration efforts were effective, and the ecological conditions improved significantly compared to 2020. The trends in Pit No. 5 were similar to those in Pit No. 4. In 2020, the vegetation coverage of Pit No. 5 was 54.37%, which peaked at 72.75% in 2021. By 2024, the vegetation coverage had increased by 16.32% compared to 2020, suggesting successful restoration over the past 5 years. The south waste dump of Pit No. 2 was restored using traditional revegetation measures in 2015. From 2020 to 2024, the average vegetation coverage remained around 50%, with little change, indicating that the effectiveness of the first restoration was limited. The background area of Jiangcang mining site showed average vegetation coverage values ranging from 77% to 84% between 2020 and 2024, indicating generally good ecological conditions. Overall, the vegetation coverage across the mining area initially increased and then decreased, with a peak in 2021 at 83.26%. Afterward, the coverage slightly decreased and stabilized around 80%. All regions showed a peak in vegetation coverage in 2021. A comparison with precipitation data indicated that there was no significant increase in rainfall in 2021, suggesting that the extended vegetation growing period due to a shorter freeze period may have contributed to the higher vegetation coverage observed that year. According to remote sensing interpretation results from 2002 to 2022, the area of land used for mining activities in the study area increased annually from 2003 to 2019, reaching a peak of 3,085.74 ha in 2019. This expansion came at the cost of reducing surrounding grasslands and bare land, with losses amounting to 11,183.26 ha and 3,667.88 ha, respectively, approximately five times the increase in mining land. Since the initiation of the second ecological restoration action in 2020, the area used for mining activities has gradually decreased to 1,911.78 ha, with a total restoration area of approximately 1,000 ha. Concurrently, the area of low-coverage grassland has recovered by 2,184.3 ha compared to 2015.

3.2 Vegetation evolution trends after restoration

The second phase of restoration in Jiangcang Pits No. 4 and No. 5 was largely completed between 2020 and the first half of 2021. Vegetation in the restoration areas quickly recovered during 2021. To further investigate whether the vegetation could safely overwinter and the sustainability of restoration effects, this study analyzed vegetation coverage trends from 2021 to 2024, as shown in Figure 4.

The vegetation evolution trend in Jiangcang Pit No. 4 from 2021 to 2024 shows an overall increase in vegetation coverage. The area with no significant increase was 1.77 km^2, accounting for 70.80% of the mining area. The area with slightly significant and significant increases combined was 0.35 km^2, covering 13.92% of the mining area, mainly distributed in the eastern and central parts of Pit No. 4. The area with no significant decrease was 0.27 km^2, representing 10.67% of the mining area, mainly in the northern and central parts of the mining area, with scattered distribution. The combined area of significant and slightly significant decreases was only 0.0032 km^2, accounting for just 0.14% of the mining area. The area with no change was 0.11 km^2, covering 4.48% of the mining area, mainly concentrated in the central part of Pit No. 4.

In Jiangcang Pit No. 5, the trend from 2021 to 2024 shows a decrease in vegetation coverage of 0.42 km^2 and an increase of 2.24 km^2, accounting for 17.66% and 76.57% of the mining area, respectively. The area with no significant increase was the largest, accounting for more than 60% of the mining area. The area with no significant decrease was 0.48 km^2, representing 16.28% of the mining area, mainly in the central and northern parts of the mining area. Significant decreases were mainly distributed in the central-western parts of the mining area, accounting for only 0.31% of the total area.

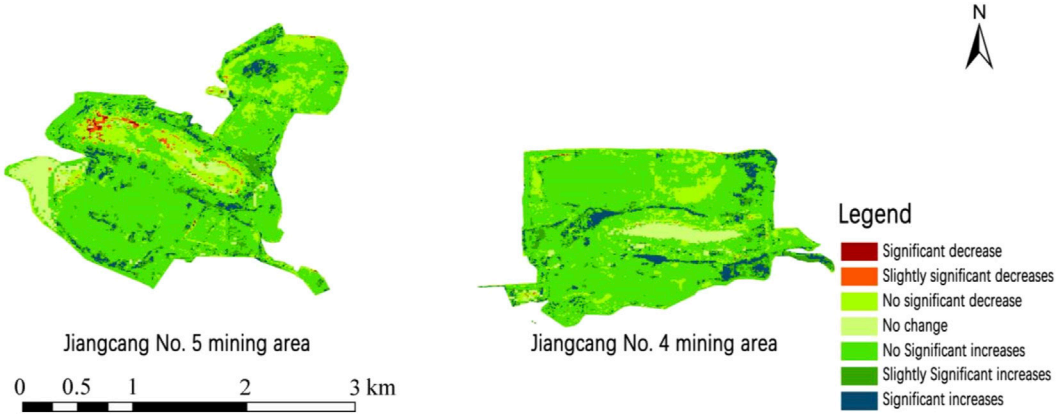

FIGURE 4
Vegetation evolution trends in jiangcang pits no. 4 and no. 5 from 2021 to 2024.

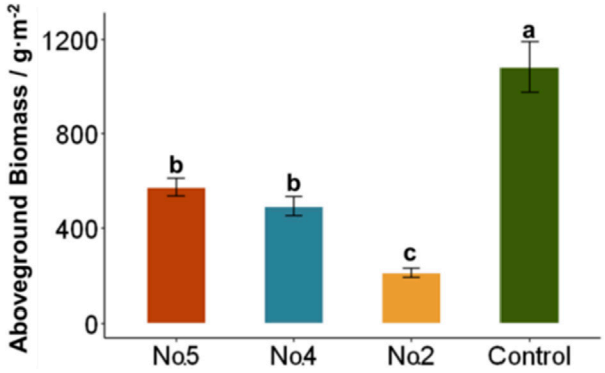

FIGURE 5
Comparison of aboveground biomass at sampling points in the study area.

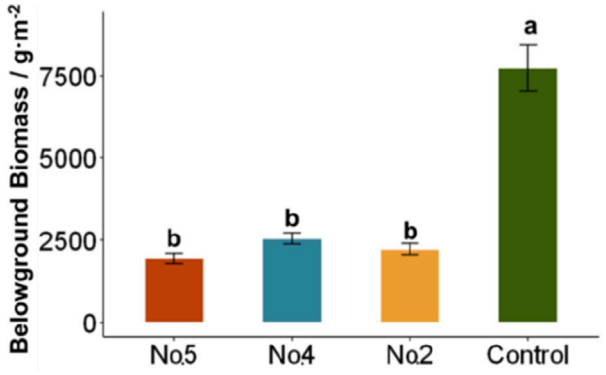

FIGURE 6
Comparison of belowground biomass at sampling points in the study area.

Significant increases were observed around the central mining area, covering 4.37% of the total area. Areas with no change in vegetation coverage were mainly located in the southwestern part of the mining area, with an area of 0.13 km^2.

The vegetation evolution trends indicate that following restoration using soil reconstruction methods, although the growing season in 2021 was slightly shortened due to restoration construction, newly established vegetation was minimally affected by winter temperatures. Over the following 3 years, vegetation did not show significant degradation, with areas showing significant or slightly significant increases in vegetation coverage accounting for more than 70% of the total mining area. This suggests that the vegetation evolution trends after restoration did not show obvious degradation, and the ecological environment of the mining area significantly improved, trending toward favorable recovery.

3.3 Plant community characteristics

Based on the 2022 biomass data from sampling points in the study area, the aboveground and belowground biomass of the natural alpine meadow background area remained higher than that of the restored waste rock platforms and slopes. The belowground biomass of the natural grassland was approximately four times that of the aboveground biomass. Figure 5 shows that after the second restoration, the aboveground biomass in Pits No. 4 and No. 5 was significantly higher than that in Pit No. 2, but still lower than that of the natural vegetation, which is highly correlated with the vegetation coverage of the sampling points. Figure 6 illustrates that belowground biomass showed little difference between the two restoration phases, both being significantly lower than the natural grassland background value, indicating that belowground biomass recovery requires long-term accumulation. Notably, the restoration in Pit No. 2 was conducted in 2015, and after 7 years of belowground biomass accumulation, there was little difference compared to Pits No. 4 and No. 5, restored in 2021, further demonstrating the effectiveness of the second soil reconstruction measures.

Statistical analysis of plant community crown width, height, abundance, and coverage in different areas of the north waste rock dump in Pit No. 5 is presented in Table 3. The natural alpine meadow background area is characterized by moderate crown

TABLE 3 Plant community characteristics in different areas.

Area type	Sunny slope	Platform	Background area
Crown Width (cm)	6.24	10.77	8.83
Height (cm)	18.13	22.33	11.95
Abundance (individuals or clumps)	2060.00	2,430.00	2,506.50
Coverage (%)	67.00	74.00	86.00

TABLE 4 Plant community diversity indices for jiangcang pit no. 5.

Area type	Sunny slope	Platform	Background area
Shannon Diversity Index	0.46	0.32	0.56
Pielou Evenness Index	0.50	0.37	0.53
Margalef Richness Index	0.712	0.4339	1.4604

TABLE 5 Community similarity coefficients for different areas in jiangcang pit no. 5.

Area type	Sunny slope	Platform	Background area
Sunny Slope	1		
Platform	0.73	1	
Background Area	0.48	0.37	1

width, low grass clusters, moderate abundance, and high coverage. The revegetated waste rock platform had higher crown width and height, with significant variability in crown width and diverse plant species distribution. The vegetation on the sunny slope of the waste rock dump exhibited lower crown width and abundance, with a wide range of coverage and significant differences in community structure. This indicates that the waste rock platform, with better water and nutrient conditions, supports rapid growth of the restored grass species (mainly Poaceae), resulting in height and crown width that even exceed those in the background area. In contrast, the sunny slope area showed poorer restoration outcomes due to limited water and nutrient availability compared to the platform area.

In-depth analysis of plant community diversity indices for the north waste rock dump in Pit No. 5 revealed that the natural grassland background area had the highest diversity, evenness, and richness indices, indicating a stable community structure with rich and evenly distributed plant species. The sunny slope of the waste rock dump also exhibited relatively high diversity, evenness, and richness indices, suggesting a diverse and evenly distributed plant community. In contrast, the platform area performed the worst in terms of species diversity. Table 4 data indicate that the restored area still requires a long period of natural succession to reach the diversity levels of the background area. The slope area showed better diversity than the platform area, likely due to the dominance of Poaceae pioneer species on the platform, which inhibited the propagation of other species. In contrast, the weaker dominance of species on the sunny slope provided more opportunities for other species to grow, resulting in better diversity.

As shown in Table 5, the similarity between the sunny slope of the waste rock dump and the natural grassland background area was relatively high after artificial restoration, indicating that revegetated slopes are more likely to return to a natural grassland community structure. However, the similarity between the platform and the natural grassland was lower, suggesting that the associated original grassland species are less prevalent on the platform, and it will take longer to restore to a natural state.

3.4 Comparison of soil properties

The soil properties of the restored mining areas (No. 5, No. 4, No. 2 pits) and the control treatment were analyzed and compared, including bulk density (BD), soil water content, soil organic carbon (SOC), pH, electrical conductivity (EC), total nitrogen (TN), total phosphorus (TP), total potassium (TK), and particle size distribution (clay, silt, and sand). Figure 7A shows that soil bulk density (BD) is higher in the restored areas (No. 5 and No. 4) compared to Pit No. 2 and the control treatment. The control treatment has the lowest BD, indicating less compaction compared to the reclaimed mining areas. This suggests that soil compaction may still be an issue in the reclaimed areas, potentially hindering root growth and overall soil quality improvement. In terms of soil water content, as depicted in Figure 7B, the control treatment exhibited significantly higher water content compared to all restored areas. The water content was lowest in Pit No. 2, suggesting that this area may have limited water retention capacity, likely due to inadequate soil structure or insufficient organic amendments during restoration. Figure 7C shows that soil organic carbon (SOC) levels are substantially higher in the control treatment compared to the restored areas, particularly in Pit No. 2, which has the lowest SOC among all the areas. This indicates that the organic matter content in the restored soils is not yet comparable to the control, which might affect soil fertility and microbial activity. Figure 7D indicates similar pH levels across all treatments, suggesting that soil acidity is relatively consistent regardless of the restoration efforts. For the nutrient content, total nitrogen (TN) depicted in Figure 7E is significantly higher in the control compared to the restored sites, with Pit No. 2 showing the lowest nitrogen content. This highlights the

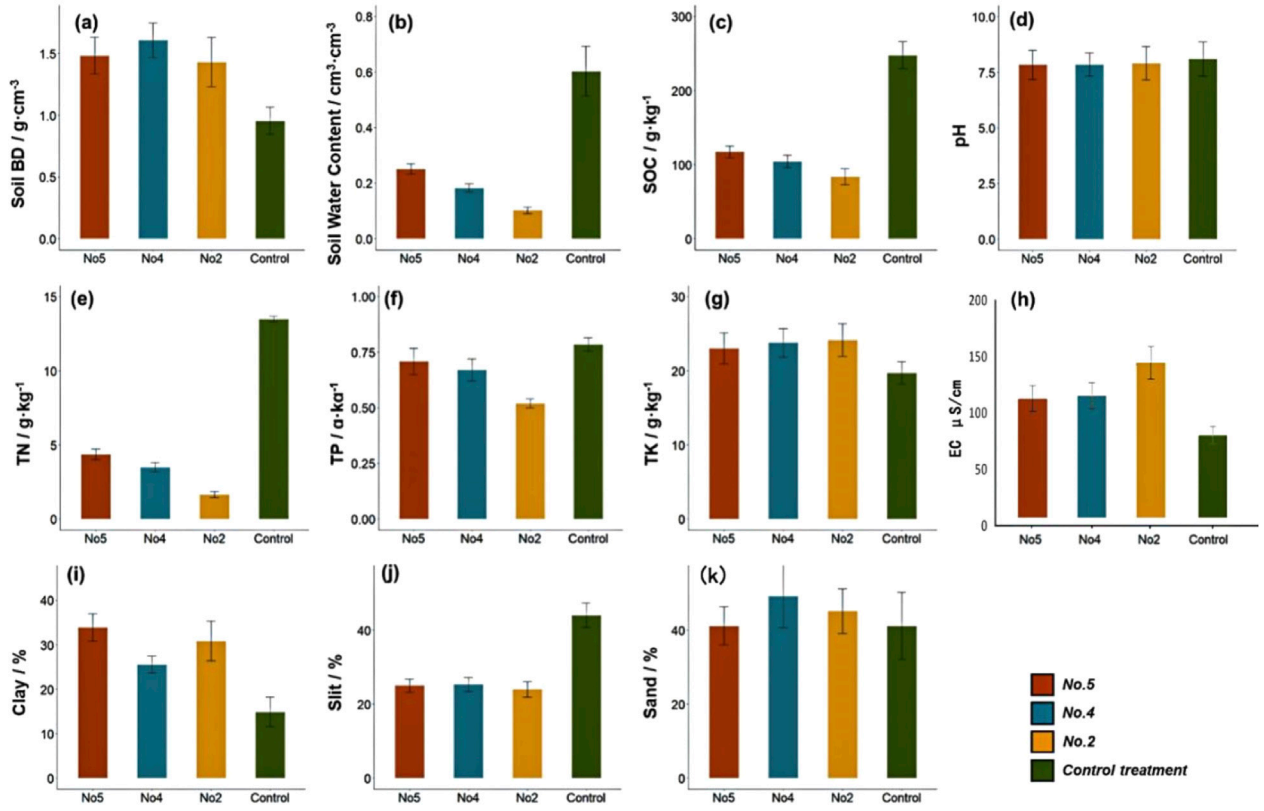

FIGURE 7
Comparison of soil properties among restored mining pits (No. 5, No. 4, No. 2) and control treatment. **(A)** Soil Bulk Density; **(B)** Soil Water Content; **(C)** Soil Organic Carbon; **(D)** pH; **(E)** Total Nitrogen; **(F)** Total Phosphorus; **(G)** Total Potassium; **(H)** Electrical Conductivity; **(I)** Clay Content; **(J)** Slit Content; **(K)** Sand Content.

challenge of replenishing soil nitrogen in reclaimed mining areas. Total phosphorus (TP) levels in Figure 7F are slightly higher in Pits No. 5 and No. 4 compared to Pit No. 2, though all remain lower than the control. Figure 7G shows that total potassium (TK) is relatively stable across all areas, with no substantial differences observed. Figure 7H shows that the electrical conductivity in the restored areas is higher than the control treatment, which is speculated to be due to the effect of the slag in the waste rock dump.

The particle size distribution analysis (Figures 7I–K) reveals variations in clay, silt, and sand contents. The clay content (Figure 7I) is highest in Pit No. 5, which suggests better aggregation and potentially improved soil stability, while Pit No. 2 has the lowest clay content. Silt content (Figure 7J) is also lowest in Pit No. 2, indicating poor soil texture compared to other areas. Conversely, sand content (Figure 7K) is highest in Pit No. 2, which could be contributing to the lower water retention and organic matter levels observed.

Overall, the comparison of soil properties across the restored areas and the control treatment shows that while there have been improvements in soil quality in Pits No. 4 and No. 5, the soil in Pit No. 2 still lags in several key properties, such as soil water content, organic carbon, and nutrient levels. The findings suggest that further amendments or different restoration strategies may be needed in Pit No. 2 to enhance its soil properties to levels comparable to the control or other restored areas.

3.5 Network analysis and relations among environmental factors

The network correlation analysis provides a visual representation of the relationships between soil physicochemical properties and vegetation attributes across the three restored mining pits (No. 5, No. 4, and No. 2) and the control treatment (Figure 8). In this analysis, the strength and direction of correlations are indicated by the color and thickness of the connecting lines, while the spatial arrangement reflects the relative proximity of interrelated variables. In Pit No. 5, soil organic matter (SOM), total nitrogen (TN), and soil water content (SWC) serve as central nodes in the network, displaying strong positive correlations with belowground biomass (BGB) and vegetation fractional cover (VFC), as indicated by thick green lines. Notably, bulk density (BD) shows a negative relationship with SOM and TN, emphasizing the detrimental impact of soil compaction on soil quality and vegetation attributes. Similarly, sand content exhibits a strong negative correlation with SWC, suggesting its adverse effect on water retention. Pit No. 4 exhibits a similar network structure, with SOM and TN again emerging as key variables positively linked to VFC and BGB. However, clay content displays a stronger correlation with SWC, implying improved soil stability and water-holding capacity in this restored area. Unlike Pit No. 5, the influence of BD is more subdued, indicating lesser soil compaction and enhanced restoration outcomes. In Pit No. 2, the relationships between soil properties and

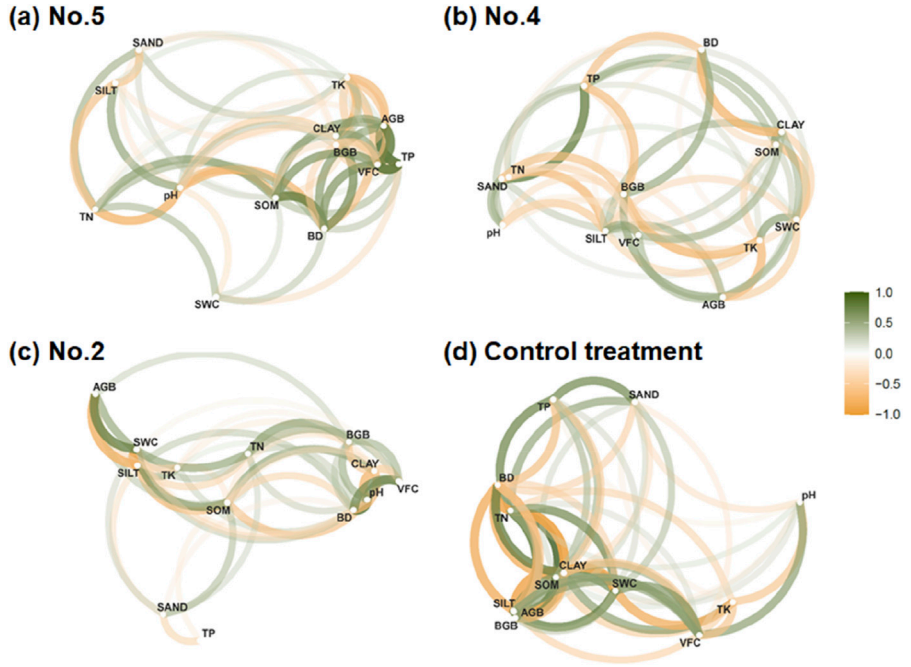

FIGURE 8
Network correlation analysis of soil physicochemical properties and vegetation attributes in restored mining areas and control treatment. **(A)** No.5. **(B)** No.4. **(C)** No.2. **(D)** Control treatment.

vegetation attributes are less pronounced. While SOM and SWC are still positively correlated with VFC and BGB, the overall network connectivity is weaker, as reflected in the thinner lines. Sand content remains negatively correlated with SWC, and the weaker centrality of SOM and TN highlights the limited soil fertility and restoration progress in this area. The control treatment (Figure 8D) reveals the most interconnected network, where SOM, TN, and SWC act as critical hubs positively influencing vegetation attributes such as aboveground biomass (AGB), BGB, and VFC. The strong positive correlation between clay content and SWC highlights the importance of soil texture in maintaining ecosystem resilience. In contrast, BD exhibits consistent negative correlations with SOM and TN, further corroborating its role as a limiting factor for soil and vegetation quality. The network correlation analysis underscores the pivotal role of SOM, TN, and SWC in supporting vegetation recovery and ecological stability across the restored areas. The control treatment serves as a benchmark, demonstrating the optimal balance between soil properties and vegetation attributes. Among the restored pits, Pit No. 5 exhibits the most promising restoration outcomes, followed by Pit No. 4, while Pit No. 2 requires additional interventions to enhance its soil and vegetation recovery.

3.6 Correlation analysis of soil physicochemical properties and vegetation attributes

To further understand the interactions between soil physicochemical properties and vegetation recovery in the restored mining areas, a correlation matrix was constructed (Figure 9). The analysis highlights key relationships among soil properties—such as pH, total nitrogen (TN), soil organic matter (SOM), and soil texture components (sand, silt, clay)—and vegetation attributes, including aboveground biomass (AGB), belowground biomass (BGB), and vegetation fractional cover (VFC).

Figure 9 illustrates a strong positive correlation between SOM and TN ($r = 0.93$) and between SOM and soil water content (SWC) ($r = 0.91$), indicating that soils with higher organic matter content have better nitrogen levels and water retention capacity. Similarly, SWC positively correlates with both BGB ($r = 0.89$) and VFC ($r = 0.76$), suggesting that enhanced soil moisture availability plays a critical role in promoting root biomass accumulation and vegetation coverage. The analysis also identifies a notable negative correlation between bulk density (BD) and SOM ($r = -0.50$), as well as BD and SWC ($r = -0.41$), underscoring the adverse effects of soil compaction on organic matter accumulation and water retention. Furthermore, the proportions of sand, silt, and clay show distinct relationships with soil nutrient dynamics and vegetation growth. For example, clay content positively correlates with SWC ($r = 0.64$), while sand content exhibits a negative correlation with TN ($r = -0.77$), indicating that finer soil textures contribute to improved nutrient retention and water availability. Vegetation attributes also reveal significant correlations with soil properties. AGB and BGB are strongly associated with TN ($r = 0.83$ and $r = 0.86$, respectively) and SOM ($r = 0.86$ and $r = 0.89$, respectively). These findings emphasize the importance of nutrient-rich soils for vegetation recovery. Additionally, VFC correlates positively with SOM ($r = 0.77$) and SWC ($r = 0.76$), highlighting the influence of soil organic content and moisture on vegetation coverage and ecosystem restoration.

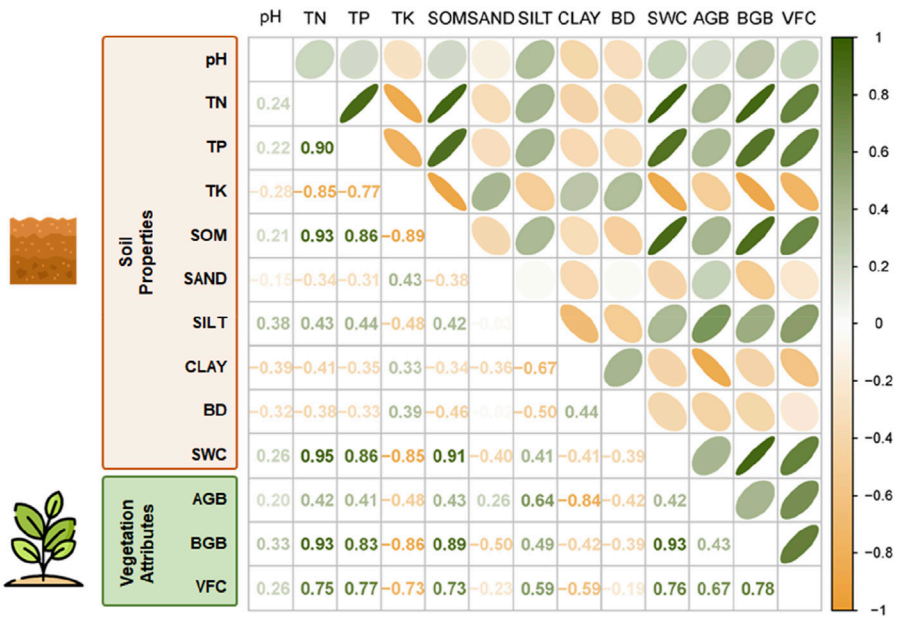

FIGURE 9
Correlation matrix of soil physicochemical properties and vegetation attributes in the restored mining areas.

4 Discussion

4.1 Vegetation coverage and evolution trends

The overall trend of vegetation coverage in the Jiangcang mining area showed a significant recovery after the second phase of restoration. The vegetation coverage of Pits No. 4 and No. 5 has increased from 50% to approximately 80%,indicating that restoration measures, such as soil reconstruction and mixed seeding of native species, were effective (Wang et al., 2018; van der Bauwhede et al., 2024). However, the comparison with the background area suggests that although vegetation recovery was considerable, it did not fully reach natural levels, especially in the initial years, which has also been reported in other high-altitude restoration projects (Sole et al., 2023; Lu et al., 2024). The increased vegetation coverage can be attributed to the use of native species adapted to the harsh environment, which has been shown to promote ecosystem resilience (Chazdon, 2008; Chaturvedi and Singh, 2017).

The differences in vegetation coverage trends between Pits No. 4, No. 5, and the south waste dump of Pit No. 2 highlight the importance of the restoration methods used. Traditional restoration measures like those in Pit No. 2 often yield limited long-term improvements, while advanced soil reconstruction techniques, including organic amendments, are more effective (Macdonald et al., 2015; He et al., 2024). These findings are consistent with results from similar restoration efforts in North America, where modernized techniques have proven to provide better revegetation outcomes (Petrova et al., 2022). The use of soil amendments, particularly sheep manure, has demonstrated a positive impact on soil moisture retention and nutrient cycling in the restored areas (Asensio et al., 2014). Sheep manure not only provides essential organic matter but also enhances soil structure, which improves water infiltration and retention, particularly in high-altitude environments where precipitation is limited (Aronson et al., 1993; Lim et al., 2022). Additionally, the gradual release of nutrients such as nitrogen, phosphorus, and potassium from manure supports microbial activity and promotes plant growth, thereby strengthening the soil-plant interactions (Lu et al., 2024). These processes collectively accelerate vegetation establishment and improve overall ecosystem stability, as observed in the increased vegetation coverage and biomass in our study. Such findings align with previous research highlighting the role of organic amendments in improving soil water dynamics and nutrient availability, which are critical for restoration success in degraded alpine ecosystems (Moreno-de las Heras, 2009; Liu et al., 2022).

The temporal trend of vegetation coverage peaking in 2021 suggests that climate factors, such as a shorter freeze period, contributed to an extended growing season and thereby enhanced recovery (Li et al., 2013; Pedrol et al., 2014). The interplay between restoration practices and climatic conditions is critical, as evidenced by similar studies in alpine regions in Europe (Madejon et al., 2021), which indicate that adaptive management strategies must consider both the restoration methods and the natural climatic variability to achieve optimal outcomes.

4.2 Plant community characteristics and diversity

The plant community characteristics, including biomass, crown width, and abundance, showed positive responses to soil reconstruction in Pits No. 4 and No. 5, aligning with studies showing that organic amendments significantly enhance plant

productivity in restored ecosystems (Asensio et al., 2013; Yang et al., 2019). Aboveground biomass was notably higher in these pits compared to earlier restoration efforts, though still lower than that of the natural background area (Bardgett et al., 2005). This is in line with global restoration practices where aboveground biomass is often a primary indicator of successful recovery (Bullock et al., 2011; Rocha et al., 2021). Belowground biomass is essential for enhancing soil stability, water retention, and nutrient cycling, forming the foundation for sustainable vegetation recovery. Previous studies have shown that organic amendments, such as sheep manure, can improve soil microbial diversity and activity, which are critical for underground biomass development and overall soil health in high-altitude mining areas (Soria et al., 2021; Zhong et al., 2021).

The diversity indices, such as Shannon diversity and Margalef richness, were lower in the restored platform areas compared to the background, reflecting the challenges of restoring full biodiversity within a short period (Cardenas-Aguiar et al., 2022; He et al., 2024). The dominance of Poaceae species in these areas has been found to suppress the establishment of other species, as observed in previous studies of restored mining sites in Australia and South Africa (Cardenas-Aguiar et al., 2022). Conversely, the sunny slope areas showed better diversity due to reduced dominance, which allowed a wider range of species to establish, supporting findings from similar studies in North America (Courtney et al., 2011; Worlanyo and Jiangfeng, 2021).

Belowground biomass in the restored areas remained significantly lower than in the natural background, suggesting that root recovery takes longer and requires a sustained accumulation of organic matter (Feng et al., 2023; Williams and Thomas, 2023). This trend has also been observed in long-term studies of alpine restoration in Europe and North America, where belowground recovery often lags behind aboveground regeneration (Bardgett et al., 2005; Kim et al., 2020). The importance of belowground processes for the long-term success of ecosystem restoration cannot be overstated, as they are crucial for nutrient cycling and soil stabilization (Pardo et al., 2014).

4.3 Community similarity and implications for ecological restoration

The similarity between the restored sunny slope areas and the natural alpine meadow suggests that these areas are more conducive to returning to a natural community structure (Reid and Naeth, 2005b; Wong, 2003). Similar outcomes have been reported in high-altitude restoration in the Rocky Mountains, where restored communities on slopes showed greater similarity to natural vegetation compared to flat, disturbed areas (Zheng et al., 2023). This indicates that the microenvironmental conditions of slopes, along with less intense competition from dominant species, can facilitate the natural re-establishment of diverse plant communities (Petrova et al., 2022; Zhang et al., 2023).

The lower similarity between the platform areas and natural grassland highlights the challenge of restoring these areas, particularly due to the dominance of pioneer species such as grasses (Pardo et al., 2014; Zhou et al., 2015). Similar results have been found in mining restoration projects in Chile, where dominant grasses inhibited the establishment of other species, reducing overall community similarity to natural areas (Aronson et al., 1993; Carabassa et al., 2020). Therefore, efforts should focus on reducing dominance through mixed seeding strategies and diversified organic amendments, as supported by research from the Mediterranean region (Cardenas-Aguiar et al., 2022). The effectiveness of restoration measures in high-altitude mining areas, such as those on the Qinghai-Tibet Plateau, aligns with findings from similar environments worldwide. For instance, studies in the Andes and the Rocky Mountains highlight that organic soil amendments, including livestock manure and biochar, significantly enhance soil fertility and facilitate vegetation recovery under harsh alpine climates (Scotton, 2021; Zhang et al., 2023). In such regions, the short growing season and limited soil nutrient availability are critical constraints for restoration success. Compared to the humid, temperate climates where restoration can rely on natural seed banks and rapid organic matter accumulation (Jones et al., 2018), high-altitude regions often require tailored interventions like soil reconstruction, organic amendments, and native species seeding to achieve long-term recovery (Zhong et al., 2021). Furthermore, restoration strategies must account for varying precipitation patterns, as areas with arid conditions may demand additional irrigation measures to support seed germination and root establishment (Zhang et al., 2023). This comparison highlights the importance of integrating climatic conditions into the design of restoration measures to optimize their effectiveness across diverse high-altitude ecosystems.

Overall, the vegetation coverage and community characteristics in the Jiangcang mining area indicate substantial recovery potential using soil reconstruction and ecological restoration. However, gaps in belowground biomass and lower community similarity in some restored areas suggest a need for adaptive management. This includes monitoring species composition, adjusting soil amendment practices, and supplementary seeding with a focus on underrepresented species, aligning with global best practices for restoring resilience and stability in degraded ecosystems (Chazdon, 2008; Feng et al., 2023; Lu et al., 2024).

5 Conclusion

The restoration efforts in the Jiangcang mining area on the Qinghai-Tibet Plateau have demonstrated important lessons and outcomes for ecological restoration in high-altitude and fragile ecosystems. The use of sheep manure as an organic amendment not only enhanced soil fertility but also contributed to increased biodiversity by introducing wild grass seeds, thereby addressing the shortage of suitable native grass species in alpine regions. This approach was crucial in improving species diversity and promoting natural regeneration, which are often challenging in such harsh environments.

A comparative analysis of the two phases of mining area restoration revealed that traditional revegetation techniques without soil reconstruction yielded limited success, whereas the second phase, which included soil reconstruction and amendments, significantly improved the stability and fertility of the substrate. This resulted in higher vegetation coverage and increased ecosystem stability, indicating the effectiveness of

enhanced restoration measures. The observed improvements in vegetation coverage and ecological conditions, without signs of degradation, further suggest that the restored mining area is on a favorable trajectory towards ecological recovery.

Although aboveground biomass showed notable recovery, approaching the levels observed in natural background areas, belowground biomass still lagged significantly behind. This indicates that while aboveground recovery can be relatively rapid, belowground biomass, which plays a crucial role in nutrient cycling and long-term ecosystem stability, requires a longer time to accumulate. The dominance of pioneer species in the restored platform areas, particularly Poaceae, was found to inhibit the development of a diverse plant community. In contrast, the slopes of the waste rock dump showed higher community similarity to natural alpine meadows, suggesting that reduced dominance of pioneer species can create opportunities for more diverse species to establish, leading to a more stable and natural community structure over time.

In summary, this study demonstrates that adaptive restoration techniques, particularly soil reconstruction and organic amendments, are essential for promoting both aboveground and belowground ecosystem recovery in high-altitude mining areas. The results underscore the need for restoration strategies that enhance soil health, manage pioneer species dominance, and support biodiversity. Moving forward, continuous long-term monitoring and adaptive management are critical to sustaining the observed ecological improvements and guiding future restoration efforts in similarly fragile ecosystems worldwide.

Data availability statement

The original contributions presented in the study are included in the article/Supplementary Material, further inquiries can be directed to the corresponding author.

Author contributions

SF: Formal Analysis, Methodology, Visualization, Writing–original draft, Writing–review and editing. ZL: Funding acquisition, Investigation, Writing–original draft, Writing–review and editing. CZ: Software, Writing–original draft, Writing–review and editing. RQ: Conceptualization, Writing–original draft, Writing–review and editing. LY: Data curation, Resources, Writing–original draft, Writing–review and editing.

Funding

The author(s) declare that no financial support was received for the research, authorship, and/or publication of this article.

Conflict of interest

Authors SF, ZL, CZ, and RQ were employed by China Geo-Engineering Corporation.

The remaining author declares that the research was conducted in the absence of any commercial or financial relationships that could be construed as a potential conflict of interest.

Generative AI statement

The author(s) declare that no Generative AI was used in the creation of this manuscript.

Publisher's note

Supplementary material

The Supplementary Material for this article can be found online at: https://www.frontiersin.org/articles/10.3389/fenvs.2024.1538243/full#supplementary-material

References

Aronson, J., Floret, C., Le Floc'h, E., Ovalle, C., and Pontanier, R. (1993). Restoration and rehabilitation of degraded ecosystems in arid and semi-arid regions: a view from the South. *Restor. Ecol.* 1 (1), 8–17. doi:10.1111/j.1526-100X.1993.tb00004.x

Asensio, V., Vega, F. A., Andrade, M. L., and Covelo, E. F. (2013). Tree vegetation and waste amendments to improve the physical condition of copper mine soils. *CHEMOSPHERE* 90, 603–610. doi:10.1016/j.chemosphere.2012.08.050

Asensio, V., Vega, F. A., and Covelo, E. F. (2014). Effect of soil reclamation process on soil C fractions. *CHEMOSPHERE* 95, 511–518. doi:10.1016/j.chemosphere.2013.09.108

Barberis, D., Lombardi, G., Enri, S. R., Pittarello, M., Viglietti, D., Freppaz, M., et al. (2023). Nitrogen fertilizer enhances vegetation establishment of a high-altitude machine-graded ski slope. *Restor. Ecol.* 31. doi:10.1111/rec.13777

Bardgett, R. D., Bowman, W. D., Kaufmann, R., and Schmidt, S. K. (2005). A temporal approach to linking aboveground and belowground ecology. *TRENDS Ecol. and Evol.* 20 (11), 634–641. doi:10.1016/j.tree.2005.08.005

Bullock, J. M., Aronson, J., Newton, A. C., Pywell, R. F., and Rey-Benayas, J. M. (2011). Restoration of ecosystem services and biodiversity: conflicts and opportunities. *TRENDS Ecol. and Evol.* 26 (10), 541–549. doi:10.1016/j.tree.2011.06.011

Carabassa, V., Domene, X., Diaz, E., and Alcaniz, J. M. (2020). Mid-term effects on ecosystem services of quarry restoration with Technosols under Mediterranean conditions: 10-year impacts on soil organic carbon and vegetation development. *Restor. Ecol.* 28, 960–970. doi:10.1111/rec.13072

Cardenas-Aguiar, E., Mendez, A., Paz-Ferreiro, J., and Gasco, G. (2022). The effects of rabbit manure-derived biochar on soil health and quality attributes of two mine tailings. *SUSTAINABILITY* 14, 1866. doi:10.3390/su14031866

Chaturvedi, R. K., and Singh, J. S. (2017). Diversity of ecosystem types in India: a review. *Proc. Indian Natl. Sci. Acad.* 83, 789–844. doi:10.16943/ptinsa/2017/41287

Chazdon, R. L. (2008). Beyond deforestation: restoring forests and ecosystem services on degraded lands. *SCIENCE* 320, 1458–1460. doi:10.1126/science.1155365

Cheng, H., Zhou, X., Dong, R., Wang, X., Liu, G., and Li, Q. (2022). Priming of soil organic carbon mineralization and its temperature sensitivity in response to vegetation restoration in a karst area of Southwest China. *Sci. TOTAL Environ.* 851, 158400. doi:10.1016/j.scitotenv.2022.158400

Courtney, R., Keith, A. M., and Harrington, T. (2011). Nematode assemblages in bauxite residue with different restoration histories. *Restor. Ecol.* 19, 758–764. doi:10.1111/j.1526-100X.2010.00734.x

Cross, A. T., and Lambers, H. (2017). Young calcareous soil chronosequences as a model for ecological restoration on alkaline mine tailings. *Sci. TOTAL Environ.* 607, 168–175. doi:10.1016/j.scitotenv.2017.07.005

Feng, T., Qi, Y., Zhang, Y., Fan, D., Wei, T., Wang, P., et al. (2024). Long-term effects of vegetation restoration and forest management on carbon pools and nutrient storages in northeastern Loess Plateau, China. *J. Environ. Manag.* 354, 120296. doi:10.1016/j.jenvman.2024.120296

Feng, T., Wei, T., Keesstra, S. D., Zhang, J., Bi, H., Wang, R., et al. (2023). Long-term effects of vegetation restoration on hydrological regulation functions and the implications to afforestation on the Loess Plateau. *Agric. For. METEOROLOGY* 330, 109313. doi:10.1016/j.agrformet.2023.109313

Figueiredo, M. A., Messias, M. C. T. B., Leite, M. G. P., and Kozovits, A. R. (2024). Topsoil volume optimization in the restoration of post-mined areas. *Restor. Ecol.* 32. doi:10.1111/rec.14222

He, Y., Tian, Z., Gu, Z., Wu, B., and Liang, Y. (2024). Controlling soil erosion of tailings from rare earth mines with paspalum wettsteinii and soil amendments. *LAND Degrad. and Dev.* doi:10.1002/ldr.5313

Heiskanen, J., Ruhanen, H., and Hagner, M. (2022). Effects of compost, biochar and ash mixed in till soil cover of mine tailings on plant growth and bioaccumulation of elements: a growing test in a greenhouse. *HELIYON* 8, e08838. doi:10.1016/j.heliyon.2022.e08838

Hu, Y.-L., Mgelwa, A. S., Singh, A. N., and Zeng, D.-H. (2018). Differential responses of the soil nutrient status, biomass production, and nutrient uptake for three plant species to organic amendments of placer gold mine-tailing soils. *LAND Degrad. and Dev.* 29, 2836–2845. doi:10.1002/ldr.3002

Jambhulkar, H. P., and Kumar, M. S. (2019). Eco-restoration approach for mine spoil overburden dump through biotechnological route. *Environ. Monit. Assess.* 191, 772. doi:10.1007/s10661-019-7873-6

Kim, M.-S., Min, H.-G., and Kim, J.-G. (2020). Integrating amendment and liquid fertilizer for aided-phytostabilization and its impacts on soil microbiological properties in arsenic-contaminated soil. *Appl. SCIENCES-BASEL* 10, 3985. doi:10.3390/app10113985

Li, S., Di, X., Wu, D., and Zhang, J. (2013). Effects of sewage sludge and nitrogen fertilizer on herbage growth and soil fertility improvement in restoration of the abandoned opencast mining areas in Shanxi, China. *Environ. EARTH Sci.* 70, 3323–3333. doi:10.1007/s12665-013-2397-9

Lim, B.-S., Kim, A.-R., Seol, J., Oh, W.-S., An, J.-H., Lim, C.-H., et al. (2022). Effects of soil amelioration and vegetation introduction on the restoration of abandoned coal mine spoils in South Korea. *FORESTS* 13, 483. doi:10.3390/f13030483

Liu, J., Zhang, S., Li, E., Zhu, Y., Cai, H., Xia, S., et al. (2022). Effects of cubic ecological restoration of mining wasteland and the preferred restoration scheme. *Sci. TOTAL Environ.* 851, 158155. doi:10.1016/j.scitotenv.2022.158155

Lu, Z., Yu, C., Liu, H., Zhang, J., Zhang, Y., Wang, J., et al. (2024). Application of new polymer soil amendment in ecological restoration of high-steep Rocky slope in seasonally frozen soil areas. *POLYMERS* 16, 1821. doi:10.3390/polym16131821

Luna, L., Vignozzi, N., Miralles, I., and Sole-Benet, A. (2018). Organic amendments and mulches modify soil porosity and infiltration in semiarid mine soils. *LAND Degrad. and Dev.* 29, 1019–1030. doi:10.1002/ldr.2830

Lupton, M. K., Rojas, C., Drohan, P., and Bruns, M. A. (2013). Vegetation and soil development in compost-amended iron oxide precipitates at a 50-year-old acid mine drainage barrens. *Restor. Ecol.* 21, 320–328. doi:10.1111/j.1526-100X.2012.00902.x

Macdonald, S. E., Landhaeusser, S. M., Skousen, J., Franklin, J., Frouz, J., Hall, S., et al. (2015). Forest restoration following surface mining disturbance: challenges and solutions. *NEW For.* 46, 703–732. doi:10.1007/s11056-015-9506-4

Madejon, P., Caro-Moreno, D., Navarro-Fernandez, C. M., Rossini-Oliva, S., and Maranon, T. (2021). Rehabilitation of waste rock piles: impact of acid drainage on potential toxicity by trace elements in plants and soil. *J. Environ. Manag.* 280, 111848. doi:10.1016/j.jenvman.2020.111848

Misebo, A. M., Pietrzykowski, M., and Wos, B. (2022). Soil carbon sequestration in novel ecosystems at post-mine sites-A new insight into the determination of key factors in the restoration of terrestrial ecosystems. *FORESTS* 13, 63. doi:10.3390/f13010063

Moreno-de las Heras, M. (2009). Development of soil physical structure and biological functionality in mining spoils affected by soil erosion in a Mediterranean-Continental environment. *GEODERMA* 149, 249–256. doi:10.1016/j.geoderma.2008.12.003

Naeth, M. A., and Wilkinson, S. R. (2014). Establishment of restoration trajectories for upland tundra communities on diamond mine wastes in the Canadian arctic. *Restor. Ecol.* 22, 534–543. doi:10.1111/rec.12106

Pardo, T., Martinez-Fernandez, D., Clemente, R., Walker, D. J., and Bernal, M. P. (2014). The use of olive-mill waste compost to promote the plant vegetation cover in a trace-element-contaminated soil. *Environ. Sci. Pollut. Res.* 21, 1029–1038. doi:10.1007/s11356-013-1988-z

Pedrol, N., Souza-Alonso, P., Puig, C. G., Gonzalez, L., Covelo, E. F., Asensio, V., et al. (2014). Improving soil fertility to support grass-legume revegetation on lignite mine spoils. *Commun. SOIL Sci. PLANT ANALYSIS* 45, 1565–1582. doi:10.1080/00103624.2013.875203

Penalver-Alcala, A., Alvarez-Rogel, J., Peixoto, S., Silva, I., Silva, A. R. R., and Gonzalez-Alcaraz, M. N. (2021). The relationships between functional and physicochemical soil parameters in metal(loid) mine tailings from Mediterranean semiarid areas support the value of spontaneous vegetation colonization for phytomanagement. *Ecol. Eng.* 168, 106293. doi:10.1016/j.ecoleng.2021.106293

Petrova, T. A., Rudzisha, E., Alekseenko, A. V., Bech, J., and Pashkevich, M. A. (2022). Rehabilitation of disturbed lands with industrial wastewater sludge. *MINERALS* 12, 376. doi:10.3390/min12030376

Reid, N., and Naeth, M. (2005a). Establishment of a vegetation cover on tundra kimberlite mine tailings: 1. A greenhouse study. *Restor. Ecol.* 13, 594–601. doi:10.1111/j.1526-100X.2005.00076.x

Reid, N., and Naeth, M. (2005b). Establishment of a vegetation cover on tundra kimberlite mine tailings: 2. A field study. *Restor. Ecol.* 13, 602–608. doi:10.1111/j.1526-100X.2005.00077.x

Rocha Martins, W. B., Schwartz, G., Ribeiro, S. S., Ferreira, G. C., Barbosa, R. de S., de Paula, M. T., et al. (2021). Ecosystem restoration after bauxite mining: favorable indicators for Technosols construction and soil management using liming and subsoiling. *NEW For.* 52, 971–994. doi:10.1007/s11056-021-09834-5

Rothman, S. E., Cole, C. A., Bruns, M. A., and Hall, M. (2021). The influence of soil amendments on a native wildflower seed mix in surface mine restoration. *Restor. Ecol.* 29. doi:10.1111/rec.13440

Scotton, M. (2021). Grassland restoration at a graded ski slope: effects of propagation material and fertilisation on plant cover and vegetation. *AGRICULTURE-BASEL* 11, 381. doi:10.3390/agriculture11050381

Sole, P., Ferrer, D., Raya, I., Pous, M., Gonzalez, R., Maranon-Jimenez, S., et al. (2023). Physical and chemical properties of limestone quarry technosols used in the restoration of mediterranean habitats. *LAND* 12, 1730. doi:10.3390/land12091730

Soria, R., Rodriguez-Berbel, N., Ortega, R., Lucas-Borja, M. E., and Miralles, I. (2021). Soil amendments from recycled waste differently affect CO_2 soil emissions in restored mining soils under semiarid conditions. *J. Environ. Manag.* 294, 112894. doi:10.1016/j.jenvman.2021.112894

van der Bauwhede, R., Troonbeeckx, J., Serbest, I., Moens, C., Desie, E., Katzensteiner, K., et al. (2024). Restoration rocks: the long-term impact of rock dust application on soil, tree foliar nutrition, tree radial growth, and understory biodiversity in Norway spruce forest stands. *For. Ecol. Manag.* 568, 122109. doi:10.1016/j.foreco.2024.122109

Wang, J., Luo, X., Zhang, Y., Huang, Y., Rajendran, M., and Xue, S. (2018). Plant species diversity for vegetation restoration in manganese tailing wasteland. *Environ. Sci. Pollut. Res.* 25, 24101–24110. doi:10.1007/s11356-018-2275-9

Williams, J. M., and Thomas, S. C. (2023). Effects of high-carbon wood ash biochar on volunteer vegetation establishment and community composition on metal mine tailings. *Restor. Ecol.* 31. doi:10.1111/rec.13861

Wong, M. (2003). Ecological restoration of mine degraded soils, with emphasis on metal contaminated soils. *CHEMOSPHERE* 50, 775–780. doi:10.1016/S0045-6535(02)00232-1

Worlanyo, A. S., and Jiangfeng, L. (2021). Evaluating the environmental and economic impact of mining for post-mined land restoration and land-use: a review. *J. Environ. Manag.* 279, 111623. doi:10.1016/j.jenvman.2020.111623

Yang, S., Liao, B., Xiao, R., and Li, J. (2019). Effects of amendments on soil microbial diversity, enzyme activity and nutrient accumulation after assisted phytostabilization of an extremely acidic metalliferous mine soil. *Appl. SCIENCES-BASEL* 9, 1552. doi:10.3390/app9081552

Yang, S., Liao, B., Yang, Z., Chai, L., and Li, J. (2016). Revegetation of extremely acid mine soils based on aided phytostabilization: a case study from southern China. *Sci. TOTAL Environ.* 562, 427–434. doi:10.1016/j.scitotenv.2016.03.208

Zhang, Y., Feng, T., Wang, L., Wang, X., Wei, T., and Wang, P. (2023). Effects of long-term vegetation restoration on soil physicochemical properties mainly achieved by the coupling contributions of biological synusiae to the Loess Plateau. *Ecol. Indic.* 152, 110353. doi:10.1016/j.ecolind.2023.110353

Zheng, T., Zeng, H., Zhang, X., Luo, J., Chen, X., Zhao, X., et al. (2023). Differential responses of soil community to reclamation with legumes versus grasses after an application of blended amendments in mining-disturbed soils. *J. Clean. Prod.* 418, 138113. doi:10.1016/j.jclepro.2023.138113

Zhong, H., Lambers, H., Wong, W. S., Dixon, K. W., Stevens, J. C., and Cross, A. T. (2021). Initiating pedogenesis of magnetite tailings using Lupinus angustifolius (narrow-leaf lupin) as an ecological engineer to promote native plant establishment. *Sci. TOTAL Environ.* 788, 147622. doi:10.1016/j.scitotenv.2021.147622

Zhou, L., Li, Z., Liu, W., Liu, S., Zhang, L., Zhong, L., et al. (2015). Restoration of rare earth mine areas: organic amendments and phytoremediation. *Environ. Sci. Pollut. Res.* 22, 17151–17160. doi:10.1007/s11356-015-4875-y

frontiers | Frontiers in Environmental Science

TYPE Original Research
PUBLISHED 22 April 2025
DOI 10.3389/fenvs.2025.1554157

OPEN ACCESS

EDITED BY
Tianjiao Feng,
Beijing Forestry University, China

REVIEWED BY
Weifeng Gong,
Qufu Normal University, China
Yaohui Liu,
Shandong Jianzhu University, China

*CORRESPONDENCE
Jianxun Zhang,
zhangjianxun@qhu.edu.cn
Runhao Zhang,
505555216@qq.com

RECEIVED 01 January 2025
ACCEPTED 07 April 2025
PUBLISHED 22 April 2025

CITATION
Jia H, Wang T, Liang P, Zhang J and Zhang R (2025) Critical evaluation on the ecosystem service levels of provincial capital cities along the Yellow River Basin.
Front. Environ. Sci. 13:1554157.
doi: 10.3389/fenvs.2025.1554157

Critical evaluation on the ecosystem service levels of provincial capital cities along the Yellow River Basin

Haifa Jia[1,2,3], Tianyou Wang[1,2,3], Pengyu Liang[1,2,3], Jianxun Zhang[1,2,3]* and Runhao Zhang[4]*

[1]School of Civil Engineering and Water Resources, Qinghai University, Xining, China, [2]Key Laboratory of Energy-Saving Building Materials and Engineering Safety, Xining, Qinghai, China, [3]Laboratory of Ecological Protection and High Quality Development in the Upper Yellow River, Xining, Qinghai, China, [4]School of Architecture and Urban Planning, Beijing University of Technology, Beijing, China

A comprehensive understanding of the spatiotemporal changes and influencing factors of ecosystem service levels is crucial for regional sustainable development and coordination. The Yellow River Basin faces challenges such as ecological degradation due to uneven regional burdens. This study constructed an ecosystem service evaluation framework based on five dimensions. A combined weighting model was used to assess the ecosystem service levels, spatiotemporal characteristics, and influencing factors of nine provincial capital cities in the Yellow River Basin from 2010 to 2020. The results indicated that: (1) There were notable differences in ecosystem service levels among cities in the Yellow River Basin. The first category of cities, rich in tourism resources, exhibited high ecosystem service levels. The second category of cities, currently undergoing industrial green transformation, urgently needed to achieve a balance between economic development and ecological protection. The third category of cities faced challenges due to poor socioeconomic conditions and limited resources. (2) Resource and energy use, Ecological environmental protection, and Socioeconomic development were the most significant dimensions influencing ecosystem service levels. (3) Indicators such as *per capita* disposable income, *per capita* road area, urban green coverage, electricity consumption per unit of GDP, and the number of higher education institutions had a considerable impact on ecosystem service levels. This study suggests optimizing the energy structure, promoting clean energy development, supporting industrial green transformation, and strengthening infrastructure to enhance and protect ecosystem services in the Yellow River Basin.

KEYWORDS

ecosystem services, sustainable development, regional coordination, mechanisms of influence, Yellow River Basin

1 Introduction

For a long time, unequal regional development has been a key factor limiting the sustainable development of the river basin (Zhang et al., 2023). Known for its abundant natural resources, strategic location, and fertile soil, the Yellow River Basin (YRB) is a key agricultural production base in China (Zhang et al., 2024), providing significant ecosystem services. However, the region's geographical expanse and distinct natural geographic

features result in ecological vulnerability and imbalanced regional pressures, thereby causing environmental deterioration and pollution (Zhang et al., 2022). In China's strategic planning for the new era, "promoting green development and fostering harmony between humans and nature" has been established as the core mission of ecological civilization construction. The "Yellow River Protection Law of the People's Republic of China," which came into effect in 2023, underscores the importance of the YRB as a critical ecological barrier for the nation. It requires cities within the basin prioritize coordinated ecological restoration and protect the environmental lifeline. With robust national policy support, ecological conservation restoration in the basin has made steady progress, significantly mitigating several key challenges. Nevertheless, ecological protection remains a long-term and formidable task. Coordinating efforts across cities within the basin to enhance ecosystem service levels is a critical component of China's national strategy and an essential practical measure for achieving ecological conservation goals.

Scholars have extensively investigated ecosystem services and developed various assessment systems and quantitative methods to measure sustainable development. These include the Human Development Index (HDI) (Bhanojirao, 1991; Lind, 2019), Environmental Sustainability Index (ESI) (Env ironmental Sustainability Index, 2002; Bui et al., 2019), and Environmental Performance Index (EPI) (Emerson et al., 2012; Pinar, 2022), among others. In evaluating urban ecosystem service functions, a range of methods and indicator systems have been employed, with common approaches including physical measurements (Dai et al., 2021), value-based evaluations (De Groot et al., 2010; Zhou et al., 2020), and emergy analysis techniques (Odum, 1996; Guan et al., 2022). Indicator systems typically encompass aspects such as biodiversity, air quality, water resources, soil quality, and urban green spaces. These methods and indicator systems provide robust tools for a comprehensive evaluation of urban ecosystem service functions. For example, Costanza et al. proposed a framework for assessing global ecosystem service values, which has served as a reference for evaluating urban ecosystem services (Costanza et al., 1997). Subsequently, more scholars, integrating the characteristics of urban ecosystems, have developed assessment systems suited for evaluating urban ecosystem service functions. Empirical research has demonstrated that the level of urban ecosystem service functions is closely related to factors such as city size, urban planning, and population density. Daily emphasized that rational urban planning and management can significantly enhance the level of urban ecosystem services (Daily, 1997).

In terms of the research scope, some scholars have conducted comprehensive evaluations at a national level (Yuan et al., 2024), analyzing internal regional differences, while others have focused on provinces (Yang et al., 2024) or cities (Kim et al., 2021), evaluating their ecosystem service conditions. Additionally, some studies have analyzed and evaluated regional ecosystem services in areas such as the Yangtze River Economic Belt (Xie et al., 2024), the Beijing-Tianjin-Hebei Region (Zhai et al., 2024), and urban agglomerations (Peng et al., 2021). Regarding the methods for assigning weights to indicators, scholars have made significant innovations, including the Delphi method (Jo et al., 2024), the entropy weight method (Amirnejad et al., 2024; Chen et al., 2024), the analytic hierarchy process (Ji et al., 2024; Jorge-García and Estruch-Guitart, 2022), fuzzy comprehensive evaluation (Fan and Ma, 2024; Sun et al., 2019), and principal component analysis (Kou et al., 2024; Salata and Grillenzoni, 2021), as well as integrate weighting methods that combine two or more weighting techniques (Chen et al., 2022).

Despite substantial theoretical advancements in measuring ecosystem service levels, several gaps remain: (1) In terms of research areas, studies frequently focus on national, provincial, or urban scales, with linear regions such as railway or canal corridors receiving more attention (Tong et al., 2021; Gao et al., 2019). Few studies have focused on river basins, especially the YRB, as their research scope. (2) In terms of evaluation system construction, much of the focus has been on ecological environment construction (Gómez-Limón et al., 2020), while the impact of ecosystem service levels has been overlooked, leading to incomplete indicator dimensions. (3) There is a lack of interregional comparative studies (Guo et al., 2017), as well as differentiated strategies for addressing regional disparities.

This study constructed and employed an ecosystem service evaluation indicator system specifically for the provincial capitals along the Yellow River. It assessed the level of ecosystem services and their influencing factors from 2010 to 2020. The findings aimed to provide valuable insights into the development of ecosystem service systems and to promote high-quality development within the YRB.

2 Study area and data sources

2.1 Study area

The Yellow River in northern China is the country's second-longest river, extending approximately 5,464 km and covering a watershed area of about 795,000 square kilometers (Cui et al., 2022a). This study focuses on the provincial capitals along the Yellow River, which serve as major urban centers within the basin. The river traverses nine provinces and autonomous regions: Qinghai, Sichuan, Gansu, Ningxia, Inner Mongolia, Shanxi, Shaanxi, Henan, and Shandong. These areas are endowed with abundant natural resources, including coal, oil, natural gas, rare earth elements, non-ferrous metals, and other minerals. Additionally, they also possess abundant biological resources such as forests, grasslands, wildlife, and diverse plant species. Despite these advantages, the basin faces pressing environmental issues like soil erosion, water pollution, water scarcity, and ecological degradation (Lu et al., 2022). In response, the Chinese government has initiated efforts to mitigate these challenges, including enhancing soil and water conservation, advancing ecological restoration projects, and promoting sustainable water use and protection (Yurui et al., 2021).

This study examines nine provincial capital cities along the Yellow River as research subjects (Figure 1), which serve as the primary urban centers within the basin. As key administrative and economic hubs, these cities are prioritized for ecological governance in the Yellow River Basin. Spanning the upper, middle, and lower reaches of the Yellow River, these cities encompass a diverse array of ecosystems from alpine regions to alluvial plains. The dynamics of their ecosystem services provide clear evidence of the spatial heterogeneity and pressures experienced across the entire basin.

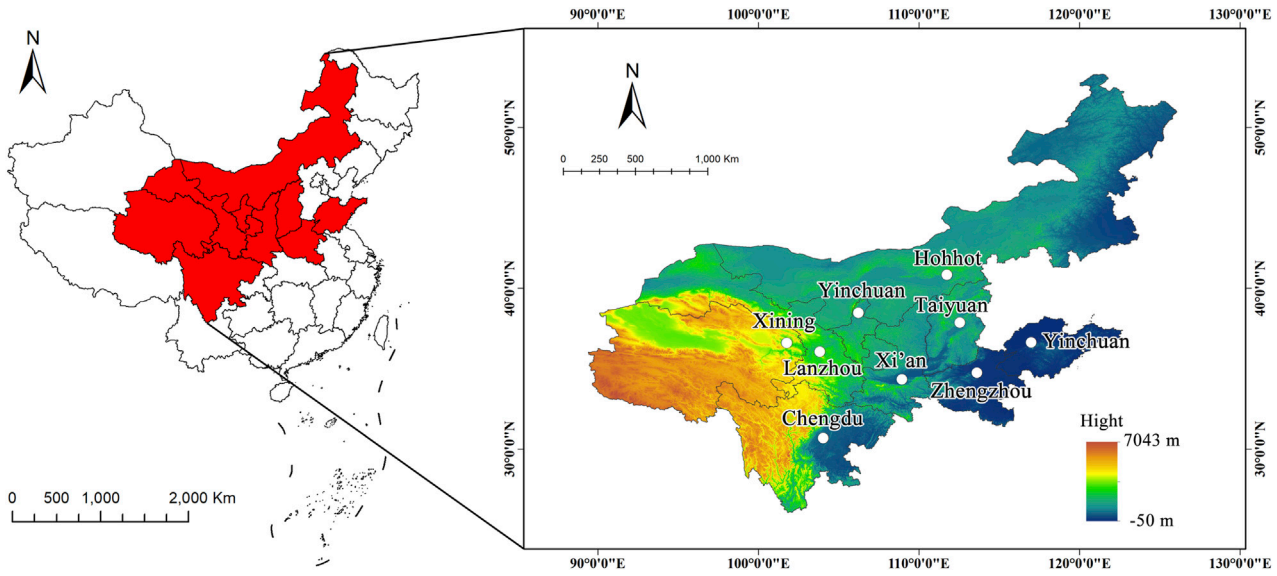

FIGURE 1
Overview of the Study area. This map is based on the standard map with the approval number GS (2024) 0650 downloaded from the national platform for common geospatial information services (Tianditu), and the base map has not been modified.

2.2 Construction of the indicator system

Adhering to principles of scientific rigor, hierarchy, operational feasibility, comprehensiveness, and purposefulness, we selected indicators based on various frameworks and research, including the Global Biodiversity and Ecosystem Services Assessment Report (Baste et al., 2024) and the 2030 Agenda for Sustainable Development (Schneider et al., 2019). We designed an indicator system to evaluate the ecosystem service development level of the provincial capitals in the YRB across five dimensions: National land space, Socioeconomic development, Resource and energy use, institutional and inputs, and ecological environmental protection.

The indicators are organized into three layers: target, standardized, and indicator layers, as shown in Table 1. This structure establishes a clear hierarchical relationship among the indicators, facilitating an integrated assessment of urban ecosystem service levels.

2.3 Data sources

This study utilized data from 2010 to 2020, primarily sourced from official statistics, provincial and city statistical yearbooks (2011–2021), and city environmental status reports (2011–2021). Calculations were performed to derive certain indicators, including GDP per unit of land, Built-up area as a proportion of urban area, afforestation area as a percentage of the jurisdictional area, and pesticide usage per unit of arable land. Economic indicators such as *per capita* GDP, Engel's coefficient, and the tertiary industry as a proportion of GDP were obtained from provincial and city statistical yearbooks. Environmental indicators such as proportion of days with good air quality, nitrogen oxide emissions per unit GDP and Sulfur dioxide emissions per unit GDP were referenced from each city's environmental status reports. Additional data on area treated for soil and water loss and nature reserves were acquired directly from relevant government departments. For missing data, we employed trend extrapolation methods.

3 Methods

The research approach of this study consists of four main steps: (1) Gather multi-period indicator data for the nine provincial capital cities in the Yellow River Basin across five dimensions: National land space, Socioeconomic development, Resource and energy use, Institutions and inputs, and Ecological environmental protection; (2) Employ a combined weighting model to determine the weights of the indicators and calculate the comprehensive scores for ecosystem service levels; (3) Visualize the ecosystem service levels and conduct cluster analysis to identify spatial-temporal patterns; (4) Utilize a panel data regression model to analyze the influencing factors and test their significance, ultimately identifying the key indicators affecting ecosystem service levels in the Yellow River Basin.

3.1 Indicator weights

To determine the weights of the indicators, both subjective and objective methods were employed. The subjective method depend on the evaluator's expertise and understanding of the subject matter but can be influenced by personal biases (Kokangül et al., 2017). The objective method, specifically the entropy weight method, quantifies the variability and disorder within the data, assigning weights accordingly. This method posits that the less variation an indicator exhibits, the lower its entropy and, consequently, its weight in the evaluation system (Žižović et al., 2020).

To mitigate the limitations of both approaches, we adopted a hybrid method combining hierarchical analysis and entropy

TABLE 1 Urban ecosystem service level evaluation indicator system for the provincial capitals of the YRB.

Target layer	Standardized layer	Indicator layer	Unit	Indicator attributes
Level of ecosystem services	National land space	GDP per unit of land	10,000 yuan/km^2	Positive
		Built-up area as a proportion of urban area	%	Positive
		Number of general higher educational institutions	Count	Positive
		Per capita road area	m^2	Positive
		Housing area *per capita*	m^2	Positive
		Population density	People/km^2	Negative
		Afforestation area as a percentage of jurisdictional area	%	Positive
		Per capita green area of parks	m^2	Positive
	Socioeconomic development	Urbanization rate of permanent resident population	%	Positive
		Tertiary industry as a proportion of GDP	%	Positive
		Engel's coefficient	%	Negative
		Investment in education	10,000 yuan	Positive
		Total labor productivity	Yuan/person	Positive
		Per capita GDP	Yuan	Positive
		Per capita disposable income	Yuan	Positive
		Urban registered unemployment rate	%	Negative
	Resource and energy use	Land use per unit GDP	m^2/10,000 yuan	Negative
		Energy consumption per unit GDP	Tons of standard coal/ 10,000 yuan	Negative
		Electricity consumption per unit GDP	kWh/10,000 yuan	Negative
		Water consumption per unit GDP	Cubic meters/10,000 yuan	Negative
		Solid waste utilization rate	%	Positive
		Per capita arable land	acre	Positive
		Pesticide usage per unit of arable land	kg/acre	Negative
		Wastewater treatment rate	%	Positive
	Institutions and inputs	R&D investment as a percentage of GDP	%	Positive
		Industrial pollution control investment	10,000 yuan	Positive
		Environmental pollution control investment	10,000 yuan	Positive
		Proportion of fiscal expenditure on energy conservation and environmental protection	%	Positive
		Green travel volume	10,000 person-trips/ 10,000 people	Positive
		Area of natural reserves as a percentage of national land	%	Positive
	Ecological environmental protection	Nitrogen oxide emissions per unit GDP	kg/10,000 yuan	Negative
		Sulfur dioxide emissions per unit GDP	kg/10,000 yuan	Negative
		Wastewater emissions per unit GDP	Cubic meters/10,000 yuan	Negative
		Greening coverage rate in built-up areas	%	Positive
		Proportion of days with good air quality	%	Positive
		Forest coverage rate	%	Positive

(Continued on following page)

TABLE 1 (*Continued*) Urban ecosystem service level evaluation indicator system for the provincial capitals of the YRB.

Target layer	Standardized layer	Indicator layer	Unit	Indicator attributes
		Rate of harmless treatment of urban domestic waste	%	Positive
		Cumulative area treated for soil and water loss	km^2	Positive

weighting. Initially, weights were calculated independently using each method. The final weights were then determined by averaging the results from both the subjective and objective calculations.

For the hierarchical analysis, we consulted 15 experts specializing in resource utilization, ecological restoration, economic development, land planning, and related fields. Using a 1-5 scale, these experts compared the importance of each indicator, assigning values to each influencing factor. A judgment matrix was then constructed, and SPSS 26.0 was used to calculate the weight of each indicator.

The entropy weight method is defined as follows: For the j-th indicator, the entropy E_J is calculated using the formula:

$$E_j = -k\sum_{i=1}^{m} P_{ij} \ln P_{ij}, 0 \le h_j \le 1 \quad (1)$$

Where: $k = \frac{1}{\ln m}$, $P_{ij} = \frac{X_{ij}}{\sum_{i=1}^{m} Xij}$, X_{ij} is the normalized value of the i-th sample for the j-th indicator, m is the number of samples.

The weight W_J derived from the entropy of the j-th indicator is given by:

$$W_J^2 = \frac{1\text{-}E_j}{\sum_{j=1}^{n}\left(1\text{-}E_j\right)} \quad (2)$$

These formulas measure the informational content of each indicator, with the final weights reflecting both the variability and significance of each factor within the comprehensive evaluation system.

3.2 Panel data regression

Panel data regression analysis, as a commonly used method in economic research, can help researchers explore the changes of observed objects over time and among individuals, and further analyze the impact of specific factors on them (Hoechle, 2007). This method is particularly effective for understanding dynamics that may not be evident in purely cross-sectional or time-series data.

The panel data regression model in this study is structured as follows:

Dependent Variable: The dependent variable represents the level of ecosystem services in each city, denoted by the comprehensive score of ecosystem services (Y_{ESS}). This score is calculated by linearly weighting the scores from five criterion layers: National Land Space, Socioeconomic Development, Resource and Energy Use, Institutions and Inputs, and Ecological Environmental Protection.

Independent Variables: The independent variables are selected based on their relevance to the ecosystem service level and encompass factors related to the economy, resources, and environment. These variables include: Number of general higher education institutions (X1), Per capita road area (X2), Per capita disposable income (X3), Electricity consumption per unit of GDP (X4), Greening coverage rate in built-up areas (X5), R&D investment as a percentage of GDP (X6), and Urban registered unemployment rate (X7).

Model Specification: The panel data regression model is formally expressed as:

$$y_{it} = \sum_{k=1}^{k} \beta_k x_{kit} + u_{it} \quad (3)$$

Where: y_{it} is the observed value of the dependent variable for city i at time t, x_{kit} the observed value of the k-th independent variable for city i at time t, β_k are the parameters to be estimated, u_{it} is the error term accounting for variations over time and across individuals, i represents each of the 9 cities analyzed, t covers the 11-year time span from 2010 to 2020.

This model allows us to assess the impact of various economic, resource, and environmental factors on the ecosystem service levels of the provincial capitals along the YRB.

3.3 Results of influencing factors

3.3.1 Unit root test

To ensure the reliability of our regression analysis, we conducted unit root tests on the time-series panel data to ascertain stationarity. Non-stationary time series, characterized by the presence of a unit root, can lead to spurious regression results. Using EViews 10, we applied four different test methods—Levin, Lin and Chu (LLC), Im, Pesaran & Shin (IPS), Augmented Dickey-Fuller (ADF), and Phillips-Perron (PP)—to evaluate the stationarity of our variables. The results are summarized in Table 2. The results indicate that all variables pass the unit root tests at the 1% or 5% significance levels, confirming that the series are stationary and suitable for further analysis.

3.3.2 Cointegration tests

After establishing stationarity, we conducted a cointegration test to verify the absence of spurious regression in our model. This test examines whether a long-term equilibrium relationship exists among the variables, assuming the differenced series are integrated of the same order. The results, presented in Table 3, indicate that four out of seven tests show statistical significance. These cointegration results affirm the presence of a stable long-term equilibrium relationship among the variables. Consequently, this confirms that the regression results are valid and not affected by spurious regression.

TABLE 2 Unit root test results.

Variable	LLC		IPS		ADF		PP	
	Statistic	Prob.	Statistic	Prob.	Statistic	Prob.	Statistic	Prob.
Y_{ESS}	−9.34017	0	−3.18153	0.0007	47.2745	0.0002	81.8532	0
X1	−9.09638	0	−2.41232	0.0079	49.5184	0.0001	86.0564	0
X2	−5.6272	0	−1.85735	0.0316	35.6621	0.0078	75.9697	0
X3	−10.8447	0	−4.94259	0	49.8171	0.0001	64.9783	0
X4	−8.45218	0	−4.11271	0	51.6041	0	65.3674	0
X5	−7.28412	0	−3.83739	0.0001	48.8299	0.0001	57.7393	0
X6	−5.75019	0	−1.51379	0.065	38.0534	0.0038	89.9891	0
X7	−8.57868	0	−2.56101	0.0052	50.0139	0.0001	63.6017	0

TABLE 3 Cointegration test results.

Statistic	Value	Prob.	Statistic	Value	Prob.
Panel v-Statistic	−2.128979	0.9834	Group rho-Statistic	4.451314	1
Panel rho-Statistic	3.216624	0.9994	Group PP-Statistic	−10.19461	0
Panel PP-Statistic	−8.584762	0	Group ADF-Statistic	−3.915962	0
Panel ADF-Statistic	−3.643833	0.0001			

TABLE 4 Model test results.

Type of test	Statistic	Prob.
F-test	10.866672	0
Lagrange Multiplier Test	73.06631	0.0003
Hausman Test	27.761655	0.0019
Heteroscedasticity Test	31.0917	0.0003
Wooldridge Autocorrelation Test	47.01284	0.0221

3.3.3 Regression results and model testing

We then performed model diagnostics to determine the most appropriate regression model. The results, summarized in Table 4, indicate that the fixed-effects model passed both the F-test and the Hausman test, suggesting it is suitable for our data. The heteroscedasticity test rejected the null hypothesis of homoscedasticity, and the Wooldridge test for auto-correlation rejected the null hypothesis of no autocorrelation. These findings support the use of the fixed-effects model for analyzing the influencing factors in our study.

3.3.4 Analysis of empirical results

Table 5 presents the regression results from various models, including hybrid model, fixed effects, random effects, and Feasible Generalized Least Squares (FGLS). The initial pooled and random effects models showed that three indicators did not pass the significance tests at the 1% or 5% levels, indicating these models may not adequately capture the relationships among variables. The fixed-effects model improved upon this but still had two indicators that were not significant, suggesting limitations in addressing within-group autocorrelation, contemporaneous correlation, and heteroscedasticity.

To resolve these issues, we applied FGLS for correction. The FGLS-corrected model effectively mitigated the problems of heteroscedasticity and autocorrelation, leading to statistically significant results across all indicators. Consequently, the FGLS-corrected panel model demonstrates its efficacy in analyzing the influencing factors in this study, providing robust and reliable results even in the presence of potential data irregularities.

4 Results

4.1 Composite scores of ecosystem service levels

Using the weighting method described earlier, we calculated the composite ecosystem service scores (Y_{ESS}) for the provincial capitals in the YRB from 2010 to 2020 (Figure 2).

The data indicate a significant upward trend in the ecosystem service levels of the nine provincial capitals from 2010 to 2020. The average comprehensive score increased from 0.3453 to 0.5173, marking a substantial rise of 49.79%. This improvement reflects the effective implementation of ecosystem service initiatives, ecological protection measures, and national high-quality development strategies that collectively enhanced the region's ecosystem services.

TABLE 5 Model regression results.

Explanatory variable	Hybrid model coefficient (Prob.)	Fixed effects coefficient (Prob.)	Random effects coefficient (Prob.)	FGLS Coefficient (Prob.)
Number of General Higher Education Institutions (X1)	0.239 (0.019)	0.231 (0.037)	−0.009 (0.839)	−0.185 (0.000)
Per Capita Road Area (X2)	0.027 (0.439)	0.078 (0.045)	−0.018 (0.636)	0.208 (0.000)
Per Capita Disposable Income (X3)	0.332 (0.000)	0.067 (0.485)	0.387 (0.000)	0.229 (0.000)
Electricity Consumption per GDP (X4)	−0.144 (0.000)	−0.112 (0.001)	−0.121 (0.000)	−0.387 (0.000)
Green Coverage Rate in Built-up Areas (X5)	0.131 (0.063)	0.160 (0.038)	0.194 (0.011)	0.201 (0.009)
R&D Investment as a Percentage of GDP (X6)	0.072 (0.003)	0.082 (0.002)	0.077 (0.003)	0.106 (0.000)
Urban Registered Unemployment Rate (X7)	−0.017 (0.697)	−0.025 (0.598)	−0.035 (0.446)	−0.099 (0.005)

From a spatial layout perspective, the upstream high-altitude and arid regions exhibit a fragile ecological foundation and relatively low ecosystem service levels compared to other cities within the Yellow River Basin. Despite significant growth due to measures such as the treatment of the Three-Rivers Source and grassland restoration, the average value in 2020 was only 0.4355, indicating that water resource constraints and climate change continue to pose long-term challenges. In contrast, the middle reaches, characterized by severe soil erosion, have seen a substantial improvement in their average value to 0.5638, attributed to initiatives like reforestation and the closure of polluting enterprises. The downstream estuarine wetlands, focusing on wetland restoration, have also witnessed a steady increase in their ecological value to 0.5302. However, there was a slight decline in 2019, which might be related to the encroachment of urban expansion on ecological space (Dong et al., 2023).

We also assessed scores for each of the five criterion layers: National Land Space, Socioeconomic Development, Resource and Energy Use, Institutions and Inputs, and Ecological Environmental Protection (Figure 3).

The results show that the contribution value of ecological environment protection indicators to ecosystem services has always ranked first, highlighting its core position in maintaining regional ecological functions. Notably, socioeconomic development indicators have shown a strong growth trend, with their score rising sharply from 0.0366 in 2010 to 0.1107 in 2020, representing a cumulative increase of 202.06%. This significant rise not only confirms the positive synergy between socioeconomic factors and ecosystem services but also highlights the profound impact of transitioning socioeconomic development models on enhancing ecological service capacity. Additionally, the national land space indicators have also achieved a significant increase of 57.98%, reflecting the optimization of land use structure and the continuous improvement of spatial governance efficiency, providing important spatial support for the enhancement of ecosystem service capacity. In contrast, the institutions and inputs indicators have only grown by 13.51%, and their relatively lagging development speed reveals the insufficiency of institutional innovation and financial guarantee mechanisms, which has become a key shortcoming restricting the continuous optimization of ecosystem service capacity.

These developments are consistent with the strategic objectives outlined in China's 12th and 13th Five-Year Plans, which prioritized ecological protection and high-quality development as key national goals. During these periods, rapid economic growth and enhancements in living standards facilitated better integration of economic and ecological goals. The promotion of green industry transformation and the adoption of sustainable development principles have propelled these cities toward higher stages of social and economic advancement, aiming to achieve a comprehensively prosperous society.

Furthermore, the average *per capita* disposable income in these cities increased from 16,368 yuan in 2010 to 37,108 yuan in 2020. Simultaneously, the average population density rose from 559 people per square kilometer to 731 people per square kilometer (Figure 4). This increase in population density highlights the growing pressure on urban space and underscores the ongoing challenges in balancing human activities with environmental sustainability. It emphasizes the need for continuous efforts to improve human-nature relationships, with sustainable urban planning and development being essential components in enhancing ecosystem services.

4.2 Time-series evolution characteristics

From 2010 to 2020, the ecosystem service levels of each city exhibited a general up-ward trend. Notably, Chengdu, Xi'an, and Zhengzhou recorded the highest comprehensive scores, reaching 0.6566, 0.5790, and 0.5643, respectively. The most significant score in-creases were observed in Chengdu, Zhengzhou, and Xining, with respective gains of 0.240, 0.238, and 0.187. In terms of percentage growth, Zhengzhou, Xining, and Lanzhou showed the most substantial improvements, increasing by 73.2%, 71.6%, and 66.6%, respectively.

Despite these overall gains, some cities experienced periodic declines. In 2012, Chengdu's score dropped by 2.82% due to

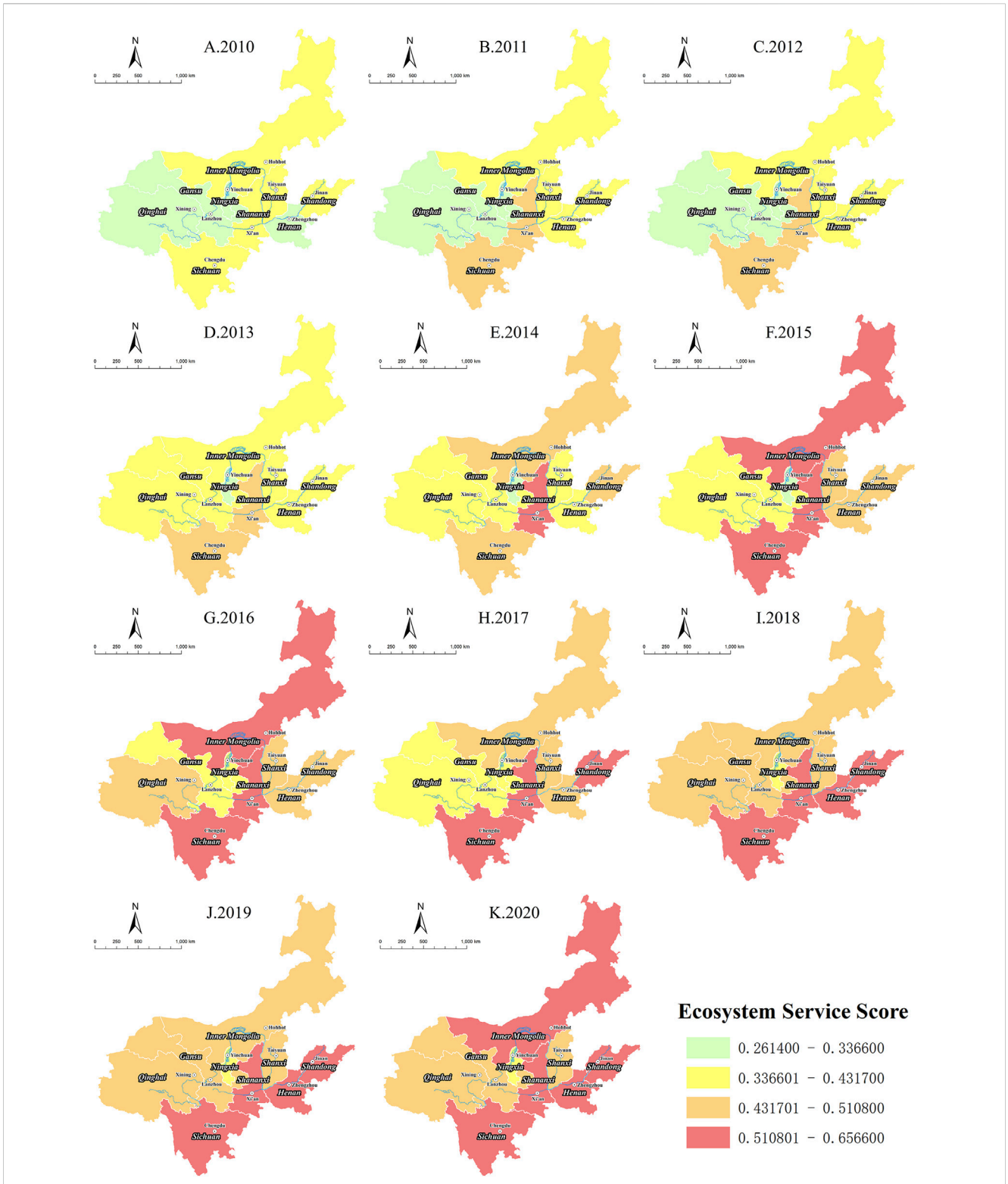

FIGURE 2
Ecosystem service scores of the provincial capitals in the YRB (2010–2020).

reduced afforestation, local climate disruptions, and increased carbon dioxide levels, which negatively affected air quality. Yinchuan's score decreased by 1.27% in 2011, largely because the effectiveness of domestic waste treatment fell by 40.2%, impacting the city's composite score. Hohhot faced downturns in 2017 and 2018, with decreases of 4.20% and 0.31%, respectively. These declines occurred during the initial phase of the "13th Five-Year Plan," a period marked by significant

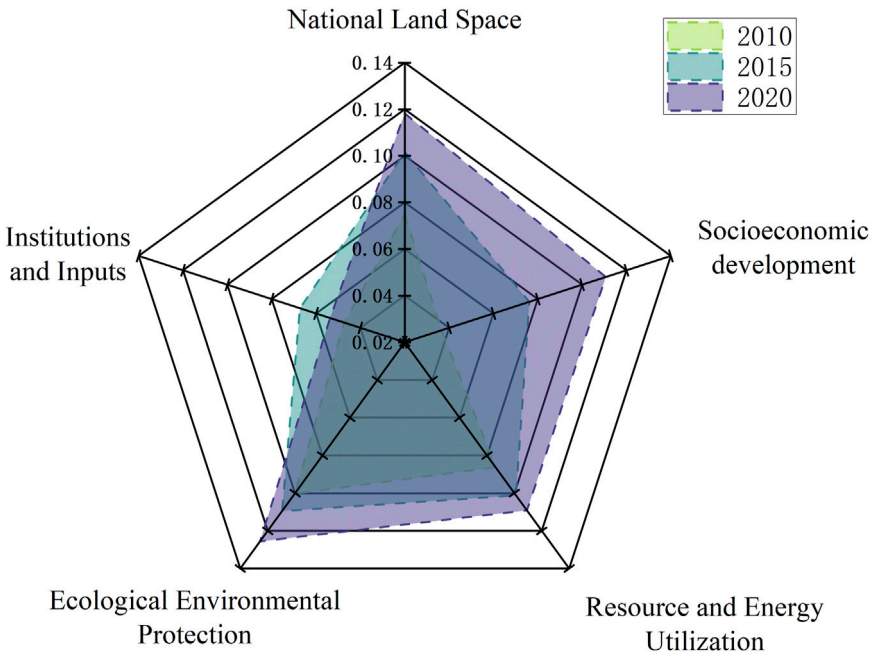

FIGURE 3
Ecosystem service scores of the provincial capitals in the YRB (2010–2020).

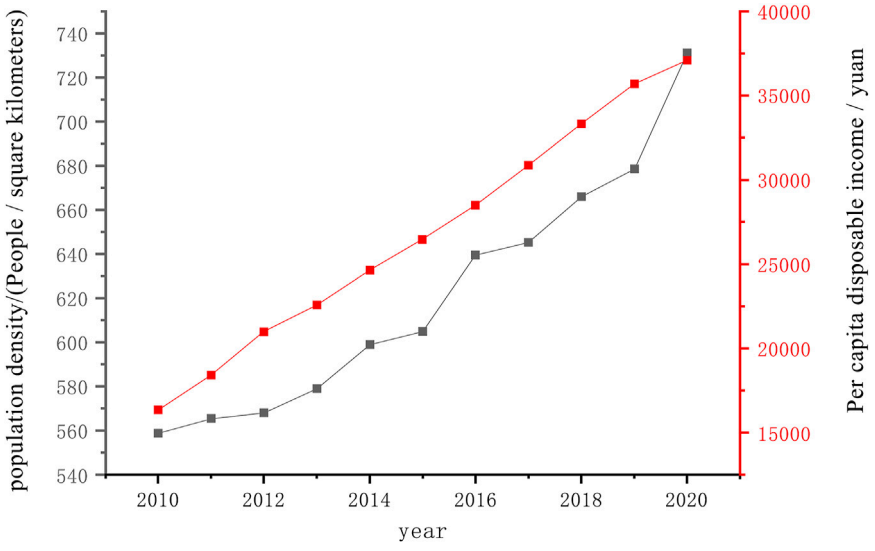

FIGURE 4
Per capita disposable income and population density of the capital cities in the YRB from 2010 to 2020.

industrial restructuring. In 2017, increases in Hohhot's electricity and water consumption per unit of GDP, along with a 17.44% reduction in soil erosion control areas, contributed to the lower scores. In 2018, further increases in electricity consumption per unit of GDP and a decline in the comprehensive utilization of solid waste exacerbated the reduction in its overall ecosystem service level.

4.3 Cluster analysis results

To deepen our understanding of the variations in ecosystem service levels among the provincial capitals of the YRB, we performed a cluster analysis using SPSS 26.0 software. This analysis produced a dendrogram that visualizes the relationships and groupings among the cities (Figure 5).

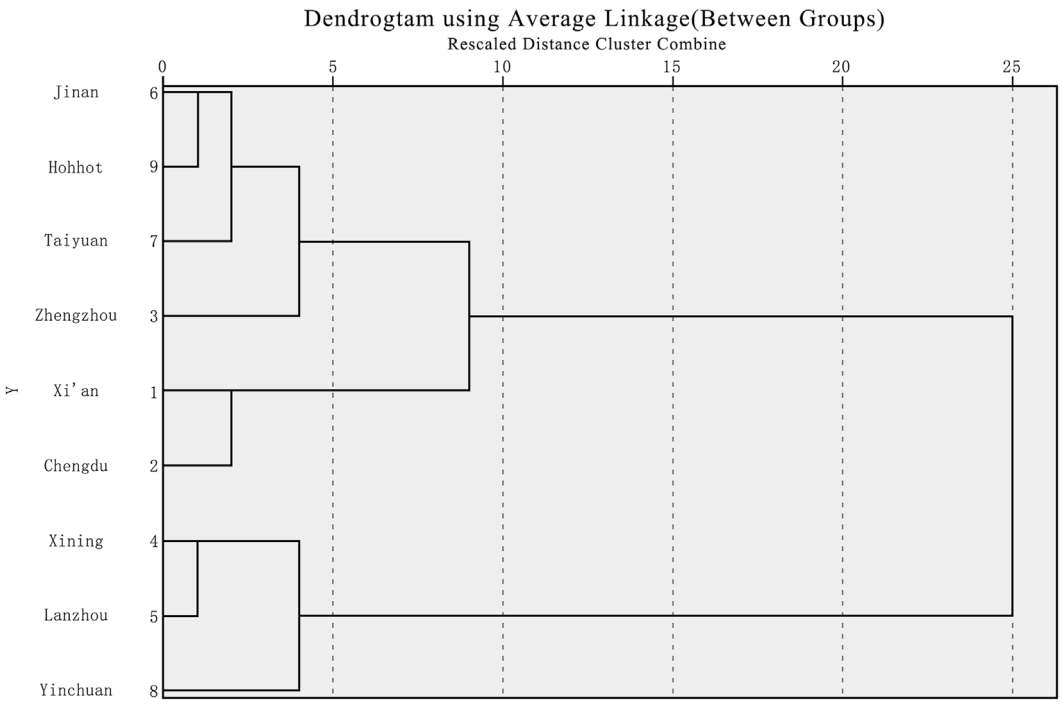

FIGURE 5
Cluster analysis dendrogram of ecosystem service levels in the provincial capitals of the YRB.

TABLE 6 Average comprehensive scores and growth for the three categories of urban ecosystem service from 2010 to 2020.

Year	First category	Second category	Third category
2010	0.4192	0.3640	0.2712
2011	0.4618	0.3860	0.2834
2012	0.4748	0.3999	0.3120
2013	0.4931	0.4166	0.3481
2014	0.5057	0.4389	0.3638
2015	0.5389	0.4793	0.3685
2016	0.5580	0.4929	0.3977
2017	0.5631	0.4965	0.4149
2018	0.5643	0.5090	0.4344
2019	0.5924	0.5221	0.4289
2020	0.6178	0.5312	0.4318
Growth	0.1986	0.1671	0.1606

The dendrogram categorizes the provincial capitals into three distinct groups based on their ecosystem service levels. First Category: Xi'an and Chengdu are classified together as cities with high ecosystem service levels. Second Category: Jinan, Hohhot, Taiyuan, and Zhengzhou form a group with medium ecosystem service levels. Third Category: Xining, Lanzhou, and Yinchuan are grouped as cities with relatively low ecosystem service levels.

A time-series analysis of these categories from 2010 to 2020, as detailed in Table 6, reveals significant improvements across all groups. The first category, comprising Xi'an and Chengdu, started with an average comprehensive score of 0.4192 in 2010 and in-creased to 0.6178 by 2020, marking the most substantial growth of 0.1986. The second category's average score rose from 0.3640 in 2010 to 0.5312 in 2020, an increase of 0.1672. The third category, despite starting with the lowest average score of 0.2712 in 2010, achieved 0.4318 by 2020, reflecting a growth of 0.1606.

5 Discussion

5.1 Urban classification discussion

The first category of cities are famous tourist cities in China, which continuously promote policies and financial investments in the field of environmental governance and protection. Tourist cities pay more attention to environmental protection and pollution control. The second category of cities is in the stage of industrial green transformation, and the lack of green industry is the main factor leading to its low level. Hohhot is rich in forest and grassland resources, but grassland degradation caused by overgrazing has resulted in its low level of ecosystem services (Qin et al., 2021). Cities in the third category are mostly in areas with underdeveloped economic development, which is due to the low level of urban development leading to inefficient environmental governance, again a factor limiting their ecosystem service level, similar to the findings of Guo et al. (2017).

5.2 Analysis of influencing factors

From the perspective of the influence mechanism of key variables, *per capita* disposable income is identified as the most significant positive driver of ecosystem service levels. Higher *per capita* disposable income not only signifies improved urban economic development but also reflects enhanced environmental awareness among residents and increased investment in environmental governance, thereby significantly boosting environmental management efficiency. In contrast, electricity consumption per unit of GDP, as the strongest negative indicator, has an impact coefficient nearly twice that of *per capita* disposable income. This result clearly demonstrates that, at comparable levels of economic development, higher energy consumption intensity leads to lower resource utilization efficiency and greater environmental pollution pressure, ultimately resulting in a marked decline in ecosystem service levels.

The indicators of *per capita* road area, greening coverage rate in built-up areas, and R&D investment as a percentage of GDP all exhibit significant positive correlations with ecosystem service levels. Specifically, the positive effect of *per capita* road area underscores the role of improved urban infrastructure in enhancing ecological service capacity; the positive impact of greening coverage rate in built-up areas confirms the critical importance of "green space" in improving urban ecological environments; and the positive correlation of R&D investment intensity highlights the significance of technological innovation in promoting green development.

Notably, the number of general higher education institutions and the urban registered unemployment rate are negatively correlated with ecosystem service levels. The negative effect of higher education institutions may stem from the associated increase in population density, which places additional pressure on the urban ecological environment. Meanwhile, the negative impact of the urban registered unemployment rate reveals the close relationship between employment status and the ecological environment: a higher unemployment rate not only indicates insufficient economic momentum but can also lead to reduced environmental governance investment, thereby intensifying environmental governance challenges.

These findings offer important policy implications: while continuing to enhance economic development, efforts must be made to reduce energy consumption intensity, optimize the allocation of higher education resources, and support ecological civilization construction through stable employment promotion. Additionally, investments in infrastructure should be increased, urban greening should be advanced, and R&D investment should be raised to enhance ecosystem service levels across multiple dimensions.

5.3 Recommendations

Effective enhancement of ecosystem services requires differentiated strategies for cities facing distinct challenges. For first category cities, maintaining regional leadership and robust ecological services growth should focus on high-quality development. Chengdu should advance park city construction by expanding urban green spaces and increasing R&D investment. Xi'an could leverage its academic resources to optimize environmental science programs, converting educational advantages into ecological innovations. Second category cities need to balance economic growth with environmental conservation through habitat improvement. Jinan requires rational urban planning to prevent ecosystem degradation from overdevelopment (Cui et al., 2022b). Hohhot should strengthen grassland conservation while developing eco-friendly husbandry and tourism. Taiyuan must accelerate green transition in coal industries and nurture renewable energy sectors. Zhengzhou should accelerate the green transformation of traditional manufacturing industries and simultaneously cultivate industrial clusters for the recycling and utilization of renewable resources to form a closed-loop resource utilization system. For third category cities, infrastructure development forms the foundation for ecological services enhancement. Key measures include expanding road networks, establishing ecological corridors, and increasing vegetation coverage. Xining could leverage its strategic location in the Three-Rivers Source region to develop ecotourism, thereby boosting local incomes. Lanzhou should prioritize employment security while constructing ecological corridors along the Yellow River. Yinchuan needs to implement water-efficient irrigation systems and strengthen wetland conservation in Yellow River basins.

Achieving both ecological protection and high-quality development in the Yellow River Basin requires a comprehensive approach. Rational allocation of water resources, coupled with optimized ecological compensation mechanisms through cross-regional cooperation, will promote both ecological and economic progress.

6 Conclusion

This study established an indicator system to evaluate ecosystem services in the provincial capital cities within the Yellow River Basin. By employing a combined weighting method, we calculated the ecosystem service levels for nine provincial capitals from 2010 to 2020. Cluster analysis was conducted to assess the spatiotemporal characteristics of ecosystem service levels across the nine provincial capital cities in the basin. Additionally, a panel regression model was applied to analyze the factors influencing ecological services and to identify the key indicators affecting the ecosystem service levels in the Yellow River Basin.

The results show that the ecosystem service levels of the nine provincial capitals in the Yellow River Basin have significantly improved, and the ecological environment has continuously improved. However, there are noticeable differences among cities. Chengdu and Xi'an exhibit the highest ecosystem service levels, while Zhengzhou, Xining, and Lanzhou show the largest increases in ecosystem service levels. The rankings of cities in the upper, middle, and lower reaches of the Yellow River are mixed, revealing a distinct spatial pattern influenced by regional ecological characteristics and restoration strategies. This suggests that the optimization and enhancement of ecosystem service functions depend on the synergistic interaction of multiple factors, including natural conditions, socio-economic elements, and policy regulations.

In terms of influencing factors, the analysis revealed that *per capita* disposable income, *per capita* road area, greening coverage rate in built-up areas, and R&D investment as a percentage of GDP all have significant positive correlations with ecosystem service levels. Notably, *per capita* disposable income shows a consistent positive correlation across three models, indicating that it plays a key role in the overall improvement of ecosystem service levels in the Yellow River Basin. On the other hand, variables such as electricity consumption per unit of GDP, the number of general higher education institutions, and the urban registered unemployment rate show significant negative correlations with ecosystem service levels. Overall, effective measures to maintain and gradually improve ecosystem service levels in the Yellow River Basin include optimizing the energy structure, promoting the development of clean energy, driving the green transformation of industrial structures, and enhancing infrastructure development.

Although this study provides valuable insights into the dynamics of ecosystem services in provincial capital cities along the Yellow River Basin, it is also necessary to recognize some limitations. The indicator system primarily focuses on socioeconomic and environmental dimensions, which may overlook nuanced cultural or governance factors that can influence ecosystem services. Additionally, due to constraints in data availability, trend extrapolation was necessary for handling missing values, potentially introducing uncertainties in the calculation of indicators. Future research could integrate high-resolution remote sensing data to capture more detailed ecological patterns. Comparative studies across different river basins, such as the Yangtze River Basin, would help identify both region-specific and universal drivers of ecosystem services.

Data availability statement

The data analyzed in this study is subject to the following licenses/restrictions: The data are not publicly available due to privacy or ethical restrictions. Requests to access these datasets should be directed to Jianxun Zhang, zhangjianxun@qhu.edu.cn.

Author contributions

HJ: Conceptualization, Methodology, Writing – original draft, Writing – review and editing. TW: Data curation, Investigation, Writing – original draft. PL: Software, Writing – review and editing. JZ: Conceptualization, Methodology, Writing – original draft, Writing – review and editing. RZ: Formal Analysis, Validation, Writing – review and editing.

Funding

The author(s) declare that financial support was received for the research and/or publication of this article. This research was funded by the National Social Science Foundation of China (Grant number 22XTJ005).

Conflict of interest

The authors declare that the research was conducted in the absence of any commercial or financial relationships that could be construed as a potential conflict of interest.

Generative AI statement

The authors declare that no Generative AI was used in the creation of this manuscript.

Publisher's note

References

Amirnejad, H., Hosseini, S., and Azadi, H. (2024). Evaluation and valuation of tajan River Basin ecosystem services. *Ecohydrol. Hydrobiol.* 25, 238–249. doi:10.1016/j.ecohyd.2024.03.005

Baste, I., Larigauderie, A., and Watson, R. T. (2024). "The intergovernmental science-policy platform on biodiversity and ecosystem services," in *Encyclopedia of biodiversity*. Editor S. M. Scheiner 3rd Edition (Oxford, United Kingdom: Academic Press), 214–235. doi:10.1016/B978-0-12-822562-2.00147-X

Bhanojirao, V. V. (1991). Human development report 1990: review and assessment. *World Dev.* 19 (10), 1451–1460. doi:10.1016/0305-750X(91)90087-X

Bui, N. T., Kawamura, A., Bui, D. D., Amaguchi, H., Bui, D. D., Truong, N. T., et al. (2019). Groundwater sustainability assessment framework: a demonstration of environmental sustainability Index for Hanoi, Vietnam. *J. Environ. Manage.* 241, 479–487. doi:10.1016/j.jenvman.2019.02.117

Chen, L., Ma, L., Jiji, J., Kong, Q., Ni, Z., Yan, L., et al. (2022). River ecosystem health assessment using a combination weighting method: a case study of Beijing section of Yongding River in China. *Int. J. Environ. Res. Public. Health* 19 (21), 14433. doi:10.3390/ijerph192114433

Chen, L., Yao, Y., Xiang, K., Dai, X., Li, W., Dai, H., et al. (2024). Spatial-temporal pattern of ecosystem services and sustainable development in representative mountainous cities: a case study of Chengdu-Chongqing urban agglomeration. *J. Environ. Manage.* 368, 122261. doi:10.1016/j.jenvman.2024.122261

Costanza, R., d'Arge, R., de Groot, R., Farber, S., Grasso, M., Hannon, B., et al. (1997). The value of the World's ecosystem services and natural capital. *Nature* 387 (6630), 253–260. doi:10.1038/387253a0

Cui, J., Zhu, M., Liang, Y., Qin, G., Li, J., and Liu, Y. (2022a). Land use/land cover change and their driving factors in the Yellow River Basin of Shandong province based on google earth engine from 2000 to 2020. *ISPRS Int. J. Geo-Inf.* 11 (3), 163. doi:10.3390/ijgi11030163

Cui, J., Zhu, M., Mi, H., and Liu, Y. (2022b). Evaluation of eco-environmental quality and analysis on spatio-temporal variation in Jinan, China. *Pol. J. Environ. Stud.* 31 (2), 1061–1072. doi:10.15244/pjoes/140297

Dai, X., Johnson, B. A., Luo, P., Yang, K., Dong, L., Wang, Q., et al. (2021). Estimation of urban ecosystem services value: a case study of Chengdu, Southwestern China. *Remote Sens.* 13 (2), 207. doi:10.3390/rs13020207

Daily, G. C., Matson, P. A., and Vitousek, P. M. (1997). "Introduction: what are ecosystem services," in *Nature's services: societal dependence on natural ecosystems*. Editor G. C. Daily (Washington, DC: Island Press), 1.

De Groot, R. S., Alkemade, R., Braat, L., Hein, L., and Willemen, L. (2010). Challenges in integrating the concept of ecosystem services and values in landscape planning, management and decision making. *Ecol. Complex.* 7 (3), 260–272. doi:10.1016/j.ecocom.2009.10.006

Dong, H., Liu, Y., Cui, J., Zhu, M., and Ji, W. (2023). Spatial and temporal variations of vegetation cover and its influencing factors in Shandong province based on GEE. *Environ. Monit. Assess.* 195 (9), 1023. doi:10.1007/s10661-023-11650-7

Emerson, J. W., Hsu, A., Levy, M. A., de Sherbinin, A., Mara, V., Esty, D. C., et al. (2012). *Environmental performance Index and pilot trend environmental performance Index*. New Haven, CT: Yale Center for Environmental Law and Policy.

Environmental Sustainability Index (2002). *An initiative of the global leaders of tomorrow environment task force*.

Fan, Y., and Ma, S. (2024). Integrating fuzzy analytic hierarchy process into ecosystem service-based spatial planning: a case study of the Shenyang Metropolitan area, China. *Ecol. Inf.* 81, 102625. doi:10.1016/j.ecoinf.2024.102625

Gao, J., Yu, Z., Wang, L., and Vejre, H. (2019). Suitability of regional development based on ecosystem service benefits and losses: a case study of the Yangtze River Delta urban agglomeration, China. *Ecol. Indic.* 107, 105579. doi:10.1016/j.ecolind.2019.105579

Gómez-Limón, J. A., Arriaza, M., and Guerrero-Baena, M. D. (2020). Building a composite indicator to measure environmental sustainability using alternative weighting methods. *Sustainability* 12 (11), 4398. doi:10.3390/su12114398

Guan, X., Fu, Y., Meng, Y., and Yan, D. (2022). Water ecology emergy analytic system construction and health diagnosis. *Energy Convers. Manag.* 270, 116254. doi:10.1016/j.enconman.2022.116254

Guo, J., Zhu, D., Wu, X., and Yan, Y. (2017). Study on environment performance evaluation and regional differences of strictly-environmental-monitored cities in China. *Sustainability* 9 (12), 2094. doi:10.3390/su9122094

Hoechle, D. (2007). Robust standard errors for panel regressions with cross-sectional dependence. *Stata J.* 7 (3), 281–312. doi:10.1177/1536867X0700700301

Ji, Z., Zou, S., Zhang, W., Song, F., Yuan, T., and Xu, B. (2024). Optimizing zoning for ecological management in alpine region by combining ecosystem service supply and demand with ecosystem resilience. *J. Environ. Manage.* 365, 121508. doi:10.1016/j.jenvman.2024.121508

Jo, J.-H., Choi, M., Kweon, D., Son, Y.-G., and Lim, E. M. (2024). Regulating ecosystem services in a local forest: navigating supply, trade-offs, and synergies. *Trees For. People* 15, 100466. doi:10.1016/j.tfp.2023.100466

Jorge-García, D., and Estruch-Guitart, V. (2022). Comparative analysis between AHP and ANP in prioritization of ecosystem services - a case study in a rice field area raised in the Guadalquivir Marshes (Spain). *Ecol. Inf.* 70, 101739. doi:10.1016/j.ecoinf.2022.101739

Kim, I., Lee, J., and Kwon, H. (2021). Participatory ecosystem service assessment to enhance environmental decision-making in a border city of South Korea. *Ecosyst. Serv.* 51, 101337. doi:10.1016/j.ecoser.2021.101337

Kokangül, A., Polat, U., and Dağsuyu, C. (2017). A new approximation for risk assessment using the AHP and fine kinney methodologies. *Saf. Sci.* 91, 24–32. doi:10.1016/j.ssci.2016.07.015

Kou, L., Wang, X., Wang, H., Wang, X., and Hou, Y. (2024). Spatiotemporal analysis of ecological benefits coupling remote sensing ecological Index and ecosystem services Index. *Ecol. Indic.* 166, 112420. doi:10.1016/j.ecolind.2024.112420

Lind, N. (2019). A development of the human development Index. *Soc. Indic. Res.* 146 (3), 409–423. doi:10.1007/s11205-019-02133-9

Lu, M., Zhao, Q., Ding, S., Wang, S., Hong, Z., Jing, Y., et al. (2022). Hydro-geomorphological characteristics in response to the water-sediment regulation scheme of the Xiaolangdi dam in the lower Yellow River. *J. Clean. Prod.* 335, 130324. doi:10.1016/j.jclepro.2021.130324

Odum, H. (1996). *Enviromental AccountEmergy and environmental decision making*. Wiley, 370.

Peng, K., Jiang, W., Ling, Z., Hou, P., and Deng, Y. (2021). Evaluating the potential impacts of land use changes on ecosystem service value under multiple scenarios in support of SDG reporting: a case study of the Wuhan urban agglomeration. *J. Clean. Prod.* 307, 127321. doi:10.1016/j.jclepro.2021.127321

Pinar, M. (2022). Sensitivity of environmental performance Index based on stochastic dominance. *J. Environ. Manage.* 310, 114767. doi:10.1016/j.jenvman.2022.114767

Qin, P., Sun, B., Li, Z., Gao, Z., Li, Y., Yan, Z., et al. (2021). Estimation of grassland carrying capacity by applying high spatiotemporal remote sensing techniques in Zhenglan Banner, inner Mongolia, China. *Sustainability* 13 (6), 3123. doi:10.3390/su13063123

Salata, S., and Grillenzoni, C. (2021). A spatial evaluation of multifunctional ecosystem service networks using principal component analysis: a case of study in Turin, Italy. *Ecol. Indic.* 127, 107758. doi:10.1016/j.ecolind.2021.107758

Schneider, F., Kläy, A., Zimmermann, A. B., Buser, T., Ingalls, M., and Messerli, P. (2019). How can science support the 2030 Agenda for sustainable development? Four tasks to tackle the normative dimension of sustainability. *Sustain. Sci.* 14 (6), 1593–1604. doi:10.1007/s11625-019-00675-y

Sun, B., Tang, J., Yu, D., Song, Z., and Wang, P. (2019). Ecosystem health assessment: a PSR analysis combining AHP and FCE methods for Jiaozhou Bay, China. *Ocean. Coast. Manag.* 168, 41–50. doi:10.1016/j.ocecoaman.2018.10.026

Tong, H., Peng, J., Zhang, Y., Fang, T., Zhang, J., Men, Z., et al. (2021). Environmental benefit analysis of "Road-to-Rail" policy in China based on a railway Tunnel measurement. *J. Clean. Prod.* 316, 128227. doi:10.1016/j.jclepro.2021.128227

Xie, Z., He, L., Mao, Z., Wan, W., Song, X., Wu, Z., et al. (2024). Spatial heterogeneity of natural and socio-economic features shape that of ecosystem services. A large-scale study on the Yangtze River Economic Belt, China. *Ecol. Indic.* 159, 111729. doi:10.1016/j.ecolind.2024.111729

Yang, Y., Yuan, X., An, J., Su, Q., and Chen, B. (2024). Drivers of ecosystem services and their trade-offs and synergies in different land use policy zones of Shaanxi province, China. *J. Clean. Prod.* 452, 142077. doi:10.1016/j.jclepro.2024.142077

Yuan, S., Mei, Z., Zhu, C., Cao, R., Li, S., Yang, L., et al. (2024). Investigating the spatio-temporal interactive relationship between land use structure and ecosystem services in Urbanizing China. *Ecol. Indic.* 158, 111315. doi:10.1016/j.ecolind.2023.111315

Yurui, L., Xuanchang, Z., Zhi, C., Zhengjia, L., Zhi, L., and Yansui, L. (2021). Towards the progress of ecological restoration and economic development in China's loess plateau and strategy for more sustainable development. *Sci. Total Environ.* 756, 143676. doi:10.1016/j.scitotenv.2020.143676

Zhai, Y., Zhai, G., Yu, Z., Lu, Z., Chen, Y., and Liu, J. (2024). Coupling coordination between urbanization and ecosystem services value in the beijing-tianjin-hebei urban agglomeration. *Sustain. Cities Soc.* 113, 105715. doi:10.1016/j.scs.2024.105715

Zhang, Z., Li, H., and Cao, Y. (2022). Research on the coordinated development of economic development and ecological environment of nine provinces (regions) in the Yellow River Basin. *Sustainability* 14 (20), 13102. doi:10.3390/su142013102

Zhang, Z., Wang, S., and Zhang, J. (2024). Spatiotemporal evolution of carbon budget and carbon compensation zoning of urban agglomerations in the Yellow River Basin. *Sci. Rep.* 14 (1), 17984. doi:10.1038/s41598-024-68614-1

Zhang, Z., Zhang, J., Liu, L., Gong, J., Li, J., and Kang, L. (2023). Spatial–temporal heterogeneity of urbanization and ecosystem services in the Yellow River Basin. *Sustainability* 15, 3113. doi:10.3390/su15043113

Zhou, J., Wu, J., and Gong, Y. (2020). Valuing wetland ecosystem services based on benefit transfer: a meta-analysis of China wetland studies. *J. Clean. Prod.* 276, 122988. doi:10.1016/j.jclepro.2020.122988

Žižović, M., Miljković, B., and Marinković, D. (2020). Objective methods for determining criteria weight coefficients: a modification of the CRITIC method. *Decis. Mak. Appl. Manag. Eng.* 3 (2), 149–161. doi:10.31181/dmame2003149z

frontiers | Frontiers in Environmental Science

TYPE Original Research
PUBLISHED 28 April 2025
DOI 10.3389/fenvs.2025.1552181

OPEN ACCESS

EDITED BY
Tianjiao Feng,
Beijing Forestry University, China

REVIEWED BY
Yaokun Fu,
China Coal Research Institute, China
Xiuli Wang,
Jiangxi University of Science and Technology, China
Bolin Li,
Chang'an University, China

*CORRESPONDENCE
Shidong Wang,
wsd0908@163.com

RECEIVED 27 December 2024
ACCEPTED 14 April 2025
PUBLISHED 28 April 2025

CITATION
Zhang H, Zhu Z, Wang S, Zou Y, Chen Z, Zhao Y, Chen Q, Jiao Y, Li Y and Du H (2025) Identifying key elements of ecological restoration in shallow-buried high-intensity mining area based on obstacle degree model a case study in Huojitu mine.
Front. Environ. Sci. 13:1552181.
doi: 10.3389/fenvs.2025.1552181

Identifying key elements of ecological restoration in shallow-buried high-intensity mining area based on obstacle degree model a case study in Huojitu mine

Hebing Zhang[1,2], Zhiyong Zhu[1], Shidong Wang[1,2]*, Youfeng Zou[1], Zhichao Chen[1], Yanling Zhao[3], Qiuji Chen[4], Yiheng Jiao[1], Yifu Li[1] and Haoyang Du[1]

[1]School of Surveying and Engineering Information, Henan Polytechnic University (HPU), Jiaozuo, China, [2]Zhengzhou Advanced Institute of Henan Polytechnic University, Zhengzhou, China, [3]College of Geoscience and Surveying Engineering, China University of Mining and Technology-Beijing, Xuzhou, China, [4]College of Geomatics, Xi'an University of Science and Technology, Xi'an, China

The idea of green mining has attracted much attention over the past decade. Accurate identification of key elements of ecological restoration in mining areas is an important prerequisite for ecosystem restoration and reconstruction and improving the quality of ecological environment. The goal of this study is to develop a five-factor index system for ecological restoration in mining areas, with the Huojitu well serving as a case study of a typical western shallow-buried high-intensity mining area in China. The factors include vegetation cove, soil, ecological landscape, land damage and site condition. An obstacle factor diagnosis model based on the coupling of obstacle degree and Shefold restriction law has been established in this research. This model is used to identify the obstacle factors and analyze the key elements of ecological restoration in the mining area. The key elements of ecological restoration are identified by combining the obstacle degree of each obstacle factor. According to the findings, out of all the areas included in the study, the one pertaining to soil conditions was the biggest at 35.29 km^2, or 31.91% of the total, followed by land damage condition (21.25 km^2 ~19.20%), site condition (19.74 km^2~17.84%), vegetation cover (3.34 km^2, ~3.02%), and ecological landscape (31.08 km^2~ 28.03%). Based on the identification results of critical elements in mining area ecological restoration, this study proposes targeted remediation strategies and formulates corresponding site-specific rehabilitation measures to facilitate efficient ecosystem recovery in mining regions. This approach not only advances the practical implementation of ecological restoration technologies but also provides a valuable reference framework for sustainable ecosystem management in post-mining landscapes.

KEYWORDS

shallow mining, land degradation, ecological restoration, obstacle factor diagnosis model, Huojitu

1 Introduction

The utilization of coal resources has led to a series of ecological problems. With the increasing popularity of green mining and carbon neutrality concepts, the ecological restoration of mining areas has attracted widespread attention and has become an important part of ecological architecture and environmental protection (Xiao et al., 2023). Recently, there has been a considerable development in mining ecological restoration theory and technology in China, forming a number of theoretical and technical achievements (Chi et al., 2024; Yao et al., 2025; Peng and Bi, 2024; Chen et al., 2024; Lei et al., 2023; Sun et al., 2024; Almassi, 2021; Bendfeldt et al., 2001). For the construction of an ecological civilization, we must adhere to the principle of "saving priority, protection priority, natural recovery" (Lei et al., 2024), which indicates that the ecological restoration of mining areas should transition from manual intervention to manual guidance (Klaus and Kiehl, 2021; Hao et al., 2025; Li et al., 2024; Du et al., 2021; Crouzeilles et al., 2017).

The Huojitu well in the northwest mining area has a shallow coal seam, thin bedrock, large coal seam thickness, and simple geological conditions. Coal occurrence conditions are ideal for mechanized one-time full height and rapid mining, which is typical of high-intensity mining (Chen et al., 2016). Large-scale long-wall high-intensity mining causes intense roof movement, stope mine pressure (Yang et al., 2020; Yang and Liu, 2020; Gao et al., 2019), and greater damage to the overlying strata and surface ecology. The western region's shallow buried depth and high intensity mining area has been the subject of increasing amounts of academic investigation. Based on the key stratum theory and CISPM (Comprehensive and Integrated Subsidence Prediction Model) comprehensive surface subsidence prediction model software, Xu et al. (2023) studied the characteristics of surface movement, the change of surface rock movement angle parameters and the development of ground fissures in the study area. Yang et al. (2019) determined the microscopic structure, mineral composition, and physical and mechanical properties of sandy mudstone mine roofs. A similar simulation test, theoretical analysis, CAN-II magnetotelluric detector, and field investigation were employed to thoroughly analyze the overburden failure. For a coordinated development of coal mining and ecological restoration, the coal industry must abandon the concept of "mining before restoration" (Guo et al., 2023) and establish the concept of "integrated development and utilization" (Hu and Xiao, 2020). Therefore, when implementing ecological restoration in mining areas, a scientific and targeted ecological restoration should be considered. Ecological restoration of mining areas must be executed meticulously to fulfill the objective of natural ecological rehabilitation.

At present, the research on the diagnosis model of obstacle factors is mainly divided into four domains: obstacle diagnosis model based on analytic hierarchy process (Zhao et al., 2023; Mao et al., 2007; Yang et al., 2022; Chai et al., 2022), obstacle diagnosis model based on principal component analysis (Li and Yang, 2010; Shi et al., 2024; Li et al., 2015), obstacle diagnosis model based on index deviation (Qu et al., 2017; Chen and Yang, 2013; Huang et al., 2018) and obstacle diagnosis model based on niche (Zhao et al., 2016; Xia et al., 2021; Sun et al., 2023; Zhao et al., 2022). These four types of models can better analyze obstacle factors and have been widely used in various fields of ecological resource research. Manhaes et al. (2022) evaluated the obstacle factors restricting forest restoration based on the functional trajectories of six forest communities 20 years of age, and identified the species that are most conducive to overcoming the obstacle factors of forest community restoration. Chen et al. (2020) employed the entropy weight TOPSIS model to assess the urban ecological level, identified the primary impediments hindering the enhancement of urban ecological standards through the obstacle factor diagnosis model, and proposed specific recommendations. Yi et al.(2023) constructed an index system for analyzing the rural resources and environment carrying capacity based on the social ecological framework given the interaction between human and environment as the core, and used the obstacle degree model to identify the key obstacles in this system. Cheng et al. (2018) used the obstacle degree model to calculate the obstacle degree of the obstacle factors affecting the green competitiveness of China's provinces, and determined the key obstacles affecting the green competitiveness of each province. Wang et al. (2022) employed the obstacle degree model to assess the degree of 25 factors within the evaluation system of agricultural sustainable development. Cui et al.(2022) thoroughly evaluated the environmental carrying capacity and identified the main obstacle factors of three major urban agglomerations in Beijing-Tianjin-Hebei, Yangtze River Delta and Pearl River Delta by using the entropy weight extension matter-element model and obstacle diagnosis model. Jiang Long (Jiang et al., 2021)[43] analyzed the main obstacle factors restricting a high-quality development through the obstacle degree model, and simulated the future development changes of the provinces in the Yellow River Basin using the system dynamics model. Jia and Du (2024) assessed the obstacle degree of each index in the ecological security evaluation using the obstacle degree model, and conducted the ecological security evaluation of Qinghai Province from 2010 to 2020. Yang et al. (2023) used the obstacle degree model to identify the key factors affecting the land use performance in Ningxia. Lei et al. (2016) combined the entropy weight TOPSIS model and the obstacle degree model to evaluate the land use performance in Anhui Province over the past 15 years. The performance change trend of the land use subsystem in Anhui Province over the next 5 years was also predicted and analyzed. Liao Yuchen used the PSR model and the obstacle factor method to construct an evaluation system from 23 indicators such as resources, environment, social economy, etc., and comprehensively evaluated the dynamic changes of ecological security in the study area (Liao et al., 2021). In summary, although the obstacle degree model has been widely used, its application is limited to the calculation of each obstacle factor's degree, and there is limited research on the identification of key obstacle factors.

In summary, this study takes the Huojitu well in a typical shallow-buried high-intensity mining area in the western region of China as the research area. We present the theory of key elements in the ecological restoration of mining areas, develop an index system for ecological restoration obstacles and establish a model for identifying key elements of ecological restoration based on the coupling of obstacle degree and Shefold's restrictive law (Erofeeva, 2021). The quantitative diagnosis of the obstacle factors affecting the ecological restoration of the mining area is carried out, and the key elements affecting the ecological restoration are identified. Different restoration strategies are formulated for different key elements in order to achieve an efficient ecological restoration of the mining area. The results have important theoretical and practical significance for dealing with the relationship between artificial restoration and natural restoration and realizing the harmonious coexistence of man and nature in mining areas.

TABLE 1 Data source.

Data type	Title	Time	Source	Application
Raster	DEM	2023	https://www.gscloud.cn/	Extract the slope data of the study area
	Landsat 8/9 OLI satellite data	May 2023	https://www.usgs.gov	Extraction of vegetation coverage in the study area
Vector	Mining subsidence data	2003–2022	CHN Energy Shendong Coal Technology Research Institute	Obtain the degree of land damage in the study area
	Land use data	2021	The third national land resource survey	Get the ecological landscape data of the study area
Fieldwork	Soil data	May 2023	Field collection	Extraction of soil nutrient distribution in the study area

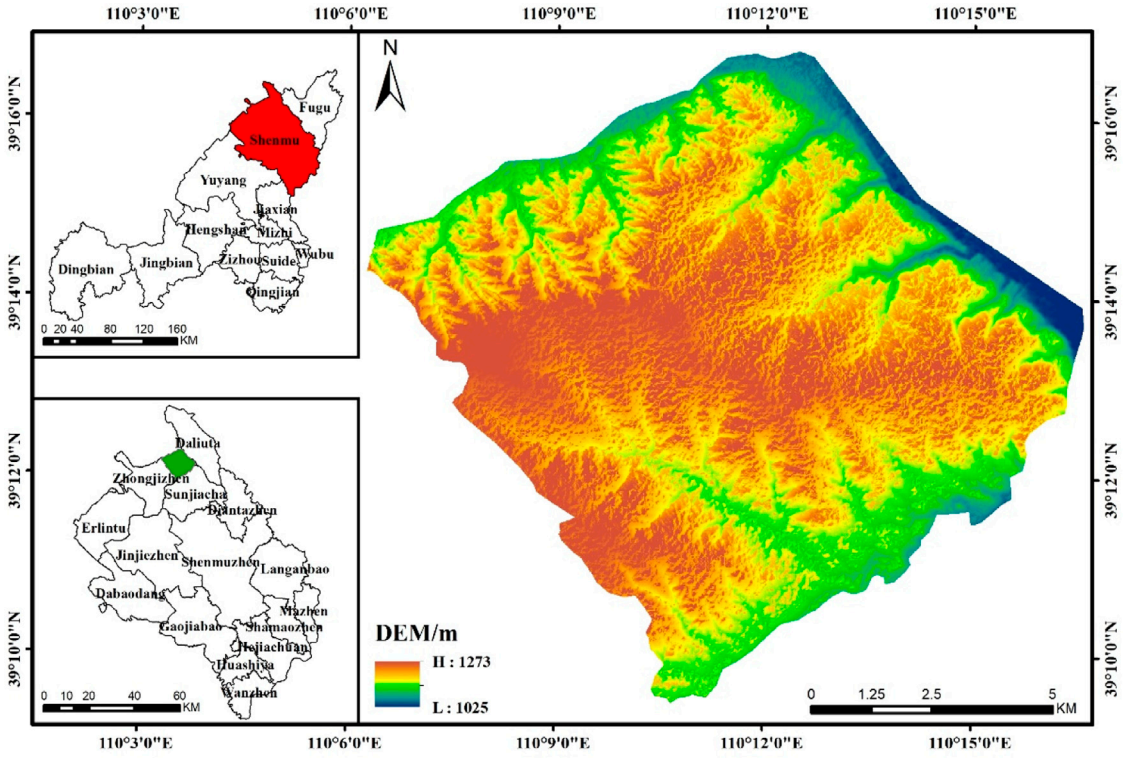

FIGURE 1
Geographical location of the study area.

2 Overview of the study area and data sources

2.1 Overview of the study area

Huojitu Mine of Daliuta Coal Mine area is located in the transition zone between the northern Loess Plateau and the Mu Us Desert between 39°9′32″~39°16′ 51″ N and 110°6′11″~110°16′32″ E, with an area of 110 km^2 (as depicted in Figure 1). This area belongs to the typical shallow-buried high-intensity mining areas in western China. As is typical of continental climates in arid and semi-arid plateau regions, the weather is dry and seldom rains more than 400 mm per year, most of which falls between the months of July and September (Wang et al., 2024). The terrain is characterized by "low around and high in the middle," with an elevation of 1,025 ~ 1,273 m. Erosion, poor corrosion resistance, and a generally loose structure characterize the soil. Vegetation is evenly distributed. Plant communities are mainly drought and cold-resistant psammophytes and xerophytes, showing a sparse shrub landscape. The ecological environment is very fragile and vulnerable to external influences. The coal reserves of the area are estimated to be approximately 950 million tons, with the recoverable reserves measuring 624 million tons. The substantial thickness of the coal mining faces, the shallow depth of the coal seam, the uncomplicated geological conditions. At the same time, the surface cracks in the study area are dense, the soil nutrients are lost and the micro-

topography is broken., and the rapid advancement of the working face result in exacerbated overburden damage and significant surface ecological degradation.

2.2 Data sources and preprocessing

The main data sources used in this research are provided in Table 1.

2.2.1 Raster data

Raster data mainly included digital elevation model (DEM) and Landsat 8/9 OLI satellite data. DEM data has a spatial resolution of 30 m (https://www.gscloud.cn/). ArcGIS 10.8 software is used to mosaic, splice and cut elevation data. Slope and aspect information were extracted using the spatial analysis module to obtain the terrain bit index. Landsat data was used to derive vegetation coverage. The data for May 2023 was obtained on the GEE cloud platform (https://code.earthengine.google.com/) with a temporal resolution of 16 days and a spatial resolution of 30 m. An NDVI image in 2023 was obtained on GEE. Finally, a vector file was used for clipping the NDVI layer to the boundary of the study area.

2.2.2 Vector data

Vector data included land use and mining subsidence data. Land use data in 2023 was provided by the department of natural resources. Mining subsidence data including the mining subsidence prediction and field subsidence monitoring data was provided by the mining enterprises. There are open-pit mines and underground mines in the study area. Open-pit mines have caused serious damage to the surface. The impact of mining activities on the surface include surface subsidence and surface cracks. Due to the timely of cracks in the mining area, the assessment of land damage in the disturbed area of the underground mine is based solely on surface subsidence data, and the evaluation results are converted into 30 m grid data.

2.2.3 Field data

The fieldwork data encompassed soil data, collected in May 2023. A total of 72 sample points was selected in the 110 km^2 study area. The distribution of sample points is shown in Figure 2. The flora in the study area predominantly consists of drought-resistant species, including sea buckthorn. The roots are extensive, with the majority concentrated within the top 20 cm layer of the soil. Therefore, soil samples at the depth of 0 ~ 20 cm were collected from each point to determine total nitrogen, total phosphorus, available nitrogen, available phosphorus and organic matter content (Table 2). The ordinary Kriging method was used to interpolate the soil data in the study area. The soil was resampled to 30 m, to maintain the spatial consistency with other data layers.

3 Research methodology

The paradigm of ecological restoration in mining areas is undergoing a strategic transition from complete reliance on artificial interventions toward moderate human assistance to facilitate natural regeneration, ultimately establishing a hybrid framework where artificial restoration serves as supplementary support to nature-driven rehabilitation. This evolving approach, profoundly aligned with the inherent mechanisms of vegetation succession, demonstrates enhanced compatibility with ecosystem self-organization processes. Under this conceptual framework, blanket interventions targeting all restoration obstacles across the study area prove scientifically unsound.

To systematically identify critical limiting factors in different subregions, this study employs an obstacle degree model for quantitative assessment of ecological constraints. Grounded in Shelford's Law of Tolerance (proposed by American ecologist Victor Ernest Shelford in 1913), which postulates that organism survival and reproduction are governed by multiple ecological factors operating within species-specific tolerance ranges, we conduct a rigorous analysis of ecosystem vulnerability thresholds. Through integration of Shelford's limiting factor theory with spatial diagnostics, this research precisely pinpoints dominant obstacles as restoration priorities—those factors exceeding biological tolerance limits and constituting primary ecological bottlenecks.

This methodology enables science-based optimization of intervention intensity, strategically removing critical barriers while preserving ecosystem autonomy. The implemented measures effectively catalyze spontaneous vegetation recovery processes, ultimately achieving sustainable self-restoration and development of regional ecosystems through minimized yet targeted human assistance.

3.1 Obstacle factor index system

Table 3 shows the results of the study's index system of ecological restoration obstacles in mining areas. The study area exhibits pronounced surface deformation induced by intensive anthropogenic excavation activities. Superimposed upon its unique geomorphic setting within the transitional zone of the Loess Plateau, this region demonstrates dramatic topographic relief. Concomitantly, the surface soil structure displays marked degradation trends, primarily manifested through enhanced sandification and organic matter depletion. Meanwhile, densely distributed industrial and mining operations have amplified regional ecological stress, while frequent human engineering activities (e.g., road construction and settlement expansion) have precipitated highly fragmented patterns in vegetation coverage zones. The synergistic interactions of these multiple stressors have resulted in direct vegetation destruction and progressive degradation of ecological functionality. Eleven factors were selected from five categories: vegetation cover, soil, ecological landscape, land damage, and site conditions.

3.2 Key elements of ecological restoration in the mining area based on the obstacle degree model

3.2.1 Obstacle factor and degree calculation based on the obstacle degree model

The identification of the key elements of ecological restoration in mining area based on obstacle degree model includes: determining the weight of each obstacle factor by entropy weight method,

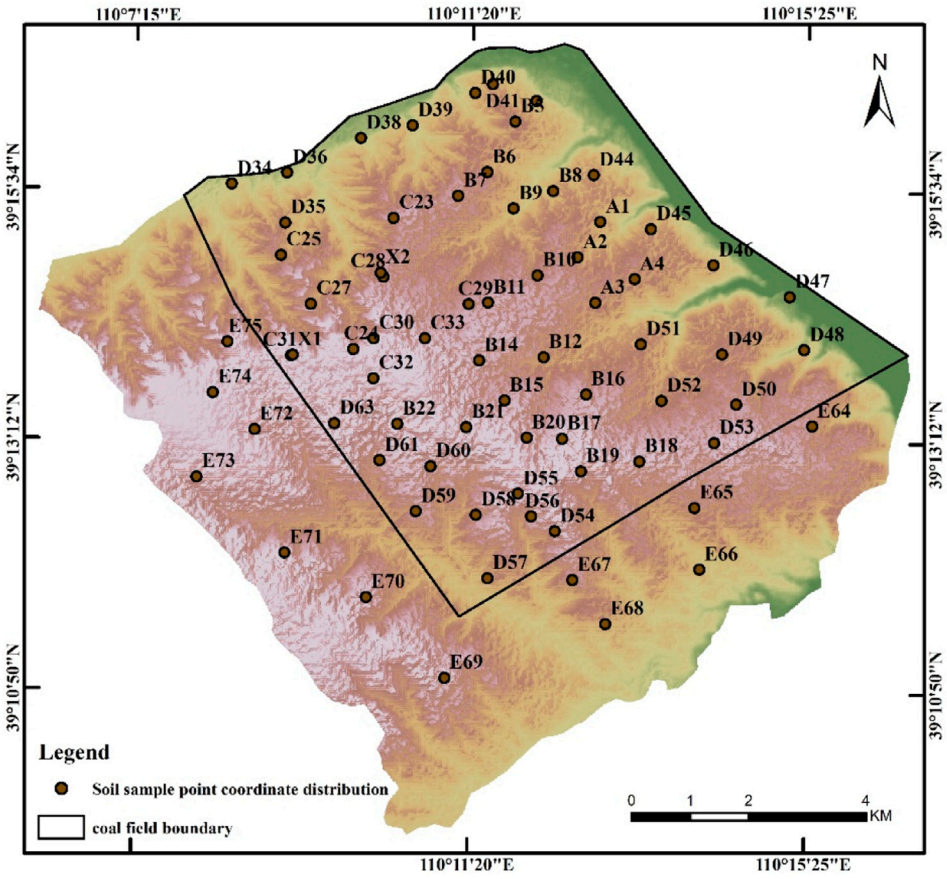

FIGURE 2
The distribution map of soil sampling points in the study area.

calculating the obstacle degree of each obstacle factor affecting the ecology of mining area, and calculating the obstacle degree of each target layer. After determining the obstacle degree of each obstacle factor, the obstacle factors are sorted. The specific steps are as follows:

(1) The entropy weight method is used to determine the factor contribution

The factor contribution reflects the importance of each obstacle factor to the ecological restoration of the mining area. This study employed the entropy weight method to ascertain the weight of each obstacle factor, effectively mitigating the impact of subjective evaluation on the weights and enhancing their accuracy. The procedure for ascertaining the weight of obstacle factors is as follows:

The values of n indicators for y evaluation objects as the initial matrix are represented by A, as shown in Formula 1:

$$A = \begin{bmatrix} a_{11} & a_{12} & \cdots & a_{1y} \\ a_{21} & a_{22} & \cdots & a_{2y} \\ \vdots & \vdots & \ddots & \vdots \\ a_{n1} & a_{n2} & \cdots & a_{ny} \end{bmatrix} \quad (1)$$

Normalized matrix A is then used to obtain the normalized matrix B, as shown in Formula 2:

$$B = \begin{bmatrix} b_{11} & b_{12} & \cdots & b_{1y} \\ b_{21} & b_{22} & \cdots & b_{2y} \\ \vdots & \vdots & \ddots & \vdots \\ b_{n1} & b_{n2} & \cdots & b_{ny} \end{bmatrix} \quad (2)$$

The meaning of b_{ij} is like the Formula 3:

$$b_{ij} = \frac{a_{ij} - min(a_i)}{max(a_i) - min(a_i)} \quad (3)$$

Here, $max(a_i)$ and $min(a_i)$ respectively represent the maximum and minimum values of the ith row of matrix A.

Then the entropy value is calculated as:

$$H_i = -\frac{1}{ln(m)} \sum_{j=1}^{m} \left(\frac{b_{ij}}{\sum_{k=1}^{m} b_{ik}} ln \frac{b_{ij}}{\sum_{k=1}^{m} b_{ik}} \right) \quad (4)$$

In Formula 4 $j = 1 \cdots m$, where m represents the number of classification levels, b_{ik} represents the sum of the ith row of matrix B, and $H_i (i = 1 \cdots n)$ denotes the ith entropy value.

Finally, n entropy weights corresponding to n indexes are calculated according to Formula 5:

$$\omega_i = \frac{1 - H_i}{n - \sum_{i=1}^{n} H_i} \quad (5)$$

The n entropy weights must satisfy the condition $\sum_{i=1}^{n} \omega_i = 1$.

TABLE 2 Sampling point data.

No	TN g/kg	TP g/kg	OM g/kg	ANN mg/kg	AP mg/kg
A1	0.42	0.35	0.58	22	1.4
A2	0.14	0.21	0.12	8	0.8
A3	0.52	0.41	0.60	16	2.0
A4	0.26	0.39	0.23	15	1.6
B5	0.36	0.43	0.33	22	2.7
B6	0.24	0.43	0.28	16	2.0
B7	0.34	0.38	0.34	26	1.2
B8	0.38	0.45	0.21	19	0.8
B9	0.56	0.60	0.55	34	4.2
B10	0.20	0.34	0.28	12	2.6
B11	0.35	0.47	0.43	38	2.1
B12	0.33	0.40	0.36	18	2.2
B14	0.43	0.51	0.48	12	2.2
B15	0.62	0.66	0.73	32	2.6
B16	0.55	0.63	0.60	26	5.0
B17	0.68	0.58	0.69	25	2.4
B18	0.44	0.50	0.44	28	2.6
B19	0.52	0.50	0.55	44	2.4
B20	0.40	0.53	0.40	28	1.0
B21	0.39	0.30	0.36	34	1.0
B22	0.45	0.35	0.33	33	2.0
C23	0.53	0.40	0.71	31	2.4
C24	0.31	0.42	0.31	26	2.1
C25	0.42	0.44	0.70	27	3.4
C27	0.51	0.73	0.76	32	3.4
C28	0.20	0.29	0.34	12	1.3
C29	0.56	0.42	0.57	30	2.2
C30	0.21	0.46	0.13	16	5.6
C31	0.68	0.43	0.70	46	33.6
C32	0.44	0.43	0.48	27	1.6
C33	0.56	0.49	0.67	30	1.8
D34	0.32	0.45	0.56	20	2.0
D35	0.15	0.77	0.16	19	1.6
D36	0.26	0.64	0.47	16	2.4
D38	0.99	0.97	1.76	76	20.6
D39	0.19	0.63	0.22	46	1.8
D40	0.32	0.64	0.47	32	1.4
D41	0.37	0.40	0.39	40	2.4

(Continued on following page)

TABLE 2 (*Continued*) Sampling point data.

No	TN g/kg	TP g/kg	OM g/kg	ANN mg/kg	AP mg/kg
D42	0.42	0.30	0.42	32	1.3
D44	0.34	0.28	0.38	25	1.8
D45	0.53	0.42	0.61	32	1.6
D46	0.52	0.41	0.69	38	4.6
D47	0.10	0.32	0.04	16	0.8
D48	0.17	0.32	0.14	18	1.1
D49	0.46	0.31	0.44	32	2.6
D50	0.46	0.41	0.44	20	3.2
D51	0.30	0.40	0.46	26	1.8
D52	0.41	0.47	0.50	33	2.9
D53	0.47	0.49	0.46	28	1.7
D54	0.39	0.58	0.37	20	1.6
D55	0.24	0.43	0.38	26	1.9
D56	0.60	0.57	0.67	22	2.4
D57	0.37	0.46	0.36	24	1.3
D58	0.23	0.51	0.20	19	3.0
D59	0.38	0.57	0.20	20	0.6
D60	0.31	0.54	0.22	23	1.8
D61	0.38	0.43	0.34	23	1.6
D63	0.44	0.37	0.32	28	2.6
E64	0.46	0.30	0.64	13	3.5
E65	0.21	0.34	0.16	22	2.6
E66	0.26	0.49	0.20	28	1.2
E67	0.74	0.45	0.74	42	2.0
E68	0.42	0.44	0.42	27	2.2
E69	0.36	0.39	0.40	19	1.8
E70	0.16	0.30	0.10	15	2.8
E71	0.24	0.33	0.18	18	0.7
E72	0.32	0.28	0.35	16	2.0
E73	0.44	0.43	0.32	10	2.0
E74	0.24	0.35	0.14	16	1.4
E75	0.24	0.42	0.14	16	0.7
X1	0.47	0.56	0.50	32	3.2
X2	0.28	1.13	0.31	18	1.4

(2) The deviation of the obstacle factor indicators is determined

The deviation of the obstacle factor indicators for the ecological restoration of the mining areas indicates the distance between each obstacle factor and the overall goal of ecological restoration in the mining area. It is calculated as:

Matrix A is normalized to obtain the standardized matrix X:

$$X = \begin{bmatrix} x_{11} & x_{12} & \cdots & x_{1y} \\ x_{21} & x_{22} & \cdots & x_{2y} \\ \vdots & \vdots & \ddots & \vdots \\ x_{n1} & x_{n2} & \cdots & x_{ny} \end{bmatrix} \quad (6)$$

TABLE 3 Index system of ecological restoration obstacle factors in mining area.

Main layer	Criterion	Indicator	Type
Evaluation of obstacle factors of ecological restoration in the mining area	Edaphic condition	Soil total phosphorus	Positive indexes
		Soil total nitrogen	Positive indexes
		Soil available phosphorus	Positive indexes
		Soil alkaline nitrogen	Positive indexes
		Soil organic matter	Positive indexes
	Site condition		Negative indicators
	Vegetation coverage conditions	Vegetation coverage	Positive indexes
	Ecological landscape conditions	Landscape fragmentation	Negative indicators
		Patch density	Negative indicators
		Shannon diversity index	Negative indicators
	Surface damage conditions	Damage degree	Negative indicators

Where x_{ij} is:

$$x_{ij} = \frac{a_{ij}}{\sqrt{\sum_{i=1}^{n} a_{ij}^2}} \tag{7}$$

Matrix I represents the indicator deviation degree, indicating the gap between the actual value of the indicator and the optimal value:

$$I = 1 - X \tag{8}$$

(3) The obstacle factor obstacle degree is determined

The obstacle degree signifies the extent to which each obstacle factor impedes ecological restoration in mining areas, which calculated as:

By assuming a matrix O_{ij} representing the indicator's obstacle degree, one would obtain:

$$O_{ij} = \frac{\omega_j I_{ij}}{\sum_{j=1}^{n} \omega_j I_{ij}} \tag{9}$$

3.2.2 Shefold's restrictive law is used to identify key elements for ecological restoration

According to Equations 6–10, the obstacle degree O_{ij} of each key element in the region is calculated, and these obstacle factors are ranked in a descending order. According to Shefold's restrictive law any deficiency in the quantity and quality of an ecological factor will lead to vegetation degradation or affect survival. The primary elements that hinder ecological restoration in mining regions are not the highest-ranked factors, but rather those with the lowest rankings, indicating the greatest obstacle degree. Therefore, the diagnostic model for the key elements in ecological restoration of mining areas can be expressed as:

$$O = \max\left(O_{ij}\right) \tag{10}$$

Where O represents the obstacle degree of the key elements in ecological restoration of mining areas.

4 Results

4.1 Indicator weight results

The weights of ecological restoration obstacle factors in the study area are provided in Table 4.

4.2 Obstacle degrees

This study divided the research area into a grid of 450 rows and 495 columns, with each grid cell measuring 30 m × 30 m, using the grid as the evaluation unit. From five aspects—soil conditions, site, vegetation cover, ecological landscape, and surface damage—and after calculating the weights and obstacle degrees of various ecological restoration obstacle factors, the natural breaks method (Jenks optimization) was systematically applied to classify obstacle intensities into four distinct tiers, the distribution of obstacle degrees for each indicator was obtained (Table 5).

4.2.1 Soil conditions

The obstacle degree of soil conditions is calculated based on five nutrient indicators: soil alkaline hydrolysis nitrogen, available phosphorus, organic matter, total nitrogen, and total phosphorus. The distribution of soil nutrient obstacle degrees are shown in Figure 3. As can be seen in Figure 4, the obstacle degree of soil condition ranges from 0.00 to 0.10. The total area of the regions with an obstacle degree less than 0.07 (i.e., Level III and IV) was 29.45 km^2, accounting for 26.62% of the total research area. The total area of the regions with an obstacle degree between 0.07 and 0.09 (i.e., Level II) was 48.26 km^2, representing 43.62% of the total research area. These regions were mainly distributed outside the underground mining area and within the secondary mining area. The total area of the regions with an obstacle degree between 0.09 and 0.10 (i.e., Level I) was 32.93 km^2, comprising 29.76% of the total research area, primarily located in the primary mining area and the eastern part of the research area. Overall, the soil condition

TABLE 4 The weights of ecological restoration obstacle factors in the study area.

Layer	Criterion	Indicator	Weight
Evaluation of obstacle factors of ecological restoration in mining area	Edaphic condition	Soil total phosphorus	0.0840
		Soil total nitrogen	0.0731
		Soil available phosphorus	0.0833
		Soil alkaline nitrogen	0.0886
		Soil organic matter content	0.0988
	Site condition	Gradient	0.1014
	Vegetation coverage conditions	Vegetation coverage	0.0884
	Ecological landscape conditions	Landscape fragmentation	0.0846
		Patch density	0.0796
		Shannon diversity index	0.1125
	Surface damage conditions	Damage degree	0.1057

TABLE 5 Statistical classification of obstacle degrees for ecological restoration factors in the research area.

Level	Obstacle degree									
	Soil conditions		Site condition		Vegetation coverage conditions		Ecological landscape conditions		Surface damage condition	
	Area/ km^2	Proportion/ %	Area/ km^2	Proportion/ %	Area/ km^2	Proportion/ %	Area/ km^2	Proportion/ %	Area/ km^2	Proportion/ %
level I	32.93	29.76	3.63	3.28	34.97	31.61	22.76	20.57	9.67	10.70
Level II	48.26	43.62	15.42	13.93	51.43	46.48	4.09	3.71	9.78	10.82
Level III	27.24	24.62	36.02	32.56	20.01	18.09	17.57	15.88	13.05	14.44
Level IV	2.21	2.00	55.57	50.23	4.23	3.82	66.21	59.84	67.50	74.68
Footing	110.64	100	110.64	100	110.64	100	110.64	100	110.64	100

in the research area was relatively good, with all regions having soil condition obstacles below 0.10.

4.2.2 Obstacle degree of site conditions

As in Figure 5, the obstacle degree of the site conditions was distributed between 0 and 0.62. However, areas with a higher obstacle degree were mainly located in the hilly regions surrounding the research area, with the eastern and northern regions being most prominent. The area where the obstacle degree of site conditions exceeds 0.24 was 3.63 km^2, accounting for 3.28% of the total area of the research zone. In other areas, the overall site condition was relatively good, with essentially no obstacles.

4.2.3 Obstacle degree of vegetation coverage conditions

From Figure 6, it can be seen that the obstacle degree of vegetation coverage conditions ranges from 0 to 0.10. The area with an obstacle degree of less than 0.08 (i.e., Level IV and Level III), primarily distributed in the southwestern part of the study area, was 24.24 km^2, accounting for 21.91% of the total area. The area with an obstacle degree between 0.08 and 0.09 (i.e., Level II) was 51.43 km^2, making up 46.48% of the total area of the research zone. The area with an obstacle degree between 0.09 and 0.10 (i.e., Level I) was 34.97 km^2, accounting for 31.61% of the total area, mainly located in the open-pit mines in the northern part and the urban areas in the eastern part of the research area.

4.2.4 Obstacle degree of ecological landscape conditions

The ecological landscape condition included landscape diversity index, landscape patch density index, and landscape separation index as shown in Figure 7. Landscape diversity can increase the complexity and stability of the ecosystems, promoting ecological restoration in mining areas. The landscape fragmentation index and patch density index directly affect the difficulty of ecological restoration. Higher patch density and landscape fragmentation

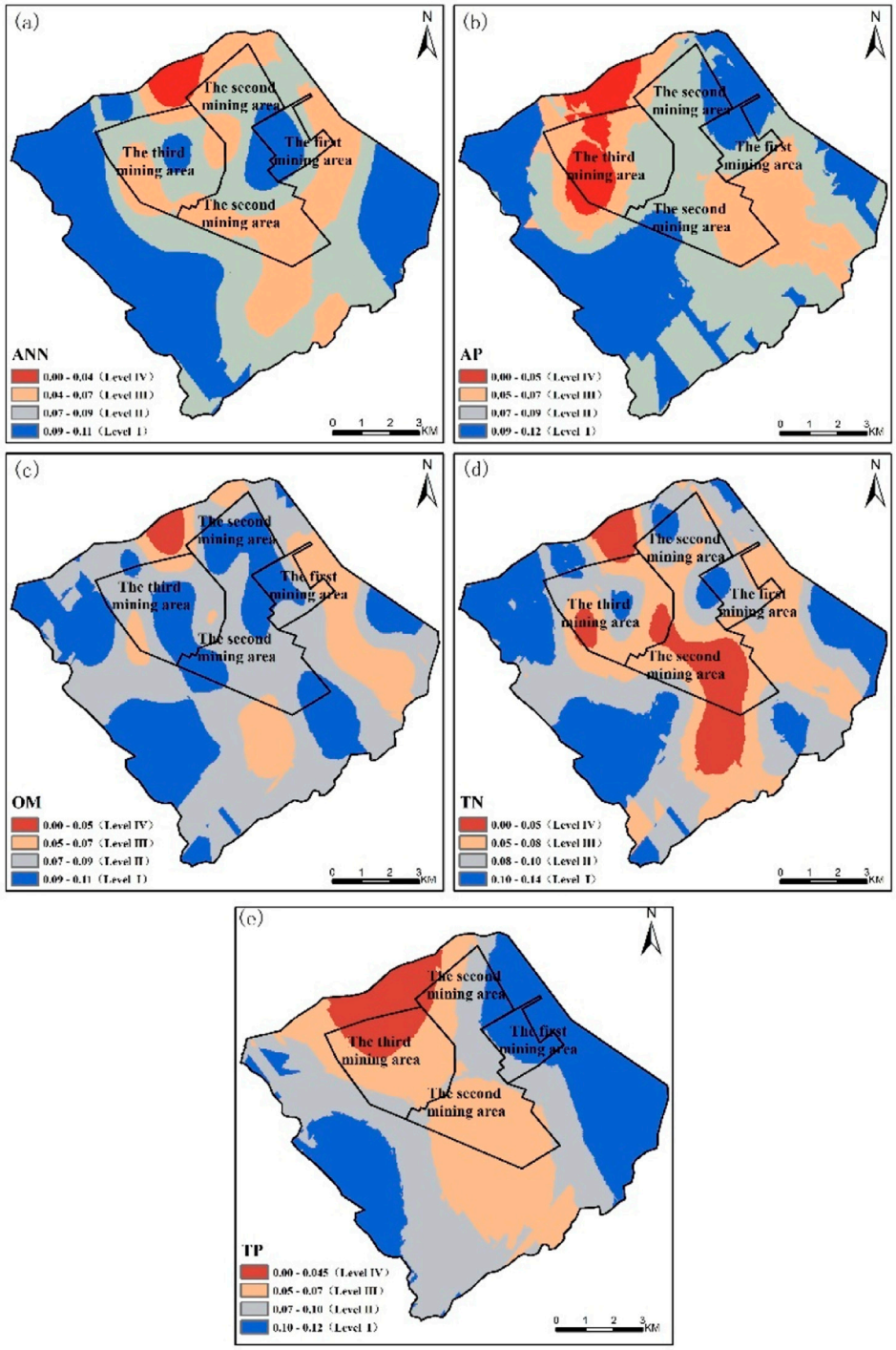

FIGURE 3
Obstacle Degree of Soil Condition **(a)** Alkaline Hydrolysis Nitrogen; **(b)** Available Phosphorus; **(c)** Organic Matter; **(d)** Total Nitrogen; **(e)** Total Phosphorus).

values indicate a higher degree of landscape fragmentation, necessitating proactive measures to reduce the number of patches, enhance patch connectivity, and promote ecological recovery. As seen in Figure 8, the obstacle degree of ecological landscape condition in the study area was relatively low, with an area greater than 0.11 (i.e., Levels I and II) covering 26.85 km^2, accounting for 24.28% of the total area. The elevated obstacle degree was primarily attributable to fragmented plots, significantly influenced by the occupation and fragmentation of construction land, resulting in increased landscape fragmentation, which subsequently impairs ecological restoration efficiency in the mining area.

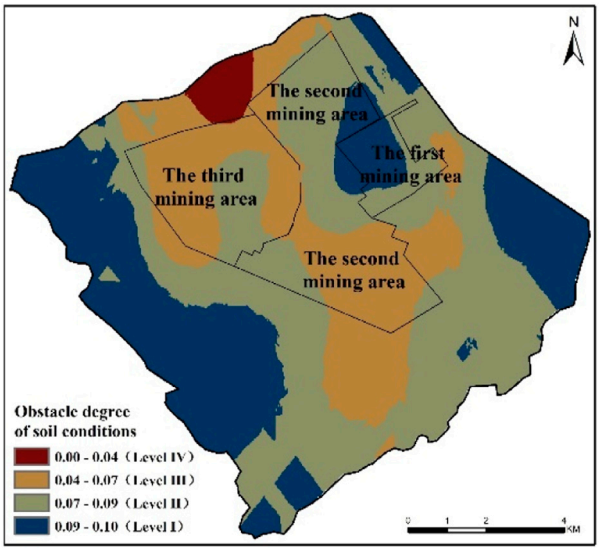

FIGURE 4
Comprehensive obstacle degree of soil condition in the research area.

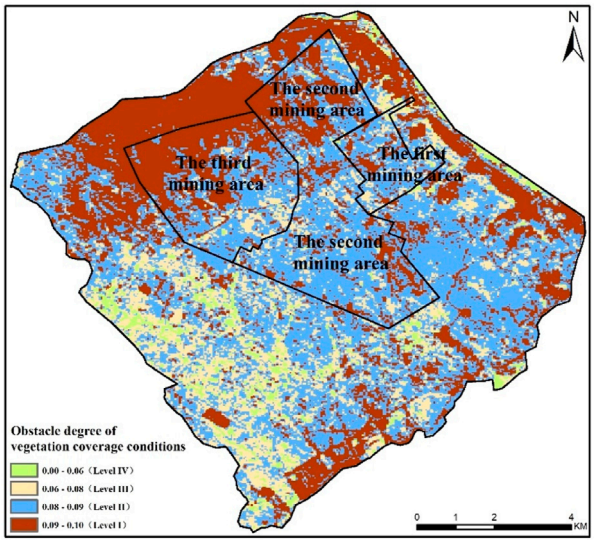

FIGURE 6
Obstacle degree of vegetation coverage conditions.

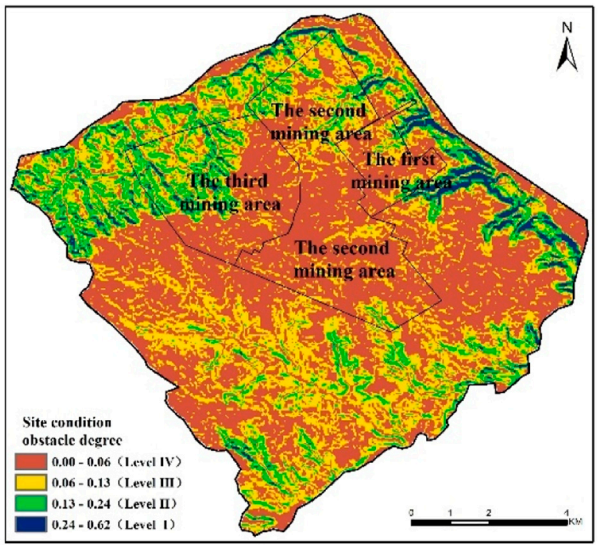

FIGURE 5
Obstacle degree of site conditions.

4.2.5 Obstacle degree of surface damage conditions

The results of the obstacle degree of surface damage condition are shown in Figure 9. The undisturbed zone covered 74.68 km^2, accounting for 67.50% of the total area. The area with an obstacle degree ranging from 0.03 to 0.22 (i.e., levels II and III) was 25.26 km^2, accounting for 22.83% of the total area. This region was predominantly located within the disturbed zone of the subterranean mines. The area with an obstacle degree ranging from 0.22 to 0.59 (i.e., level I) covered 10.70 km^2, accounting for 9.67% of the total. It was mainly located in the disturbed area of the open-pit mines in the northern part of the study area.

4.3 Identification of key elements for ecological restoration in mining areas

Ecological restoration in mining regions must identify the most pressing needs and key elements affecting restoration efforts, in order to specifically mitigate these obstacles during the restoration process and tackle the primary issues. Therefore, this paper analyzes the obstacle degree of various ecological restoration obstacle factors and calculates the key elements for ecological restoration in each region based on the Shefold's restrictive law. The distribution of the key elements for ecological restoration in the study area is shown in Table 6; Figure 10.

The distribution of key factors for ecological restoration in the study area is shown in Figures 5–8. The region affected by land degradation, which is pivotal for ecological restoration, spans 21.25 km^2, representing 19.20% of the total study area, predominantly located in the open-pit mining zone, secondary mining zone, and tertiary mining zone. This is followed site condition (19.74 km^2~ 17.84%) in the hilly areas surrounding the study area; soil condition (35.29 km^2~31.91%) located in the cultivated land in the western and central parts of the study area, the observed phenomenon primarily stems from the gentle topography and peripheral positioning beyond underground mining disturbance zones in these areas, where land degradation remains comparatively mild. Such geomorphological advantages create fundamentally favorable edaphic conditions for spontaneous vegetation recovery. Paradoxically, despite these advantageous preconditions, soil nutrient constraint intensity emerges as the predominant limiting factor, presenting a critical bottleneck that substantially impedes ecological restoration progress in these

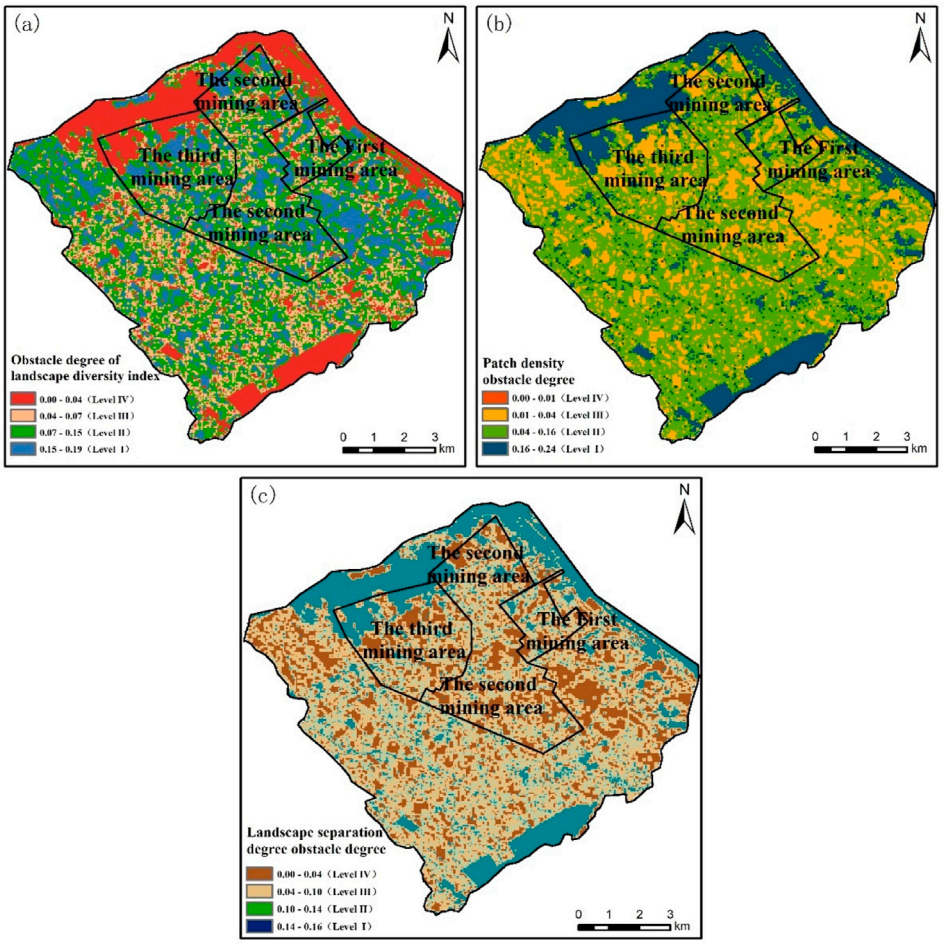

FIGURE 7
Obstacle degree of ecological landscape condition **(a)** landscape diversity index; **(b)** patch density; **(c)** landscape separation degree).

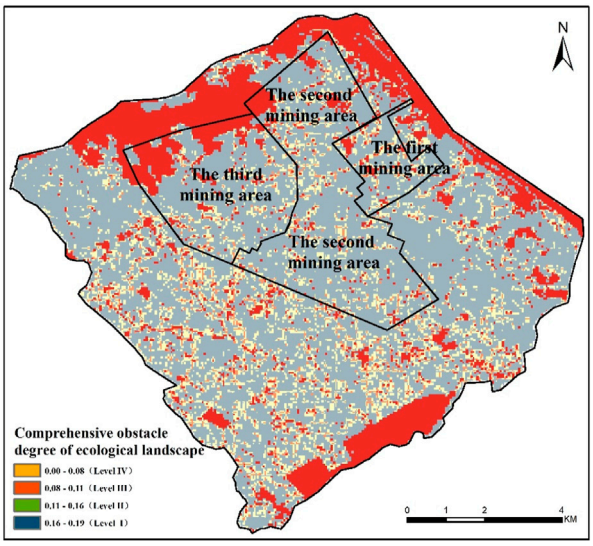

FIGURE 8
Comprehensive obstacle degree of ecological landscape condition.

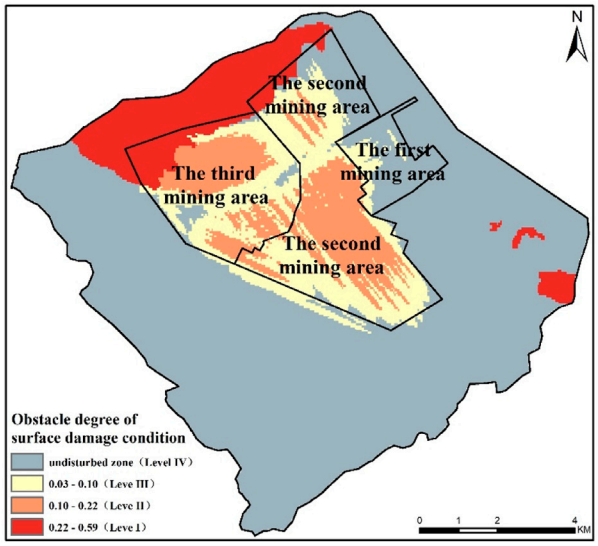

FIGURE 9
Obstacle degree of land damage level.

TABLE 6 Key elements Areal cover for ecological restoration in the study area.

Layer	Criterion	Indicator	Area/ km^2	Proportion/ %
Evaluation of obstacle factors of ecological restoration in mining area	Edaphic condition	Total phosphorus content of soil	15.06	13.61
		Soil total nitrogen	8.48	7.66
		Soil available phosphorus content	6.48	5.86
		Soil alkaline nitrogen content	2.56	2.33
		Organic matter content	2.71	2.45
	Site condition	Gradient	19.74	17.84
	Vegetation coverage conditions	Vegetation coverage	3.34	3.02
	Ecological landscape conditions	Landscape fragmentation	13.40	12.11
		Patch density	15.06	13.61
		Shannon diversity index	2.56	2.31
	Surface damage conditions	Damage degree	21.25	19.20

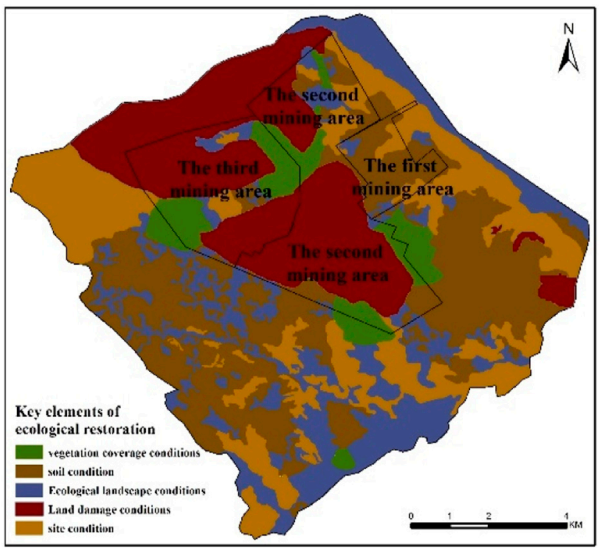

FIGURE 10
Distribution of key elements for ecological restoration in the study area.

specific sectors; vegetation cover (3.34 km^2~ 3.02%) distributed at the boundary between the disturbed open-pit mining area and the tertiary mining area, as well as the boundary of the primary mining area; and, ecological landscape (31.08 km^2~ 28.03%) located within the urban disturbance area.

Various levels of focused intervention strategies are necessary depending on the kinds of key elements for ecological restoration in the research region. In terms of area, regions where soil conditions and ecological landscape conditions were considered as key factors had the widest range, primarily distributed in relatively flat areas outside the disturbed zones of underground and open-pit mining area. This area poses relatively low restoration difficulty. Improving soil conditions and restoring surface vegetation are crucial steps in the subsequent ecological restoration process. These actions will help achieve the specific restoration goals of enhancing the continuity and diversity of the ecological landscape.

From the perspective of restoration difficulty, regions where land degradation and site conditions were the key factors for ecological restoration posed the greatest challenges. These areas were mainly distributed in the open-pit mining, underground mining, and the gully zones disturbed areas surrounding the study area. For those areas with significant site condition obstacles, techniques such as slope protection and anchor reinforcement should be employed for vegetation recovery, with long-term monitoring and maintenance afterward to prevent vegetation degradation. For areas with significant surface damage obstacles, different restoration methods should be applied based on the types of surface damage. It is recommended to employ geomorphological reconstruction and soil improvement techniques to make the restored ecosystem more self-sufficient in areas where land degradation has occurred as a result of excavation and compaction. In regions significantly impacted by surface subsidence, it is essential to consider factors such as mining face and extraction intensity parameters, and to develop a cooperative restoration model for source damage mitigation and vegetation rehabilitation.

Within subsurface mining zones exhibiting moderate disturbance intensities, soil nutrient deficiency emerges as the dominant constraint factor. Conversely, in intensively disturbed sectors and surface mining areas, geomorphological destruction constitutes the primary restoration bottleneck, where catastrophic terrain alterations necessitate landform reconstruction as the prerequisite rehabilitation objective. This spatial divergence in constraint mechanisms reveals a fundamental dichotomy between edaphic limitation and geotechnical challenges in post-mining ecosystem recovery.

5 Discussion

In this study, when calculating the degree of obstacles, the degrees of obstacles related to soil conditions, vegetation cover conditions, and ecological landscape conditions are generally low, distributed in the ranges of 0–0.1, 0–0.094, and 0–0.194, respectively. In contrast, the degrees of obstacles associated with site conditions and land damage conditions are relatively high, concentrated in the ranges of 0–0.62 and 0.033–0.589.

In the distribution of key ecological restoration factors, the area where soil conditions, vegetation cover conditions, and ecological landscape conditions are considered key factors for ecological restoration reaches 69.71 km^2, accounting for 62.96% of the total area of the study area. This indicates that in the study area, the maximum degree of obstacle factors is primarily below 0.2 in most regions, suggesting that only positive interventions are needed in the subsequent restoration process to achieve ecological self-recovery. In contrast, the total area where site conditions and land damage conditions are key factors for ecological restoration is 40.99 km^2, making up 37.04% of the total area, and the degree of obstacle factors in this portion is high, resulting in greater restoration difficulty.

Based on the Shefold restrictive theorem, this study identifies the obstacle factor with the highest degree of obstruction in the region as a key element for ecological restoration. Targeted restoration measures are further applied to different key ecological restoration factors to reduce the negative impacts of obstacle factors on the ecology of the mining area, enhance the ecological stability of the area, and promote ecological construction. The proposed management measures and recommendations are as follows:

(1) Conventional obstacle degree models predominantly focus on quantifying constraint intensities and analyzing their spatial distributions, yet critically lack systematic prioritization mechanisms for multiple coexisting constraints within defined geographical units. Addressing this methodological gap, our study introduces an innovative identification framework that integrates maximum constraint screening with traditional obstacle degree calculations. This advancement enables systematic identification of the dominant limiting factor—the variable exhibiting peak obstacle intensity—which constitutes the pivotal restoration determinant in target areas.

(2) This study reveals the spatial differentiation characteristics of key elements in mining area ecological restoration and their coupling mechanisms with mining activities. Spatial analysis demonstrates significant spatial coupling between regions where land damage constitutes the critical ecological restoration element and the distribution of underground mining subsidence zones and open-pit mining areas, indicating that mining engineering directly induces the destruction of surface soil structures. Restoration areas where site conditions are identified as the key ecological restoration element exhibit pronounced spatiotemporal heterogeneity, with their spatial distribution patterns showing a significant positive correlation with topographic factors (slope), which highlights the foundational control of terrain elements on ecological restoration processes. Notably, restoration units constrained by vegetation cover conditions and soil physicochemical properties display spatial distribution characteristics distinct from secondary mining disturbance zones, primarily concentrated in primary mining disturbance zones and non-disturbed areas. This phenomenon suggests that mining activities, by altering surface stress fields and material migration pathways, generate specific ecological degradation gradients. The spatial overlap between ecological degradation units and mining subsidence ranges in the study area conclusively corroborates mining disturbance as the primary driver of regional ecosystem degradation, with impact mechanisms involving multiple stressors such as physical destruction, chemical pollution, and biodiversity loss.

(3) For areas with high obstacle degrees in surface damage conditions, differentiated restoration techniques should be applied based on damage types. In regions impacted by surface excavation and compaction, landform reshaping and soil improvement technologies should be employed to enhance the self-sustaining capacity of reconstructed ecosystems. For areas severely affected by surface subsidence, parameters such as coal mining face configurations and extraction intensity must be considered to establish a collaborative restoration model integrating source damage control and vegetation reconstruction.

(4) In identifying key ecological restoration elements, this study utilized the entropy weight method to determine indicator weights. While this approach enhances objectivity, it assigns weights solely based on data dispersion without distinguishing between positive or negative directional impacts of indicators on ecological restoration. Future research could optimize directional sensitivity by incorporating models such as TOPSIS (Technique for Order Preference by Similarity to Ideal Solution).

6 Conclusion

This article takes the Huojitu mine in a typical shallow buried high-intensity mining area in the western region of China as the research area. From five aspects—vegetation cover, soil, ecological landscape, land degradation, and site conditions—an index system was constructed for the ecological restoration obstacles in the mining area. An identification model for key ecological restoration factors was established, which was based on the coupling of obstacle degree and Shefold's restrictive law. The identification of key ecological restoration factors in the research area was carried out with the main conclusions as follows:

(1) The entropy weight method enhances objectivity in index weighting. The obstacle degree model quantifies deviation from ideal states. Their combination achieves precise identification of critical restoration elements.

(2) Soil condition emerges as the predominant obstacle (35.29 km^2, 31.91%), followed by ecological landscape (31.08 km^2), land damage (21.25 km^2), and site conditions (19.74 km^2).

(3) Differentiated strategies: Soil improvement (micro-topography remodeling + vegetation restoration), site condition areas (lattice slope protection + anchor reinforcement + long-term monitoring), land damage zones (landform reconstruction + source control collaborative restoration).

Data availability statement

The raw data supporting the conclusions of this article will be made available by the authors, without undue reservation.

Author contributions

HZ: Writing – original draft, Writing – review and editing. ZZ: Writing – original draft, Writing – review and editing. SW: Writing – original draft, Writing – review and editing. YoZ: Writing – original draft, Writing – review and editing. ZC: Writing – original draft. YaZ: Writing – original draft. QC: Writing – original draft. YJ: Writing – review and editing. YL: Writing – review and editing. HD: Writing – review and editing.

Funding

The author(s) declare that financial support was received for the research and/or publication of this article. This work was supported by the National Natural Science Foundation of China (Grants: U22A20620, U21A20108), Double First Class Discipline Creation Project of Surveying and Mapping Science and Technology (GCCRC202402). Heartfelt appreciation is also expressed to the anonymous reviewers and the editors, whose insightful comments significantly enhanced the quality of this manuscript.

Conflict of interest

The authors declare that the research was conducted in the absence of any commercial or financial relationships that could be construed as a potential conflict of interest.

Generative AI statement

The author(s) declare that no Generative AI was used in the creation of this manuscript.

Publisher's note

All claims expressed in this article are solely those of the authors and do not necessarily represent those of their affiliated organizations, or those of the publisher, the editors and the reviewers. Any product that may be evaluated in this article, or claim that may be made by its manufacturer, is not guaranteed or endorsed by the publisher.

References

Almassi, B. (2021). Value disputes in urban ecological restoration: lessons from the Chicago Wilderness. *Stud. Hist. Philosophy Sci. Part A* 87, 93–100. doi:10.1016/j.shpsa.2021.03.007

Bendfeldt, E. S., Burger, J. A., and Daniels, W. L. (2001). Quality of amended mine soils after sixteen years. *Soil Sci. Soc. Am. J.* 65, 1736–1744. doi:10.2136/sssaj2001.1736

Chai, N., Zhou, W., and Wan, B. (2022). Research on performance evaluation and obstacle diagnosis for urban water ecological civilization construction based on GFAHP-cloud-FSE model: the case of Shizuishan, China. *Stoch. Environ. Res. Risk Assess.* 36, 3439–3465. doi:10.1007/s00477-022-02203-4

Chen, J. J., Nan, H., Yan, W. T., Guo, W. B., and Zou, Y. F. (2016). Features of surface dynamic movement and deformation caused by high intensity mining with shallow depth. *Coal Sci. Technol.* 44, 158–162. doi:10.13199/j.cnki.cst.2016.03.030

Chen, X. H., and Yang, L. (2013). Obstacle diagnosis model based on the catastrophe progression method and its applications for the small and medium-sized enterprises. *Systeins Engineering-Theory and Pract.* 33, 1479–1485. doi:10.12011/1000-6788(2013)6-1479

Chen, F., Song, X. J., Dong, W. X., Zhu, Y. F., You, Y. N., and Ma, J. (2024). Effects of land reclamation on soil bacterial community assembly and carbon sequestration function in coal mine subsidence area: taking Dongtan Mining Area as an example. *Coal Sci. Technol.* 52, 345–354. doi:10.12438/cst.2023-1221

Cheng, X., Long, R. Y., and Chen, H. (2018). Obstacle diagnosis of green competition promotion: a case study of provinces in China based on catastrophe progression and fuzzy rough set methods. *Environ. Sci. Pollut. Res.* 25, 4344–4360. doi:10.1007/s11356-017-0762-z

Chen, Y., Zhu, M. K., Lu, J. L., Zhou, Q., and Ma, W. B. (2020). Evaluation of ecological city and analysis of obstacle factors under the background of high-quality development: taking cities in the Yellow River Basin as examples. *Ecol. Indic.* 118, 106771. doi:10.1016/j.ecolind.2020.106771

Chi, G. M., Chen, S. S., Wang, W., Wang, S. D., Zhu, Z. Y., Jiao, Y. H., et al. (2024). Research on ecological restoration area delineation in mining area based on Entropy-weighted Extension Matter-element Model: a case study in Huojitu Mine. *J. Henan Polytech. Univ. Sci.*, 1–16. doi:10.16186/j.cnki.1673-9787.2024030082

Crouzeilles, R., Ferreira, M. S., Chazdon, R. L., Lindenmayer, D. B., Sansevero, J. B. B., Monteiro, L., et al. (2017). Ecological restoration success is higher for natural regeneration than for active restoration in tropical forests. *Sci. Adv.* 3, e1701345. doi:10.1126/sciadv.1701345

Cui, Z., Wang, Z. G., Zhang, X. R., Wang, Y. Y., and Zhang, M. (2022). Evaluation of regional environmental carrying capacity and its obstacle indicators diagnosis: evidence from three major urban agglomerations in China. *Front. Environ. Sci.* 10. doi:10.3389/fenvs.2022.1015158

Du, H. D., Cao, Y. C., Nie, W. J., and Song, S. J. (2021). Evolution of soil properties under artificial and natural revegetation in loess gully coal mining subsidence area. *J. China Coal Soc.* 46, 1641–1649. doi:10.13225/j.cnki.jccs.st20.1784

Erofeeva, E. A. (2021). Plant hormesis and Shelford's tolerance law curve. *J. For. Res.* 32, 1789–1802. doi:10.1007/s11676-021-01312-0

Gao, C., Xue, N. Z., He, B. Q., and Deng, W. N. (2019). Study on influence of key strata on surface subsidence law of fully mechanized caving mining in extra-thick coal seam. *Coal Sci. Technol.* 47, 229–234. doi:10.13199/j.cnki.cst.2019.09.029

Guo, W. B., Wu, D. T., Bai, E. H., Zhang, P., Hou, J. J., and Zhang, Y. Z. (2023). Current situation and prospect of intelligent green mining technology in coal mines in China. *J. Henan Polytech. Univ. Sci.* 42, 1–17. doi:10.16186/j.cnki.1673-9787.2022060037

Hao, C. M., Wang, Y. T., Yi, S. H., and Liu, S. (2025). Evolution of microbial carbon sequestration potential in farmland soil driven by natural restoration in coal mine subsidence area. *Coal Sci. Technol.*, 1–15. doi:10.12438/cst.2024-0681

Hu, Z. Q., and Xiao, W. (2020). Some thoughts on green development strategy of coal industry: from aspects of ecological restoration. *Coal Sci. Technol.* 48, 35–42. doi:10.13199/j.cnki.cst.2020.04.002

Huang, H. P., Li, Y. L., and Qiao, X. Z. (2018). Evaluation and barrier factors analysis of agricultural circular economy based on lUOCE: a case study of Jiangxi Province. *Chin. J. Eco-Agriculture* 26, 916–925. doi:10.13930/j.cnki.cjea.170963

Jia, H. F., and Du, P. Y. (2024). Ecological security evaluation and obstacle factor diagnosis in Qinghai Province based on DPSIR-TOPSIS and obstacle degree models. *Res. Agric. Mod.* 45, 296–305. doi:10.13872/j.1000-0275.2024.0020

Jiang, L., Zuo, Q. T., Ma, J. X., and Zhang, Z. Z. (2021). Evaluation and prediction of the level of high-quality development: a case study of the Yellow River Basin, China. *Ecol. Indic.* 129, 107994. doi:10.1016/j.ecolind.2021.107994

Klaus, V. H., and Kiehl, K. (2021). A conceptual framework for urban ecological restoration and rehabilitation. *Basic Appl. Ecol.* 52, 82–94. doi:10.1016/j.baae.2021.02.010

Lei, S. G., Wang, W. Z., Li, Y. Y., Yang, X. C., Zhou, Y. L., Zhao, X. T., et al. (2023). Study on disturbance and restoration of soil organic carbon pool in large-scale open-pit mining areas in Northern China. *Coal Sci. Technol.* 51, 100–109. doi:10.12438/cst.2023-0965

Lei, S. G., Xia, J. N., Bian, Z. F., and Cheng, W. (2024). Near-natural ecological restoration in open-pit mine area. *J. China Coal Soc.* 49, 2021–2030. doi:10.13225/j.cnki.jccs.XH23.1689

Lei, X. P., Qiu, R., and Liu, Y. (2016). Evaluation of regional land use performance based on entropy 'TOPSIS model and diagnosis of its obstacle factors. *Trans. Chin. Soc. Agric. Eng.* 32, 243–253. doi:10.11975/j.issn.1002-6819.2016.13.035

Li, C. H., Huo, H. Y., Li, Y. J., and Hou, Y. (2015). Evaluation of low-carbon city competitiveness and its obstacle indicators analysis in Shandong Province. *Resour. Sci.* 37, 1474–1481. doi:10.12438/cst.2023-1221

Li, J. Y., Chen, X. X., Li, M. W., Zhang, N. N., Zhou, Z. Q., Li, X. M., et al. (2024). Community composition and structure pathways in subalpine forest, Sichuan Province, China. *Aeta Ecol. Sin.* 44, 3471–3482. doi:10.20103/j.stxb.202308151766

Li, X. M., and Yang, J. S. (2010). Indication of diagnosing salinity-alkalinity hazard of typical area in the huanghuaihai plain. *J. Irrigation Drainage* 29, 56–58. doi:10.13522/j.cnki.ggps.2010.04.001

Liao, Y. C., Xie, Y., Liu, J. Y., Zhu, Z. F., and Wu, Y. (2021). Ecological security dynamic assessment and obstacle factors analysis in Jiuzhaigou National Nature Reserve. *Acta Ecol. Sin.* 41, 5950–5960. doi:10.5846/stxb202002130243

Manhaes, A. P., Pantaleao, L. C., Moraes, L. F. D., Amazonas, N. T., Saavedra, M. M., Mantuano, D., et al. (2022). Functional trajectory for the assessment of ecological restoration success. *Restor. Ecol.* 30. doi:10.1111/rec.13665

Mao, X. M., Yang, Q. Y., Xin, G. X., Lu, C. Y., and Peng, K. (2007). Analysis of the main barrier factors for large-scale management of farmland in chongqing municipality. *J. Southwest Univ. Nat. Sci. Ed.*, 146–150. doi:10.13718/j.cnki.xdzk.2007.12.032

Peng, S. P., and Bi, Y. L. (2024). Properties of ecological environment damage and their mechanism of restoration in arid and semi-arid coal mining area of western China. *J. China Coal Soc.* 49, 57–64. doi:10.13225/j.cnki.jccs.YH24.0156

Qu, Y. B., Zhu, W. Y., Y, W. J., Zhang, Y., and Gao, Y. (2017). Land consolidation spatial pattern and diagnosis of its obstacle factors based on pressure-state-response model. *Trans. Chin. Soc. Agric. Eng.* 33, 241–249. doi:10.11975/j.issn.1002-6819.2017.03.033

Shi, H. L., Zhang, L. X., Gan, F. L., Pu, J. B., Gou, J. F., and Liu, J. (2024). Soil quality evaluation and obstacle factors of erosion slop in karst trough valley area. *J. Soil Water Conservation* 38, 126–135. doi:10.13870/j.cnki.stbcxb.2024.02.007

Sun, X. B., Cai, W. M., Kong, X. B., Li, Q. F., and Zhao, J. (2023). Quality regulation pattern and consolidation time zone of county-level-cultivated land based on multi agent collaboration. *Trans. Chin. Soc. Agric. Eng.* 39, 232–245. doi:10.11975/j.issn.1002-6819.202308105

Sun, H., Deng, W., and Zhang, H. (2024). Spatial analysis and planning strategy of Linpan in Western Sichuan based on productionliving-ecological space: a case study of Tianma Town, Dujiangyan. *J. Spatio-temporal Inf.* 31, 431–443. doi:10.20117/j.jsti.202403008

Wang, D. D., Xiao, L., Bi, Y. L., Nie, W. J., and Zhang, K. (2024). Effects of AMF inoculation on plant-soil ecological stoichiometry and nutrient recovery in Shendong mine. *Coal Sci. Technol.* 52, 354–363. doi:10.12438/cst.2023-0273

Wang, Z. G., Huang, L. F., Yin, L. S., Wang, Z. X., and Zheng, D. D. (2022). Evaluation of sustainable and analysis of influencing factors for agriculture sector: evidence from jiangsu province, China. *Front. Environ. Sci.* 10. doi:10.3389/fenvs.2022.836002

Xia, M. F., Yu, H. M., Li, S., and Dan, C. L. (2021). Obstacle factor diagnosis of well-facilitated farmland construction based on ecological niche in Poyang Lake Plain. *J. China Agric. Univ.* 26, 182–190. doi:10.11841/j.issn.1007-4333.2021.07.18

Xiao, W., Ren, H., Zhao, Y. L., Wang, Q. Y., and Hu, Z. Q. (2023). Monitoring and early warning the spontaneous combustion of coal waste dumps supported by unmanned aerial vehicle remote sensing. *Coal Sci. Technol.* 51, 412–421. doi:10.13199/j.cnki.cst.2022-1901

Xu, F. Y., Guo, W. B., and Wang, C. (2023). Research on surface subsidence law in high-intensity mining of shallow buried with thick coal seam. *Coal Sci. Technol.* 51, 11–20. doi:10.13199/j.cnki.cst.2021-0821

Yang, D. M., Guo, W. B., Tan, Y., Wang, Y. X., Ma, X. C., and Li, Z. (2019). Lithology and fissure characteristics of overburden in high-intensity mining. *J. China Coal Soc.* 44, 786–795. doi:10.13225/j.cnki.jccs.2018.6044

Yang, J. Z., and Liu, Q. J. (2020). Analysis and measured of strata behavior law and mechanism of 8.8 m ultra-high mining height working face. *Coal Sci. Technol.* 48, 69–74. doi:10.13199/j.cnki.cst.2020.01.009

Yang, Z. K., Zhang, J. H., and Zhang, N. (2020). Key technology in complete set of equipment for high cutting fully mechanized caving face in extra-thick soft coal. *Coal Eng.* 52, 123–126. doi:10.11799/ce202008026

Yang, F., Chen, Z. M., and Gong, S. L. (2022). Evaluation of land resource carrying capacity in Liaoning Province based on AHP-entropy weight TOPSIS model. *Bull. Soil Water Conservation* 42, 144–149. doi:10.13961/j.cnki.stbctb.2022.01.020

Yang, Z., Li, C. W., Ren, Z. Y., Li, P., Xu, Y. T., Han, J. C., et al. (2023). Evaluation of land use performance in ningxia, China based on entropy-weight TOPSIS model and diagnosis of its obstacle factors. *J. Earth Sci. Environ.* 45, 796–805+766. doi:10.19814/j.jese.2022.08039

Yao, Q. L., Yu, L. Q., Chen, S. Y., Lil, Y. H., and Li, X. H. (2025). Mining-affected water resources and ecological effects in ecologically fragile mining areas of western China. *J. China Coal Soc.*, 1–22. doi:10.13225/j.cnki.jccs.2023.1695

Yi, D., Ding, G. Q., Han, Y., Yi, J. L., Guo, J., and Ou, M. H. (2023). Integrated assessment and critical obstacle diagnosis of rural resource and environmental carrying capacity with a social-ecological framework: a case study of Liyang county, Jiangsu Province. *Enviroment Sci. Pollut. Res.* 30, 76026–76043. doi:10.1007/s11356-023-27509-w

Zhao, B. H., Huang, J. H., Li, Z. B., Li, Q., and Zhou, C. Y. (2023). Comprehensive evaluation and influencing factor analysis of urban ecological water security in Gansu Province based on AHP-entropy method. *Bull. Soil Wateronservation* 43, 167–173+213. doi:10.13961/j.cnki.stbctb.2023.01.020

Zhao, S. X., Niu, H. P., Zhang, H. W., Zhang, H. B., and Zhang, X. H. (2016). Suitability evaluation on high quality capital farmland consolidation based on niche-fitness model. *Trans. Chin. Soc. Agric. Eng.* 32, 220–228. doi:10.11975/j.issn.1002-6819.2016.12.032

Zhao, Z. T., Kong, X. B., Zhang, X. L., Chen, W. G., Liao, Y. B., and Yao, D. H. (2022). Method for zoning high-standard ecological farmland construction using multi-dimensional super-volume ecological niche. *Trans. Chin. Soc. Agric. Eng.* 38, 253–263. doi:10.11975/j.issn.1002-6819.2022.13.028

frontiers | Frontiers in Environmental Science

TYPE Original Research
PUBLISHED 15 May 2025
DOI 10.3389/fenvs.2025.1574870

OPEN ACCESS

EDITED BY
Tianjiao Feng,
Beijing Forestry University, China

REVIEWED BY
Peng Zhou,
Henan Polytechnic University, China
Peng Chen,
Yangtze University, China

*CORRESPONDENCE
Yun Tang,
tangyun23@whu.edu.cn

RECEIVED 11 February 2025
ACCEPTED 29 April 2025
PUBLISHED 15 May 2025

CITATION
Tang Y, Wang Y and Yang Q (2025) Multiscale effects of climate change and anthropogenic activity on vegetation dynamics in Guangdong-Hong Kong-Macao greater bay area. *Front. Environ. Sci.* 13:1574870. doi: 10.3389/fenvs.2025.1574870

Multiscale effects of climate change and anthropogenic activity on vegetation dynamics in Guangdong-Hong Kong-Macao greater bay area

Yun Tang[1]*, Yuanyuan Wang[2] and Quanming Yang[3]

[1]School of Computer Science, Huainan Normal University, Huainan, China, [2]China Water Huaihe Planning, Design and Research Co, LTD, Hefei, China, [3]School of Environment and Spatial Informatics, Suzhou University, Suzhou, China

As a crucial indicator of terrestrial ecosystems, vegetation plays a significant role in reflecting the interactions and coupled coordination between anthropogenic activities and natural ecosystems. Understanding the drivers of vegetation change is paramount for achieving sustainable development of socio-ecological systems. Climate change and anthropogenic activities are the primary influencing factors of vegetation change. Given the current research gap in understanding the impacts of climate factors and anthropogenic activities on vegetation change at different temporal scales within the rapid urbanization process of urban agglomerations, based on the Normalized Difference Vegetation Index (NDVI), nighttime light intensity and climatic factors, this paper explores the spatial-temporal distribution of vegetation change trend through trend analysis, and uses empirical mode decomposition and partial correlation analysis to analyzes the correlation between vegetation change and climate factors and anthropogenic activities at different time scales. The relative contributions of climate factors and anthropogenic activities to vegetation change were analyzed by residual trend method. The results reveal that: NDVI exhibits an increasing trend in most regions, Land Surface Temperature (LST) has significantly increased, and the intensity of anthropogenic activities has significantly intensified in half of the regions. The correlation between vegetation change and anthropogenic activities and climate factors shows spatiotemporal heterogeneity, with significantly correlated areas increasing with the extension of temporal scales. A strong negative correlation between vegetation change and anthropogenic activity intensity is mainly distributed in the core urban areas of various cities. The regions where vegetation change is significantly negatively correlated with LST are primarily located in Zhaoqing, Jiangmen, and Huizhou. Increases in precipitation and sunshine duration promote vegetation growth. Vegetation change is primarily influenced by anthropogenic activities in the short term. In the long-term trend, most areas are dominated by climate factors, and vegetation changes caused by anthropogenic activities are mainly distributed in the core areas of cities. These findings contribute to a comprehensive understanding of the driving mechanisms

of vegetation dynamic changes in the context of urbanization and provide a scientific basis for formulating more effective urban ecological management and sustainable development strategies.

KEYWORDS

vegetation dynamics, climate factors, anthropogenic activity, multiscale effects, Guangdong-Hong Kong-Macao greater bay area

1 Introduction

Terrestrial ecosystems, critical components of the global carbon cycle, are vital for climate stability and biodiversity conservation (Ge et al., 2021; Li Y. et al., 2021). However, rapid urbanization is causing unprecedented changes in these ecosystems. Driven by both climate change and anthropogenic activity, alterations in vegetation cover, a prominent feature of terrestrial ecosystems, have garnered widespread attention (Chang et al., 2022). Vegetation is crucial for carbon regulation, climate maintenance, and fragile ecosystem protection, and its dynamics directly impact ecological sustainability. Climate change (e.g., rising temperatures, altered precipitation) and anthropogenic activity (e.g., land-use change) profoundly reshape global vegetation patterns. Therefore, quantifying the relative contributions of climate change and anthropogenic activity to vegetation change is key to understanding terrestrial ecosystem change mechanisms and for developing effective strategies to address climate change and promote socio-economic and ecological sustainability.

Remote sensing provides important data for studying vegetation dynamics and their drivers. Vegetation indices derived from remote sensing are critical indicators for assessing plant biophysical parameters (Wang et al., 2003). The NDVI has characteristics with long temporal record, broad spatial coverage, and high sensitivity, is the most widely used index for measuring vegetation growth. NDVI is applied in vegetation dynamics studies at global (Funk and Brown, 2006; Liu et al., 2022), national (Prăvălie et al., 2022; Mehmood et al., 2024a), regional (Li et al., 2015; Liu et al., 2023; Qi et al., 2024), and city scales (Aburas et al., 2015; Barboza et al., 2021; Singh et al., 2024). In China, long-term NDVI-based monitoring reveals a significant increase in vegetation cover, with spatio-temporal heterogeneity in the rate of increase. For example, studies in the Shaanxi-Gansu-Ningxia region of the Loess Plateau (Li et al., 2015), the northern Loess Plateau (Ning et al., 2015), the Heilongjiang River Basin (Chu et al., 2019), the Yangtze and Yellow River Basins (Zhang et al., 2020), the Yangtze River Delta (Yuan et al., 2019; Tian et al., 2024), the Pearl River Delta (Hu and Xia, 2019; Abbas et al., 2021; Ruan et al., 2020; Chen et al., 2022), the Pearl River Basin (Chen et al., 2022), Jilin Province (Ren H. et al., 2023), Northern China (Lin et al., 2020; Sun et al., 2021), and Southwest China (Qi et al., 2024) demonstrate this trend. Common NDVI-based vegetation change detection methods include linear regression (Wu et al., 2020), the continuous change detection and classification (CCDC) algorithm (Lasaponara et al., 2024), LandTrendr (Eckert et al., 2015; Wuyun et al., 2024), DBEST (detecting breakpoints and estimating segments in trends) (Rhif et al., 2022). The Mann-Kendall test offers several advantages for vegetation trend analysis. This non-parametric method does not require specific data distributions and is suitable for non-normally distributed remote sensing data. In addition, it is resistant to outliers, improving the accuracy of vegetation trend identification (Li P. et al., 2021; Mehmood et al., 2024b).

Climatic factors, topography, nitrogen deposition, CO_2 concentration, and anthropogenic activity are major drivers of vegetation change in terrestrial ecosystems (Potter and Brooks, 1998; Jiang, 2022). Climatic factors significantly influence regional vegetation distribution and growth; rising temperatures, altered precipitation patterns, and extreme climate events are profoundly changing global vegetation growth, distribution, and phenology (Jiang et al., 2017; Afuye and et al., 2021; Zhang et al., 2018). Numerous studies indicate that temperature and precipitation are key factors influencing vegetation change. Increased temperature and summer precipitation extend growing seasons and accelerate growth, promoting vegetation cover (Fang et al., 2003). For example, precipitation patterns significantly affect vegetation dynamics in China's northern agro-pastoral transitional zone (Jiang et al., 2020), and increased temperature and precipitation lead to increased growing season NDVI on the Qinghai-Tibet Plateau (Pang et al., 2017). Vegetation response to climate change in the Yangtze and Yellow River Basins varies with temporal scale (Zhang et al., 2020). In West Bengal, India, temperature and precipitation jointly influence the Enhanced Vegetation Index (Banerjee et al., 2024). Research further suggests that vegetation growth environment, type, and the spatial heterogeneity of climate change can modify vegetation responses to climatic factors. For instance, NDVI in the Pearl River Delta and Yangtze River Delta is more responsive to temperature than precipitation (Chen et al., 2022; Yuan et al., 2019; Abbas et al., 2021), whereas vegetation in the arid, semi-arid, and sub-humid regions of Northern China, temperate grasslands and deserts, and the northern Loess Plateau is more sensitive to precipitation changes (Sun et al., 2021; Lin et al., 2020; Ning et al., 2015). Grassland NDVI in the Heilongjiang River Basin is positively correlated with precipitation year-round. Coniferous, broadleaf, mixed forests, and woodlands show significant positive correlation between NDVI and air temperature, and significant negative correlation with autumn precipitation (Chu et al., 2019). Grassland NDVI in relatively arid regions of Northern China is more sensitive to heavy precipitation than to moderate or light rainfall (Yuan et al., 2015). In semi-humid Northeast Asia, vegetation sensitivity to growing-season temperature differs based on species and elevation (Cao et al., 2019).

Urbanization and population growth amplify the impact of anthropogenic activity on the ecological environment. Anthropogenic activity increasingly influence vegetation, sometimes more profoundly than climate change. For instance, anthropogenic factors and land use are the primary combined

influences on vegetation change in eastern China (Zou et al., 2025). Land use change due to urbanization is a major driver of vegetation cover decline in the Yangtze River Delta (Yuan et al., 2019). Urban expansion in Shenzhen leads to regional net primary productivity loss (Yu et al., 2009). In Northern China, reduced population density and afforestation have promoted desertification recovery (Wang J. et al., 2024). Population growth and migration may explain significant vegetation cover changes in the African Sahel (Boschetti et al., 2013), and anthropogenic activity are the dominant factor in vegetation changes near Kolkata, India (Banerjee et al., 2024). Studies indicate that anthropogenic activity can have both promoting and inhibiting effects on vegetation cover. Large-scale ecological projects promote vegetation greening and NDVI increases (Zheng et al., 2021; Shi et al., 2020), such as the Grain for Green program, increased crop planting, and remediation of coal mining areas (Chen et al., 2022; Ning et al., 2015). Afforestation promotes NDVI growth in Shaanxi, Shanxi, and Hebei provinces, and much of Southern China (Lin et al., 2020; Liu et al., 2022). However, anthropogenic activity are also a major cause of vegetation degradation in China's agro-pastoral belt. Over-cultivation, overgrazing, and unsustainable farming lead to degradation in Northeast China (Chu et al., 2019; Zhang, 2014). Construction land expansion in the Pearl River Basin causes NDVI decline (Wenyu et al., 2022), and energy production, chemical infrastructure, and mineral resource development increase the risk of vegetation degradation in northern Shaanxi (Li et al., 2015).

Given the complex interactions of climate change and anthropogenic activity on vegetation (Zou et al., 2025; Georgescu et al., 2014; Wang et al., 2021), various quantitative methods are used to distinguish their relative contributions. These include Hurst exponent analysis (Wang et al., 2020), geostatistical methods (Zhang et al., 2024), Geodetector models (Zou et al., 2025), partial correlation analysis (Xu et al., 2023), and residual trend analysis (RESTREND) (Yan et al., 2021; Wang W. et al., 2024). RESTREND, based on regression between vegetation indices and climatic factors, calculates the residual between actual and climate-driven vegetation change, representing the impact of anthropogenic activity. Due to its simplicity and suitability for large-scale analysis, RESTREND is chosen as the primary method to quantify the impact of climate and anthropogenic activity on vegetation change.

Regarding analysis of vegetation change drivers, most existing studies rely on traditional methods focused on a single temporal scale. However, long-term climate factor variations are often non-linear, non-stationary, and complex, with different temporal scales or periodic oscillations. Anthropogenic activity intensities, such as urban expansion, over-cultivation, overgrazing, and afforestation, demonstrate spatio-temporal heterogeneity (Zhang et al., 2020; Gao et al., 2022). The relative importance of climate and anthropogenic activity on vegetation change is significantly affected by temporal scale (Ge et al., 2021). Single-scale analyses cannot accurately reflect vegetation responses to different drivers (Qi et al., 2019). Therefore, incorporating multi-temporal scale analysis into assessing the relative importance of climate change and anthropogenic activity, studying vegetation change drivers at annual, interannual, decadal scales, and long-term trends, is crucial for analyzing spatio-temporal differences in the dominant factors affecting vegetation change.

In recent years, China's regional development strategy has prioritized urban agglomerations. In this model, vegetation change in urban agglomerations exhibits more complex spatio-temporal heterogeneity, posing new challenges for ecological protection and sustainable development. The Guangdong-Hong Kong-Macao Greater Bay Area (GBA) is one of China's most densely populated regions, with high levels of openness, economic activity, and social and economic development. The GBA has experienced significant climate change and intensive anthropogenic activity, resulting in noticeable vegetation changes (Geng et al., 2022). Climate change increases the magnitude of effects on ecosystem vulnerability, and anthropogenic activity are the primary drivers of these changes (Zhang P. et al., 2023), making it a suitable location for studying vegetation dynamics during urbanization. Multi-scale analyses of the relationships between climate, anthropogenic activity, and vegetation dynamics in the GBA are lacking. This study focuses on multi-temporal scale differences in the impacts of anthropogenic activity and climate change on vegetation, aiming to reveal the driving mechanisms of vegetation change more comprehensively and provide a basis for sustainable urban development and spatial planning.

Based on these considerations, this study proposes a multi-timescale effects model to quantify the relative importance of climate factors and anthropogenic activity on vegetation change in the GBA at different temporal scales. The NDVI and nighttime light intensity are used to represent vegetation change and anthropogenic activity, respectively. Surface temperature, precipitation, and sunshine duration are selected as climate factors. The analysis comprises four aspects: (1) analyzing trends in vegetation change, anthropogenic activity, and climate factors; (2) detecting multi-temporal scale characteristics; (3) calculating the spatial heterogeneity of correlations between vegetation change and climate/anthropogenic activity across different temporal scales; (4) quantifying the relative contributions of climate and anthropogenic activity to vegetation change at different temporal scales.

2 Materials and methods

2.1 Study area

The Guangdong-Hong Kong-Macao Greater Bay Area (GBA), composed of nine cities in the Pearl River Delta urban agglomeration, the Hong Kong Special Administrative Region and the Macao Special Administrative Region, and is one of the five key national city clusters. Covering an area of approximately 56,000 km^2, the GBA had a permanent population of 86.884 million at the end of 2023, accounting for about 6% of the total population of China. Its geographical location is situated between 111°12′E–115°35′E and 21°25′N-24°30′N, as shown in Figure 1. The GBA is located in a subtropical monsoon climate zone, characterized by significant cloud cover for most of the year, resulting in a cloudy and rainy environment. It experiences high

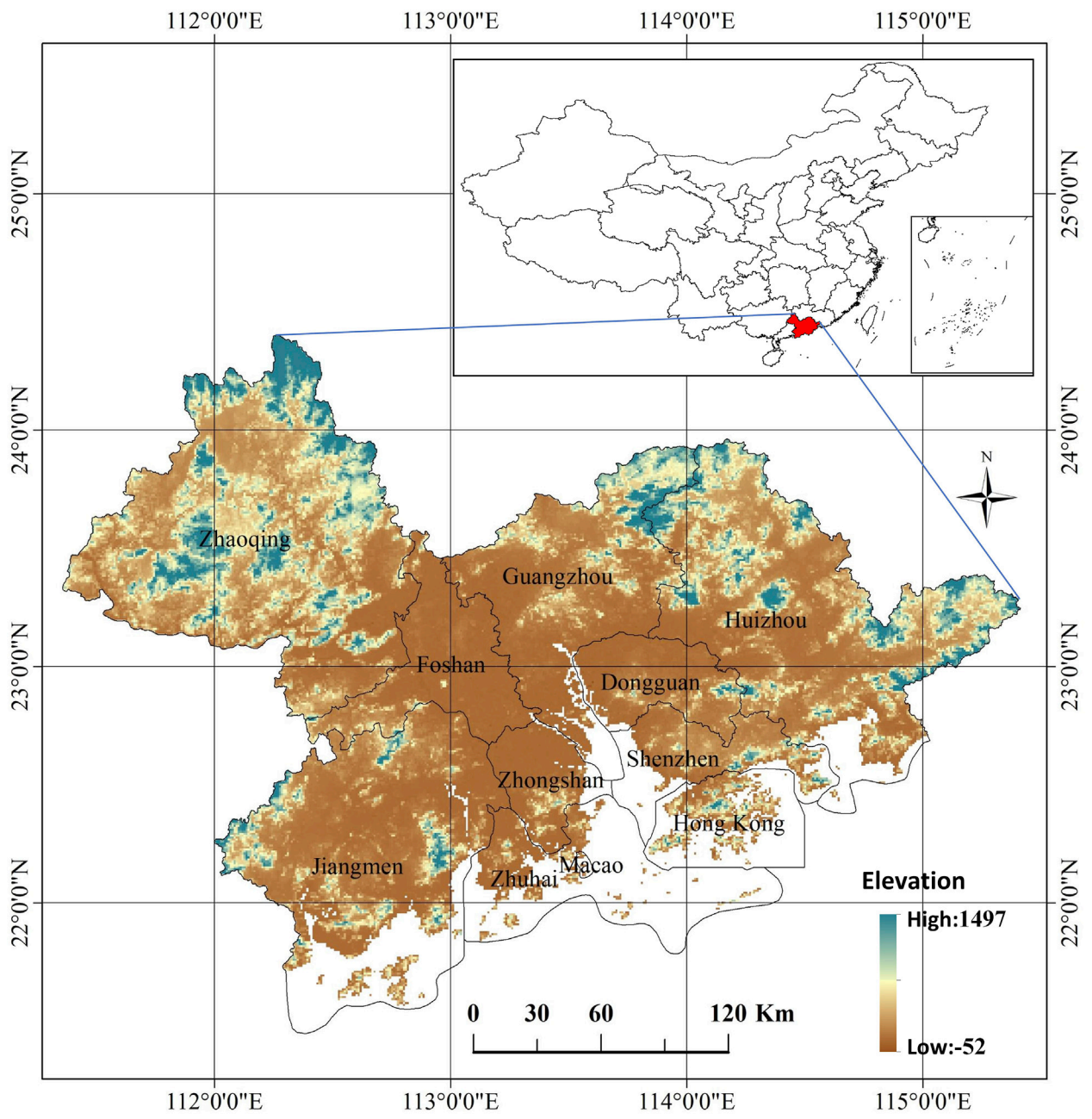

FIGURE 1
The location of the study area Guangdong–Hong Kong–Macao Greater Bay.

temperatures and heavy rainfall in summer and mild, low-rainfall conditions in winter, with synchronous rain and heat, abundant rainfall, and sufficient heat. The annual average precipitation reaches 1800 mm, the total annual sunshine duration is 2000 h, and the annual average temperature ranges from 21.4°C to 22.4°C. Subtropical evergreen broad-leaved forests flourish in the GBA, and vegetation growth is vigorous. The economic development level of the GBA exhibits internal imbalances, with an economic pattern characterized by "strong east and weak west." Over the past 2 decades, Hong Kong's total economic output has surpassed that of other cities. After the recent decade of development, Shenzhen and Guangzhou have also reached leading economic positions comparable to Hong Kong. The economic level of Foshan and Dongguan has developed steadily, with relatively high total economic output, while other cities have relatively lower total economic outputs (Wu et al., 2021).

2.2 Data preparation

The data selected for this study include nighttime light imagery, vegetation index, land surface temperature, and meteorological data, covering a period from April 2012 to December 2020, totaling 105 months. All data were reprojected to the WGS84 coordinate

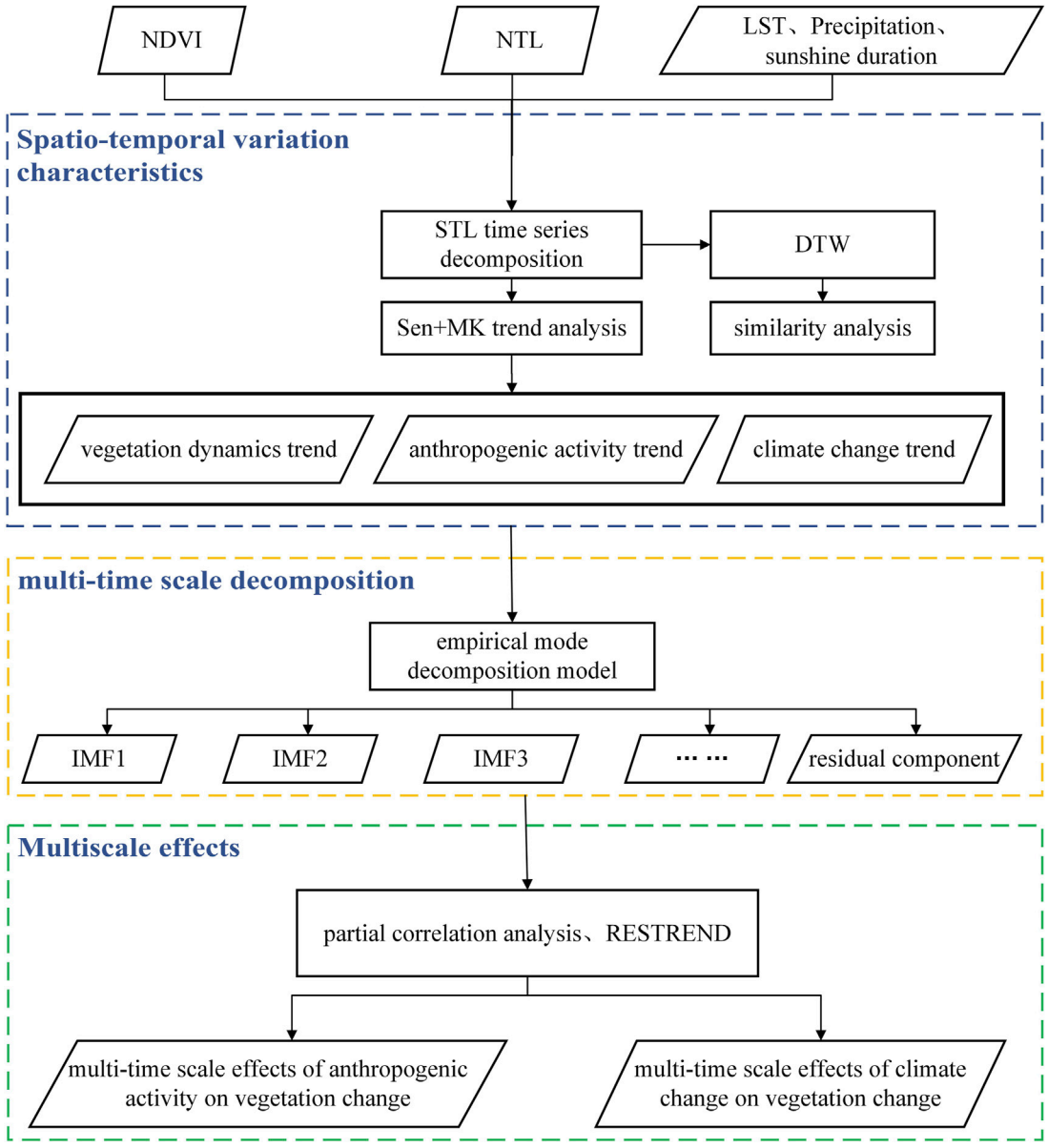

FIGURE 2
The flowchart of methods.

system and resampled to a spatial resolution of 0.004167 ° × 0.004167 ° (approximately 500 m at the equator). The Seasonal and Trend decomposition using Loess (STL) algorithm was applied to the original data to decompose the time series into trend, seasonal, and residual components, respectively. Based on the trend components of the data sources, relevant calculations and analyses were conducted to remove the influences of seasonality and noise.

2.2.1 NDVI data

The NDVI is sensitive to chlorophyll and quantifies vegetation change by measuring the contrast between the reflection of solar radiation in the red band and near infrared band. With the advancement of remote sensing technology, NDVI has been widely used for monitoring vegetation change. This study employed NDVI to monitor vegetation changes. The 16-day composite NDVI product provided by MYD13A1 data was selected, and monthly averages were calculated.

2.2.2 Climate data

Climate factors included LST, precipitation, and sunshine duration. LST data were selected from the 8-day composite LST product provided by MOD11A2, and monthly LST averages were calculated. Meteorological data were obtained from the National Meteorological Science Data Center, providing data from national standard meteorological stations for the period 2012–2020 (http://data.cma.cn/), and monthly average temperature, monthly total precipitation, and monthly total solar radiation data were extracted. Given the limited number of existing meteorological stations and the complex topography of the study area, inverse

distance weighting interpolation was performed on the meteorological data using ArcGIS 10.6 software to match the remote sensing images. The rasterized meteorological data spatial distribution maps had the same spatial resolution and projection information as the nighttime remote sensing imagery.

2.2.3 Nighttime light data

In 2012, the Visible Infrared Imaging Radiometer Suite (VIIRS) onboard the National Polar-Orbiting Partnership (NPP) satellite, launched by the National Aeronautics and Space Administration (NASA), became available for capturing nighttime lights. The NPP-VIIRS nighttime light remote sensing imagery provides daily raw data, monthly composite data, and some annual composite data, and these products have already eliminated the effects of cloud cover, lightning, and moonlight. The NPP-VIIRS/DNB data were obtained from the Earth Observation Group at the Payne Institute for Public Policy, Colorado School of Mines (https://eogdata.mines.edu/products/vnl/), with a temporal coverage from April 2012 to December 2020. Nighttime light intensity (NTL) was used in this study to represent the intensity of anthropogenic activities.

2.3 Methods

This study develops a multi-timescale effects model (Figure 2) to quantify the influence of climatic factors and anthropogenic activity on vegetation change across multiple temporal scales within the GBA. The analytical framework comprises the following: First, trend analysis of vegetation, anthropogenic activity, and climate factor time series is conducted using the Theil-Sen median trend estimator and the Mann-Kendall test. Second, Empirical Mode Decomposition (EMD) is applied to extract multi-temporal scale characteristics from vegetation change, anthropogenic activity intensity, and climatic factors. Subsequently, partial correlation analysis is performed to assess the relationships between vegetation change at different temporal scales and both climatic factors and anthropogenic activity. Finally, the Residual Trend (RESTREND) method is utilized to quantify the relative contributions of climate factors and anthropogenic activity to vegetation change across each temporal scale. Adopting a multi-temporal perspective, this research aims to provide an in-depth analysis of vegetation dynamics and their underlying drivers, with the goal of providing a scientific basis for refining existing ecosystem models and enabling fine-grained temporal monitoring of human-environment interactions in rapidly urbanizing regions.

2.3.1 Mann-Kendall trend analysis

The temporal trend of a time series was calculated using a combination of the Theil-Sen median trend estimator and the Mann-Kendall test. The Theil-Sen median trend estimator, which can reduce the influence of outliers, is widely used for dynamic detection in long time series. The Mann-Kendall test is employed to determine the significance of the trend. The calculation equation for the Theil-Sen median trend estimator is as follows (Li et al., 2021a):

$$\beta = median\left(\frac{x_j - x_i}{j - i}\right), \forall j > i \tag{1}$$

In the equation Equation 1, β represents the rate of change; *median* is the median value of a dataset; and x_i and x_j are the observed values for the *i*th month and the *j*th month, respectively. $\beta > 0$ indicates an increasing trend, and $\beta < 0$ indicates a decreasing trend.

The significance of the trend change was calculated using the Mann-Kendall non-parametric statistical test. The calculation process of the Mann-Kendall trend test is as follows:

For a time series $(x_1, x_2, \ldots, x_n)$, the test statistic for the trend test is:

$$\tau = \sum_{i=1}^{n-1} \sum_{j=i+1}^{n} sign\left(x_j - x_i\right), \forall j > i \tag{2}$$

$$sign\left(x_j - x_i\right) = \begin{cases} 1, if\ x_j - x_i > 0 \\ 0, if\ x_j - x_i = 0 \\ -1, if\ x_j - x_i < 0 \end{cases} \tag{3}$$

In the Equations 2, 3 n is the length of the time series, and x_i and x_j are the observed values for the *i*th month and the *j*th month, respectively. When the observed values are independent and identically distributed, the calculation of the variance, as given in Equation 4:

$$Var(\tau) = \frac{n*(n-1)*(2n-5)}{18} \tag{4}$$

The formula for calculating the Mann-Kendall significance (Z), as given in Equation 5:

$$Z = \begin{cases} \frac{\tau - 1}{\sqrt{Var(\tau)}}, if\ \tau > 0 \\ 0, if\ \tau = 0 \\ \frac{\tau + 1}{\sqrt{Var(\tau)}}, if\ \tau < 0 \end{cases} \tag{5}$$

A trend is considered significant when $|Z| \geq 1.96$.

The combination of the Theil-Sen median trend estimator and the Mann-Kendall test can effectively reflect the spatial distribution characteristics of the change trends in vegetation, anthropogenic activities, and climate factors. Since pixels with a rate of change strictly equal to 0 are essentially nonexistent, pixels with a rate of change between −0.0005 and 0.0005 were classified as stable, pixels with a rate of change less than −0.0005 were classified as degraded areas, and pixels with a rate of change greater than 0.0005 were classified as improved areas. The results of the Mann-Kendall test for significance at the 0.05 confidence level were classified into significant change ($|Z| \geq 1.96$) and non-significant change ($|Z| \leq 1.96$).

2.3.2 Dynamic Time Warping method

Dynamic Time Warping (DTW) is an algorithm used to measure the similarity between two time series. The DTW algorithm can achieve high classification accuracy when the number of samples or the length of the time series of satellite imagery is reduced, and it is widely applied in land use/cover mapping and farmland detection.

With the advancement of the DTW algorithm in the automatic identification and shape matching of time series of different lengths, the DTW algorithm has been widely applied to analyze the consistency of time series. The calculation formula is as follows (Csillik et al., 2019):

For time series of observed values A and B with lengths of n and m, respectively, construct an n × m matrix:

$$\begin{cases} A = a_1, a_2, \ldots, a_i, \ldots, a_n \\ B = b_1, b_2, \ldots, b_j, \ldots, b_m \end{cases} \quad (6)$$

In the Equation 6, the (i_{th}, j_{th}) element is the Euclidean distance between points A_i and B_j. This represents the similarity between every point in sequence A and every point in sequence B, where a smaller distance indicates a higher similarity. The Dynamic Programming algorithm seeks a path through a set of points in the matrix grid. These points are the aligned points used in the calculation of the cumulative distance between the two sequences. This warping path W is calculated as Equations 7, 8:

$$W = \bar{\omega}1, \bar{\omega}2, \ldots, \bar{\omega}k \quad \max(n, m) \le k \le n + m + 1 \quad (7)$$

$$\bar{\omega}k = \sqrt{\left(a_i - b_j\right)^2} \quad (8)$$

The path needs to satisfy three constraints.

(1) Boundary Condition: $\bar{\omega}1 = (1, 1)$, $\bar{\omega}k = (m, n)$, meaning that the selected path must start at (1,1) and end at point (m, n).
(2) Continuity: The path cannot skip over a point for matching, but must align with points adjacent to itself. That is, if $\bar{\omega}(k-1) = (a', b')$, then $\bar{\omega}k = (a, b)$ needs to satisfy $(a - a') \le 1$ and $(b - b') \le 1$.
(3) Monotonicity: If $\bar{\omega}(k-1) = (a', b')$, then $\bar{\omega}k = (a, b)$ needs to satisfy $0 \le (a - a')$ and $0 \le (b - b')$.

The optimal matching path between the two sequences is found in the distance matrix as the path that minimizes the accumulated distance between sequences A and B:

$$DTW(A, B) = \frac{1}{K} \times \min\left(\sum_1^k W_k\right) = \frac{1}{K} \times \gamma_K = \frac{\gamma(i, j)}{K} \quad (9)$$

In the Equation 9, $\gamma(i, j)$ is the accumulated distance. It starts by matching the two time series, A and B, from point (1,1), and accumulates the distance corresponding to each point passed through until reaching the end point (n, m). This accumulated distance represents the similarity between sequences A and B. The denominator K is used to compensate for different warping paths.

The accumulated distance $\gamma(i, j)$ is the sum of the distance $d(A_i, B_j)$ of the current grid point (A_i, B_j) and the minimum accumulated distance of the neighboring elements that can reach this grid point. This is derived using the following recursive function as Equation 10:

$$\gamma(i, j) = d\left(A_i, B_j\right) + min\{\gamma(i-1, j-1), \gamma(i-1, j), \gamma(i, j-1)\} \quad (10)$$

Given the classification advantages of the DTW algorithm, anthropogenic activity, climatic factors, and vegetation change can be flexibly analyzed using DTW similarity measures within urban areas exhibiting natural phenological variability. Both anthropogenic activity and climatic factors represent major influences on vegetation change. The heterogeneity in NDVI induced by anthropogenic activity is examined based on the similarity of NDVI time series corresponding to varying levels of nighttime light intensity. In parallel, the heterogeneity in vegetation change arising from climatic factor variations is assessed by calculating the similarity of NDVI time series associated with varying magnitudes of LST, precipitation, and sunshine duration.

2.3.3 Empirical mode decomposition method

This study analyzed the change characteristics of vegetation, climate factors, and anthropogenic activities at the pixel scale across multiple temporal scales using the Empirical Mode Decomposition (EMD) method.

The EMD method decomposes the original time series data $X(t)$ into n components and a residual component, i.e., Intrinsic Mode Functions $(IMF_i, i = 1, 2, \ldots, n)$. Each IMF component and the residual component represent the change characteristics and long-term trends of the time series at a specific temporal scale. The specific decomposition process of empirical mode decomposition is as follows (Zhang et al., 2020):

(1) Identify all the extrema points of the original time series signal $h(t)$ from the study data source.
(2) Fit the upper and lower envelopes of these extrema points using spline interpolation. Calculate the mean of these envelopes, denoted as $s(t)$. Then, subtract $s(t)$ from the original time series signal $h(t)$ to obtain $r(t)$.
(3) Determine whether $r(t)$ meets the criteria to be classified as an Intrinsic Mode Function.
(4) If $r(t)$ is not an Intrinsic Mode Function, replace $h(t)$ with $r(t)$ and repeat steps (1) through (3) iteratively until $r(t)$ satisfies the conditions to be considered an Intrinsic Mode Function. This process yields an IMF, denoted as $x_i(t)$. Each IMF then represents oscillatory variations in observed values within a specific frequency band.
(5) Once an IMF is obtained, subtract this mode function from the original time series signal. Repeat steps (1) through (4) to continuously obtain the next IMF until the remaining sequence after subtraction is either monotonic or constant.

Based on this procedure, the original time series is decomposed using EMD into several IMFs and a residual component, as given in Equation 11:

$$h(t) = \sum_{i=1}^{n} x_i(t) + r \quad (11)$$

where n is the number of decomposed IMFs, $x_i(t)$ epresents each of the decomposed IMF signals, and r represents the residual component.

The average period of the ith IMF component is calculated by dividing the length of the time series by the number of peaks (local maximum). To evaluate the relative importance of each IMF and the residual component, the variance contribution is calculated:

$$V_i = V_r(x_i) \Big/ \left[\sum_{i=1}^{n} V_r(x_i) + V_r(r)\right] \quad (12)$$

$$V_r = V_r(r) \Big/ \left[\sum_{i=1}^{n} V_r(x_i) + V_r(r)\right] \quad (13)$$

In the Equations 12, 13 $V_r(x_i)$ and $V_r(r)$ represent the variance of the ith IMF component and the residual component, respectively.

2.3.4 Partial correlation analysis

Climate factors, anthropogenic activities, and vegetation change are interrelated; altering one element affects the others. Partial correlation analysis calculates the correlation between a dependent variable and an independent variable while excluding the influence of related variables on the dependent variable. The magnitude of the partial correlation coefficient reflects the influence of each factor on the dependent variable, with other factors acting as control variables. Second-order partial correlation coefficients are based on correlation analysis and first-order partial correlation analysis, and third-order partial correlation coefficients are based on correlation analysis, first-order partial correlation analysis, and second-order partial correlation analysis. The calculation formula for partial correlation analysis is as follows (Xu et al., 2023):

$$R_{xy} = \frac{\sum_{i=1}^{n}(x_i - \bar{x})(y_i - \bar{y})}{\sqrt{\sum_{i=1}^{n}(x_i - \bar{x})^2}\sqrt{\sum_{i=1}^{n}(y_i - \bar{y})^2}} \tag{14}$$

In the Equation 14, R_{xy} represents the correlation coefficient; x_i and y_i represent the values of variables x and y in the ith period, respectively; $\bar{x}$ and $\bar{y}$ represent the average values of variables x and y, respectively; and n represents the sample size. The range of R_{xy} is from −1 to 1.

The equation for calculating the first-order partial correlation is as follows:

$$R_{xy,1} = \frac{R_{xy} - R_{x1}R_{y1}}{\sqrt{(1 - {R_{x1}}^2)(1 - {R_{y1}}^2)}} \tag{15}$$

In the Equation 15, $R_{xy,1}$ represents the partial correlation coefficient between variables x and y when variable one is held constant, and R_{xy}, R_{x1}, R_{y1} represent the correlation coefficients between variables x and y, x and 1, and y and 1, respectively.

The equation for calculating the second-order partial correlation, as given in Equation 16:

$$r_{xy.12} = \frac{r_{xy.1} - r_{x2.1}r_{y2.1}}{\sqrt{(1 - {r_{x2.1}}^2)(1 - {r_{y2.1}}^2)}} \tag{16}$$

where $r_{xy.12}$ is the second-order partial correlation coefficient; x and y represent the elements for which the partial correlation coefficient is calculated; one and two represent the control variables; and $r_{xy.1}$, $r_{x2.1}$, $r_{y2.1}$ represent first-order partial correlation coefficients.

The equation for calculating the third-order partial correlation, as given in Equation 17:

$$r_{12.345} = \frac{r_{12.35} - r_{14.35}r_{24.35}}{\sqrt{(1 - {r_{14.35}}^2)(1 - {r_{24.35}}^2)}} \tag{17}$$

where $r_{12.345}$ represents the third-order partial correlation coefficient between vegetation and a certain variable, after controlling for three other variables sequentially; and $r_{12.35}$, $r_{14.35}$, $r_{24.35}$ represent the corresponding second-order partial correlation coefficients.

2.3.5 Residual trend method

Vegetation change is influenced by both climate factors and anthropogenic activities. The RESTREND analyzes the relative roles of climate factors and anthropogenic activities on vegetation change by establishing a relationship model between vegetation change and climate factors. The RESTREND method analyzes the residual trend between the observed NDVI values ($NDVI_{obs}$)and the predicted NDVI values ($NDVI_{pre}$)by using climate factors (precipitation, LST, and sunshine duration) as explanatory variables in a regression model. The basic principle of the RESTREND method is as follows (Qi et al., 2019):

Establish a regression model between $NDVI_{pre}$ and climate factors:

$$NDVI_{pre_{i,j}} = b_0 + b_1P_{i,j} + b_2T_{i,j} + b_3S_{i,j} \tag{18}$$

In the equation, $P_{i,j}$, $T_{i,j}$, $S_{i,j}$ represent the monthly total precipitation, land surface temperature, and monthly total sunshine duration at spatial location (i, j), respectively, and b_0, b_1, b_2, b_3 are the coefficients determined by the least squares method.

Based on the results of Equation 18, the residual $NDVI_{res}$ between $NDVI_{obs}$ and $NDVI_{pre}$ is calculated. The change trend of $NDVI_{pre}$ is used to measure the impact of climate factor changes on vegetation change, and the change trend of $NDVI_{res}$ is used to represent the impact of anthropogenic activities on vegetation change, thus extracting the influences of climate factors and anthropogenic activities on vegetation change. Subsequently, the Sen's slope method was used to calculate the relative roles of climate factors and anthropogenic activities in vegetation change.

3 Results

3.1 Change trend analysis

The combination of the Theil-Sen median trend estimator and the Mann-Kendall test can effectively reflect the temporal trends of vegetation, anthropogenic activities, and climate factors in GBA.

3.1.1 Vegetation change trend

By overlaying the classification results of the Theil-Sen median trend estimator and the Mann-Kendall test, the change trends of NDVI at the pixel scale were obtained, as shown in Figure 3. The proportions of the five change types were as follows: significant increase: 17.36%, slight increase: 46.23%, no change: 7.41%, slight decrease: 24.09%, and significant decrease: 4.9%. The area of land with improved vegetation was significantly larger than the area with degraded vegetation. The GBA experienced widespread vegetation greening during the study period, with the total area of significantly improved vegetation accounting for 17.36% and the total area of slightly improved vegetation accounting for 46.23%. Areas with significant vegetation improvement were mainly distributed in Zhaoqing, Huizhou, and Jiangmen. The cities with the highest proportions of improved vegetation area were Zhaoqing, Hong Kong, and Shenzhen, with percentages of 76.89%, 72.9%, and 71.23%, respectively.

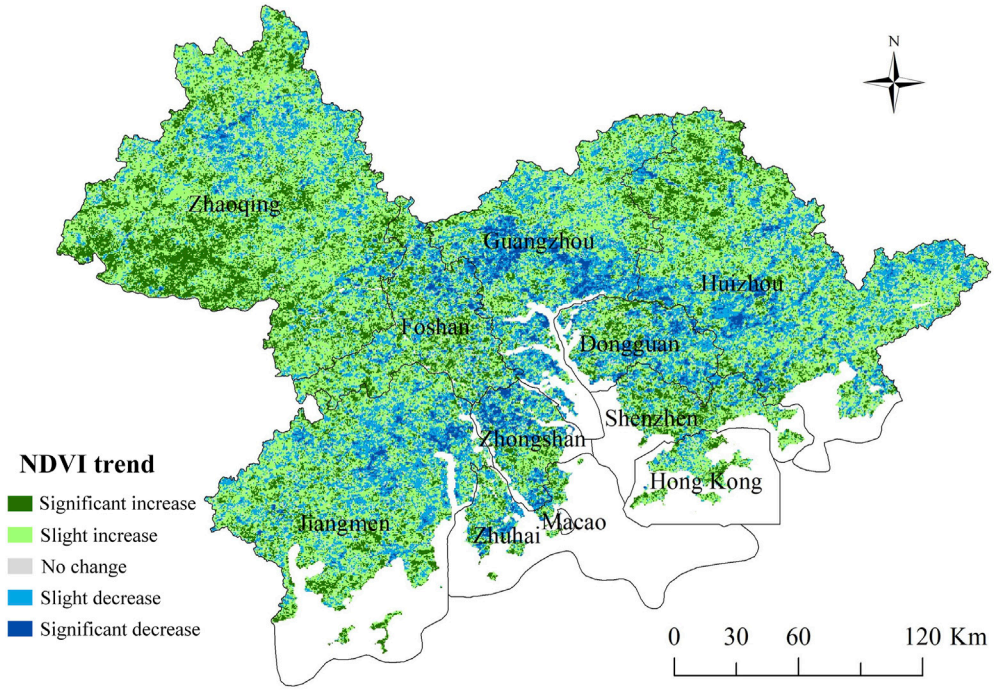

FIGURE 3
Spatial distribution of NDVI change trend.

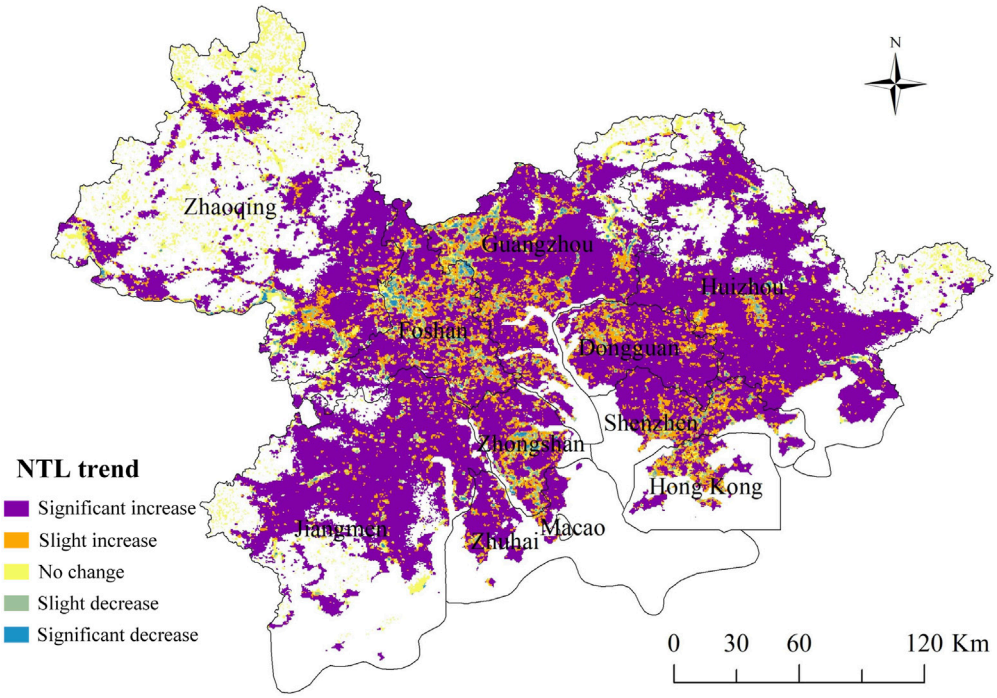

FIGURE 4
Spatial distribution of NTL change trend.

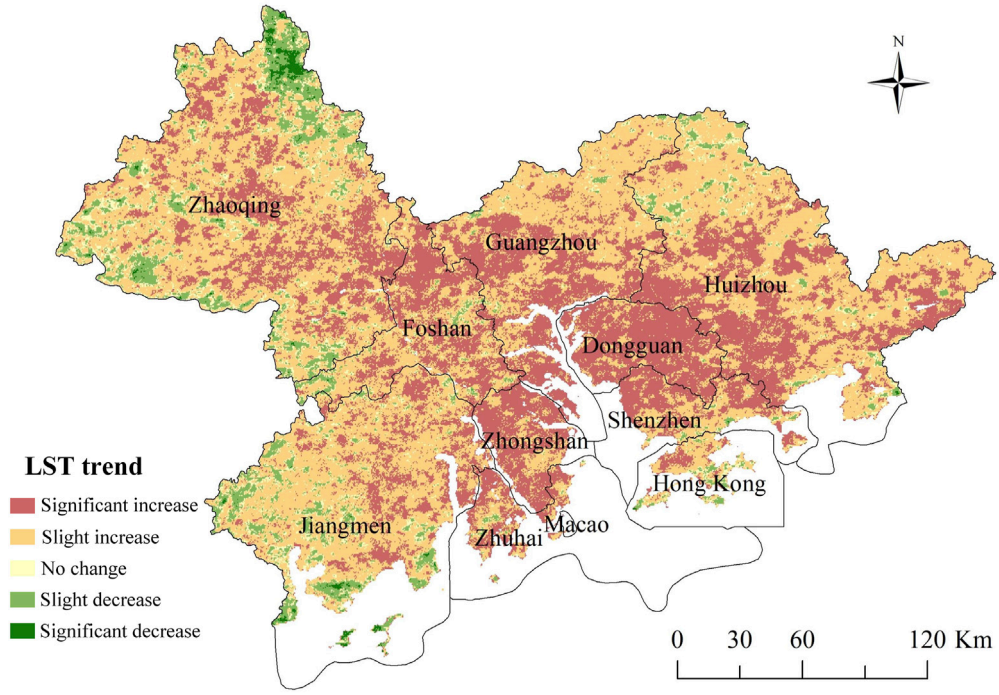

FIGURE 5
Spatial distribution of LST change trend.

The total area of vegetation degradation in the GBA reached 28.99%, with relatively significant degradation in Zhongshan, Dongguan, and Guangzhou, the total area of vegetation degradation accounted for 46.99%, 43.21% and 41.31%, respectively. These three cities have experienced more rapid urbanization and significant expansion of built-up areas compared to other cities. This rapid urbanization process has led to noticeable degradation of surface vegetation cover.

3.1.2 Trend of anthropogenic activity intensity

The spatial distribution of the change trends in anthropogenic activity intensity is shown in Figure 4. The proportions of the five change types were as follows: significant increase: 51.47%, slight increase: 8.77%, no change: 6.69%, slight decrease: 2.43%, and significant decrease: 0.71%. The proportions of areas with increased anthropogenic activity intensity were relatively lower in the three cities of Zhaoqing, Huizhou, and Jiangmen.

3.1.3 Trends of climate factors

The spatial distribution of LST change trends is shown in Figure 5. The proportions of the five change types were as follows: significant increase: 34%, slight increase: 53.42%, no change: 5.29%, slight decrease: 6.8%, and significant decrease: 0.48%. With the rapid urbanization of the GBA, the LST in various cities also showed varying degrees of increase. Dongguan, Zhongshan, Zhuhai, and Shenzhen had relatively high proportions of areas with increased LST, with the percentages of significantly increased areas being 80.11%, 71.49%, 53.77%, and 52.08%, respectively. Jiangmen had the lowest proportion of areas with significantly increased LST, at 19.15%.

3.2 Similarity analysis

The heterogeneity of NDVI induced by anthropogenic activity was explored, as shown in Figure 6, the DTW distance of NDVI time series exhibited a clear increasing trend with the increase in the difference between nighttime light intensities, indicating that the differences in NDVI became larger. As shown in Figure 7, with the increase in the difference between climate factors, the DTW distances of the NDVI time series corresponding to the three climate factors also showed an increasing trend. Among them, the DTW distance corresponding to different sunshine durations was relatively lower.

3.3 Multi-time scale characteristics analysis

3.3.1 Multi-time scale characteristics of vegetation change

Based on the EMD method, multi-temporal scale analysis was performed on the NDVI time series at the pixel scale from April 2012 to December 2020. The mean period of each IMF and the mean variance contribution of each IMF and the residual component for all pixels were calculated as the change period and variance contribution of vegetation at different temporal scales, respectively. The average periods and average variance contributions are shown in Table 1, and the spatial distribution of variance contributions to vegetation change at different temporal scales is shown in Figure 8.

As shown in Table 1, the vegetation changes in the GBA are mainly characterized by periods of 10 months, 36 months, and

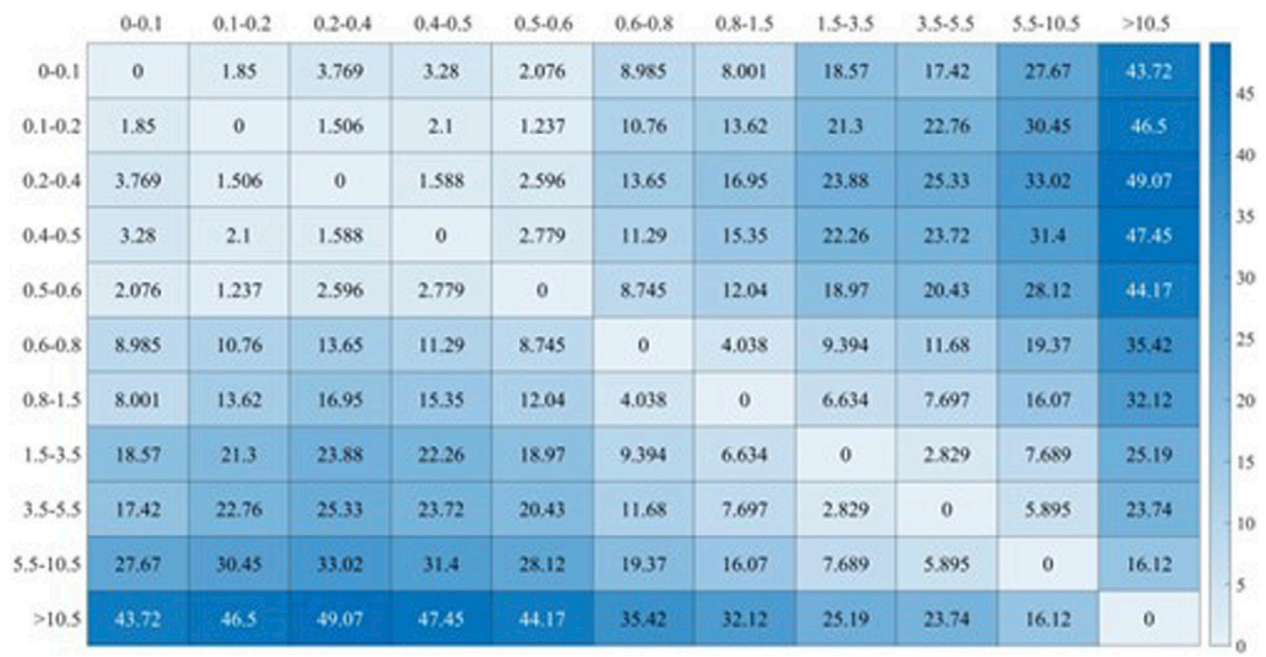

FIGURE 6
DTW distance of NDVI sequence corresponding to different NTL intensity.

86 months. The increasing trend in residual component indicate an overall increase in vegetation cover, which is consistent with the Mann-Kendall trend. Based on the decomposition of vegetation change time series, the multi-temporal scales of vegetation change in the GBA are categorized as annual (1-year), interannual (3-year), sub-decadal (7-year), and long-term trend.

Figures 8A–D present the variance contributions of the 1-year, 3-year, 7-year temporal scales and the long-term trend to vegetation change in the GBA, respectively. For the 1-year temporal scale, the variance contributions of most cities are below 50%, except for a small region in Zhaoqing. Regions where the 3-year variance contribution exceeds 50% account for 15% of the GBA and are mainly distributed in Huizhou, Guangzhou, and Zhaoqing. The 7-year variance contribution exceeds 50% in 10.3% of the study area, primarily in Huizhou and Guangzhou. Long-term trends account for over 50% variance in 17.2% of the GBA, with a higher prevalence in Zhaoqing, Jiangmen, and Zhongshan.

3.3.2 Multi-time scale characteristics of climate factors and anthropogenic activity

Table 2 indicates that the dominant periodicities for anthropogenic activity intensity in the GBA are 12 months, 36 months, and 86 months. The residual components of anthropogenic activity intensity exhibit an increasing trend, with the variance contribution reaching 62.2%, demonstrating a marked increase in anthropogenic activity intensity, which is consistent with the Mann-Kendall trend analysis. The multitemporal scales of anthropogenic activity intensity change in the GBA are then categorized as 1-year, 3-year, 7-year and long-term trends to facilitate the analysis of their impact upon vegetation change.

Figures 9A–D present the variance contributions of the 1-year, 3-year, and 7-year temporal scales, and the long-term trend to anthropogenic activity intensity in the GBA, respectively. The variance contributions of the 1-year, 3-year, and 7-year temporal scales were generally below 30%, indicating minimal fluctuation in anthropogenic activity intensity at shorter temporal scales. The regions with variance contributions greater than 50% in the long-term trend accounted for 65%, indicating that most regions are dominated by long-term trends in anthropogenic activity intensity, and the long-term trend of anthropogenic activity intensity has a significant impact on vegetation change.

As shown in Table 3, the LST is mainly characterized by 10 months, 36 months, and 79 months periodicities, with the residual component exhibiting an increasing trend and a variance contribution of 25.32%, indicating an increase in LST. This study summarized the multi-temporal scales of LST change as 1-year, 3-year, 7-year temporal scale, and a long-term trend.

Figures 10A–D respectively show the variance contributions of the 1-year, 3-year, and 7-year temporal scales, and the long-term trend to LST change in the GBA. The 1-year and 7-year temporal scales generally have variance contributions to LST that are less than 50%. The regions with variance contributions greater than 50% at the 3-year temporal scale accounted for 25.26%, Zhaoqing, Guangzhou, and Huizhou are dominated by 3-year LST changes. The regions with variance contributions greater than 50% in the long-term trend accounted for 12.46%, mainly distributed in the core urban areas, indicating that LST changes in the core urban areas are dominated by long-term trends.

According to Table 3, multi-temporal scales of precipitation and sunshine duration changes are summarized as 1-year, 3-year, and 7-year temporal scales, and a long-term trend. The variance contribution of the long-term trend to precipitation was 25.49%, and the precipitation showed a decreasing trend, and there was no clear long-term trend in sunshine duration.

10.3389/fenvs.2025.1574870

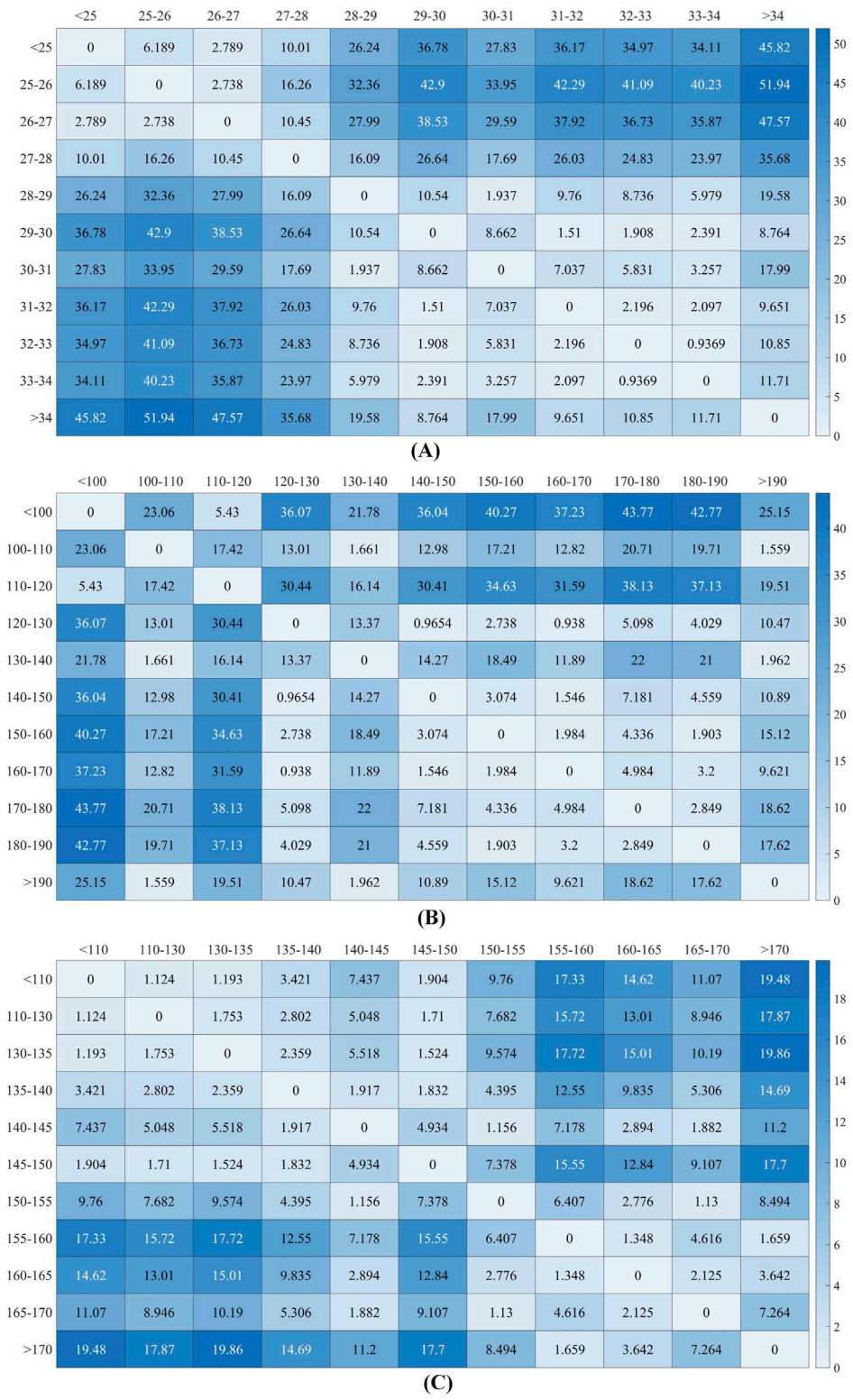

FIGURE 7
DTW distance of NDVI sequence corresponding to climatic factors **(A)** LST, **(B)** precipi-tation, **(C)** sunshine duration.

TABLE 1 Mean period and variance contribution of vegetation change at different time scales.

Description	IMF1	IMF2	IMF3	IMF4	IMF5	Residual component
period	10	36	86	100	100	
variance contribution	19.15%	30.05%	20.59%	1.82%	0	28.39%

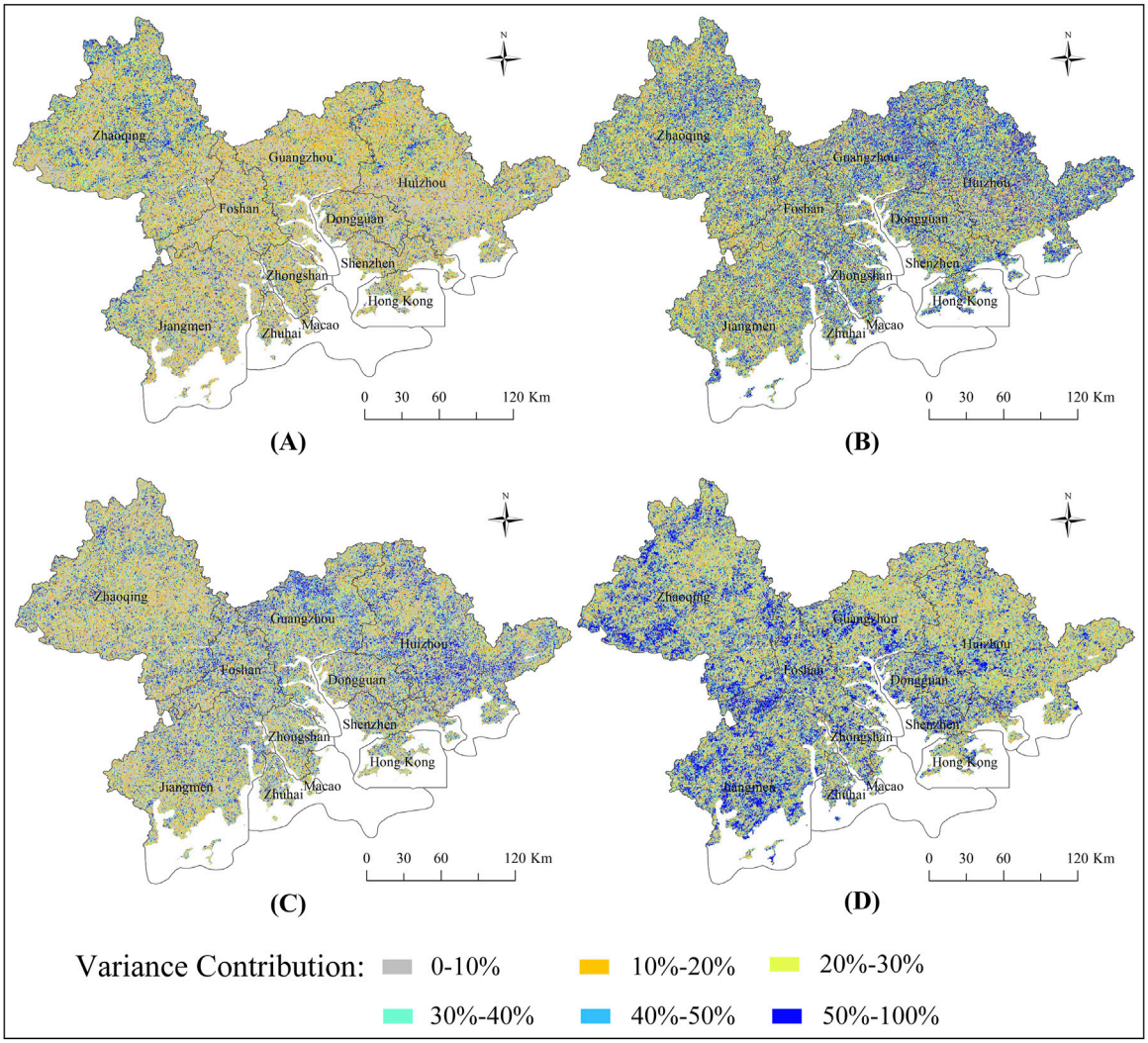

FIGURE 8
Variance contribution of different time scales to vegetation change **(A)** 1-year, **(B)** 3-year, **(C)** 7-year, **(D)** long-term trend.

TABLE 2 Mean period and variance contribution of anthropogenic activity intensity at different time scales.

Description	IMF1	IMF2	IMF3	IMF4	IMF5	Residual component
period	12	36	86	100	100	
variance contribution	11.91%	16.42%	8.98%	0.49%	0	62.2%

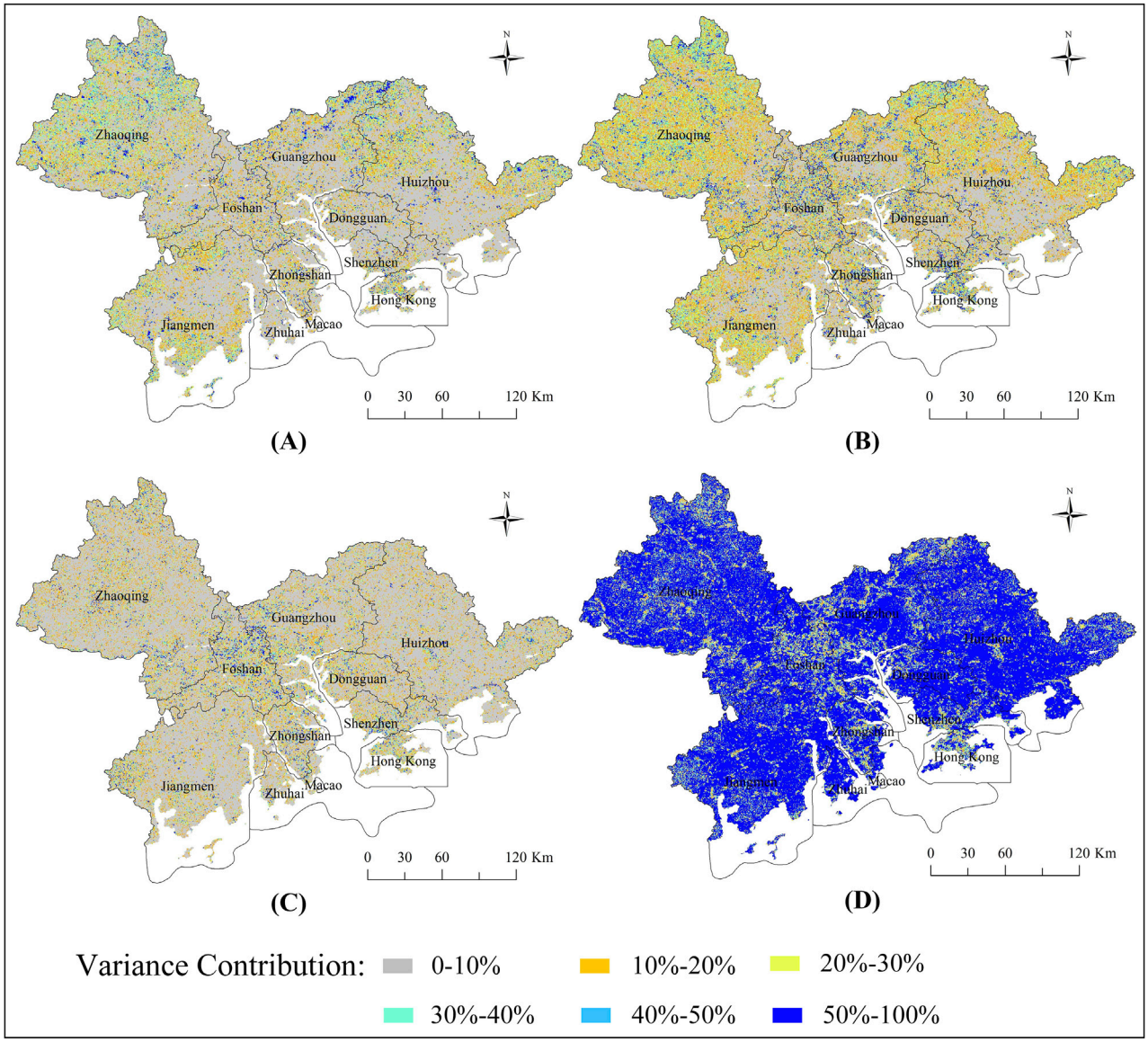

FIGURE 9
Variance contribution of different time scales to anthropogenic activity intensity **(A)** 1-year, **(B)** 3-year, **(C)** 7-year, **(D)** long-term trend.

TABLE 3 Mean period and variance contribution of climate factors at different time scales.

Climate factors	Description	IMF1	IMF2	IMF3	IMF4	IMF5	Residual component
LST	period	10	36	79	92	88	
	variance contribution	17.3%	36.48%	19.75%	1.16%	0	25.32%
precipitation	period	10	36	84	99	99	
	variance contribution	22.85%	34.51%	15.92%	1.22%	0	25.49%
sunshine duration	period	10	34	84	84	72	
	variance contribution	36.86%	30.02%	19.07%	3.54%	0	10.52%

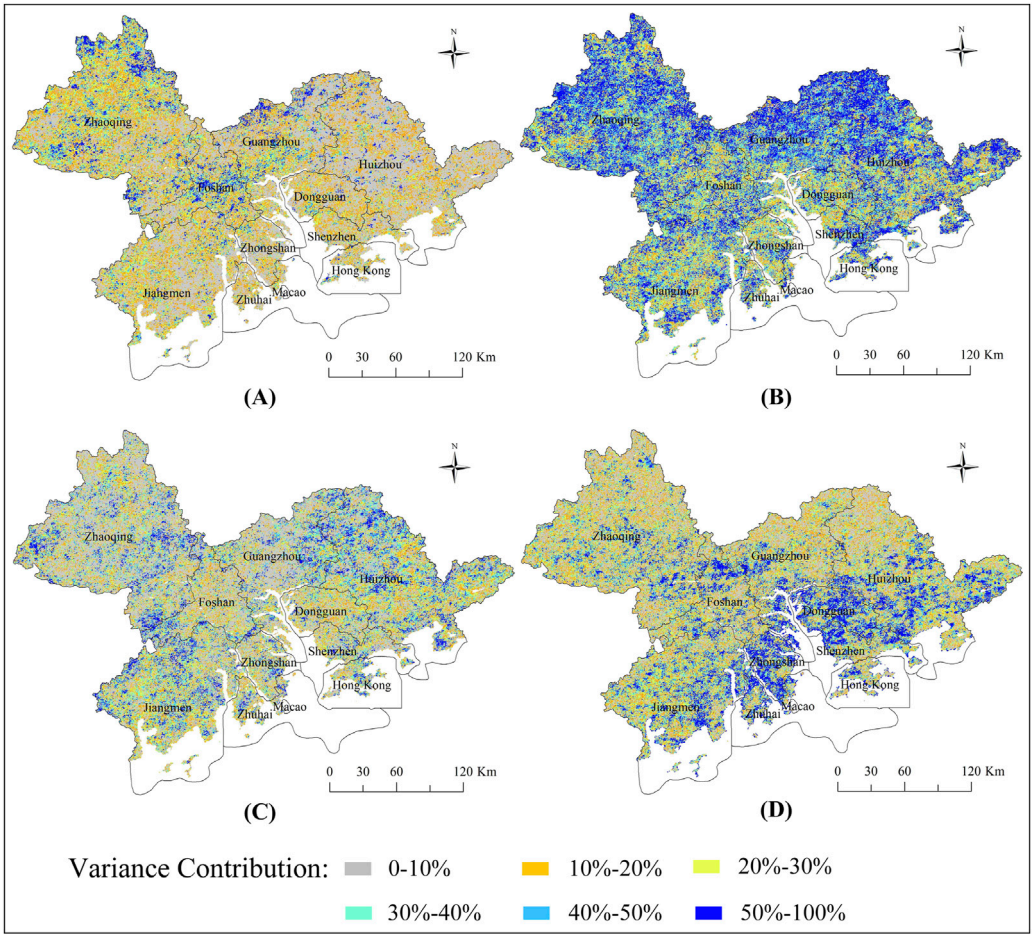

FIGURE 10
Variance contribution of different time scales to LST **(A)** 1-year, **(B)** 3-year, **(C)** 7-year, **(D)** long-term trend.

TABLE 4 The proportion of correlation between vegetation change and anthropogenic activity intensity at different time scales.

Correlation	IMF1	IMF2	IMF3	Residual component	Raw values
$R < 0$, $p < 0.05$	22.35	31.97	41.34	24.96	32.87
$R < 0$, $p > 0.05$	26.58	18.87	10.54	26.84	16.94
$R > 0$, $p < 0.05$	23.51	30.30	37.58	22.25	32.45
$R > 0$, $p > 0.05$	27.56	18.86	10.54	25.95	17.74

3.4 Effects of climatic factors and anthropogenic activity on vegetation

3.4.1 Correlation between anthropogenic activity intensity and vegetation change

Using the influence of climate factors (LST, precipitation, and sunshine duration) on vegetation change as control variables, a pixel-by-pixel partial correlation analysis was performed on the relationship between vegetation change and anthropogenic activity intensity at 1-year, 3-year, and 7-year temporal scales, as well as the long-term trend and overall values. Based on the spatial distribution of the partial correlation coefficients, the spatial heterogeneity of the correlation between vegetation change and anthropogenic activity intensity in the GBA at different temporal scales was analyzed. The area percentages of different correlations are shown in Table 4.

Figures 11A–E respectively show the spatial distribution of the partial correlation between vegetation change and anthropogenic activity intensity in the GBA at the 1-year, 3-year, and 7-year temporal scales, the long-term trend, and the overall values. At the 1-year temporal scale in the GBA, the relationship between vegetation change and anthropogenic activity intensity was not significant in 54.14% of the regions, while 22.35% and 23.51% of the regions showed significant negative or positive correlations, respectively. Pixels with negative and positive correlations were evenly distributed in the GBA. The areas with significant correlations between vegetation change and anthropogenic activity intensity increased at the 3-year and 7-year temporal scales. The

TABLE 5 The proportion of correlation between vegetation change and LST at different time scales.

Correlation	IMF1	IMF2	IMF3	Residual component	Raw values
$R < 0$, $p < 0.05$	17.84	28.99	37.62	12.70	30.24
$R < 0$, $p > 0.05$	22.25	18.05	10.58	38.97	18.39
$R > 0$, $p < 0.05$	33.14	34.02	41.28	10.85	32.67
$R > 0$, $p > 0.05$	26.77	18.95	10.52	37.48	18.70

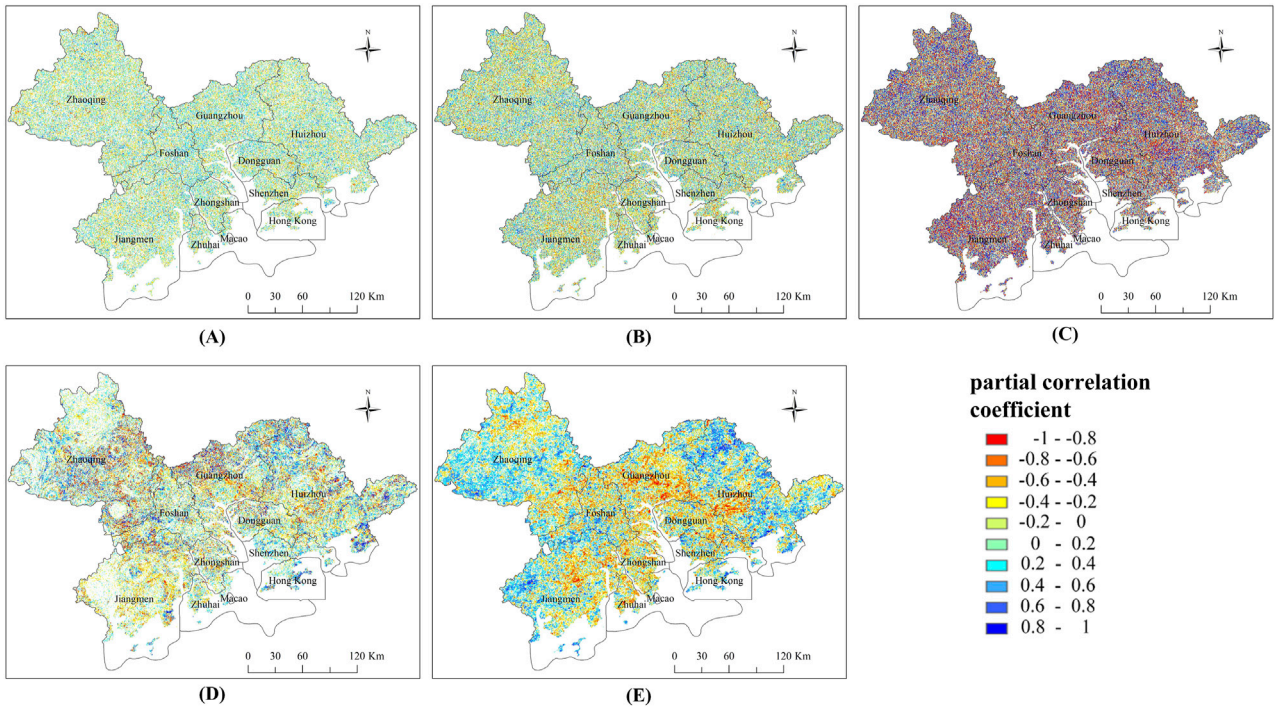

FIGURE 11
Spatial distribution of partial correlation between vegetation change and anthropogenic activity intensity at different time scales **(A)** 1-year, **(B)** 3-year, **(C)** 7-year, **(D)** long-term trend, **(E)** overall values.

contribution of the long-term trend to anthropogenic activity intensity was 62.2%, significantly greater than that of other temporal scales. The partial correlation analysis for the long-term trend showed a significant correlation between vegetation change and anthropogenic activity intensity in 47.21% of the regions, with negative correlations mainly distributed in Guangzhou, Huizhou, Zhaoqing, and Jiangmen. The partial correlation analysis for the overall values showed a significant correlation between vegetation change and anthropogenic activity intensity in 65.32% of the regions in the GBA, with negative correlations mainly distributed in the core urban areas of each city, indicating that urbanization development has a negative impact on vegetation.

3.4.2 Correlation between climatic factors and vegetation change

To reveal the spatial heterogeneity of the correlation between vegetation change and LST change at different temporal scales, partial correlation analyses were performed pixel-by-pixel on the relationship between vegetation change and LST at 1-year, 3-year, and 7-year temporal scales, the long-term trend, and the overall values, using the influence of anthropogenic activity intensity, precipitation, and sunshine duration on vegetation change as control variables. Similarly, the partial correlations between vegetation change and precipitation, between vegetation change and sunshine duration at different temporal scales were analyzed.

As shown in Table 5 and Figures 12A–E, at the 1-year, 3-year, and 7-year temporal scales, the change trends of regions with significant correlations between vegetation change and LST were similar to those of regions with significant correlations between vegetation change and anthropogenic activity intensity. For the overall values, the relationship between vegetation change and LST was not significant in 37.09% of the regions. The regions with significant negative correlations between vegetation change and LST accounted for 30.24%, mainly distributed in Zhaoqing, Jiangmen, and Huizhou. The regions with significant positive correlations between vegetation change and LST reached 32.67%, concentrated in the built-up areas of Guangzhou, Foshan, Zhongshan, Zhuhai, Hong Kong, Shenzhen, and Dongguan. The GBA is located in a humid region with abundant precipitation. The increase in temperature has a small impact on the available water for vegetation,

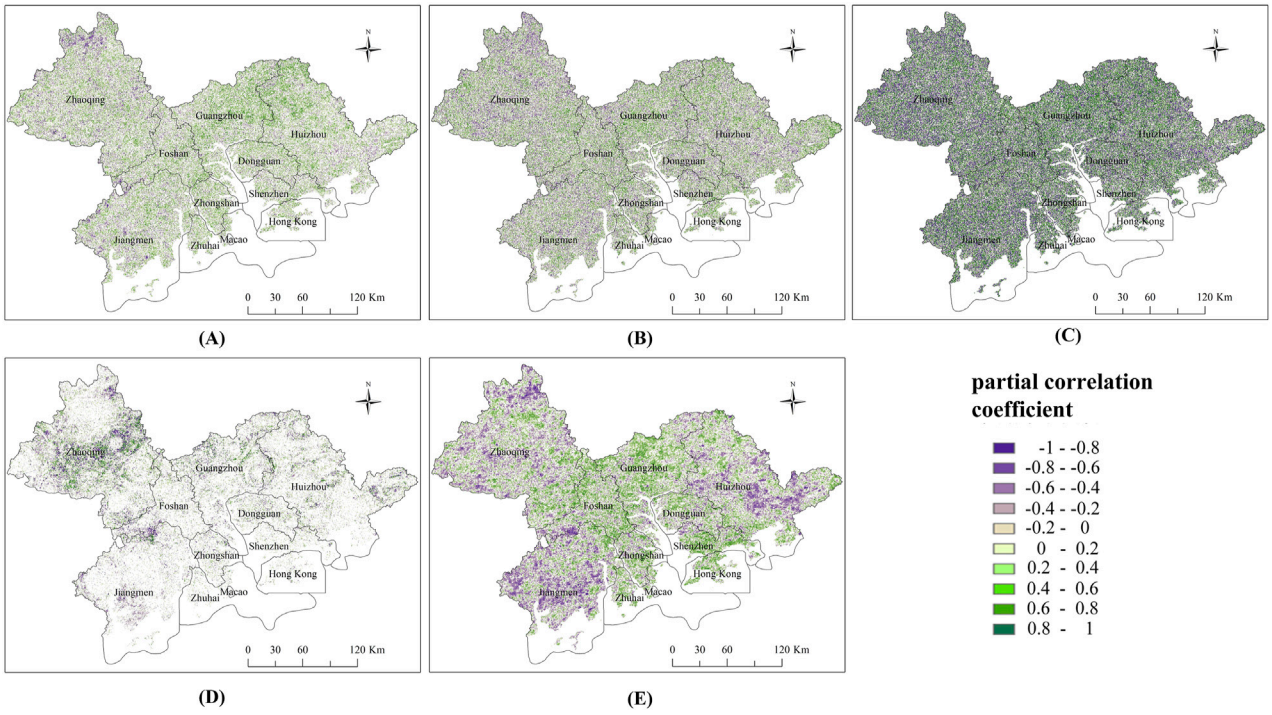

FIGURE 12
Spatial distribution of partial correlation between vegetation change and LST at different time scales **(A)** 1-year, **(B)** 3-year, **(C)** 7-year, **(D)** long-term trend, **(E)** overall values.

TABLE 6 The proportion of correlation between vegetation change and precipitation at different time scales.

Correlation	IMF1	IMF2	IMF3	Residual component	Raw values
$R < 0$, $p < 0.05$	27.81	38.88	36.87	30.07	42.60
$R < 0$, $p > 0.05$	26.36	18.17	11.09	24.89	23.23
$R > 0$, $p < 0.05$	21.41	26.50	41.11	22.23	16.14
$R > 0$, $p > 0.05$	24.43	16.45	10.93	22.80	18.03

but it can promote vegetation photosynthesis, and the increase in land surface temperature promotes vegetation growth.

As shown in Table 6 and Figures 13A–E, the correlations between vegetation change and precipitation in the GBA were significantly correlated in most regions at the 3-year and 7-year temporal scales and the long-term trend. In the built-up areas of Guangzhou, Foshan, Jiangmen, Zhongshan, and Dongguan, an increase in precipitation promoted vegetation growth.

As shown in Table 7 and Figures 14A–E, for the overall values, an increase in sunshine duration promoted vegetation growth in the built-up areas of Guangzhou, Foshan, Zhongshan, Hong Kong, and Jiangmen.

3.5 The contribution of climatic factors and anthropogenic activity to vegetation change

The RESTREND method was used to analyze the response of vegetation change to climate factors and anthropogenic activities in the GBA. Areas with extremely low proportions of impervious surfaces, where vegetation change is only affected by climate factors and not by anthropogenic activities, were randomly selected. The coefficients of a multiple regression model were calculated as the coefficients of the RESTREND model. Based on these coefficients, the predicted values of NDVI were calculated, and the differences between the predicted and observed values were compared. The IMF1 of NDVI was used as the dependent variable in the RESTREND model, and the IMF1 of LST, precipitation, and sunshine duration were used as independent variables. Based on this method, the relative importance of climate factors and anthropogenic activities on vegetation change was determined at the 1-year temporal scale. Similarly, the relative importance of climate factors and anthropogenic activities at the 3-year and 7-year temporal scales and the long-term trend were determined. When the relative contribution of climate factors to vegetation change was greater than 50%, vegetation change was considered to be dominated by climate factors. When the relative contribution of climate factors to vegetation change was less than 50%, vegetation change was considered to be dominated by anthropogenic activities.

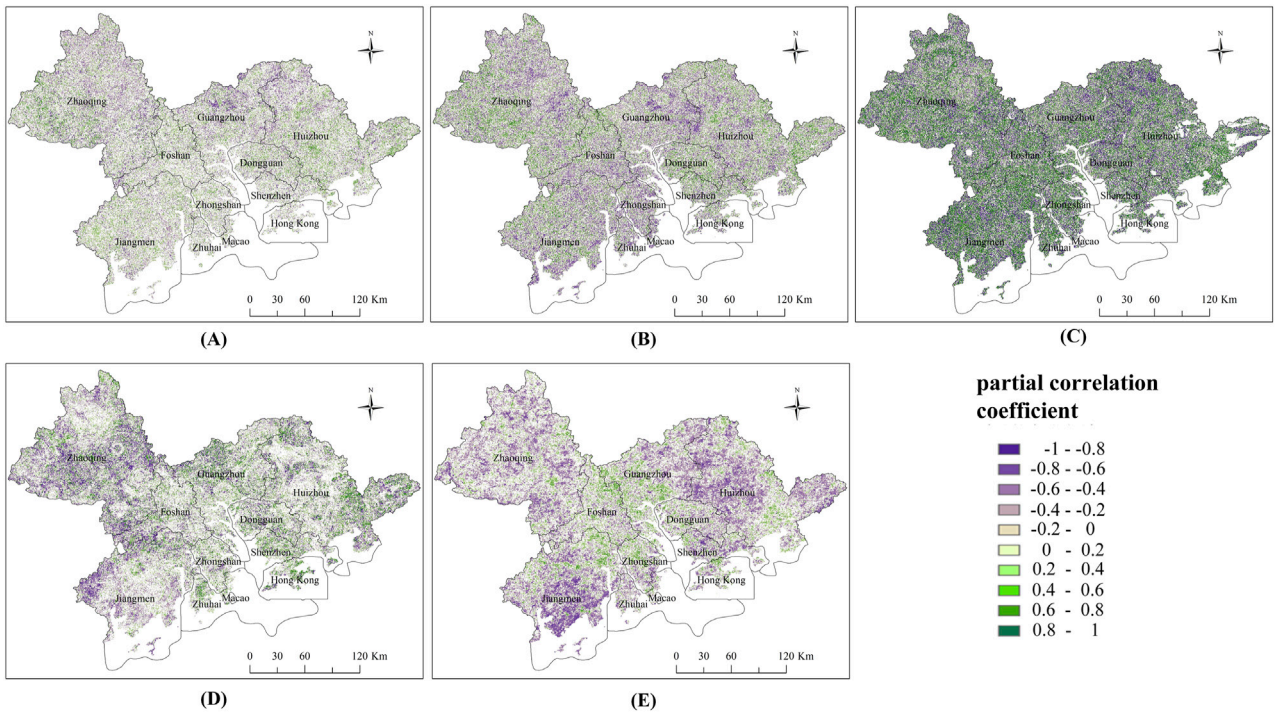

FIGURE 13
Spatial distribution of partial correlation between vegetation change and precipitation at different time scales **(A)** 1-year, **(B)** 3-year, **(C)** 7-year, **(D)** long-term trend, **(E)** overall values.

TABLE 7 The proportion of correlation between vegetation change and sunshine duration at different time scales.

Correlation	IMF1	IMF2	IMF3	Residual component	Raw values
$R < 0$, $p < 0.05$	22.33	27.42	41.04	10.49	31.04
$R < 0$, $p > 0.05$	27.24	20.20	11.84	38.89	23.53
$R > 0$, $p < 0.05$	25.96	31.66	35.39	11.79	23.37
$R > 0$, $p > 0.05$	24.47	20.72	11.73	38.82	22.07

As shown in Figure 15, at the 1-year, 3-year, and 7-year temporal scales, the relative contribution of the predicted NDVI values, i.e., vegetation changes induced by climate factors, was low in most regions of the GBA. The regions with a contribution greater than 50% accounted for 23.33%, 22.50%, and 18.79%, respectively, and these regions did not exhibit a clustered distribution, indicating that vegetation change was mainly driven by anthropogenic activities at short temporal scales, and the impact of urbanization on vegetation was significant. The GBA has experienced rapid urbanization in the past decade, with a significant expansion of high-intensity anthropogenic activity areas, which has significantly affected the distribution of vegetation. For the long-term trend, the regions with a relative contribution of predicted NDVI values greater than 50% accounted for 81.81%, and the regions with a contribution greater than 75% accounted for 69.85%, indicating that climate factors played a dominant role in vegetation change. The regions with a relative contribution of predicted NDVI values less than 50% in the long-term trend, i.e., where anthropogenic activities played a dominant role in vegetation change, were mainly distributed in the core urban areas. Among them, the regions with a contribution less than 25% accounted for 10.54%, indicating that with the expansion of the temporal scale, climate factors played a dominant role in vegetation change in most regions of the GBA in the long-term trend. However, in the core urban areas that were significantly affected by urbanization, vegetation change was determined by the intensity of anthropogenic activities.

4 Discussion

4.1 Mapping anthropogenic activity from nighttime lights

Since 1992, NTL data have been extensively utilized in urbanization research, characterizing the intensity and extent of anthropogenic activity from a nocturnal perspective and demonstrating itself as a reliable indicator (Bennett and Smith,

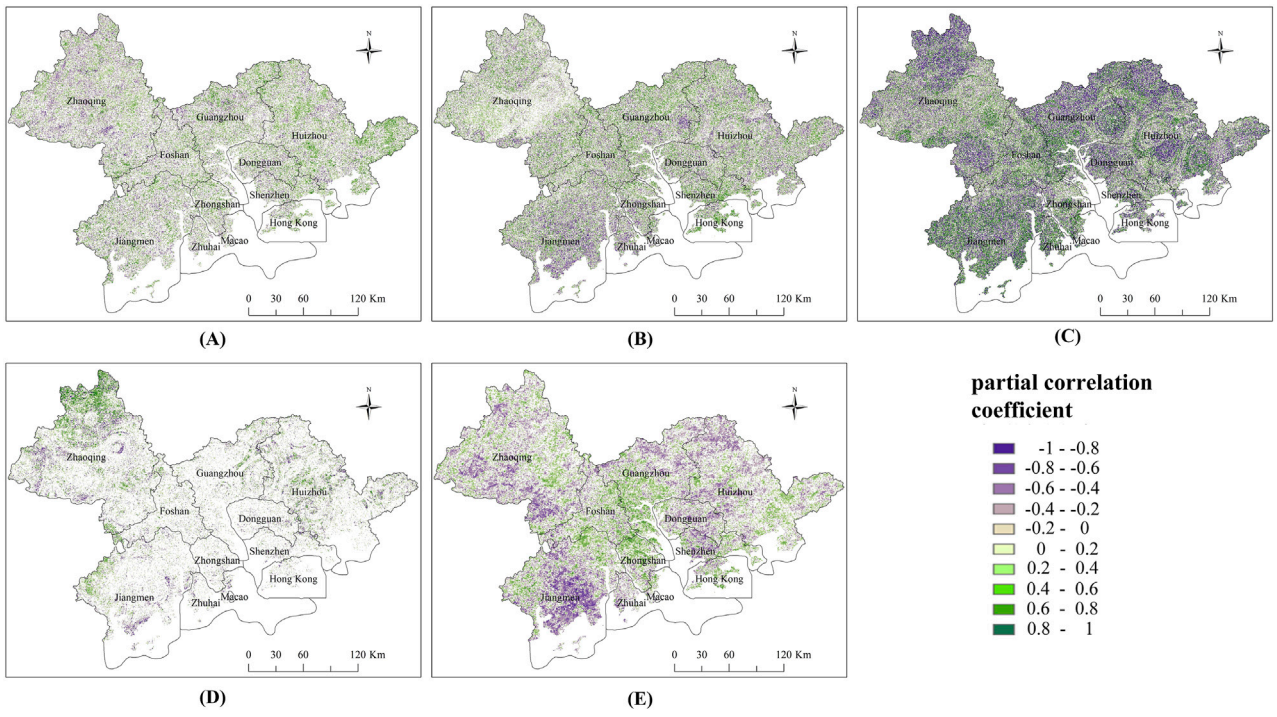

FIGURE 14
Spatial distribution of partial correlation between vegetation change and sunshine duration at different time scales **(A)** 1-year, **(B)** 3-year, **(C)** 7-year, **(D)** long-term trend, **(E)** overall values.

2017). With the proliferation of NTL sensors, algorithms, and data products, NTL data are poised to provide enhanced insight into the socio-economic and environmental changes associated with urbanization. However, limitations persist in NTL-based urban applications. For example, scale effects introduce uncertainties across both spatial and temporal dimensions; differing spatial resolutions can lead to significant discrepancies in the spatial patterns identified in research findings, while varying temporal scales (e.g., annual, monthly, daily) can elicit different NTL patterns and outcomes. Beyond anthropogenic activity influences, NTL variations are also affected by angular effects, seasonal changes, transient light sources, cloud-mask failures, and noise. This can result in inconsistencies between NTL intensity and actual anthropogenic activity intensity (Zhang R. et al., 2023), such as in some rural areas or urban peripheries (Goldblatt et al., 2018). Furthermore, anthropogenic activity mapping presents a complex challenge encompassing factors like population, infrastructure, and land cover. To improve the accuracy of NTL data in urban applications, it is essential to integrate them with geospatial data and other multi-source remote sensing data.

Electricity consumption and urban development are positively correlated; increased electricity consumption primarily stems from sustainable economic growth, urban population, and expanded construction land. Taking Beijing, Shanghai, and Guangzhou as examples, high levels of anthropogenic activity and power consumption frequently coincide (Xu, 2023). Based on this observation, this study utilizes electricity consumption data as a secondary means of validating the characteristics of anthropogenic activity intensity. As shown in Figure 16, Guangzhou and Shenzhen exhibit the highest electricity consumption in the Pearl River Delta region, followed by Foshan and Dongguan. Although Huizhou's electricity consumption is lower, its average annual growth rate is high (Figure 4), indicating a widespread distribution of areas experiencing increasing anthropogenic activity intensity. These results align with findings based on NTL intensity, providing indirect confirmation of the reliability of NTL intensity as a proxy for anthropogenic activity intensity.

4.2 Impact of climate change on vegetation dynamics

This study delved into the impact of climate change on vegetation dynamics in the GBA. Climate change is a key factor influencing vegetation dynamics. During the study period, land surface temperatures in the GBA generally increased, with the percentages of significantly increased areas in Dongguan and Zhongshan reaching 80.11% and 71.49%, respectively, while the long-term trend of precipitation showed a decrease, and sunshine duration showed no significant long-term changes. The greater the differences in land surface temperature, precipitation, and sunshine duration, the greater the differences in NDVI time series (Mondal and Jeganathan, 2018; Ding et al., 2023), which together constitute a scenario in which climate change has a complex impact on vegetation dynamics in the GBA.

The results showed that the impact of climate factors on vegetation in the GBA exhibited spatial heterogeneity, which is similar to the results of previous studies in northern China, the

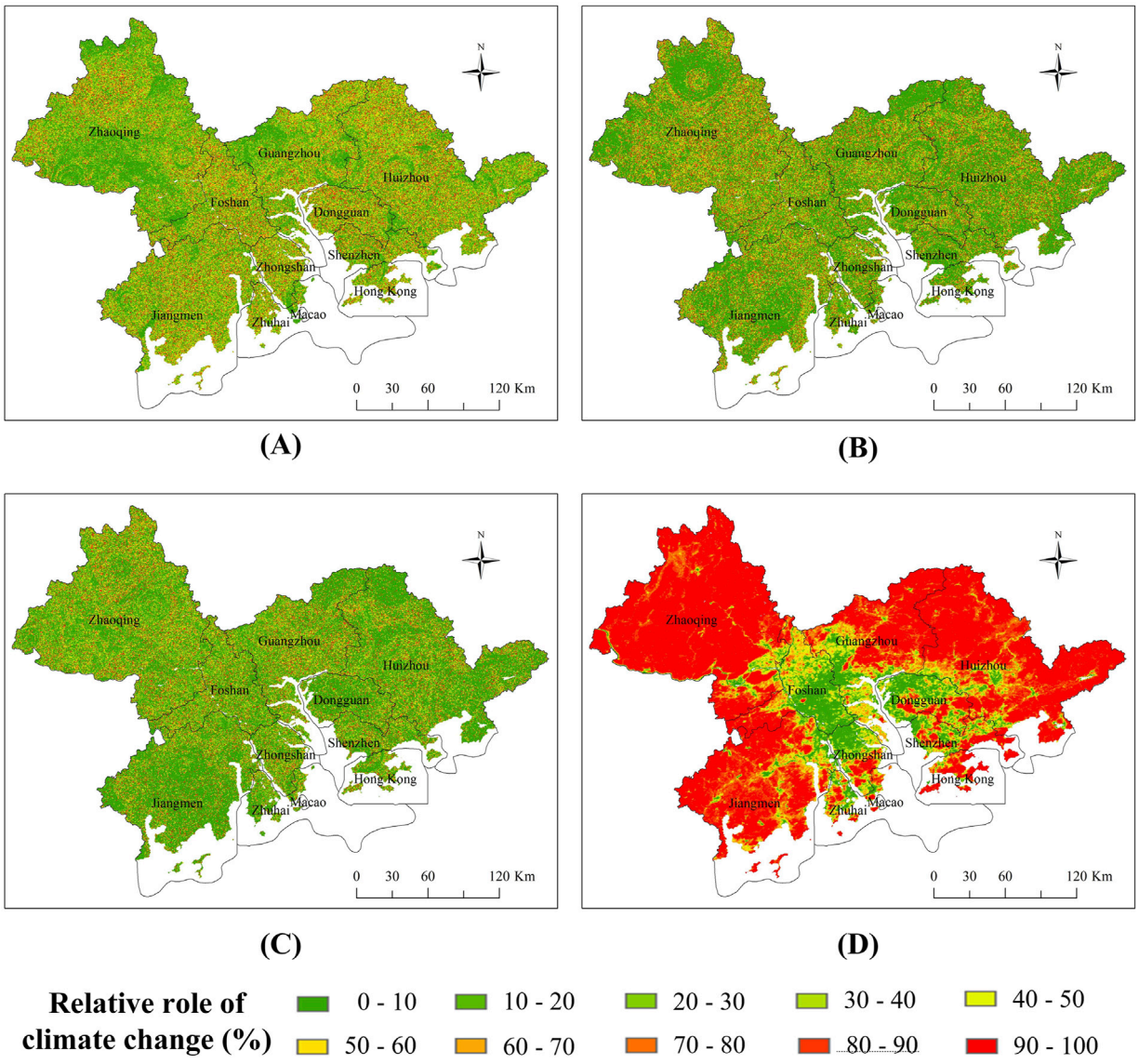

FIGURE 15
Spatial distribution of relative contributions of climate factors to vegetation change **(A)** 1-year, **(B)** 3-year, **(C)** 7-year, **(D)** long-term trends.

Yangtze and Yellow River basins, the Qinghai-Tibet Plateau, and West Bengal, India (Yuan et al., 2015; Banerjee et al., 2024; Xu et al., 2023). We found that the positive correlation between LST and vegetation was more pronounced in areas with higher urbanization levels, which is consistent with some studies that show rising temperatures cause earlier spring warming and delayed autumn cooling, extending the growing season and increasing the leaf area index, resulting in regional greening (Li et al., 2022). In contrast, Zhaoqing, Jiangmen, and Huizhou exhibiting a negative correlation between LST and vegetation were more common, where urbanization levels were relatively lower, increased temperatures can lead to enhanced vegetation transpiration, exacerbating water stress and inhibiting vegetation growth.

The decrease of precipitation have a limiting effect on vegetation growth in the long-term scale, which is consistent with the conclusions of relevant studies that indicate negative impacts of low precipitation and aridification on vegetation (Tuo et al., 2024). In Guangzhou, Foshan, and Zhongshan, precipitation and sunshine duration both showed a positive correlation with vegetation, which is similar to the research results from northern China, the Hengduan Mountains, the Qinghai-Tibet Plateau, and the Central Yunnan Urban Agglomeration (Chen et al., 2020; Chen et al., 2021; Zhang et al., 2019; He et al., 2024). From a mechanistic perspective, climate factors directly influence plant physiological processes such as photosynthesis, respiration, and transpiration, thereby affecting vegetation growth and distribution. Different vegetation types also exhibit varying sensitivities to these influences (Ren Y. et al., 2023), which may be the cause of spatial differences.

In the short-term scales, vegetation change may be driven by anthropogenic activities, but in the long-term trends, climate factors gradually become dominant. Some studies also point out that climate change is the main driver of vegetation change over long periods (Ge et al., 2021; Wang J. et al., 2024). This further emphasizes the key role of climate change in shaping vegetation

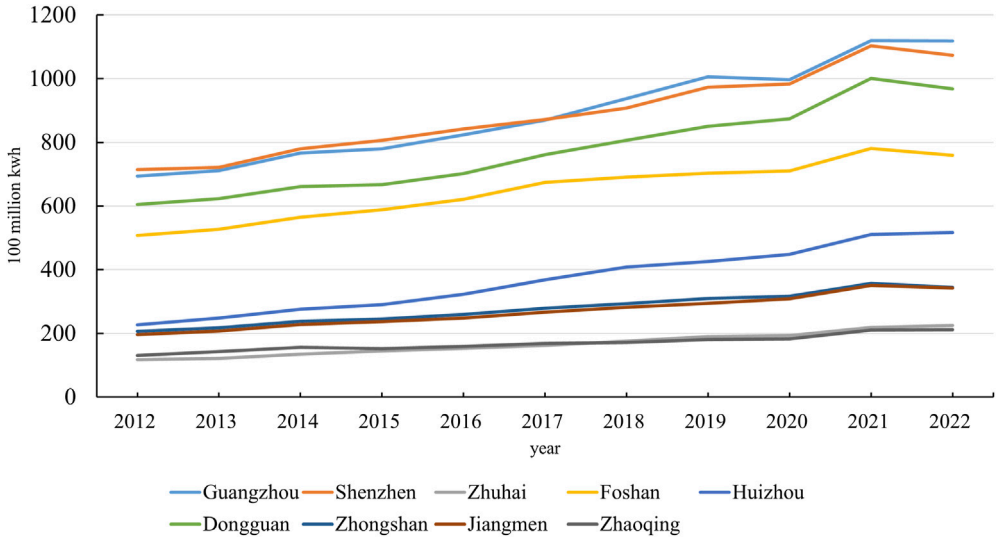

FIGURE 16
Electricity consumption by city in the Pearl River Delta.

dynamics, and the long-term impact of climate change needs to be fully considered when formulating ecological environment protection strategies.

4.3 Impact of anthropogenic activity on vegetation dynamics

From a spatial distribution perspective, the increase in anthropogenic activity intensity was mainly concentrated in the core urban areas, such as Guangzhou, Shenzhen, and Foshan, where the rate of urban expansion was faster. Zhaoqing, Huizhou, and Jiangmen showed relatively lower proportions of increased anthropogenic activity intensity, indicating that there is obvious spatial heterogeneity in the urbanization process within the GBA, which is similar to the results of research in many regions (Gao et al., 2024; Fan et al., 2022). Although the GBA generally exhibited a greening trend, with vegetation improving in 63.59% of the region, the problem of vegetation degradation remained prominent, especially in areas such as Zhongshan, Dongguan, and Guangzhou, where the total area of degradation accounted for as much as 28.99%. This indicates that rapid urbanization has a negative impact on vegetation cover (Yu et al., 2009; Ruas et al., 2022; Zhang et al., 2023a).

A significant negative correlation between anthropogenic activity intensity and vegetation change existed in some regions, particularly evident in the core urban areas (Gao et al., 2022; Zheng et al., 2021). Zhongshan, Dongguan, and Guangzhou experienced rapid expansion of impervious surfaces during the study period. Anthropogenic activity intensity increased significantly, and the proportion of vegetation degradation was relatively high, indicating that the urbanization process caused significant degradation of vegetation cover, which is similar to the research results in the GBA and the Lanzhou-Xining urban agglomeration (Wu et al., 2022; Wang J. et al., 2024). The results of the partial correlation analysis further confirmed this: as the temporal scale increased, the areas with significant correlations between vegetation change and anthropogenic activity intensity increased. In the long-term trend, anthropogenic activity intensity and vegetation change exhibited a significant negative correlation, particularly in the core urban areas, indicating that the urbanization development had a negative impact on vegetation. This is consistent with previous research that pointed out that urban expansion leads to a decrease in vegetation cover (Zou et al., 2025; Zhang et al., 2023b; Yang et al., 2021). The urbanization process leads to an increase in impervious areas and a decrease in green space areas, which directly results in a reduction of vegetation cover. At the same time, urbanization also changes surface hydrological processes and energy balance, further inhibiting vegetation growth (White and Greer, 2006; Zhou et al., 2021). For example, the dense distribution of buildings and the hardening of roads may lead to a decrease in soil moisture content, which is not conducive to vegetation growth. However, some studies have shown that anthropogenic activities promote vegetation cover, with ecological restoration projects, afforestation activities, and decreased population density becoming important factors for increased vegetation cover (Liu et al., 2023; Jin et al., 2020; Shi et al., 2020; Wang J. et al., 2024).

The impact of anthropogenic activities on vegetation varies at different temporal scales. In the short-term temporal scales, vegetation change is mainly driven by anthropogenic activities, such as the reduction of vegetation cover area caused by urban expansion, which is similar to the conclusions of some studies that found the short-term impacts of urban expansion on vegetation are more significant (Qi et al., 2023). In the long-term trend, areas with higher levels of urbanization showed a stronger dominance of anthropogenic activities, while non-urbanized areas tended to be dominated by climate factors (Prăvălie et al., 2022; Li P. et al., 2021; Pang et al., 2017; Banerjee et al., 2024; Yu et al., 2009; Hu et al., 2023). Studies have found that vegetation types and their specific ecological adaptation strategies determine their different response patterns to

climate change, which also explains why vegetation changes in different regions exhibit different patterns under the same climatic conditions. For example, Zhaoqing, Huizhou, and Jiangmen had higher proportions of vegetation improvement, while Zhongshan and Dongguan showed obvious vegetation degradation.

4.4 Limitations and future directions

This study used remote sensing and meteorological data and employed various time series analysis methods to explore vegetation dynamics in the GBA and their relationship with climate change and anthropogenic activities. However, there are still some limitations, which are mainly reflected in the following aspects: 1. Data source limitations: This study relied on MODIS data and NPP-VIIRS/DNB nighttime light data, although these data have good applicability at the regional scale, there are still certain shortcomings in their spatiotemporal resolutions. This may lead to some bias in the detailed depiction of vegetation change and its influencing factors, especially for the evaluation of the lagged effects of extreme climatic events on vegetation. 2. Insufficient representation of meteorological data: Although this study used the monthly total precipitation and sunshine duration data from meteorological stations, the distribution of meteorological stations may not fully represent the climate conditions of the entire study area, especially in topographically complex regions, where the results of data interpolation may have some uncertainties. 3. Methodological limitations: In conducting multi-factor analysis, this study may not have fully captured the non-linear relationships between vegetation change and influencing factors. The selected indicators may not fully represent all climate factors when using the RESTREND method to evaluate the relative contribution of climate factors and anthropogenic activities to vegetation change, which may simplify or underestimate the complex influence of climate change on vegetation.

Future studies could be improved in the following aspects: 1. Improve data quality and resolution: Future research can try to use remote sensing data with higher spatial and temporal resolutions to monitor vegetation dynamics more precisely, and better evaluate the lagged effects of extreme climate events on vegetation. 2. Multi-source data integration: Combining remote sensing data with ground observation data can compensate for the shortcomings of remote sensing data in accuracy and validation. For example, field vegetation surveys and flux observations can be used to improve the accuracy and reliability of research results.

5 Conclusion

This study analyze the spatiotemporal patterns of vegetation change in the GBA, its response characteristics to anthropogenic activities and climate factors, and to quantify the relative contributions of climate factors and anthropogenic activities to vegetation change. According a comprehensive analysis of multi-source data, this study seeks to reveal the driving mechanisms of dynamic vegetation change in the context of urbanization.

The results of this study showed that the GBA as a whole experienced a significant vegetation greening process. The area with improved vegetation was significantly greater than that with degraded vegetation, indicating an overall increasing trend in vegetation cover in the region. Specifically, vegetation in Zhaoqing, Huizhou, and Jiangmen showed significant improvement, while vegetation degradation was more pronounced in the core urban areas of Zhongshan, Dongguan, and Guangzhou. Simultaneously, anthropogenic activities in the region also underwent significant changes. The intensity of anthropogenic activities showed a significant increase in half of the regions, reflecting the impact of the rapid urbanization process on anthropogenic activity intensity. In addition, LST also underwent significant changes, LST increased more noticeably in cities such as Dongguan, Zhongshan, Zhuhai, and Shenzhen, which may be related to the urban heat island effect. Further analysis showed that the dynamics of vegetation change are influenced by driving factors at different temporal scales. The intensity of anthropogenic activities showed smaller fluctuations at short temporal scales, while 65% of the region showed anthropogenic activity intensity fluctuations dominated by long-term trends, indicating that the changes in anthropogenic activities have a cumulative effect over long temporal scales. LST changes in core urban areas were also dominated by long-term trends, which may be the result of the combined effects of long-term urbanization and climate change.

The correlations between vegetation change and anthropogenic activity intensity, and between vegetation change and climate factors exhibited obvious spatiotemporal heterogeneity. As the temporal scale increased, the regions exhibiting significant correlations between vegetation change and anthropogenic activity intensity and between vegetation change and LST gradually increased, indicating that at longer temporal scales, the influences of anthropogenic activities and temperature on vegetation were more pronounced. Notably, vegetation change was significantly correlated with anthropogenic activity intensity in two-thirds of the regions, and the negative correlations were mainly distributed in the core urban areas of various cities, indicating that the urbanization process had a negative impact on vegetation. Simultaneously, regions where vegetation change was significantly negatively correlated with LST were mainly distributed in Zhaoqing, Jiangmen, and Huizhou, while regions with significant positive correlations were concentrated in the built-up areas of Guangzhou, Foshan, Zhongshan, Zhuhai, Hong Kong, Shenzhen, and Dongguan, reflecting the complex impact of temperature changes on vegetation growth in different regions. In addition, increases in precipitation and sunshine duration both promoted vegetation growth to a certain extent.

This study revealed the temporal characteristics of the impacts of climate factors and anthropogenic activities on vegetation change. At short temporal scales, vegetation change was mainly driven by anthropogenic activities, indicating that the short-term impact of urbanization on vegetation was more significant, while the influence of climate factors was relatively small. However, in the long-term trend, vegetation change in most regions was mainly dominated by climate factors, while the vegetation changes caused by anthropogenic activities were mainly distributed in the core urban areas, indicating that over the long-term, the influence of climate factors on vegetation gradually became apparent, while the influence of anthropogenic activities was mainly reflected in urbanized areas.

Data availability statement

The original contributions presented in the study are included in the article/supplementary material, further inquiries can be directed to the corresponding author.

Author contributions

YT: Conceptualization, Data curation, Formal Analysis, Funding acquisition, Investigation, Methodology, Software, Supervision, Validation, Visualization, Writing – original draft, Writing – review and editing. YW: Data curation, Resources, Software, Writing – review and editing. QY: Conceptualization, Data curation, Project administration, Writing – review and editing.

Funding

The author(s) declare that financial support was received for the research and/or publication of this article. This research was funded by the PhD research startup foundation with grant number 622187-BSKYQDJ.

Conflict of interest

Author YW was employed by China Water Huaihe Planning, Design and Research Co, LTD.

The remaining authors declare that the research was conducted in the absence of any commercial or financial relationships that could be construed as a potential conflict of interest.

Generative AI statement

The author(s) declare that no Generative AI was used in the creation of this manuscript.

Publisher's note

References

Abbas, S., Nichol, J. E., and Wong, M. S. (2021). Trends in vegetation productivity related to climate change in China's Pearl River Delta. *PLoS One* 16, e0245467. doi:10.1371/journal.pone.0245467

Aburas, M. M., Abdullah, S. H., Ramli, M. F., Ash' aari, Z. H., and Firdaus, M. (2015). Measuring land cover change in Seremban, Malaysia using NDVI index. *Procedia Environ. Sci.* 30, 238–243. doi:10.1016/j.proenv.2015.10.043

Afuye, G. A., Kalumba, A. M., and Orimoloye, I. R. (2021). Characterisation of vegetation response to climate change: a review. *Sustainability* 13, 7265. doi:10.3390/su13137265

Banerjee, A., Kang, S., Meadows, M. E., Sajjad, W., Bahadur, A., Moazzam, M. F. U., et al. (2024). Evaluating the relative influence of climate and human activities on recent vegetation dynamics in West Bengal, India. *Environ. Res.* 250, 118450. doi:10.1016/j.envres.2024.118450

Barboza, E. P., Cirach, M., Khomenko, S., Iungman, T., Mueller, N., Barrera-Gómez, J., et al. (2021). Green space and mortality in European cities: a health impact assessment study. *Lancet Planet. Health* 5, e718–e730. doi:10.1016/S2542-5196(21)00229-1

Bennett, M. M., and Smith, L. C. (2017). Advances in using multitemporal night-time lights satellite imagery to detect, estimate, and monitor socioeconomic dynamics. *Remote Sens. Environ.* 192, 176–197. doi:10.1016/j.rse.2017.01.005

Boschetti, M., Nutini, F., Brivio, P. A., Bartholomé, E., Stroppiana, D., and Hoscilo, A. (2013). Identification of environmental anomaly hot spots in West Africa from time series of NDVI and rainfall. *ISPRS J. Photogramm. Remote Sens.* 78, 26–40. doi:10.1016/j.isprsjprs.2013.01.003

Cao, J., Liu, H., Zhao, B., Li, Z., Drew, D. M., and Zhao, X. (2019). Species-specific and elevation-differentiated responses of tree growth to rapid warming in a mixed forest lead to a continuous growth enhancement in semi-humid Northeast Asia. *For. Ecol. Manage.* 448, 76–84. doi:10.1016/j.foreco.2019.05.065

Chang, J., Liu, Q., Wang, S., Li, X., Chen, W., Zhao, J., et al. (2022). Vegetation dynamics and their influencing factors in China from 1998 to 2019. *Remote Sens.* 14, 3390. doi:10.3390/rs14143390

Chen, S., Zhu, Z., Liu, X., and Yang, L. (2022). Variation in vegetation and its driving force in the Pearl river delta region of China. *Int. J. Environ. Res. Public Health* 19, 10343. doi:10.3390/ijerph191610343

Chen, S. T., Guo, B., Zhang, R., Zang, W. Q., Wei, C. X., Wu, H. W., et al. (2021). Quantitatively determine the dominant driving factors of the spatial—temporal changes of vegetation NPP in the Hengduan Mountain area during 2000–2015. *J. Mt. Sci.* 18, 427–445. doi:10.1007/s11629-020-6404-9

Chen, W., Xia, L., Xu, G., Yu, S., Chen, H., Chen, J., et al. (2022). Dynamic variation of NDVI and its influencing factors in the Pearl River Basin from 2000 to 2020. *Ecol. Environ.* 31, 1306. doi:10.16258/j.cnki.1674-5906.2022.07.003

Chen, Z., Wang, W., and Fu, J. (2020). Vegetation response to precipitation anomalies under different climatic and biogeographical conditions in China. *Sci. Rep.* 10, 830. doi:10.1038/s41598-020-57910-1

Chu, H., Venevsky, S., Wu, C., and Wang, M. (2019). NDVI-based vegetation dynamics and its response to climate changes at Amur-Heilongjiang River Basin from 1982 to 2015. *Sci. Total Environ.* 650, 2051–2062. doi:10.1016/j.scitotenv.2018.09.115

Csillik, O., Belgiu, M., Asner, G. P., and Kelly, M. (2019). Object-based time-constrained dynamic time warping classification of crops using Sentinel-2. *Remote Sens.* 11, 1257. doi:10.3390/rs11101257

Ding, H., Yuan, Z., Yin, J., Shi, X., and Shi, M. (2023). Evaluating ecosystem stability based on the dynamic time warping algorithm: a case study in the Minjiang river Basin, China. *Ecol. Indic.* 154, 110501. doi:10.1016/j.ecolind.2023.110501

Eckert, S., Hüsler, F., Liniger, H., and Hodel, E. (2015). Trend analysis of MODIS NDVI time series for detecting land degradation and regeneration in Mongolia. *J. Arid. Environ.* 113, 16–28. doi:10.1016/j.jaridenv.2014.09.001

Fan, P. Y., Chun, K. P., Mijic, A., Mah, D. N. Y., He, Q., Choi, B., et al. (2022). Spatially-heterogeneous impacts of surface characteristics on urban thermal environment, a case of the Guangdong-Hong Kong-Macau Greater Bay Area. *Urban Clim.* 41, 101034. doi:10.1016/j.uclim.2021.101034

Fang, J. Y., Piao, S. L., He, J. S., Zhao, Q. S., and Liu, G. H. (2003). Vegetation activity in China has been increasing in recent 20 years. *Sci. China Ser. C Life Sci.* 33, 545–552. doi:10.1360/03c0906

Funk, C. C., and Brown, M. E. (2006). Intra-seasonal NDVI change projections in semi-arid Africa. *Remote Sens. Environ.* 101, 249–256. doi:10.1016/j.rse.2005.12.014

Gao, K., Yang, X., Wang, Z., Lai, F., Zhang, H., Shi, T., et al. (2024). Sensing the multi-scale landscape functions heterogeneity by big geodata from parcel to urban agglomerations-a case of the Greater Bay Area, China. *Int. J. Digit. Earth* 17, 2304073. doi:10.1080/17538947.2024.2304073

Gao, W., Zheng, C., Liu, X., Lu, Y., Chen, Y., Wei, Y., et al. (2022). NDVI-based vegetation dynamics and their responses to climate change and human activities from 1982 to 2020: a case study in the Mu Us Sandy Land, China. *Ecol. Indic.* 137, 108745. doi:10.1016/j.ecolind.2022.108745

Ge, W., Deng, L., Wang, F., Zhang, H., Zhao, Y., Li, S., et al. (2021). Quantifying the contributions of human activities and climate change to vegetation net primary productivity dynamics in China from 2001 to 2016. *Sci. Total Environ.* 773, 145648. doi:10.1016/j.scitotenv.2021.145648

Geng, S., Zhang, H., Xie, F., Li, L., and Yang, L. (2022). Vegetation dynamics under rapid urbanization in the guangdong–Hong Kong–macao greater bay area urban agglomeration during the past two decades. *Remote Sens.* 14, 3993. doi:10.3390/rs14163993

Georgescu, M., Morefield, P. E., Bierwagen, B. G., and Weaver, C. P. (2014). Urban adaptation can roll back warming of emerging megapolitan regions. *Proc. Natl. Acad. Sci. U. S. A.* 111, 2909–2914. doi:10.1073/pnas.1322280111

Goldblatt, R., Stuhlmacher, M. F., Tellman, B., Clinton, N., Hanson, G., Georgescu, M., et al. (2018). Using Landsat and nighttime lights for supervised pixel-based image classification of urban land cover. *Remote Sens. Environ.* 205, 253–275. doi:10.1016/j.rse.2017.11.026

Gregg, J. W., Jones, C. G., and Dawson, T. E. (2003). Urbanization effects on tree growth in the vicinity of New York City. *Nature* 424, 183–187. doi:10.1038/nature01728

He, Y., Lin, C., Wu, C., Pu, N., and Zhang, X. (2024). The urban hierarchy and agglomeration effects influence the response of NPP to climate change and human activities. *Glob. Ecol. Conserv.* 51, e02904. doi:10.1016/j.gecco.2024.e02904

Hu, M., and Xia, B. (2019). A significant increase in the normalized difference vegetation index during the rapid economic development in the Pearl River Delta of China. *Land Degrad. Dev.* 30, 359–370. doi:10.1002/ldr.3221

Hu, T., Dong, J., Qiu, S., Yang, Z., Zhao, Y., Cheng, X., et al. (2023). Stage response of vegetation dynamics to urbanization in megacities: a case study of Changsha City, China. *Sci. Total Environ.* 858, 159659. doi:10.1016/j.scitotenv.2022.159659

Jiang, H., Xu, X., Guan, M., Lu, Y., Li, L., Chen, L., et al. (2020). Determining the contributions of climate change and human activities to vegetation dynamics in agro-pastural transitional zone of northern China from 2000 to 2015. *Sci. Total Environ.* 718, 134871. doi:10.1016/j.scitotenv.2019.134871

Jiang, L., Bao, A., Guo, H., Ndayisaba, F., Kurban, A., and De Maeyer, P. (2017). Vegetation dynamics and responses to climate change and human activities in Central Asia. *Sci. Total Environ.* 599, 967–980. doi:10.1016/j.scitotenv.2017.05.012

Jiang, P. (2022). *Analysis of vegetation change in China and its sensitivity to climate variability from 1982 to 2015 [D]*. Lanzhou, China: Lanzhou University. doi:10.27204/d.cnki.glzhu.2022.000377

Jin, K., Wang, F., Han, J. Q., Wu, Z. S., Tang, Y. L., Li, J. M., et al. (2020). Contribution of climatic change and human activities to vegetation NDVI change over China during 1982-2015. *Acta Geogr. Sin.* 75, 961–974.

Lasaponara, R., Abate, N., and Masini, N. (2024). Early identification of vegetation pest diseases using Sentinel 2 NDVI time series 2016-2023: the case of Toumeyella Parvicorvis at Castel Porziano (Italy). *IEEE Geosci. Remote Sens. Lett.* 21, 1–5. in press. doi:10.1109/lgrs.2024.3386218

Li, M., Wu, P., Ma, Z., and Liu, J. (2022). Prominent vegetation greening in spring and autumn across China during the 1981–2018 period. *Environ. Res. Lett.* 17, 124043. doi:10.1088/1748-9326/aca8be

Li, P., Wang, J., Liu, M., Xue, Z., Bagherzadeh, A., and Liu, M. (2021a). Spatio-temporal variation characteristics of NDVI and its response to climate on the Loess Plateau from 1985 to 2015. *Catena* 203, 105331. doi:10.1016/j.catena.2021.105331

Li, S., Yang, S., Liu, X., Li, L., and Zhao, Y. (2015). NDVI-based analysis on the influence of climate change and human activities on vegetation restoration in the Shaanxi-Gansu-Ningxia Region, Central China. *Remote Sens.* 7, 11163–11182. doi:10.3390/rs70911163

Li, Y., Zheng, Z., Qin, Y., Wang, J., Liu, J., Feng, Q., et al. (2021b). Relative contributions of natural and man-made factors to vegetation cover change of environmentally sensitive and vulnerable areas of China. *J. Clean. Prod.* 321, 128917. doi:10.1016/j.jclepro.2021.128917

Lin, X., Niu, J., Berndtsson, R., Yu, X., Zhang, L., and Chen, X. (2020). NDVI dynamics and its response to climate change and reforestation in northern China. *Remote Sens.* 12, 4138. doi:10.3390/rs12244138

Liu, C., Liu, J., Zhang, Q., Ci, H., Gu, X., and Gulakhmadov, A. (2022). Attribution of NDVI dynamics over the globe from 1982 to 2015. *Remote Sens.* 14, 2706. doi:10.3390/rs14112706

Liu, Y., Xie, Y., Guo, Z., and Xi, G. (2023). Effects of climate variability and human activities on vegetation dynamics across the Qinghai–Tibet Plateau from 1982 to 2020. *Remote Sens.* 15, 4988. doi:10.3390/rs15204988

Mehmood, K., Anees, S. A., Muhammad, S., Hussain, K., Shahzad, F., Liu, Q., et al. (2024a). Analyzing vegetation health dynamics across seasons and regions through NDVI and climatic variables. *Sci. Rep.* 14, 11775. doi:10.1038/s41598-024-62464-7

Mehmood, K., Anees, S. A., Rehman, A., Tariq, A., Zubair, M., Liu, Q., et al. (2024b). Exploring spatiotemporal dynamics of NDVI and climate-driven responses in ecosystems: insights for sustainable management and climate resilience. *Ecol. Inf.* 80, 102532. doi:10.1016/j.ecoinf.2024.102532

Mondal, S., and Jeganathan, C. (2018). Mountain agriculture extraction from time-series MODIS NDVI using dynamic time warping technique. *Int. J. Remote Sens.* 39, 3679–3704. doi:10.1080/01431161.2018.1444289

Ning, T., Liu, W., Lin, W., and Song, X. (2015). NDVI variation and its responses to climate change on the northern Loess Plateau of China from 1998 to 2012. *Adv. Meteorol.* 2015, 1–10. doi:10.1155/2015/725427

Pang, G., Wang, X., and Yang, M. (2017). Using the NDVI to identify variations in, and responses of, vegetation to climate change on the Tibetan Plateau from 1982 to 2012. *Quat. Int.* 444, 87–96. doi:10.1016/j.quaint.2016.08.038

Potter, C. S., and Brooks, V. (1998). Global analysis of empirical relations between annual climate and seasonality of NDVI. *Int. J. Remote Sens.* 19, 2921–2948. doi:10.1080/014311698214352

Pradhan, B., Yoon, S., and Lee, S. (2024). Examining the dynamics of vegetation in South Korea: an integrated analysis using remote sensing and *in situ* data. *Remote Sens.* 16, 300. doi:10.3390/rs16020300

Prăvălie, R., Sîrodoev, I., Nita, I. A., Patriche, C., Dumitraşcu, M., Roşca, B., et al. (2022). NDVI-Based ecological dynamics of forest vegetation and its relationship to climate change in Romania during 1987–2018. *Ecol. Indic.* 136, 108629. doi:10.1016/j.ecolind.2022.108629

Pravalie, R., Sîrodoev, I., and Peptenatu, D. (2014). Detecting climate change effects on forest ecosystems in Southwestern Romania using Landsat TM NDVI data. *J. Geogr. Sci.* 24, 815–832. doi:10.1007/s11442-014-1122-2

Qi, G., Cong, N., Luo, M., Qiu, T., Rong, L., Ren, P., et al. (2024). Contribution of climatic change and human activities to vegetation dynamics over southwest China during 2000–2020. *Remote Sens.* 16, 3361. doi:10.3390/rs16183361

Qi, T., Ren, Q., Zhang, D., Lu, W., and He, C. (2023). Impacts of urban expansion on vegetation in drylands: a multiscale analysis based on the vegetation disturbance index. *Ecol. Indic.* 147, 109984. doi:10.1016/j.ecolind.2023.109984

Qi, X., Jia, J., Liu, H., Qin, X., Zhang, Y., Liu, H., et al. (2019). Relative importance of climate change and human activities for vegetation changes on China's silk road economic belt over multiple timescales. *Catena* 180, 224–237. doi:10.1016/j.catena.2019.04.027

Ren, H., Wen, Z., Liu, Y., Lin, Z., Han, P., Shi, H., et al. (2023a). Vegetation response to changes in climate across different climate zones in China. *Ecol. Indic.* 155, 110932. doi:10.1016/j.ecolind.2023.110932

Ren, Y., Zhang, F., Zhao, C., and Cheng, Z. (2023b). Attribution of climate change and human activities to vegetation NDVI in Jilin Province, China during 1998–2020. *Ecol. Indic.* 153, 110415. doi:10.1016/j.ecolind.2023.110415

Rhif, M., Abbes, A. B., Martinez, B., de Jong, R., Sang, Y., and Farah, I. R. (2022). Detection of trend and seasonal changes in non-stationary remote sensing data: case study of Tunisia vegetation dynamics. *Ecol. Inf.* 69, 101596. doi:10.1016/j.ecoinf.2022.101596

Ruan, Z., Kuang, Y., He, Y., Zhen, W., and Ding, S. (2020). Detecting vegetation change in the Pearl River Delta region based on time series segmentation and residual trend analysis (TSS-RESTREND) and MODIS NDVI. *Remote Sens.* 12, 4049. doi:10.3390/rs12244049

Ruas, R. D. B., Laís, M. S. C., and Bered, F. (2022). Urbanization driving changes in plant species and communities–A global view. *Glob. Ecol. Conserv.* 38, e02243. doi:10.1016/j.gecco.2022.e02243

Shi, Y., Jin, N., Ma, X., Wu, B., He, Q., Yue, C., et al. (2020). Attribution of climate and human activities to vegetation change in China using machine learning techniques. *Agric. For. Meteorol.* 294, 108146. doi:10.1016/j.agrformet.2020.108146

Singh, P., Verma, P., Chaudhuri, A. S., Singh, V. K., and Rai, P. K. (2024). Evaluating the relationship between Urban Heat Island and temporal change in land use, NDVI and NDBI: a case study of Bhopal city, India. *Int. J. Environ. Sci. Technol.* 21, 3061–3072. doi:10.1007/s13762-023-05141-y

Sun, R., Chen, S., and Su, H. (2021). Climate dynamics of the spatiotemporal changes of vegetation NDVI in northern China from 1982 to 2015. *Remote Sens.* 13, 187. doi:10.3390/rs13020187

Tian, X., Tao, Z., Xie, Y., Shao, W., and Zhang, S. (2024). Spatiotemporal evolution and driving mechanism of fractional vegetation coverage in the Yangtze River Delta. *IEEE J. Sel. Top. Appl. Earth Obs. Remote Sens.* 17, 10979–10997. In Press. doi:10.1109/jstars.2024.3407727

Tuo, M., Xu, G., Zhang, T., Guo, J., Zhang, M., Gu, F., et al. (2024). Contribution of climatic factors and human activities to vegetation changes in arid grassland. *Sustainability* 16, 794. doi:10.3390/su16020794

Wang, B., Xu, G., Li, P., Li, Z., Zhang, Y., Cheng, Y., et al. (2020). Vegetation dynamics and their relationships with climatic factors in the Qinling Mountains of China. *Ecol. Indic.* 108, 105719. doi:10.1016/j.ecolind.2019.105719

Wang, J., and Liu, D. (2022). Vegetation green-up date is more sensitive to permafrost degradation than climate change in spring across the northern permafrost region. *Glob. Change Biol.* 28, 1569–1582. doi:10.1111/gcb.16011

Wang, J., Wang, Y., and Xu, D. (2024a). Desertification in northern China from 2000 to 2020: the spatial–temporal processes and driving mechanisms. *Ecol. Inf.* 82, 102769. doi:10.1016/j.ecoinf.2024.102769

Wang, M., Peng, J., Du, Y., Ma, J., Feng, Q., and Hu, Y. (2021). Scale consistency for investigating urbanization level, vegetation coverage, and their correlation. *Urban For. Urban Green.* 59, 126998. doi:10.1016/j.ufug.2021.126998

Wang, W., Luan, W., Jing, H., Zhu, J., Zhang, K., Ma, Q., et al. (2024b). Quantitative assessment of urban expansion impact on vegetation in the lanzhou–xining urban agglomeration. *Appl. Sci.* 14, 8615. doi:10.3390/app14198615

Wang, Z. X., Liu, C., and Huete, A. (2003). Progress in vegetation index research: from AVHRR-NDVI to MODIS-EVI. *Acta Ecol. Sin.* 5, 979–987. doi:10.3321/j.issn:1000-0933.2003.05.020

White, M. D., and Greer, K. A. (2006). The effects of watershed urbanization on the stream hydrology and riparian vegetation of Los Penasquitos Creek, California. *Landsc. Urban Plan.* 74, 125–138. doi:10.1016/j.landurbplan.2004.11.015

Wu, G., Dang, A., Tian, Y., and Kan, C. (2021). Study on the urban agglomerations structure of the Guangdong-Hong Kong-Macao Greater Bay Area based on spatiotemporal big data. *J. Remote Sens.* 25, 665–676. doi:10.11834/jrs.20210590

Wu, X., Sun, X., Wang, Z., Li, C., Gao, X., Lu, Y., et al. (2020). Vegetation changes and their response to global change based on NDVI in the Koshi river Basin of central Himalayas since 2000. *Sustainability* 12, 6644. doi:10.3390/su12166644

Wu, Y., Luo, Z., and Wu, Z. (2022). The different impacts of climate variability and human activities on NPP in the Guangdong–Hong Kong–Macao Greater Bay Area. *Remote Sens.* 14, 2929. doi:10.3390/rs14122929

Wuyun, D., Duan, M., Sun, L., Crusiol, L. G. T., Wu, N., and Chen, Z. (2024). Pixel-wise parameter assignment in LandTrendr algorithm: enhancing cropland abandonment monitoring using satellite-based NDVI time-series. *Comput. Electron. Agric.* 227, 109541. doi:10.1016/j.compag.2024.109541

Xu, B., Li, J., Pei, X., and Yang, H. (2023). Decoupling the response of vegetation dynamics to asymmetric warming over the Qinghai-Tibet plateau from 2001 to 2020. *J. Environ. Manage.* 347, 119131. doi:10.1016/j.jenvman.2023.119131

Xu, L. (2023). *A study on the impact of urban development and its transmission effect on carbon emission in China [D]*. Lanzhou, China: Lanzhou University. doi:10.27204/d.cnki.glzhu.2023.000245

Yan, W., Wang, H., Jiang, C., Jin, S., Ai, J., and Sun, O. J. (2021). Satellite view of vegetation dynamics and drivers over southwestern China. *Ecol. Indic.* 130, 108074. doi:10.1016/j.ecolind.2021.108074

Yang, K., Sun, W., Luo, Y., and Zhao, L. (2021). Impact of urban expansion on vegetation: the case of China (2000–2018). *J. Environ. Manage.* 291, 112598. doi:10.1016/j.jenvman.2021.112598

Yu, D., Shao, H., Shi, P., Li, X., and Ji, C. (2009). How does the conversion of land cover to urban use affect net primary productivity? a case study in shenzhen city, China. *Agric. For. Meteorol.* 149, 2054–2060. doi:10.1016/j.agrformet.2009.07.012

Yuan, J., Xu, Y., Xiang, J., Wu, L., and Wang, D. (2019). Spatiotemporal variation of vegetation coverage and its associated influence factor analysis in the Yangtze River Delta, eastern China. *Environ. Sci. Pollut. Res.* 26, 32866–32879. doi:10.1007/s11356-019-06378-2

Yuan, X., Li, L., Chen, X., Liu, X., Li, H., and Chen, Z. (2015). Effects of precipitation intensity and temperature on NDVI-based grass change over Northern China during the period from 1982 to 2011. *Remote Sens.* 7, 10164–10183. doi:10.3390/rs70810164

Zhang, P., Dong, Y., Ren, Z., Wang, G., Guo, Y., Wang, C., et al. (2023a). Rapid urbanization and meteorological changes are reshaping the urban veg-etation pattern in urban core area: a national 315-city study in China. *Sci. Total Environ.* 904, 167269. doi:10.1016/j.scitotenv.2023.167269

Zhang, Q. (2014). *Contributions of climate change and human activities to vegetation dynamics of Loess Plateau [D]*. Lanzhou, China: Lanzhou Jiaotong University. doi:10.7666/d.D539465

Zhang, R., Chen, S., Gao, L., and Hu, J. (2023b). Spatiotemporal evolution and impact mechanism of ecological vulnerability in the Guangdong–Hong Kong–Macao Greater Bay Area. *Ecol. Indic.* 157, 111214. doi:10.1016/j.ecolind.2023.111214

Zhang, W., Wang, L., Xiang, F., Qin, W., and Jiang, W. (2020). Vegetation dynamics and the relations with climate change at multiple time scales in the Yangtze River and Yellow River Basin, China. *Ecol. Indic.* 110, 105892. doi:10.1016/j.ecolind.2019.105892

Zhang, X., Jia, W., Lu, S., and He, J. (2024). Ecological assessment and driver analysis of high vegetation cover areas based on new remote sensing index. *Ecol. Inf.* 82, 102786. doi:10.1016/j.ecoinf.2024.102786

Zhang, Y., Xu, G., Li, P., Li, Z., Wang, Y., Wang, B., et al. (2019). Vegetation change and its relationship with climate factors and elevation on the Tibetan plateau. *Int. J. Environ. Res. Public Health* 16, 4709. doi:10.3390/ijerph16234709

Zhang, Z., Chang, J., Xu, C. Y., Liu, D., Yu, Z., Yang, H., et al. (2018). The response of lake area and vegetation cover variations to climate change over the Qinghai-Tibetan Plateau during the past 30 years. *Sci. Total Environ.* 635, 443–451. doi:10.1016/j.scitotenv.2018.04.113

Zheng, K., Tan, L., Sun, Y., Wu, Y., Duan, Z., Xu, Y., et al. (2021). Impacts of climate change and anthropogenic activities on vegetation change: evidence from typical areas in China. *Ecol. Indic.* 126, 107648. doi:10.1016/j.ecolind.2021.107648

Zhou, S., Zhang, W., Wang, S., Zhang, B., and Xu, Q. (2021). Spatial–temporal vegetation dynamics and their relationships with climatic, anthropogenic, and hydrological factors in the Amur River basin. *Remote Sens.* 13, 684. doi:10.3390/rs13040684

Zou, Y., Chen, W., Li, S., Wang, T., Yu, L., Zhang, X., et al. (2025). Assessing vegetation dynamics and human impacts in natural and urban areas of China: insights from remote sensing data. *J. Environ. Manage.* 373, 123632. doi:10.1016/j.jenvman.2024.123632

frontiers | Frontiers in Environmental Science

TYPE Original Research
PUBLISHED 22 May 2025
DOI 10.3389/fenvs.2025.1601695

OPEN ACCESS

EDITED BY
Tianjiao Feng,
Beijing Forestry University, China

REVIEWED BY
Ling Han,
Grassland Ecology, Nitrogen Cycle, Nitrogen Deposition, China
Wang Hongyi,
Heilongjiang Bayi Agricultural University, China
Ran Zhang,
Beijing Forestry University, China

*CORRESPONDENCE
Yanying Han,
1064336015@qq.com

†These authors share first authorship

RECEIVED 28 March 2025
ACCEPTED 06 May 2025
PUBLISHED 22 May 2025

CITATION
Zhang X, Ye Y, Tao J, Niu Z, Cui Z, Li J and Han Y (2025) Responses of alpine grassland plant communities on Sejila Mountain in the Qinghai-Tibet Plateau to phosphorus addition. *Front. Environ. Sci.* 13:1601695. doi: 10.3389/fenvs.2025.1601695

Responses of alpine grassland plant communities on Sejila Mountain in the Qinghai-Tibet Plateau to phosphorus addition

Xizhe Zhang†, Yanhui Ye†, Jiang Tao, Ziyou Niu, Zhipan Cui, Jianlin Li and Yanying Han*

Resources and Environment College, Xizang Agriculture and Animal Husbandry University, Nyingchi, Tibet, China

Introduction: As an important global ecological security barrier, the Qinghai-Tibet Plateau is a key region for exploring how global climate change affects the grassland ecosystem. Therefore, this study explored the mechanism of the impact of intensified atmospheric Phosphorus (P) deposition on the alpine grassland plant communities in Sejila Mountain, Nyingchi, Tibet.

Methods: A field experiment with four different gradients of phosphate fertilizer application (0, 50, 75, and 100 kg hm^{-2} a^{-1}) was designed. The variation patterns of plant morphology, biomass, nutrient content, and stoichiometric ratio characteristics in response to P were systematically analyzed.

Results: P addition significantly affected the total community biomass and root-shoot ratio, showing a trend of initial increase followed by decline ($P < 0.05$). Additionally, P addition significantly influenced the plant traits (average height, total coverage, and abundance) and aboveground biomass of plant community (Poaceae, Cyperaceae, and Forbs). The plant traits and aboveground biomass of Poaceae and Forbs increased significantly with increasing of P addition levels. At a P addition of 100 kg hm^{-2} a^{-1}, a decline in these parameters was observed. The total coverage and aboveground biomass of Cyperaceae plants showed a significant downward trend. P addition had limited effects on plant carbon (C) and nitrogen (N) contents and their respective stoichiometric ratios. However, it significantly increased P contents in both aboveground and belowground plant parts ($P < 0.05$), consequently reducing the C:P and N:P stoichiometric ratios in plants. This effectively enhanced plant P use efficiency.

Discussion: This study highlights the significant role of P addition in shaping the plant community structure and nutrient cycling of alpine grasslands. However, excessive P addition may exacerbate ecological competition among plants, potentially leading to nutritional imbalances and soil environmental degradation.

KEYWORDS

phosphorus addition, alpine grassland, plant traits, nutrient content, stoichiometric ratio

1 Introduction

Phosphorus (P) deposition encompasses contributions from both natural and anthropogenic sources. As a critical nutrient for plant growth, P plays an indispensable role in ecosystem functioning by influencing plant productivity, carbon sequestration, and nutrient cycling through atmospheric deposition (Dissanayaka et al., 2020). Atmospheric P deposition has gained increasing attention due to its dual natural and human-driven origins, including weathering processes, volcanic activities, agricultural runoff, dust transport, and emissions from combustion sources (Pan et al., 2021). In recent decades, global climate change and intensified human activities have substantially increased P deposition, particularly in regions such as Asia and Europe (Penuelas et al., 2020). This trend is primarily attributed to agricultural fertilization practices, windborne dust from arid and semi-arid areas, and industrial emissions. While P deposition enhances nutrient availability in terrestrial ecosystems, it is also associated with a suite of environmental challenges. Alpine grassland ecosystems, particularly those on the Qinghai-Tibet Plateau, are highly sensitive to changes in nutrient availability due to their nutrient-limited conditions and harsh environmental constraints. These ecosystems provide vital ecosystem services, such as climate regulation, water conservation, soil fertility maintenance, and support for pastoral livelihoods (Yang et al., 2020). The addition of P promotes the increase in aboveground biomass of alpine grasslands, drives the proliferation of bacteria and fungi, enhances their activity levels, and further regulates the functional traits of plants, thereby propelling changes in the overall ecological balance and ecological functions of alpine grasslands (Sun J. et al., 2022). Plant biomass is a key metric for assessing grassland ecosystem health and restoration, as it reflects the system's capacity for carbon storage and primary production. Biomass production in grasslands is intricately linked to the availability and stoichiometry of carbon (C), nitrogen (N), and P. Among these elements, P is often the most limiting nutrient in alpine ecosystems due to its low bioavailability and slow turnover rates (Mesquita et al., 2020).

P addition can profoundly affect the structure and functioning of alpine grassland ecosystems (Sun Y. et al., 2022). Experimental studies have shown that P inputs promote plant biomass accumulation, enhance vegetation cover, and increase primary productivity (Mao et al., 2021). However, these benefits are accompanied by significant alterations in plant community composition. P addition tends to favor species with higher P demands, such as grasses and forbs, while suppressing species less dependent on P, such as sedges. This shift in community structure can lead to a decline in plant diversity, particularly in nutrient-poor environments where competition for P is a key driver of species coexistence. Over the long term, P addition may result in soil P accumulation, altering the chemical and biological properties of soils and complicating the long-term trajectory of plant biomass dynamics. P enrichment can increase soil microbial activity and alter the composition of microbial communities, which play a critical role in nutrient cycling. Enhanced microbial activity may accelerate the mineralization of organic matter, thereby influencing the availability of other essential nutrients such as nitrogen. Moreover, the interaction between P and nitrogen availability can lead to imbalances in nutrient ratios, potentially reducing the efficiency of nutrient uptake and utilization by plants.

In addition to its effects on plant biomass, P addition significantly influences the stoichiometry of C, N, and P within alpine grassland (Sun Y. et al., 2022). Changes in stoichiometric ratios are particularly important as they regulate key ecological processes, including nutrient cycling, plant-microbe interactions, and ecosystem productivity. P addition exerts profound effects on the contents of C, N, and P in alpine grasslands. It can alter the structure of soil bacterial communities, influence nitrogen forms in the soil, and affect plant nitrogen uptake (Zhang Z. et al., 2024). Additionally, P addition regulates plant growth and microbial activity in soils, indirectly impacting soil carbon content. In alpine grasslands, P addition enhances plant P uptake, influencing the forms of P in the soil. More importantly, P addition significantly affects the stoichiometric ratios of plants, soil, and microbial biomass, notably reducing C:P and N:P ratios, while its effects on the C:N ratio are relatively limited (Sun Y. et al., 2022). Such imbalances in stoichiometric ratios could have potential negative consequences for the functionality of grassland ecosystems.

The alpine grasslands of Sejila Mountain, located in Nyingchi, southeastern Tibet, are representative of high-altitude ecosystems characterized by cool winters, mild summers, and distinct wet and dry seasons. These grasslands are nutrie nt-limited and highly sensitive to external nutrient inputs, making them an ideal system for studying the effects of P deposition. Most of the current studies on the impact of P addition on alpine grasslands are short-term experiments. In this study, we conducted a long-term P addition experiment to study its impacts on the plant traits, biomass, nutrient contents (C, N, and P), and stoichiometric characteristics of the alpine grasslands in Sejila Mountain. The main objectives are as follows: (1) Analyze the responses of different plant functional groups to P addition; (2) Reveal the impacts of P addition on the plant communities in alpine grasslands; (3) Explore the relationships among plant traits, biomass, and nutrient contents under P addition. This is of great significance for clarifying the potential mechanisms of the changes in plant communities and the dynamics of nutrient cycling in alpine grasslands under P deposition, and provides a scientific basis for the protection and restoration of alpine grasslands.

2 Materials and methods

2.1 Study area

The experiment was conducted on the alpine grasslands of the western slope of Sejila Mountain in Nyingchi City, Tibet Autonomous Region (29°37′30″N, 94°37′13″E). The site exhibits an elevation of 4,400 m and an average slope of 21.4° (Figure 1). This plot is located in the humid mountain warm temperate zone and semi-humid mountain temperate zone. The annual average temperature is −0.73°C, and the annual average precipitation is 1,134.1 mm. Precipitation is mainly concentrated from April to October. The frost - free period is 180 days, and the average relative humidity ranges from 60% to 80%. The primary vegetation types include Poaceae, Cyperaceae, and Forbs. The soil types in the area

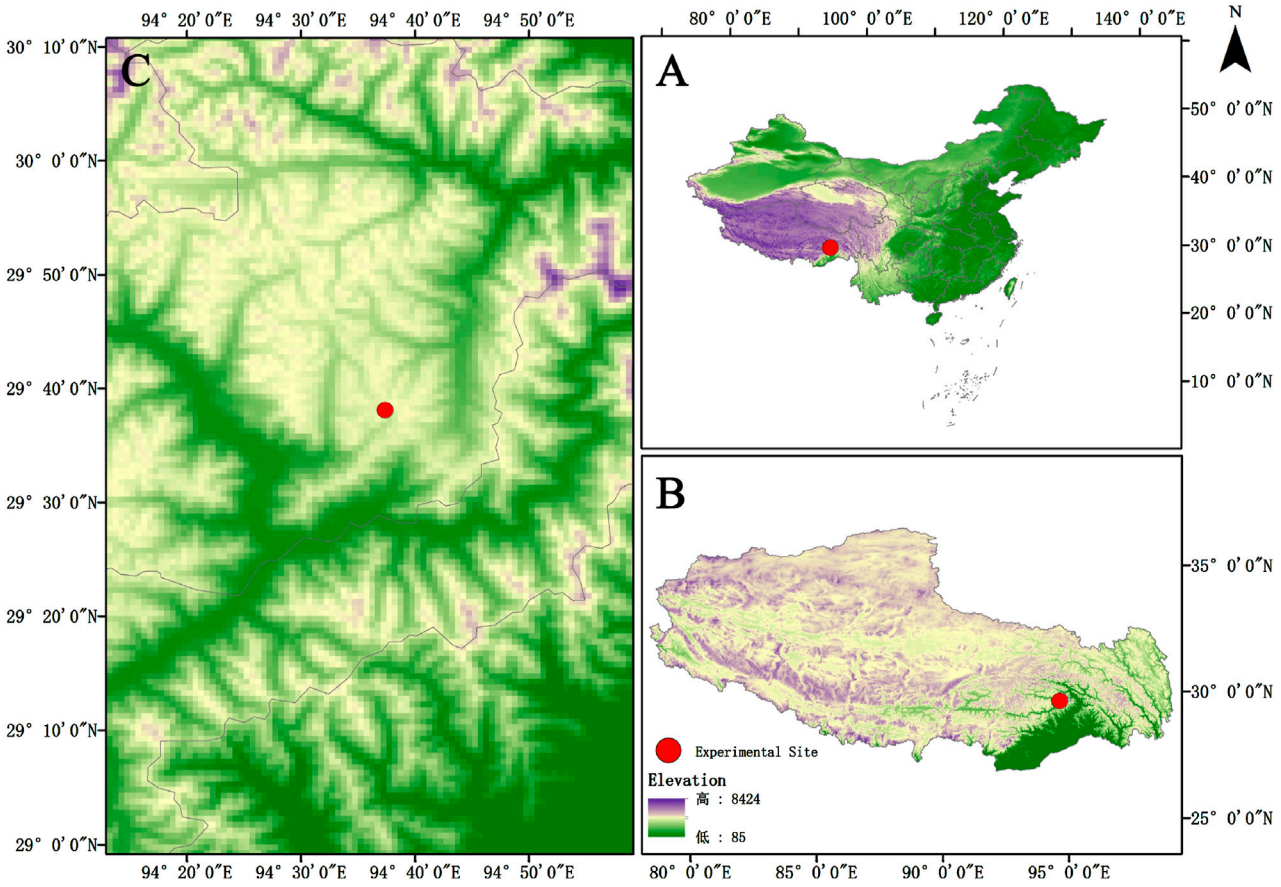

FIGURE 1
Geographical Location Map of the Research Area. **(A)** map of China; **(B)** map of Xizang; **(C)** Specific location of research site.

TABLE 1 Soil parameters and measurement methods of the test site.

Physical and chemical properties of soil	Test method	Unit	Value
pH	pH meter determination		5.83
OC	Potassium dichromate oxidation-external heating method	mg/g	54.60
TN	Kjeldahl nitrogen determination method	mg/g	4.65
TP	Molybdenum anti-colorimetric method	mg/g	0.91
$NH4^+$-N	Potassium chloride leaching-UV spectrophotometry	mg/kg	4.53
$NO3^-$-N	Calcium chloride leaching-UV spectrophotometry	mg/kg	0.32
AP	Ammonium bicarbonate leaching-molybdenum anti-colorimetric method	mg/kg	3.62

are dominated by mountain brown soils and acidic brown soils. Basic soil parameters are presented in Table 1.

2.2 Experimental design

The experiment employed a field P fertilizer application approach with controlled treatments. P addition is drawn from the P addition treatment test standard (50 kg hm^{-2} a^{-1}) carried out by Zhai Jiaying in 2009 for alpine grasslands. Considering that the atmospheric P sedimentation has shown an increasing trend year by year over time, high concentration addition tests have been carried out based on the above P addition standards. Three replicated blocks of equal area were established, with a 5 m wide buffer zone between blocks. Each block contained four treatment groups, corresponding to P application rates of 0, 50, 75, and 100 kg hm^{-2} a^{-1}, designated as CK, P50, P75, and P100, respectively. Each treatment group consisted of a plot measuring 3 m × 3 m, with a 1 m wide buffer zone between plots. A total of 12 plots were established. Translated from what was initiated in 2019, at the beginning of August each

year, dissolve calcium superphosphate [$Ca(H_2PO_2)$] in water at the specified concentration, and evenly sprinkle it within the sample plot with the help of a watering can. The amount of water applied each time is roughly equivalent to a natural precipitation of 2.0 mm. In the control sample plot, the same amount of water is applied. After evaluation, the amount of water addition during fertilization will not have an impact on the ecosystem processes.

2.3 Measurement of plant traits and biomass

In the middle of August 2024, the number of species in each experimental area was recorded in detail. The heights and quantities of plants in each functional group were measured through the direct measurement method and the quadrat method, and the coverage rate was measured by using the line transect method. Randomly select three small plots of 30 cm × 30 cm. Plants within the subplots were clipped at ground level according to their functional groups, and subsequently oven-dried at 105°C for 30 min to deactivate enzymes, followed by drying at 80°C to constant weight. The aboveground biomass of each functional group was then determined by weighing. Plant roots were collected from the soil layer of 0–20 cm in depth using a soil auger with a diameter of 5 cm (Contains 95% of underground plant biomass). For each small sample plot, the auger was used to drill three times in an S-shape pattern, and the root samples obtained from the drilling were then mixed. Subsequently, the root samples were rinsed thoroughly with deionized water, and stones and humus mixed in them were carefully picked out. The treated root samples were placed in an oven at 80°C and dried to a constant weight before being weighed, so as to calculate the belowground biomass per unit area. The root-shoot ratio of the community was calculated by dividing the belowground biomass of the community by the aboveground biomass of the community.

2.4 Determination of the nutrient contents of C, N, and P in plants

The collected aboveground and belowground plant samples were ground into powder using a mechanical grinder. Organic carbon content was measured using the potassium dichromate oxidation method, total nitrogen was determined using the Kjeldahl method, and total P was quantified using the molybdenum-antimony anti-colorimetric method. By dividing the molar content of any two elements in the plant by each other, calculated the plants C:N, C:P, N:P.

2.5 Data analyses

Data processing was performed using Microsoft Excel 2019. Statistical analysis was carried out with IBM SPSS Statistics 20. One - way analysis of variance (ANOVA) was used to evaluate the responses of plant biomass, plant traits of different functional groups, and nutrient contents under different P addition gradients. Multiple comparisons were conducted using the Least Significant Difference (LSD) test, with the significance level set at $P < 0.05$. The figures were plotted using Origin 2021 software, and the results were presented as Mean ± Standard Error (Mean ± SE). The Spearman correlation analysis method was employed to investigate the relationships among plant biomass, plant traits, and nutrient contents in alpine grasslands under P addition.

3 Results

3.1 Effect of P addition on various plant functional groups

3.1.1 Effects of P addition on the Poaceae

The traits of the plant and aboveground biomass of the Poaceae showed a trend of increasing first and then decreasing under P treatment (Figure 2), and the highest value was reached under P75 treatment, with each plant trait increasing by 34.20%, 62.03% and 450.00% compared with CK, respectively, and the increase effect of average height and abundance of the Poaceae plants was more significant ($P < 0.05$); the aboveground biomass increased significantly by 140.35% compared with the control ($P < 0.05$); but under P100 treatment, each plant trait and aboveground biomass began to show a downward trend, indicating that excessive P addition has an adverse effect on the traits of the Poaceae and aboveground biomass. The addition of P addition not significantly affect the C content of Poaceae, and the N content showed a trend of decrease first and then increase (Figure 3). With the increase of P addition level, the P content of Poaceae plants increased significantly ($P < 0.05$); under P100 treatment, the P content of Poaceae plants increased by 122.10% compared with the control group. In the stoichiometric ratio characteristics, C:N showed a trend of increasing first and then falling; both C:P and N:P showed a significant trend of downward, which were 109.37 and 4.58 under P100 treatment.

3.1.2 Effects of P addition on the Cyperaceae

In this study, the mean height and abundance of Cyperaceae plants showed an upward trend with the increase in P addition, but the difference was not significant, indicating that P addition had no significant effect on the mean height and abundance of Cyperaceae (Figure 4). P addition resulted in a significant downward trend in the total coverage and aboveground biomass of Cyperaceae ($P < 0.05$). The total coverage and aboveground biomass were the lowest under P100 treatment, with a decrease of 62.85% compared with CK treatment, and aboveground biomass decreased to 8.83 g m^{-2}. P addition had no significant effect on C and N content in Cyperaceae (Figure 5). However, P addition significantly affected the P content of Cyperaceae ($P < 0.05$). With the increase in P addition level, the P content of Cyperaceae significantly increased, and under P100 treatment, the P content of Cyperaceae increased by 140.52% compared with the control group. P addition had no significant effect on C:N in Cyperaceae, but C:P and N:P showed a significant downward trend with the increase in P addition concentration ($P < 0.05$), which decreased to 110.01 and 6.12 under P100 treatment.

3.1.3 Effects of P addition on the Forbs

The plant traits and aboveground biomass of Forbs showed a trend of increasing first and then decreasing with P addition, and the

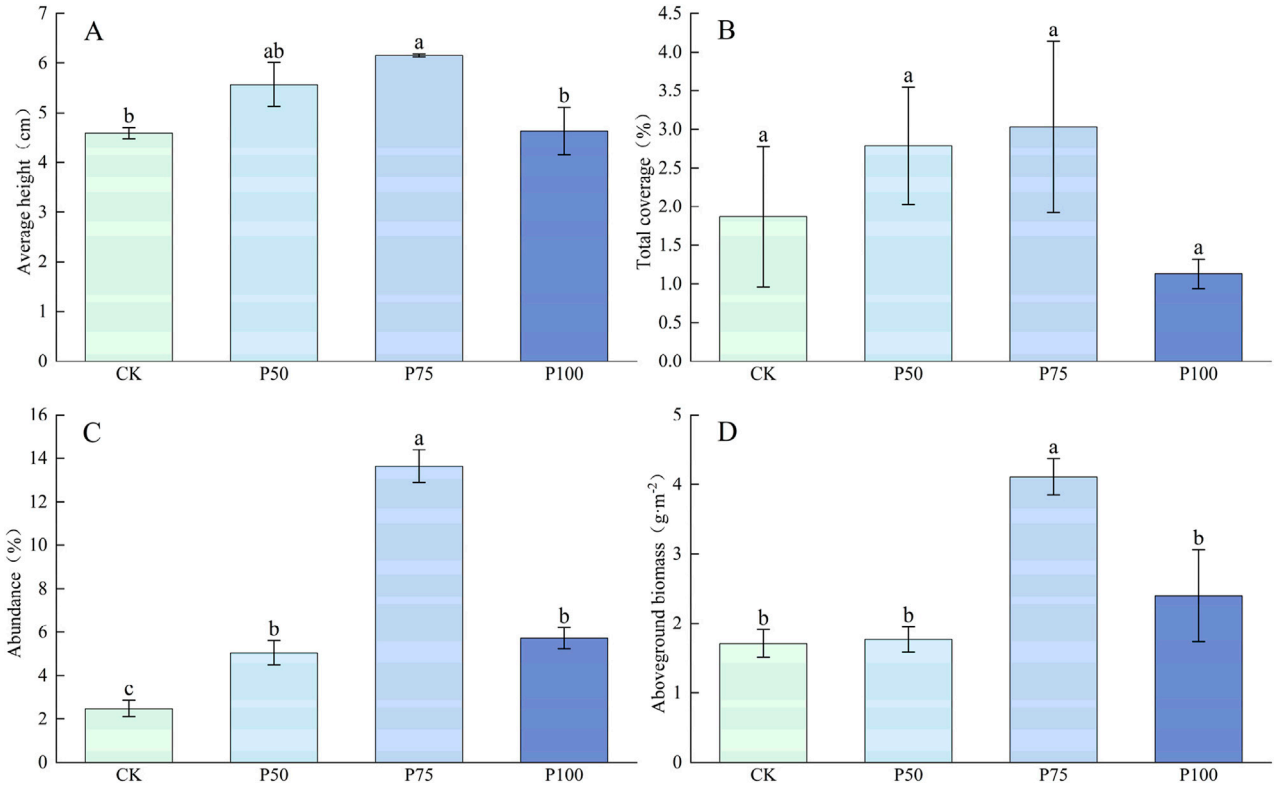

FIGURE 2
Changes in the traits and aboveground biomass of the Poaceae under P addition. **(A)** Average height, **(B)** Total coverage, **(C)** Abundance, **(D)** Aboveground biomass. Lower case letters in the graphs indicate significant differences mong the different level of P addition ($P < 0.05$, LSD test).

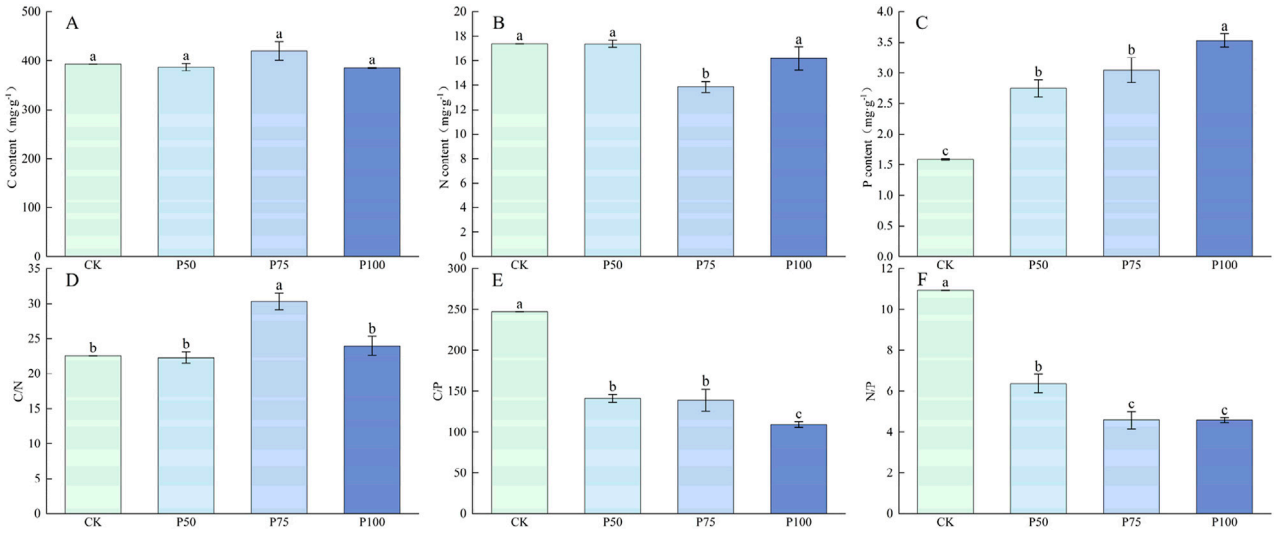

FIGURE 3
Changes in the nutrient content and stoichiometric ratio characteristics of the Poaceae under P addition. **(A)** C content, **(B)** N content, **(C)** P content, **(D)** C/N, **(E)** C/P, **(F)** N/P. Lower case letters in the graphs indicate significant differences mong the different level of P addition ($P < 0.05$, LSD test).

changes were significant ($P < 0.05$, Figure 6), and reached the maximum value under P75 treatment. Compared with CK treatment, the average height, total coverage and abundance of Forbs increased by 73.86%, 51.55%, and 42.04%, and the aboveground biomass increased to 105.23 g m^{-2}. In the case of P addition, the C content of Forbs showed a tendency to decrease first

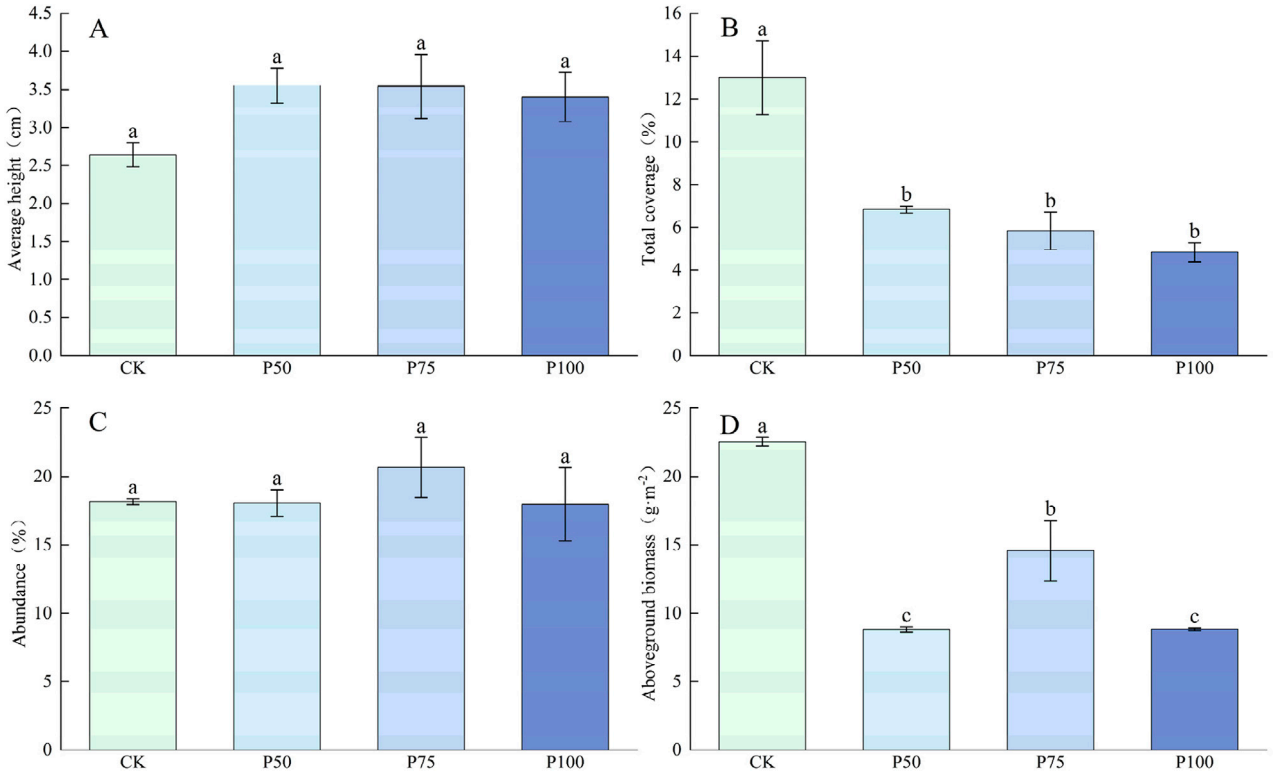

FIGURE 4
Changes in the traits and aboveground biomass of the Cyperaceae under P addition. **(A)** Average height, **(B)** Total coverage, **(C)** Abundance, **(D)** Aboveground biomass. Lower case letters in the graphs indicate significant differences mong the different level of P addition ($P < 0.05$, LSD test).

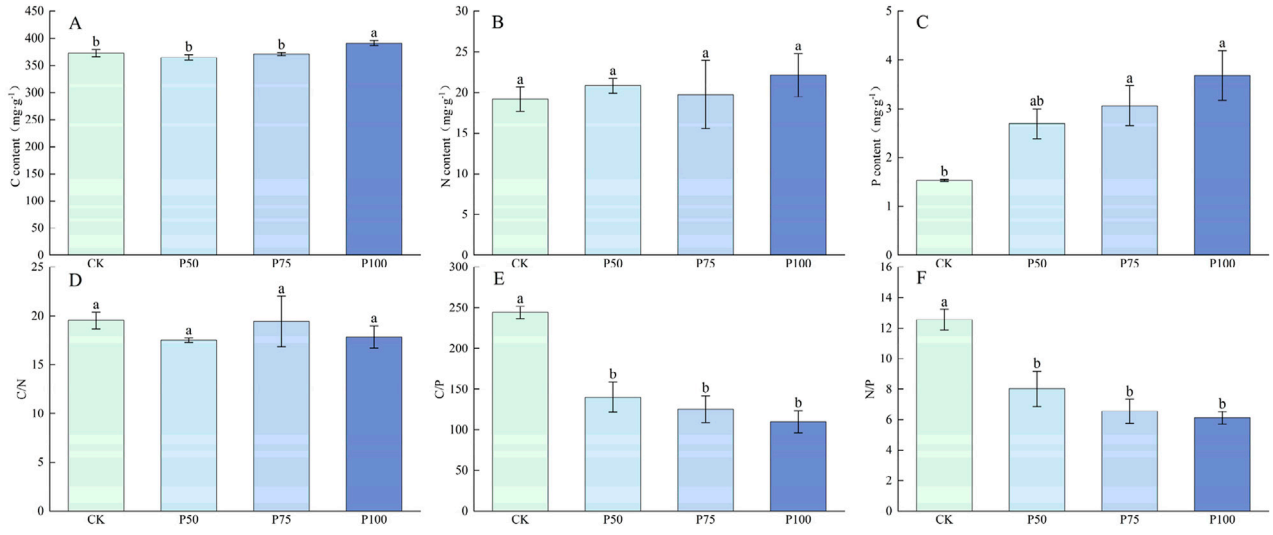

FIGURE 5
Changes in the nutrient content and stoichiometric ratio characteristics of the Cyperaceae under P addition. **(A)** C content, **(B)** N content, **(C)** P content, **(D)** C/N, **(E)** C/P, **(F)** N/P. Lower case letters in the graphs indicate significant differences mong the different level of P addition ($P < 0.05$, LSD test).

and then increase (Figure 7), with no significant effect on the N content, which significantly affected the P content of Forbs ($P < 0.05$). Under P100 treatment, the P content of Forbs increased by 117.50% compared with the control group. The C:N of Forbs did not change significantly with the increase of P addition level, but both the C:P and N:P ratios decreased significantly with the increase of P addition level ($P < 0.05$), with the lowest under P100 treatment, at 82.40 and 5.39.

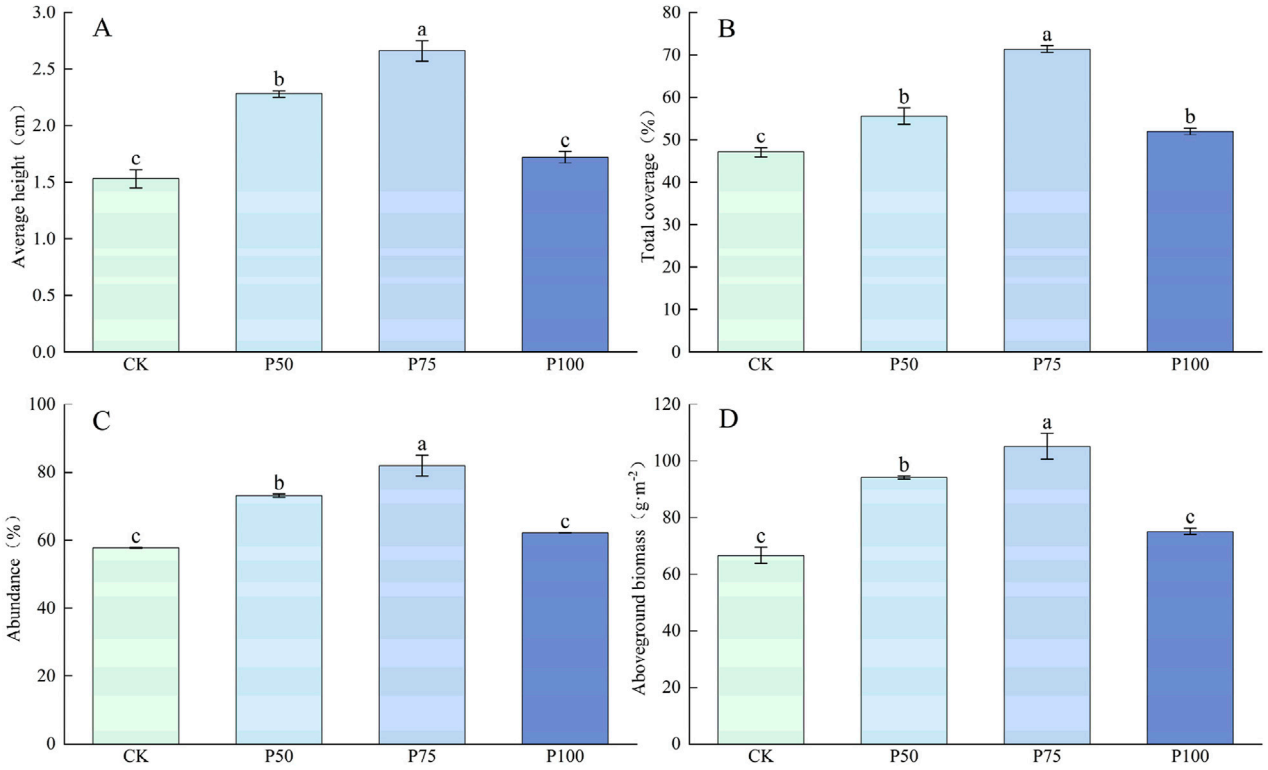

FIGURE 6
Changes in the traits and aboveground biomass of the Forbs under P addition. **(A)** Average height, **(B)** Total coverage, **(C)** Abundance, **(D)** Aboveground biomass. Lower case letters in the graphs indicate significant differences mong the different level of P addition ($P < 0.05$, LSD test).

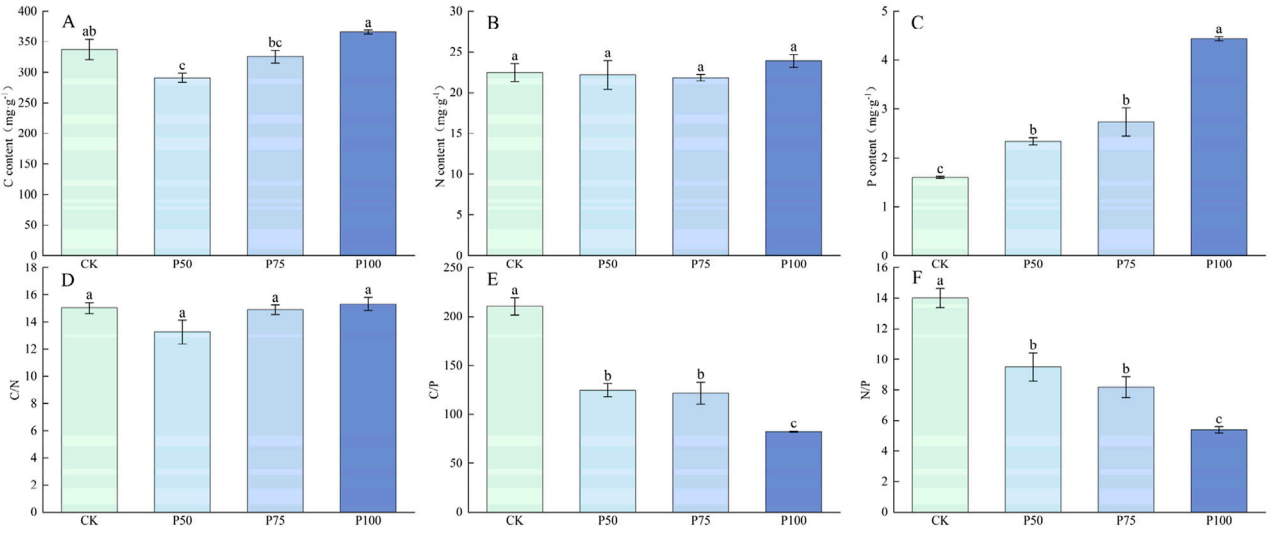

FIGURE 7
Changes in the nutrient content and stoichiometric ratio characteristics of the Forbs under P addition. **(A)** C content, **(B)** N content, **(C)** P content, **(D)** C/N, **(E)** C/P, **(F)** N/P. Lower case letters in the graphs indicate significant differences mong the different level of P addition ($P < 0.05$, LSD test).

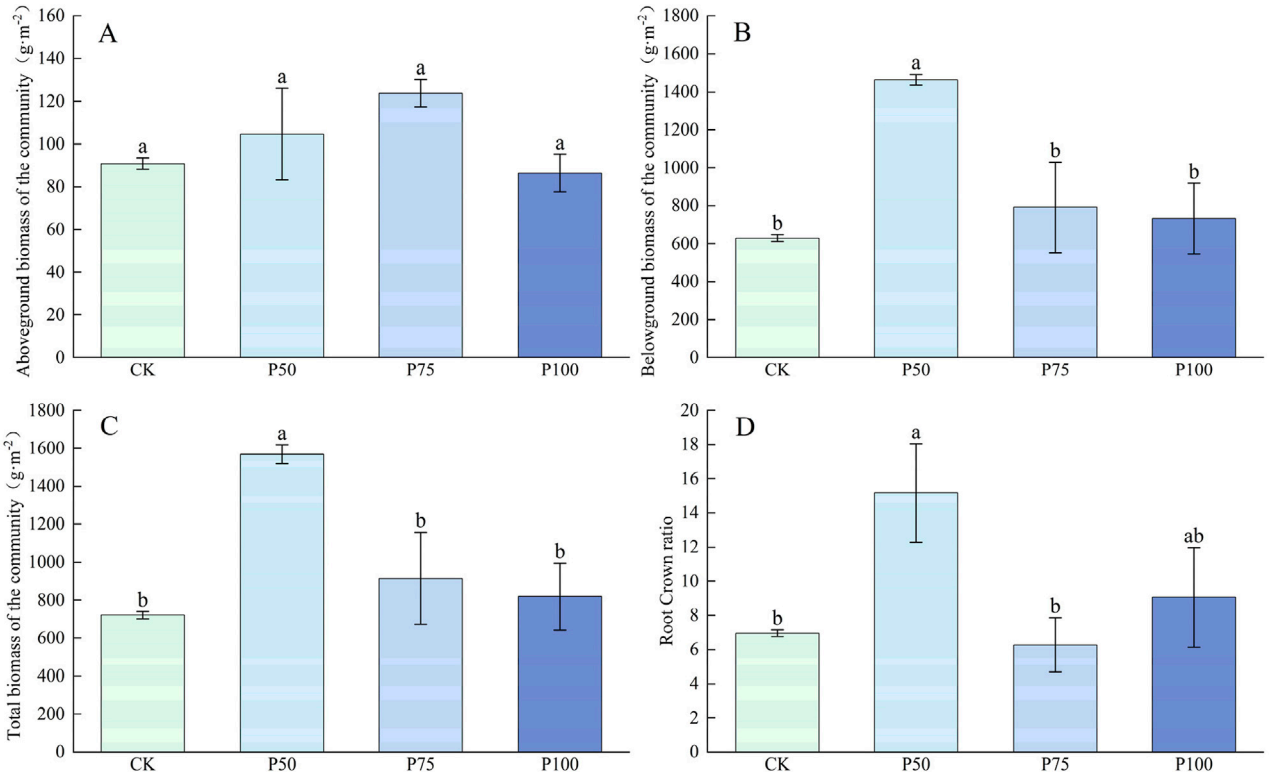

FIGURE 8
Changes in plant community biomass and root crown ratios by addition of P. **(A)** Aboveground biomass of the community, **(B)** Belowground biomass of the community, **(C)** Total biomass of the community, **(D)** Root crown ratio. Lower case letters in the graphs indicate significant differences mong the different level of P addition ($P < 0.05$, LSD test).

3.2 Effects of P addition on plant communities

P addition significantly affected the plant community biomass and root crown ratio in the alpine grasslands of Sejila Mountain ($P < 0.05$, Figure 8). The aboveground biomass, belowground biomass, total biomass, and root crown ratios of plant communities showed a consistent response pattern characterized by increased first and then decreased. Under P50 treatment, the belowground biomass, total biomass and root crown ratios of the plant community reached peaks, which were 1,464.12 g m^{-2}, 1,568.80 m^{-2} and 15.16, which increased by 132.34%, 117.60% and 118.13% respectively compared with the control group; under P75 treatment, the above-ground biomass of the plant community reached the highest value of 123.91 g m^{-2}. This trend may be due to the fact that excessive P addition changes soil conditions, thus exerting an inhibitory effect on plant growth.

In the alpine grasslands plant community of Sejila Mountain, P addition had no significant effect on the C and N content of the aboveground and belowground plant parts (Figure 9). P addition significantly affected the P content of the aboveground and belowground parts of the plant community ($P < 0.05$). With the increase in the level of P addition, the P content in the plant community increased significantly, and under the P100 treatment, the P content of the aboveground and belowground parts of the plant community increased to 3.88 mg g^{-1} and 2.00 mg g^{-1}. C:N in the aboveground and belowground parts of the plant community did not change significantly under the gradual increase in P addition levels. However, C:P and N:P showed a significant downward trend. Under P100 treatment, the C:P of the aboveground and belowground parts was 98.30 and 181.32, a decrease of 58.03% and 60.14% compared with the control treatment; N:P was 5.35 and 5.56, a decrease of 57.34% and 81.60% compared with the control treatment.

3.3 Characteristics correlation analysis of P addition with plant traits, biomass, and nutrient contents

Spearman correlation analysis was conducted on plant traits, biomass and community nutrient contents in the alpine grasslands of Sejila Mountain under different gradients of P addition (Figure 10). The results showed that there were mostly positive correlations among the average height, total coverage and abundance within the Poaceae, Cyperaceae and Forbs respectively, indicating that these traits within the same group would affect each other and change jointly. The aboveground biomass of each plant group was significantly correlated with some of its own traits. The aboveground biomass of Poaceae had an extremely significant positive correlation with abundance ($P < 0.001$). The aboveground biomass of Forbs had extremely significant positive correlations with all its traits ($P < 0.001$). Notably, the aboveground biomass of Cyperaceae was negatively correlated with

its average height, but positively correlated with total coverage and abundance. Meanwhile, there were also certain correlations among the aboveground biomasses of different plant groups, suggesting that they would influence the accumulation of biomass in the community. Community biomass was positively correlated with the aboveground biomasses of Poaceae and Forbs, but negatively correlated with that of Cyperaceae. The C, N and P contents of the community were not only correlated with each other, but also significantly related to the traits and biomass of plant groups. Specifically, the C and N contents had extremely significant negative correlations with the total coverage of Poaceae, there was an extremely significant positive correlation between C and N contents, and the P content had an extremely significant negative correlation with the total coverage of Cyperaceae. This indicates that nutrient contents can affect plant growth, and conversely, the growth status of plants can also have an impact on the nutrient cycling of the community.

4 Discussion

P is a component of important substances such as nucleic acids and phospholipids in plants, and is crucial for physiological processes such as energy metabolism and photosynthesis (Dissanayaka et al., 2020). Research has found that within the moderate range of P addition, grassland plants gain more abundant nutrients, enhance photosynthesis, and accelerate growth (Fan et al., 2021). In this study, it was found that moderate P supply can help improve material synthesis and accumulation in Poaceae and Forbs, thereby increasing height, coverage, and abundance. But when P addition exceeds a certain threshold, it can cause a series of problems. Excessive application of phosphate fertilizers leads to a surplus of P in the soil, increasing the risk of P loss (Zhang W. et al., 2020). These changes can interfere with the absorption of other nutrients by plants, affect their normal physiological functions, and thus inhibit plant growth. The P demand characteristics of Cyperaceae may be different from those of Poaceae and Forbs, and their growth may not be significantly regulated by the amount of P addition, so the average height and abundance changes are not significant. The decrease in total coverage may be due to P addition promoting the growth of other plants, intensifying interspecific competition, and putting Cyperaceae at a disadvantage in resource acquisition, resulting in a decrease in their coverage in the community (Yang et al., 2020).

Studies have shown demonstrated that P addition significantly increased the aboveground biomass of Poaceae in alpine grassland (Zhang W. et al., 2024). In this study, at a P application rate of 75 kg hm^{-2} a^{-1} (P75 treatment), the aboveground biomass of Poaceae and Forbs reached 4.11 g m^{-2} and 105.23 g m^{-2}, respectively, representing increases of 140.35% and 58.20% compared to the control. However, this trend reversed at higher P levels. These results indicate that P addition initially promotes the growth of Poaceae and Forbs, but this stimulatory effect diminishes and may even turn inhibitory as P concentration continues to rise. Pedro et al. (2021) also supported the notion that P addition increases the aboveground biomass of non-nitrogen-fixing plants. However, when soil P concentration exceeds plant demand, a phenomenon of P saturation occurs. Excess P not only fails to further promote plant growth but may also intensify ecological competition among plant species (Kuang et al., 2021), leading to a decline in the aboveground biomass of Poaceae and Forbs. Similarly, observed in a multi-gradient nitrogen and P addition experiment in alpine grassland that the aboveground biomass of Cyperaceae significantly decreased with increasing P levels (Dong et al., 2022). This finding aligns with our study and may be attributed to Cyperaceae being more limited by nitrogen availability. In contrast, P addition promotes the growth of competing plant species, which intensify competition for

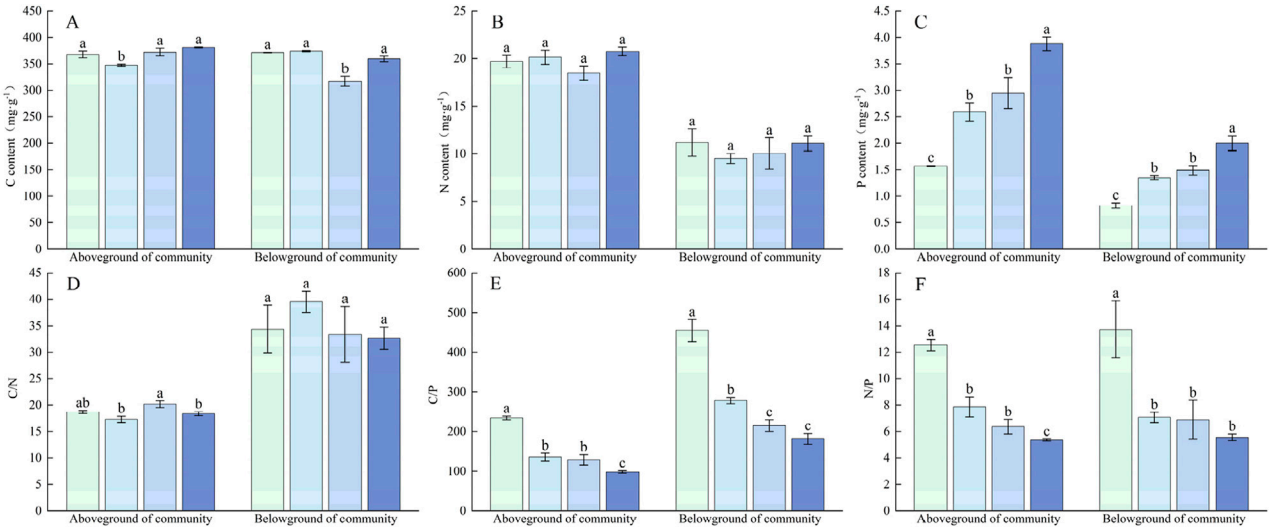

FIGURE 9
Changes in nutrient content and stoichiometric characteristics of P application on plant communities. **(A)** C content, **(B)** N content, **(C)** P content, **(D)** C/N, **(E)** C/P, **(F)** N/P. Lower case letters in the graphs indicate significant differences mong the different level of P addition ($P < 0.05$, LSD test).

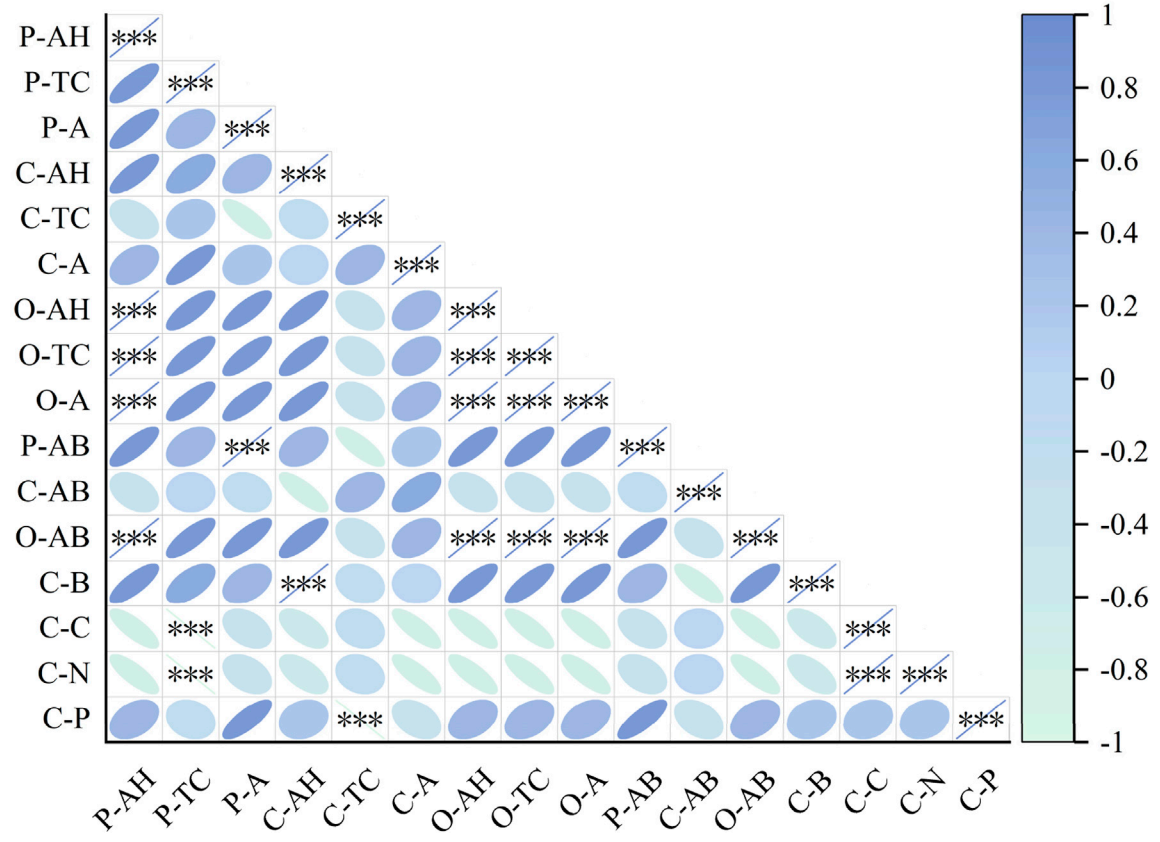

FIGURE 10
Spearman correlation heat map of plant traits, biomass and nutrient contents. P-AH, Average height of Poaceae; P-TC, Total coverage of Poaceae; P-A, Abundance of Poaceae; C-AH, Average height of Cyperaceae; C-TC, Total coverage of Cyperaceae; C-A, Abundance of Cyperaceae; O-AH, Average height of Forbs; O-TC, Total coverage of Forbs; O-A, Abundance of Forbs; P-AB, Aboveground biomass of Poaceae; C-AB, Aboveground biomass of Cyperaceae; O-AB, Aboveground biomass of Forbs; C-B, Community biomass; C-C, Community carbon content; C-N, Community nitrogen content; C-P, Community P content. *, ** and *** indicate significant correlations at the 0.05, 0.01 and 0.001 levels respectively.

resources such as light, water, and nutrients (Kuang et al., 2021), thereby suppressing the growth of Cyperaceae.

Plant biomass, as a core indicator of grassland ecosystem productivity, plays a crucial role in ecosystem stability and functionality (Gaowen et al., 2021). In a 5-year P addition experiment conducted in the alpine grasslands of Sejila Mountain, we observed a trend of initial increase followed by a decline in aboveground biomass, belowground biomass, total biomass, and root-to-shoot ratio of the plant community. Notably, the increase in belowground biomass was more pronounced than that in aboveground biomass under different P addition treatments, consistent with findings by Chen and Xiao (2023), which highlighted the stronger stimulatory effect of P addition on belowground biomass. P, as an essential nutrient for plant growth, can enhance plant growth, increase biomass, and optimize root-to-shoot ratio when applied in appropriate amounts (Lekberg et al., 2021). However, excessive P addition can induce adverse changes in the soil environment, such as salinity accumulation and pH imbalance (Yong et al., 2019), which disrupt soil microbial community structure and function, inhibiting the activity of certain microorganisms (Zhan et al., 2020). These environmental stresses eventually feedback onto plants, causing a decline in biomass and root-to-shoot ratio.

The contents of C, N, and P in plants are directly linked to primary productivity, species composition, and diversity in grassland ecosystems, playing a critical role in ecosystem function and regulation (De et al., 2019). Our results indicated that P addition had no significant effect on the C and N contents of the aboveground and belowground components of the plant community. Carbon, as a structural component in plants, is relatively stable and less influenced by external environmental factors (Sterner and Elser, 2017). Although P addition may alter soil microbial community structure, these changes did not significantly affect plant nitrogen content (Wang et al., 2020). However, the P content of the plant community significantly increased under P addition. The P contents of Poaceae, Cyperaceae, and Forbs responded similarly to P addition. Under the P100 treatment, the P contents of these functional groups increased by 122.1%, 140.52%, and 117.50%, respectively, compared to the control. This is likely because P addition elevated the concentration of available P (AP) in the soil (Cheng et al., 2020), providing a richer P source for plants and enhancing P uptake.

The C:N ratio is often regarded as an important indicator of nutrient balance in plants (Zhang J. et al., 2020). In this study, P addition had no significant effect on the C:N ratio in the aboveground and belowground components of the plant

community. This suggests that P addition is not strongly correlated with nitrogen uptake or that plants can adjust nitrogen uptake and utilization to maintain a stable C:N balance (Sun Y. et al., 2022). In contrast, the C:P and N:P ratios of the plant community declined significantly with increasing P levels. This trend is attributed to enhanced P uptake efficiency, which increased P content in plants, while the absorption of carbon and nitrogen did not increase proportionally, thereby reducing C:P and N:P ratios (Mao et al., 2021; Sun Y. et al., 2022). In this study, Poaceae demonstrated stronger P uptake and utilization efficiency under P addition (Liu et al., 2020), resulting in faster growth and greater accumulation of nutrients. Conversely, Cyperaceae and Forbs showed weaker responses to P addition. The differential responses of plant species to P addition may be due to variations in their P uptake and utilization efficiency (Luor et al., 2022), as well as the influence of microbial communities altering the mineralization rate of organic P to affect P availability (Deforest and Moorhead, 2020). Despite these differences, the overall trend observed was a significant decline in C:P and N:P ratios with increasing P addition levels.

In the study of the alpine grasslands on Sejila Mountain, the correlations among plant traits, biomass, and community nutrient contents under different gradients of P addition exhibit unique patterns. Some scholars have found that within a certain range, P addition can promote the growth of Poaceae plants (Huang et al., 2018), and there is a positive correlation between their biomass and abundance, which is consistent with the extremely significant positive correlation between the aboveground biomass and abundance of Poaceae plants in this study. However, for Forbs, in this study, their aboveground biomass has an extremely significant positive correlation with all traits. This may be due to the unique environmental conditions of the alpine grasslands on Sejila Mountain, which make Forbs more sensitive to P addition and enable them to make more full use of P to promote their own growth. The results that the aboveground biomass of Cyperaceae is negatively correlated with the average height and positively correlated with the total coverage and abundance are relatively rare. It may be because P addition has changed the intra-specific or inter-specific competition relationships of Cyperaceae plants. Under high coverage and abundance, the competition among individuals intensifies, resulting in a decrease in the average height, but the overall biomass accumulation is more influenced by the total coverage and abundance. At the community level, in this study, the community biomass is positively correlated with Poaceae and Forbs, and negatively correlated with Cyperaceae. Studies on grasslands at different altitudes have shown that community biomass is affected by dominant plant groups (Chen et al., 2021). In the alpine grasslands on Sejila Mountain, Poaceae and Forbs play a positive and dominant role in the construction of community biomass, while Cyperaceae shows different correlations due to its own characteristics. In addition, the relationship between community nutrient contents and the traits and biomass of plant groups is consistent with previous studies on the interaction between nutrient cycling and plant growth, further emphasizing the importance of the complex feedback mechanism between the two in the alpine grassland ecosystem.

Given the complexity of P deposition, future research should focus on long-term monitoring and modeling to capture the spatiotemporal variability of P inputs. Additionally, integrated management strategies are needed to mitigate the environmental risks associated with excessive P deposition. Such strategies could include optimizing agricultural fertilization practices, controlling industrial emissions, and implementing land management practices that enhance the retention and utilization of P within ecosystems. By addressing these challenges, we can promote the sustainability and resilience of alpine grassland ecosystems in the face of global environmental change.

5 Conclusion

We conducted an in-depth analysis of a 5-year P addition experiment with varying gradients in the alpine grasslands of Sejila Mountain and drew the following key conclusions: P addition had significant and profound effects on plant traits, biomass, C, N, and P contents, as well as their stoichiometric ratios. These effects exhibited a high degree of consistency across plant communities and their constituent functional groups. Poaceae and Forbs' overground biomass increase most under P75 treatment, but when P addition exceeds 100 kg hm^{-2} a^{-1}, it will inhibit its growth, and P addition reduces the total coverage and biomass of the Cyperaceae. At the community level, however, P addition led to a notable increase in total biomass. Additionally, P addition substantially altered the elemental composition within plants, as evidenced by a significant increase in P content and a notable decrease in the C:P and N:P ratios. However, excessive P addition (P100) intensified ecological competition among plant species, posing potential threats to the functional stability and ecological balance of grassland ecosystems. Based on the above research results, in order to empirically test the impact of P addition on the ecosystem stability of the alpine grasslands in Sejila Mountain, it is very necessary to closely monitor the changes in plant community structure, and pay attention to the impact of precipitation on the effect of nutrient addition, and pay special attention to the dynamics of Cyperaceae plants. It is crucial to prevent ecological imbalances caused by fierce interspecies competition and achieve sustainable development of grassland ecosystems.

Data availability statement

The raw data supporting the conclusion of this article will be made available by the authors, without undue reservation.

Author contributions

XZ: Conceptualization, Methodology, Software, Formal analysis, Investigation, Data curation, Writing – original draft, Writing – review and editing, Visualization. YY: Conceptualization, Software, Investigation, Resources, Writing – review and editing, Visualization, Supervision, Project administration, Funding acquisition. JT: Conceptualization, Methodology, Validation, Formal analysis, Investigation, Data curation, Writing – original draft, Writing – review and editing, Visualization. ZN: Writing – original draft. ZC: Writing – original draft. JL: Writing – original draft. YH: Conceptualization, Methodology, Formal analysis, Investigation, Data curation, Writing – original draft, Writing – review and editing, Visualization.

Funding

The author(s) declare that financial support was received for the research and/or publication of this article. This research was funded by the National Natural Science Foundation of China (31860141; 31360119); Graduate Education Innovation Program of Tibet Agriculture and Animal Husbandry University (YJS2024-26; YJS2024-28; YJS2024-31); National College Student Innovation and Entrepreneurship Training Program (2024-02); Linzhi Apple Science and Technology Academy of Tibet (XY2024-03); Key Discipline Construction Project of Tibet Agriculture and Animal Husbandry University (XK2024-04); Xizang Agriculture and Animal Husbandry University Doctoral Program in Forestry (Phase I) funded by Grant 533325001.

Acknowledgments

The author thanks Associate Professors YH for providing technical assistance.

Conflict of interest

The authors declare that the research was conducted in the absence of any commercial or financial relationships that could be construed as a potential conflict of interest.

Generative AI statement

The author(s) declare that no Generative AI was used in the creation of this manuscript.

Publisher's note

All claims expressed in this article are solely those of the authors and do not necessarily represent those of their affiliated organizations, or those of the publisher, the editors and the reviewers. Any product that may be evaluated in this article, or claim that may be made by its manufacturer, is not guaranteed or endorsed by the publisher.

References

Chen, C., and Xiao, W. (2023). The global positive effect of phosphorus addition on soil microbial biomass. *Soil Biol. and Biochem.* 176, 108882. doi:10.1016/j.soilbio.2022.108882

Chen, Z., Xiong, P., Zhou, J., Lai, S., Jian, C., Xu, W., et al. (2021). Effects of plant diversity on semiarid grassland stability depends on functional group composition and dynamics under N and P addition. *Sci. Total Environ.* 799, 149482. doi:10.1016/j.scitotenv.2021.149482

Cheng, H. Y., Yuan, M. S., Duan, Q. Y., Sun, R., Shen, Y., Yu, Q., et al. (2020). Influence of phosphorus fertilization patterns on the bacterial community in upland farmland. *Industrial Crops and Prod.* 155, 112761. doi:10.1016/j.indcrop.2020.112761

De, L. J. R., Jackson, B. G., Wilkinson, A., Pritchard, W. J., Oakley, S., Mason, K. E., et al. (2019). Relationships between plant traits, soil properties and carbon fluxes differ between monocultures and mixed communities in temperate grassland. *J. Ecol.* 107, 1704–1719. doi:10.1111/1365-2745.13160

Deforest, L. J., and Moorhead, L. D. (2020). Effects of elevated pH and phosphorus fertilizer on soil C, N and P enzyme stoichiometry in an acidic mixed mesophytic deciduous forest. *Soil Biol. Biochem.* 150, 107996. doi:10.1016/j.soilbio.2020.107996

Dissanayaka, S., Ghahremani, M., Siebers, M., Wasaki, J., and Plaxton, W. C. (2020). Recent insights into the metabolic adaptations of phosphorus deprived plants. *J. Exp. Bot.* 72 (2), 199–223. doi:10.1093/jxb/eraa482

Dong, J., Cui, X., Niu, H., Zhang, J., Zhu, C., Li, L., et al. (2022). Effects of nitrogen addition on plant properties and microbiomes under high phosphorus addition level in the alpine steppe. *Front. Plant Sci.* 13, 894365. doi:10.3389/fpls.2022.894365

Fan, L. L., Mekrovar, O., Li, Y. M., Li, K. H., Ma, X. X., and Mao, J. F. (2021). Effect of nutrient addition on the productivity and species richness of grassland along with an elevational gradient in Tajikistan. *Front. Plant Sci.* 12, 765077. doi:10.3389/fpls.2021.765077

Gaowen, Y., Masahiro, R., Julien, R., Hempel, S., and Rillig, M. C. (2021). Plant and soil biodiversity have non-substitutable stabilising effects on biomass production. *Ecol. Lett.* 24 (8), 1582–1593. doi:10.1111/ele.13769

Huang, J., Yu, H., Liu, J., Luo, C., Sun, Z., Ma, K., et al. (2018). Phosphorus addition changes belowground biomass and C:N:P stoichiometry of two desert steppe plants under simulated N deposition. *Sci. Rep.* 8 (1), 3400. doi:10.1038/s41598-018-21565-w

Kuang, X. L., Si, K. Y., Song, H. J., Peng, L., and Chen, A. (2021). Lime-phosphorus fertilizer efficiently reduces the Cd content of rice: physicochemical property and biological community structure in Cd-polluted paddy soil. *Front. Microbiol.* 12, 749946. doi:10.3389/fmicb.2021.749946

Lekberg, Y., Arnillas, C. A., Borer, E. T., Bullington, L. S., Fierer, N., Kennedy, P. G., et al. (2021). Nitrogen and phosphorus fertilization consistently favor pathogenic over mutualistic fungi in grassland soils. *Nat. Commun.* 12, 3484. doi:10.1038/s41467-021-23605-y

Liu, C. J., Gong, X. W., Dang, K., Li, J., Yang, P., Gao, X., et al. (2020). Linkages between nutrient ratio and the microbial community in rhizosphere soil following fertilizer management. *Environ. Res.* 184, 109261. doi:10.1016/j.envres.2020.109261

Luor, Y., Kuzyakov, Y., Zhu, B., Qiang, W., Zhang, Y., and Pang, X. (2022). Phosphorus addition decreases plant lignin but increases microbial necromass contribution to soil organic carbon in a subalpine forest. *Glob. Change Biol.* 28 (13), 4194–4210. doi:10.1111/gcb.16205

Mao, Q. G., Chen, H., Wang, C., Pang, Z., Mo, J., and Lu, X. (2021). Effect of long-term nitrogen and phosphorus additions on understory plant nutrients in a primary tropical forest. *Forests* 12 (6), 803. doi:10.3390/f12060803

Mesquita, C. P. B. D., Brigham, L. M., Sommers, P., Porazinska, D. L., Farrer, E. C., Darcy, J. L., et al. (2020). Evidence for phosphorus limitation in high-elevation unvegetated soils, Niwot Ridge, Colorado. *Biogeochemistry* 147 (7), 1–13. doi:10.1007/s10533-019-00624-y

Pan, Y., Liu, B., Cao, J., Liu, J., Tian, S., and Du, E. (2021). Enhanced atmospheric phosphorus deposition in Asia and Europe in the past two decades. *Atmos. Ocean. Sci. Lett.* 14 (05), 100051. doi:10.1016/j.aosl.2021.100051

Pedro, M. T., Suzanne, M. P., Selene, B., Chaneton, E. J., Firn, J., Risch, A. C., et al. (2021). Negative effects of nitrogen override positive effects of phosphorus on grassland legumes worldwide. *Proc. Natl. Acad. Sci. U. S. A.* 118 (28), 1–8. doi:10.1073/pnas.2023718118

Penuelas, J., Janssens, I. A., Ciais, P., Obersteiner, M., and Sardans, J. (2020). Anthropogenic global shifts in biospheric N and P concentrations and ratios and their impacts on biodiversity, ecosystem productivity, food security, and human health. *Glob. Change Biol.* 26 (4), 1962–1985. doi:10.1111/gcb.14981

Sterner, R. W., and Elser, J. J. (2017). *Ecological Stoichiometry: The Biology of Elements from Molecules to the Biosphere*. Princeton University Press. Publication date: 2017-02-15. doi:10.1515/9781400885695

Sun, J., Wang, Y., Liu, S., Li, J., Zhou, H., Wu, G., et al. (2022). Editorial: patterns, functions, and processes of alpine grassland ecosystems under global change. *Front. Plant Sci.* 13, 1048031. doi:10.3389/fpls.2022.1048031

Sun, Y., Wang, C. T., Chen, X. L., Liu, S., Lu, X., Chen, H. Y. H., et al. (2022). Phosphorus additions imbalance terrestrial ecosystem C:N:P stoichiometry. *Glob. Change Biol.* 28 (24), 7353–7365. doi:10.1111/gcb.16417

Wang, S. H., Mori, T., Mo, J. M., and Zhang, W. (2020). The responses of carbon- and nitrogen-acquiring enzymes to nitrogen and phosphorus additions in two plantations in southern China. *J. For. Res.* 31 (04), 1319–1324. doi:10.1007/s11676-019-00905-0

Yang, J., Liu, Q. R., and Wang, X. T. (2020). Plant community and soil nutrient of alpine meadow in different degradation stages on the Tibetan plateau, China. *J. Appl. Ecol.* 31 (12), 4067–4072. doi:10.13287/j.1001-9332.202012.008

Yong, J., Zhu, W. X., Ru, Z. W., Li, H., and Zhang, Y. G. (2019). Effects of long-term fertilization and water addition on soil properties and plant community characteristics in a semiarid grassland. *J. Appl. Ecol.* 30 (7), 2470–2480. doi:10.13287/j.1001-9332.201907.034

Zhan, Y. N., Wang, Z., and Meng, Y. L. (2020). Biochar addition improves soil phosphorus availability: a meta-analysis. *J. Appl. Ecol.* 31 (4), 1185–1193. doi:10.13287/j.1001-9332.202004.024

Zhang, J., He, N., Liu, C., Xu, L., Chen, Z., Li, Y., et al. (2020). Variation and evolution of C:N ratio among different organs enable plants to adapt to N-limited environments. *Glob. Change Biol.* 26, 2534–2543. doi:10.1111/gcb.14973

Zhang, W., Gong, J., Zhang, S., Lambers, H., Dong, X., Hu, Y., et al. (2024). Soil phosphorus availability affects niche characteristics of dominant C3 perennial and sub-dominant C4 annual species in a typical temperate grassland of northern China. *Plant Soil* 504, 737–761. doi:10.1007/s11104-024-06655-1

Zhang, W., Zhang, Y., An, Y., and Chen, X. (2020). Phosphorus fractionation related to environmental risks resulting from intensive vegetable cropping and fertilization in a subtropical region. *Environ. Pollut.* 269, 116098. doi:10.1016/j.envpol.2020.116098

Zhang, Z., Wang, L., Li, T., Fu, Z., Sun, J., Hu, R., et al. (2024). Effects of short-term nitrogen and phosphorus addition on soil bacterial community of different halophytes. *mSphere* 9, e0022624. doi:10.1128/msphere.00226-24

frontiers | Frontiers in Environmental Science

TYPE Original Research
PUBLISHED 13 June 2025
DOI 10.3389/fenvs.2025.1552447

OPEN ACCESS

EDITED BY
Tianjiao Feng,
Beijing Forestry University, China

REVIEWED BY
Xiaojing Qin,
Henan Polytechnic University, China
Yan Shen,
Ningxia University, China

*CORRESPONDENCE
Zhongju Meng,
mengzhongju@126.com

RECEIVED 02 January 2025
ACCEPTED 07 March 2025
PUBLISHED 13 June 2025

CITATION
Zhao F, Meng Z, Liu Y, Li P and Tang G (2025) Soil carbon and nitrogen changes due to soil particles redistribution caused by photovoltaic array.
Front. Environ. Sci. 13:1552447.
doi: 10.3389/fenvs.2025.1552447

Soil carbon and nitrogen changes due to soil particles redistribution caused by photovoltaic array

Feiyan Zhao[1], Zhongju Meng[1]*, Yang Liu[2], Peng Li[1,3] and Guodong Tang[4]

[1]College of Desert Control Science and Engineering, Inner Mongolia Agricultural University, Hohhot, China, [2]Inner Mongolia Water Conservancy Research Institute, Hohhot, China, [3]The Comprehensive Support Center of Audit Bureau of Ulanqab City, Ulanqab, China, [4]Institute of Water Resources for Pastoral Area Ministry of Water Resources, Hohhot, China

There is an inevitable relationship between the size of soil particles and the distribution of organic matter. The soil texture in desert photovoltaic areas is poor, with variations in soil particle size and organic matter. This study explores the heterogeneity of soil particle size and organic matter distribution at different zonal scales, aiming to clarify the impact of photovoltaic array construction on microtopography and, consequently, on these indicators. This will facilitate precise vegetation restoration based on the distribution of nutrients within the region. Baced on the Kubuqi Desert photovoltaic area as the research area, the soil particle size in the 0–30 cm soil layer and the distribution of soil organic matter in the main particle size range (<250 μm, <500 μm) in this area were analyzed. Fine sand (particle size 100–250 μm) was the main component of the soil; the carbon and nitrogen stocks in the upper 0–30 cm of soil diminished linearly with escalating wind speed gradient, from 70.76 Mg C ha^{-1} to 53.82 Mg C ha^{-1} and from 13.96 Mg N ha^{-1} to 8.12 Mg N ha^{-1}. The total carbon and nitrogen levels in the two soil particle sizes, together with their contribution to total soil organic carbon, diminished as the wind speed gradient intensified, with the reduction in organic carbon content becoming stronger. The organic carbon content of soil particles <250 μm accounted for 63.7%–98.6% of the total soil organic carbon, while that of particles 250μm–500 μm only accounted for 3.32%–33.34%. SOC was significantly higher in the 0–5 cm layer than in the 5–30 cm layer in all areas of the photovoltaic array. Wind causes changes in sand particle transport in PV arrays, and may also alter the microclimate environment leading to differences in soil decomposition cycling processes, which can exhibit uneven organic carbon and nitrogen distribution between particles. Our research demonstrates the internal distribution of soil carbon and nitrogen reserves in each region of the photovoltaic array, establishing a robust foundation for subsequent vegetation restoration and plant species selection in each region, thereby implementing the "photovoltaic + ecological" governance model.

KEYWORDS

photovoltaic, soil particle-size fraction, soil organic C, wind speed, arid desert region

1 Introduction

Soil constitutes the most extensive carbon storage within terrestrial ecosystems. The organic carbon content in the soil to a depth of 1 m is approximately three fold the total carbon reservoir in the biosphere and double that of the total carbon reservoir in the atmosphere. (Li et al., 2024). Particles of different sizes store soil organic carbon, and the physicochemical properties of silt and even clay positively correlate with more than half of the organic carbon (Lavallee et al., 2020; Sokol et al., 2022). The distribution of particle sizes in various soils significantly influences the concentration of soil organic carbon, form of existence, migration process, decomposition rate, and stability of the organic carbon pool (Zhang et al., 2023). In the degradation of soil organic carbon, active organic carbon is predominantly found in soil particles sized >50 μm and <2 μm. (Lützow et al., 2006). Coarse–free particles of organic carbon constitute 70.63%–76.53% of the total amount of organic carbon in the soil, representing the primary type of soil organic carbon sequestration. It is also unprotected, highly active organic carbon, which is more likely to be released due to the influence of the environment and human activities (He et al., 2023). It typically interacts with a mineral surface that contains a lower amount of organic carbon. Contact with microorganisms reduces the rate of decomposition (Heckman et al., 2022). Enhancing plant diversity and productivity gradually alters the process of soil organic carbon input through vegetation restoration. (Deng et al., 2014; Qu et al., 2024; Liu et al., 2020b; Qu et al., 2022). This alters the rate of soil organic carbon turnover. (Liu et al., 2020a; Li et al., 2020; Qu et al., 2022). The accumulation of organic carbon in soil results from the equilibrium between carbon input and output. (Srivastava et al., 2020). The quantity, distribution, and dynamics of clay and silt associated organic carbon are reliably observed throughout a wide range of ecosystems and climate zones (Cotrufo et al., 2019; Georgiou et al., 2022). Organic carbon and total nitrogen in sand grains are generally thought to be the primary active organic carbon and nitrogen components. On the other hand, organic carbon and total nitrogen in clay and silt grains are considered to be inactive carbon and nitrogen components. (Christensen, 1992). Desertified land accounts for about 25% of the global land area, and soil carbon reserves in desert areas account for 9.5% of the total soil carbon reserves (Poulter et al., 2014). Despite the fact that desert ecosystems are a substantial portion of terrestrial ecosystems, they display distinctive traits that are associated with the presence of soil organic carbon in the soil particle size fraction. In desert areas, we may observe the following phenomena: extremely low land productivity; coarse particles dominate the soil's mechanical composition; natural climate influences reduce the intensity of microbial activity; and the accumulation of organic carbon in coarse particles (Sokol and Bradford, 2019). The minimal intake of organic matter renders the organic carbon in clay and silt independent of their respective contents (Hassink, 1997). Wind erosion is the main factor controlling the particle size composition. High wind erosion intensity results in a large proportion of coarse particles. The arrangement of soil particles, encompassing their clay and silt proportions, affects wind erosion and dictates the role of soil particle–bound carbon in soil organic carbon. (Liu J. et al., 2021; Lei et al., 2019; Zhao et al., 2019). However, wind erosion accumulation affects the desert photovoltaic area, where the landform primarily consists of undulating sand dunes. Less agglomeration disperses the particles, and their resistance to wind erosion is low. The soil nutrients are poor, which is not conducive to plant growth. The vegetation is extremely sparse, the psammophytes are scattered, and the economic value utilization rate is small. The primary reason for this is that sandy land has a single mineral particle composition, with a concentration of particles between 0.05 and 1 mm. Vegetation restoration can be carried out on this basis, and the particle size composition and mineral composition can be changed to completely change its nutrient coordination and supply, water holding capacity, and sand fixation resistance. It is the fundamental measure to improve the productivity and ecosystem service value of sandy land (Ni et al., 2018). In recent years, some researchers have linked SOC grouping with soil particle classification and systematically classified the *status quo* by combining SOC with soil particles of different particle sizes, such as sand (>53 μm), silt (2–53 μm), and clay (<2 μm). Vegetation construction within the environmental tolerance threshold is the key to reversing the trend of land desertification, promoting sand and soil formation, and creating productivity (Zhang et al., 2014).

The Kubuqi Desert is surrounded by the Yellow River on the north-west, north-east, east sides, and a large amount of sand and dust from the Yellow River is deposited here. The large-scale development of the photovoltaic industry based on sufficient sunshine has not only changed the microenvironment of the surface but also affected the structure of the sand and dust flow. The spatial distribution of particles dictates the composition of soil particles (Lopez and Bacilio, 2020; Slessarev et al., 2022). The desert area has changed the original radiation balance through the construction of photovoltaic power stations. At the same time, the physical existence of photovoltaic panels has a shading effect on the surface and also affects the air flow on the surface, thus affecting the air temperature and relative humidity pattern. Barron-Gafford's on-site observation of the Tucson photovoltaic electric field in the United States found that the photovoltaic electric field has a heat island effect, with an average annual temperature increase of 2.4°C at a height of 2.5 m and a nighttime temperature increase of 3°C–4°C (Barron-Gafford et al., 2016). Parrat's wind tunnel test shows that the photovoltaic panel only reduces the turbulence intensity above and around it but has no significant effect on the average wind speed and wind direction. The photovoltaic field primarily influences air turbulence in the wind field (Pratt and Kopp, 2013). At the same time, during the operation period of the photovoltaic electric field, the layout of the photovoltaic array will increase the surface roughness and change the law of surface sediment transport and sedimentation. Our research team has concluded that the average particle size in the windward direction of the photovoltaic electric field is larger than that in the leeward direction. The soil particles in the leeward direction show a trend of refinement, while the soil particles in the main wind direction show a trend of coarsening. The accumulation degree of very fine sand and fine sand particles in the soil particle size from the outer edge of the photovoltaic electric field to the center of the photovoltaic electric field gradually increases. Studies have shown that the construction of photovoltaic power plants significantly increased soil organic matter, total nitrogen, and ammonium nitrogen content (Ding and Liu, 2021). The construction of a photovoltaic power station in a desert area can realize the

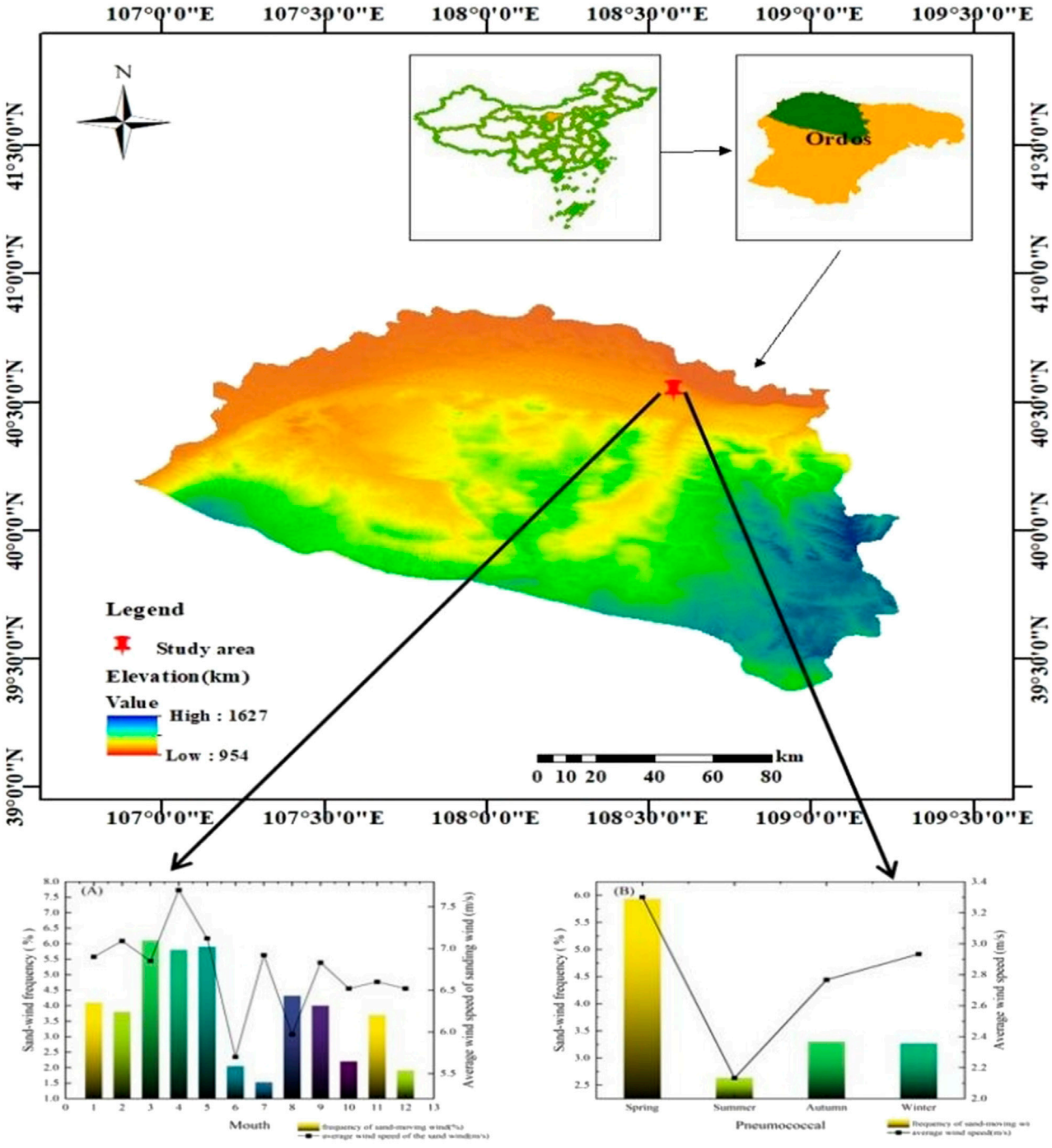

FIGURE 1
Overview map of the research area.

ecological value of windbreak and sand fixation, improving microclimate, carbon fixation, and efficiency enhancement. Therefore, the construction of this project in a desert area considers the mutual benefits of energy supply and ecological enhancement. Thus far, limited research has examined the correlation between soil particle size and organic carbon in desert photovoltaic regions. This gap in knowledge hinders our understanding of the influence of soil texture on the accumulation and storage of organic carbon and nitrogen in this area, as well as soil management measures and vegetation restoration.

In general, the construction of photovoltaic power stations in desert areas has the potential to reduce the harm caused by strong winds and sand. However, the current research mostly focuses on changes in wind speed and soil texture between different positions of photovoltaic panels. There are few studies on organic reserves in

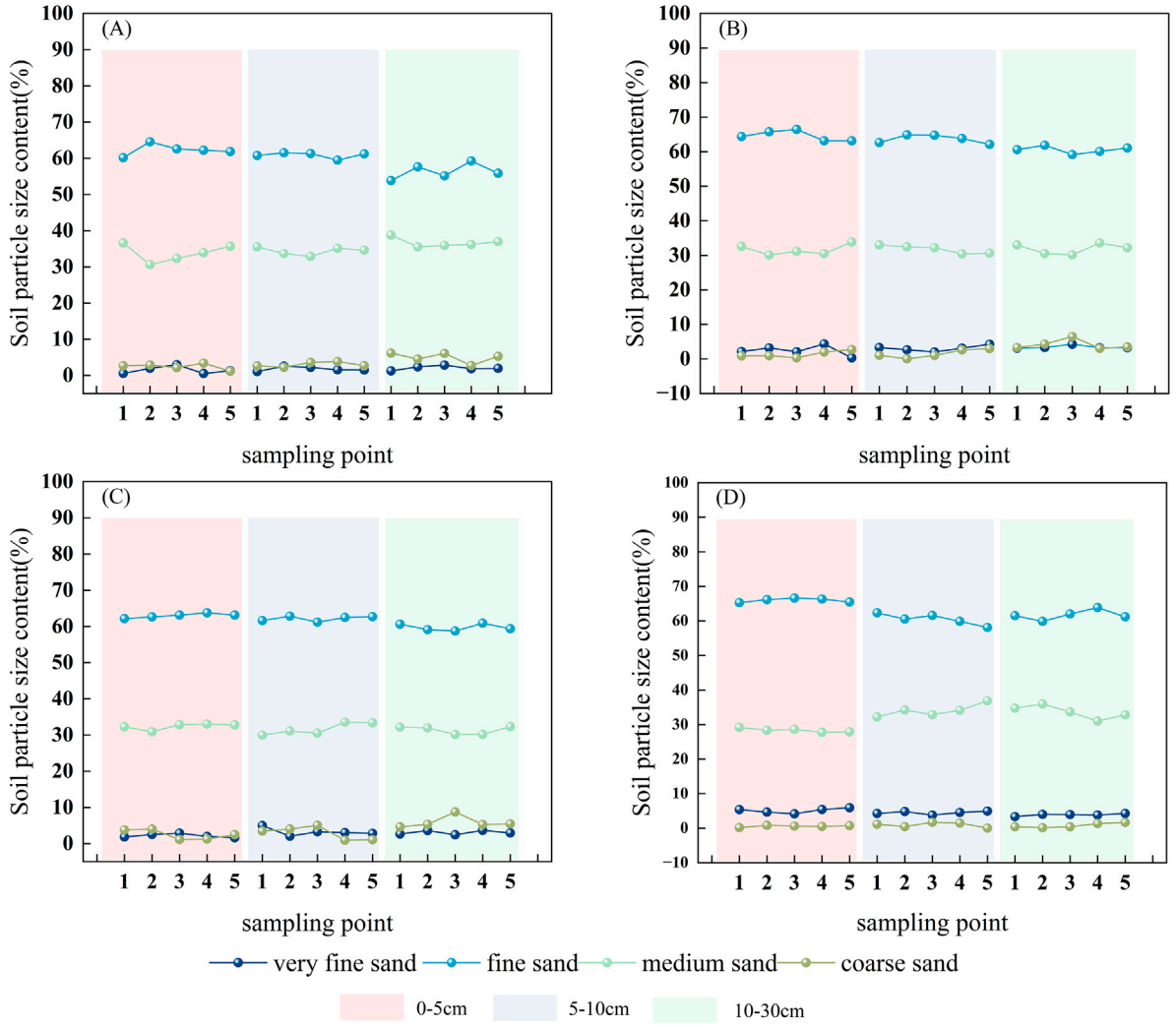

FIGURE 2
Soil particle size composition by region **(A–D)** in the figure represent 4 samples respectively).

photovoltaic array space. It is necessary to systematically carry out this evaluation study to clarify the direction of vegetation restoration and the photovoltaic industry in the later stage. Therefore, this study takes the photovoltaic array in the middle of the Kubuqi Desert as an example to evaluate the soil particle size distribution and the content of organic matter in the particle size range of each level in the region in order to provide a reference for the efficient use of the existing resources within the array to develop a sustainable new energy industry.

2 Materials and methods

2.1 Study site description

The research region exhibits characteristic climatic characteristics (arid and semi-arid) and soil types (calcium-rich grey soil, grey desert soil, and loess) prevalent in the deserts of northern China. The latitude ranges from 37.2°N to 39.5°N, and the longitude is from 107.1°E ~ 111.5°E. The mean annual precipitation (MAP) is between 150 mm and 400 mm, while the mean annual temperature (MAT) varies between 5°C and 8°C. The mean evapotranspiration (ET) ranges from 2,100 mm to 2,700 mm, the aridity index (1-AI) varies between 0.85 and 0.93, and the predominant flora in this region consists of sand willow (*Salix psammophila*), sand whip (*Psammochloa villosa*), small-leaved golden chicken (*Caragana microphylla*), and sand wormwood (*Artemisia desertorum*) (Figure 1).

2.2 Field sampling

Soil samples were collected at 12 sample points throughout the photovoltaic array, including 3 sample points from an open area outside the photovoltaic array (A), 3 sample points from the outer perimeter of the photovoltaic array near the wind measurement (B), 3 sample points from the middle of the photovoltaic array (C), and 3 sample points from the inner part of the photovoltaic array near

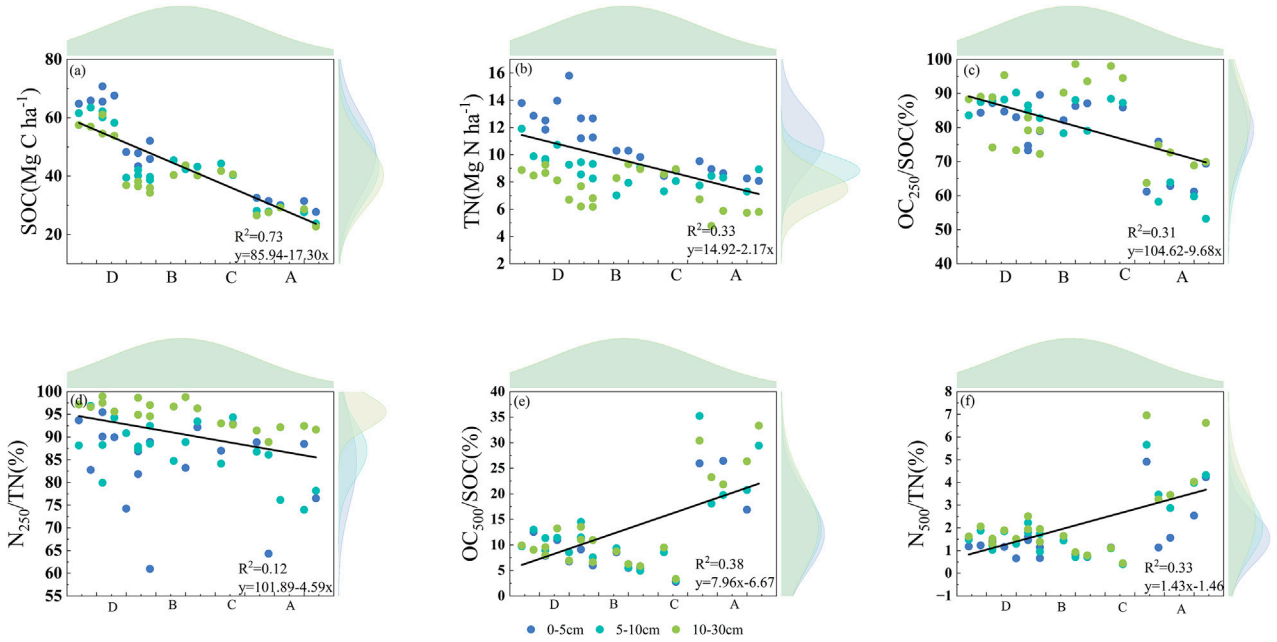

FIGURE 3
The proportion of organic C and N reserves in the two particle size groups to the soil organic reserves in the 0–30 cm soil layer as a function of wind speed **(a–d)** in the figure represent 4 samples respectively; Wind speeds show an increasing trend from D to A, at the same time, **(a, c, e)** represents C index, **(B, D, F)** represents N index.).

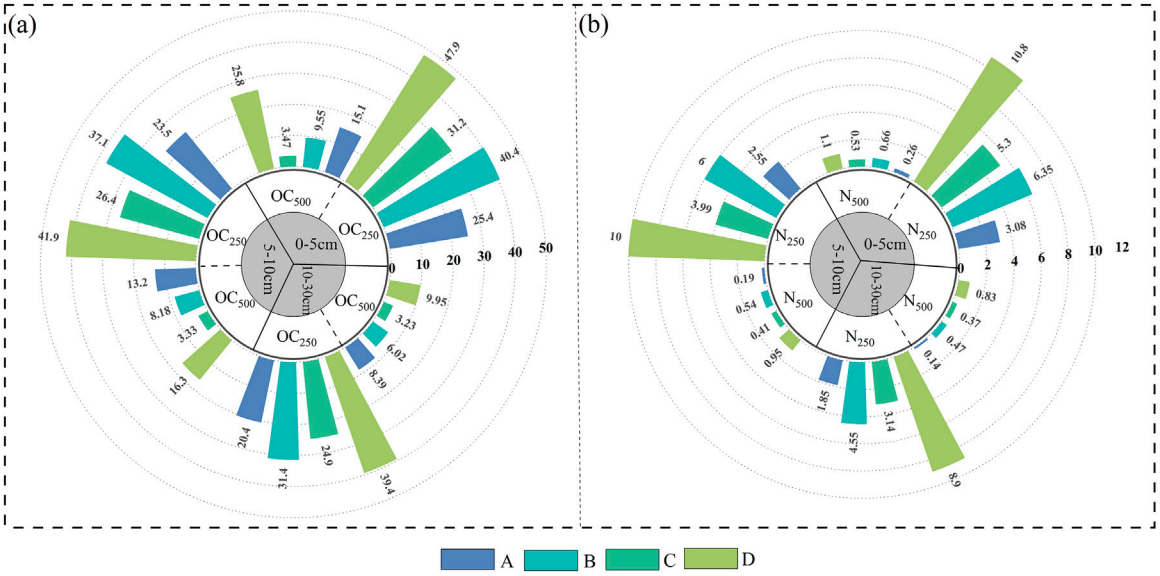

FIGURE 4
Relationship between organic carbon (nitrogen) storage and soil organic carbon (nitrogen) storage in two of the three soil layers in each region **(a–d)** in the figure represent 4 samples respectively, **(a)** the content of OC_{250} and OC_{500} in each soil layer, **(b)** the content of N_{250} and N_{500} in each soil layer).

the leeward measurement (D). The average wind speed of the four regional sampling points is A>C>B > D. For each sample point, a 1 m × 1 m plot was established, and five samples were obtained using a soil auger from the four corners and center. We mixed soil samples from the same depth (0–5 cm, 5–10 cm, and 10–30 cm) for each plot. In the lab, the soil was sieved through a 2.0 mm sieve and divided into two subsamples: one for air-dried physical and chemical analysis, including particle size classification and organic carbon

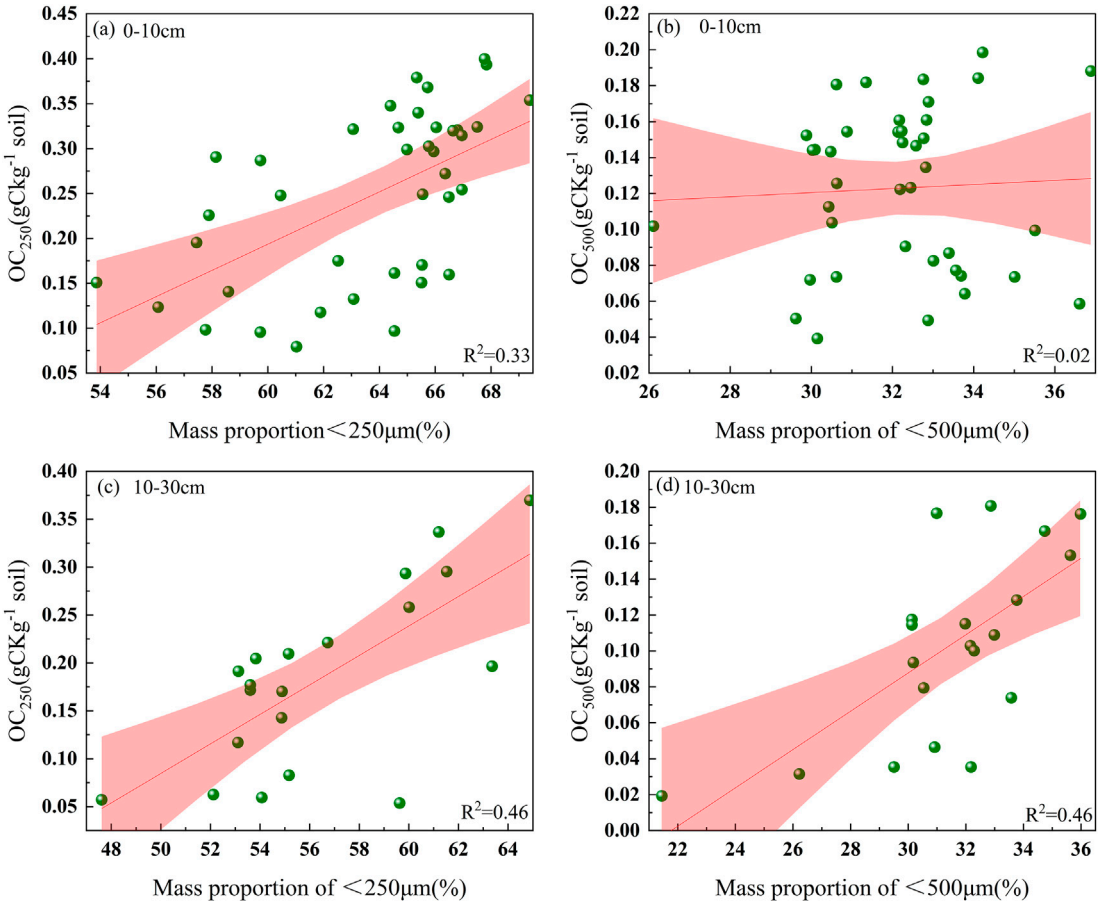

FIGURE 5
Relationship between soil organic carbon content in the two grain sizes and the mass fractions of organic carbon in the 0–10 cm and 10–30 cm grain sizes **(a)**: OC_{250} content at 0–10 cm, **(b)**: OC_{500} content at 0–10 cm, **(c)**: OC_{250} content at 10–30 cm, **(d)**: OC_{500} content at 0–10 cm).

and nitrogen determination, and one for ring knife soil bulk density (BD) sampling Equation 1.

$$BD\ (g/cm^3) = \frac{W_1 - W_0}{V} \quad (1)$$

where V is the ring knife volume (cm^3); W_1 is the weight of the soil + ring knife after drying (g); and W_0 is the ring knife weight (g).

2.3 Soil particle size determination and classification

The soil samples were air-dried, sieved through 2 mm, then evaluated using PSD. The material was dispersed with sodium hexametaphosphate, organic debris removed with 10% hydrogen peroxide, and carbonates removed with 10% hydrochloric acid. We assessed PSD for each sample after pretreatment. We used a Mastersizer 3,000 laser particle size analyzer to make the measurements. Each sample was measured three times, and the average was used as the final measurement. We used a volume percentage unit with a repeatability of less than 0.5% and an accuracy error of less than 1%. USDA soil texture classification standard (Folk and Ward, 1957), and the soil particle size is divided into four grades according to the actual situation of the sample plot: very fine sand particles (50–100 μm), fine sand particles (100–250 μm), medium sand particles (250–500 μm), and coarse sand particles (500–1,000 μm). Soil particle size classification methods are important because different methods often lead to different conclusions depending on the technology used (Smith and Waring, 2019; Xu et al., 2017). Ultrasonic dispersion, chemical and density classification, and wet and dry sieving are the most commonly used methods (Gregorich et al., 2006; Moni et al., 2012). The tiny proportion of clay in the soil distribution of the experimental plot is even undetectable, so dry sieving has a less significant effect on the organic carbon of sandy soil. Place 100 g of soil in a sieve containing fine sand and medium sand, and connect the sieve cover to the sieve shaker (Mendes et al., 1999; Schutter and Dick, 2002). The soil particles were dried at 120°C for 48 h and weighed after shaking the sieve at 600 r min−1 for 2 min until no change in soil mass occurred. We repeated these steps twice for each soil sample. We held the soil in plastic bags until we determined C and N. We estimated

the soil mass fractions for each particle size class using the Equations 2, 3.

$$\text{Mass proportion (\%)} = \frac{\text{Dry weight of soil (g)}}{\text{Total soil dry mass (g)}} \quad (2)$$

The soil quality recovery rate R is calculated and announced as follows:

$$R = \frac{\text{Total soil dry mass (g)}}{100\ \text{(g)}} \times 100\% \quad (3)$$

2.4 Determination of soil organic carbon and nitrogen

Soil particles <250 μm and <500 μm were used to measure organic carbon and nitrogen levels. 1.0 g of dry soil was treated with 0.1 mol/L HCl at 25°C for 24 h to remove carbonates (Midwood and Boutton, 1998), washed with ultrapure water until neutral, air-dried, crushed, and sieved through a 0.149 mm SOC, and TN were measured with a complete C/N analyzer. Soil organic C (g C kg−1), total N (g N kg−1), and particle size <250 and <500 μm concentrations were estimated from dry soil mass (1 g) before HCl treatment. Soil organic carbon (Mg C ha^{-1}) and nitrogen (Mg N ha^{-1}) stocks were calculated as follows Equations 4, 5:

$$\text{SOC (TN)} = T \times BD \times C(N) \times 10 \quad (4)$$

where T represents the soil thickness (cm), BD represents soil bulk density (g/cm^{-3}), C represents soil organic C concentration (g/kg),N represents soil total N concentration (g/kg).

$$OC(TN)_{250(500)=} T \times BD \times C(N) \times 10/R \quad (5)$$

3 Results and analysis

3.1 Soil particle size composition

In the four areas of this study, the wind speed decreased from CK to the interior of the photovoltaic array and then increased before decreasing again. The overall trend was A > C > B > D. As can be seen in Figure 2, in the 0–30 cm soil of the study area, particle composition is dominated by fine sand (53.83%–66.62%) and medium sand (27.76%–38.77%), with a low content of very fine sand (0.57%–4.92%). The volume percentage of fine sand in the soil generally decreases with increasing soil depth, while the volume

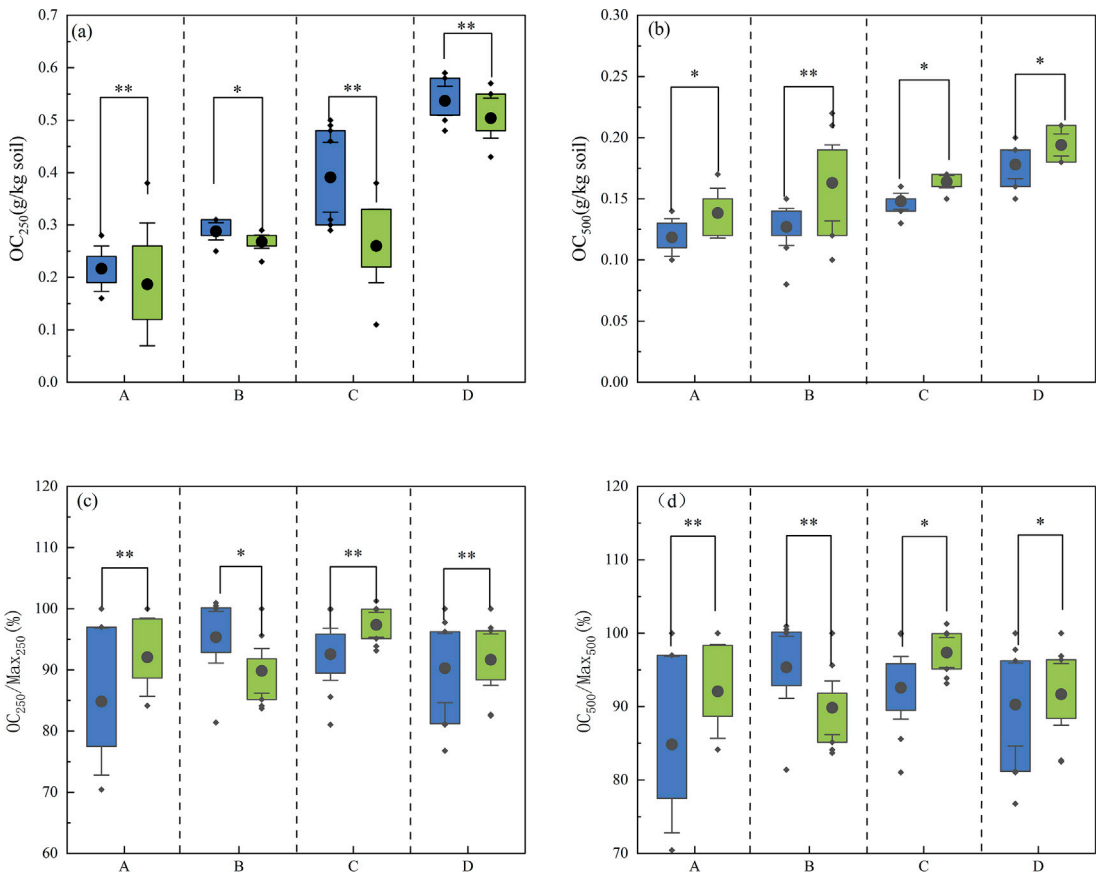

FIGURE 6
Soil organic C content in each region and its proportion of the maximum organic C content in each particle size class **(a)**: OC_{250} content of two soil layers in four sampling sites, **(b)**: OC_{500} content of two soil layers in four sampling sites, **(c)**: OC_{250}/Max_{250} in two soil layers at four sampling sites,**(d)**: OC_{500}/Max_{500} in two soil layers at four sampling sites, at the same time, blue represents 0–10 cm and green represents 10–30 cm).

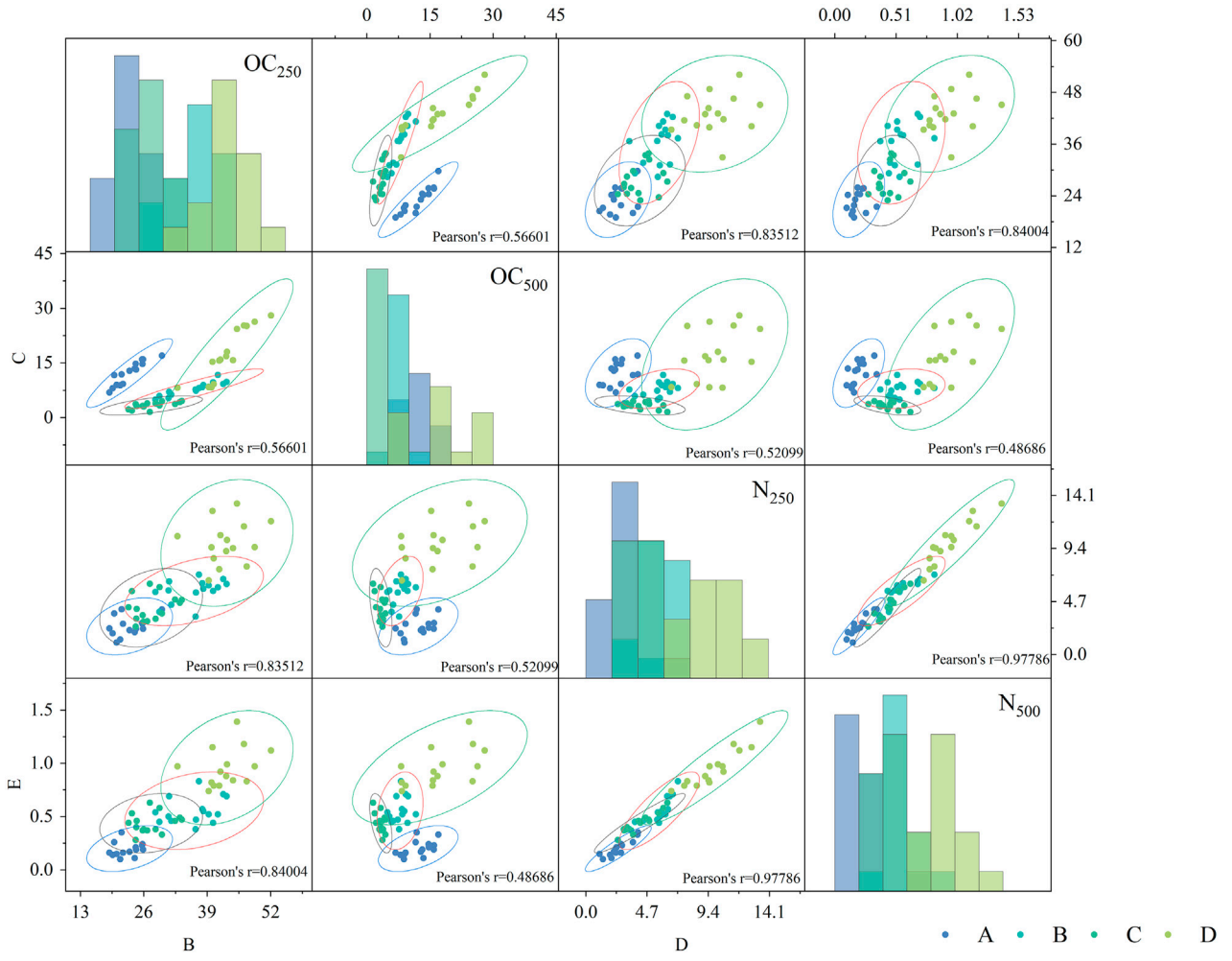

FIGURE 7
Correlation between organic matter and nitrogen storage for each grain size in each region **(A-D)** represents four sampling points).

percentage of coarse particles changes with soil depth in the opposite direction to fine sand. There are significant differences in the soil particle size distribution in each region of the same soil layer with wind speed. The content of medium and fine sand in 0–5 cm is significantly higher than that in other regions at each wind speed gradient. The content of coarse particles in different soil layers at points A and B is significantly different. Wind speed activities also clearly affect fine particles.

3.2 Soil carbon and nitrogen storage and particle size distribution

The C and N storage in the top 30 cm of soil decreased linearly with increasing wind speed gradient, from 70.76 Mg C ha^{-1} to 53.82 Mg C ha^{-1} and from 13.96 Mg N ha^{-1} to 8.12 Mg N ha^{-1}, respectively (Figures 3, 4). The soil organic C (OC_{250}) and N (N_{250}) contents of the <250 μm particle size decreased linearly with the increase of wind speed gradient. The organic C (OC_{500}) and N (N_{500}) in soil particles <500 μm increased with the wind speed gradient, among which N_{500}, but the difference was not significant. With the increase of wind speed gradient, the proportion of soil organic carbon reserves in <250 μm soil to total soil carbon reserves (OC_{250}/SOC) decreased from 98.6% to 63.70%, and the proportion of N (N_{250}/TN) decreased from 98.6% to 60.3%. At the same time, the proportion of soil particle composition with organic carbon reserves of <500 μm (OC_{500}/SOC) decreased from 35.2% to 0.8%, and N $_{500}$/TN decreased from 7.8% to 0.4%.

3.3 Relationship between soil organic carbon and nitrogen stocks and soil particle size and non-particle size

Soil carbon and nitrogen stocks in the two particle size ranges are positively correlated with soil stocks throughout the soil depth and in each part of the photovoltaic array. In the soil of each part, the OC_{250} stock linearly increases with the increase of organic C stock. Ordinary least squares regression analysis of the slopes in each location ranged from 0.01 to 1.60 for C and 0.01 to 1.37 for N, and the relationship between soil organic C and soil fine-particle organic

C had a higher coefficient of determination. The relationship between soil organic carbon and OC_{500} was not affected by depth across the entire soil depth range (Figure 5). In addition, the organic carbon content of both soil particle sizes increased linearly with the total organic carbon content of the soil, indicating that the soil was not saturated with organic carbon. The relationship between soil particle size nitrogen content and total soil nitrogen content was similar to that of organic carbon.

3.4 Distribution of soil organic carbon by particle size

Both OC_{250} and OC_{500} showed a continuous increase with their mass fraction (Figure 6); in addition, the mass fraction of the OC_{250} soil particle size component explained the 95% confidence interval of the organic carbon content to a greater extent. The soil organic carbon content in areas C and D was higher than in areas A and B. Moreover, the soil organic carbon content in all areas was essentially 10–30 cm higher than that in 0–10 cm areas. The soil <250 μm particle size component ($OC_{250}/OCmax_{250}$) organic carbon content as a percentage of the maximum organic carbon content was basically the same in each soil layer. The OC_{250} content in area D was extremely low, with an average value of 0.24 g/kg. OC_{500} is low in area D and high in areas A and B. Area D shows the lowest $OC_{500}/OCmax_{500}$ (76.78%) and the highest $OC_{250}/OCmax_{250}$ (104.29%) (Figure 7). Overall, area D shows a higher $OC_{250}/OCmax_{250}$.

4 Discussion

Wind is caused by the movement of air currents, and changes in wind speed and direction serve as important indicators of local airflow variations (Ehrenberg, 1847). While causing deformation of the Earth's surface, wind also alters other soil properties. The installation of solar panels in photovoltaic (PV) power stations alters the properties of the underlying surface and modifies the surrounding airflow. Research has shown that photovoltaic arrays can create a range of effects on nearby airflow, including blocking and dragging, which subsequently impacts wind speed and direction, leading to changes in the wind field (Zhao et al., 2022). It has been observed that, compared to open areas (A), the establishment of photovoltaic arrays acts as a windbreak in desert regions. Wind speeds within the photovoltaic array are significantly lower than those in open areas, dropping to as low as 44.5% of the wind speed in the surrounding open regions as one moves inward from the edges. Additionally, fluctuations in wind speed correspond with minor changes in soil particle size, mainly concentrated at depths of 0–10 cm. This may be related to the alteration of the local microclimate due to the construction of the photovoltaic power station, which reduces surface wind speeds and diminishes the transport capacity of sand materials, resulting in more fine particles remaining on the soil surface. Previous studies have concluded that when the intersection angle exceeds 45°, the photovoltaic panel array exhibits a notable "sand interception effect," with an average sand transport rate above the array reduced by 82.58% compared to moving dunes, while significant wind and sand activity primarily occurs at the edges (Tang et al., 2021). Furthermore, reduced wind speeds increase the potential surface moisture content and enhance soil temperature and humidity, making soil particles less susceptible to erosion (Tanner et al., 2020). The negative correlation between fine particles and wind speed observed in this study is consistent with these findings.

Changes in terrain within photovoltaic (PV) areas in deserts can lead to variations in microclimate, resulting in increased ground temperatures and altered precipitation patterns. These factors affect the accumulation and decomposition rates of soil organic matter, the mineralization of organic carbon, and the nutrient content in the soil (Aryal, 2022), all of which influence the carbon storage and distribution in the region. Research indicates that rising temperatures can further promote the decomposition of soil organic matter, thereby increasing the availability of nutrients and enhancing mineralization rates (Williams et al., 2009). This study shows that soil organic carbon (SOC) and total nitrogen (TN) levels are higher within the PV arrays compared to the external areas, with a more pronounced increase on nutrient content found in the fine particles of the surface soil. The construction of PV stations alters the surface microenvironment, raising surface temperatures and moisture levels while potentially stimulating soil microbial and enzymatic activity, which accelerates the decomposition process. Additionally, the interception of rainfall by PV panels redistributes precipitation, concentrating acidic substances on the soil surface, which further speeds up microbial decomposition. Furthermore, reduced wind speeds lead to a greater retention of fine particles on the soil surface, enriching the nutrient content. The changes in soil nutrient levels within the PV arrays may be influenced by variations in wind speed that affect the deposition of particles or differences in parent material. The nitrogen levels in this area exhibit greater stability, likely due to the low vegetation cover in desert regions that limits external nitrogen consumption; moreover, the efficiency of nitrogen-decomposing soil microorganisms and enzymes is significantly lower under drought and sandstorm conditions compared to those decomposing carbon. As illustrated in the data, there is a positive correlation between fine sand content and organic carbon across various sampling locations. The correlation of soil organic carbon with different particle sizes follows a consistent pattern, with the strongest correlation in the size range of 100–250 μm, followed by 250–500 μm, 50–100 μm, and finally 500–1,000 μm (Harry et al., 2000; Zhang et al., 2017). This finding aligns with previous research, indicating that soil with predominant particle sizes contains higher levels of organic carbon.

5 Conclusion

The research investigated the composition of soil particle size components in the three soil depths inside and outside the photovoltaic power plant, the content and storage of organic carbon, and organic nitrogen in the two soil particle size components of the main particle size composition. Fine sand particles (particle size 100–250 μm) are the main component of the soil in this area. Compared with other particle size components,

soil components with a particle size of <250 μm can better estimate soil organic carbon and nitrogen reserves. Wind speed From the outside to the inside of the photovoltaic array, the wind speed experienced a weakening-strengthening-weakening process. Particle size and wind speed showed an opposite trend, and the organic matter and total nitrogen reserves also showed an increasing-decreasing-increasing trend, while the reserves stored in the surface layer were more abundant. In future photovoltaic projects, it is necessary to carry out scientific vegetation construction based on the threshold of soil environment in the region, long-term ecological research results, the growth status of sand-fixing vegetation and the demand of plant species for nutrient elements.

Data availability statement

The datasets generated during and/or analyzed during the current study are available from the corresponding author on reasonable request. Requests to access the datasets should be directed to 1109592302@qq.com.

Author contributions

FZ: Conceptualization, Writing–original draft. ZM: Writing–review and editing. YL: Investigation, Writing–original draft, Writing–review and editing. PL: Writing–review and editing. GT: Writing–review and editing, Methodology.

Funding

The author(s) declare that financial support was received for the research, authorship, and/or publication of this article. This research was supported by Ordos Science and Technology Major Project (2022EEDSKJZDZX020-4); National Natural Science Foundation of China (NSFC)(42201012). Inner Mongolia Autonomous Region Forestry Research Institute Open Subjects (KF2024ZD02). Sub-project of Science and Technology Project of China Huaneng Group Co., Ltd. - Research on Low-cost and Biodegradable Sand Barriers for Flow Sand Fixation in Sandy Areas for Photovoltaic Power Stations.

Acknowledgments

Thank you to all the authors and to the editors and reviewers who contributed to the improvement of this article!

Conflict of interest

The authors declare that the research was conducted in the absence of any commercial or financial relationships that could be construed as a potential conflict of interest.

Generative AI statement

The author(s) declare that no Generative AI was used in the creation of this manuscript.

Publisher's note

References

Arayal, D. R. (2022). Grazing intensity in grassland ecosystems: implications for carbonstorage and functional properties. *CABI Rev.* 13 (12), 2162. doi:10.1079/cabireviews202217032

Barron-Gafford, G. A., Minor, R. L., Allen, N. A., Cronin, A. D., Brooks, A. E., and Pavao-Zuckerman, M. A. (2016). The Photovoltaic Heat Island Effect:Larger solar power plants increase local temperatures. *Sci. Rep.* 6, 35070–35077. doi:10.1038/srep35070

Christensen, B. T. (1992). Physical fractionation of soil and organic matter in primary particle size and density separates. *Adv. Soil Sci. N. Y.*, 20. doi:10.1007/978-1-4612-2930-8_1

Cotrufo, M. F., Ranalli, M. G., Haddix, M. L., Six, J., and Lugato, E. (2019). Soil carbon storage informed by particulate and mineral-associated organic matter. *Nat. Geosci.* 12, 989–994. doi:10.1038/s41561-019-0484-6

Deng, L., Zhang, Z. N., and Shangguan, Z. P. (2014). Long-term fencing effects on plant diversity and soil properties in China. *Soil and Tillage Res.* 137, 7–15. doi:10.1016/j.still.2013.11.002

Ding, C. X., and Liu, Y. (2021). Effects of solar photovoltaic park construction on soil microbial community in alpine desert of qinghai tibet plateau. *ACTA AGRESTIA SIN.* 29, 1061–1069. doi:10.11733/j.issn.1007-0435.2021.05.023

Ehrenberg, C. G. (1847). The sirocco dust that fell at genoa on the 16th may. 1846. *QJ Geol. Soc. Lond* 3, 25–26. doi:10.1007/978-3-642-11476-2

Folk, R. L., and Ward, W. C. (1957). A study in the significance of grain-size parameters. *J. Sediment. Petrology* 27, 3–27. doi:10.1306/74d70646-2b21-11d7-8648000102c1865d

Georgiou, K., Jackson, R. B., Vindušková, O., Abramoff, R. Z., Ahlstr¨om, A., Feng, W., et al. (2022). Global stocks and capacity of mineral-associated soil organic carbon. *Nat. Commun.* 13, 3797. doi:10.1038/s41467-022-31540-9

Gregorich, E. G., Beare, M. H., McKim, U. F., and Skjemstad, J. O. (2006). Chemical and biological characteristics of physically uncomplexed organic matter. *Soil Sci. Soc. Am. J.* 70, 975–985. doi:10.2136/sssaj2005.0116

Harry, J. P., Roger, L. P., and Neal, A. S. (2000). Factors controlling soil carbon levels in New Zealand grasslands:Isclay content important? *Soil Sci. Soc. Ameri-ca J.* 64, 1623–1630. doi:10.2136/sssaj2000.6451623x

Hassink, J. (1997). The capacity of soils to preserve organic C and N by their association with clay and silt particles. *Plant Soil* 191, 77–87. doi:10.1023/a:1004213929699

He, Y. T., He, Y. J., Wang, P., and Xie, H. S. (2023). Effects of different forest management regimes on soil organic carbon in aggregate fractions in natural secondary Quercus mongolica forests. *Ecol. Environ. Sci.* 32, 11–17. doi:10.16258/j.cnki.1674-5906.2023.01.002

Heckman, K., Hicks Pries, C. E., Lawrence, C. R., Rasmussen, C., Crow, S. E., Hoyt, A. M., et al. (2022). Beyond bulk: density fractions explain heterogeneity in global soil carbon abundance and persistence. *Glob. Change Biol.* 28, 1178–1196. doi:10.1111/gcb.16023

Lavallee, J. M., Soong, J. L., and Cotrufo, M. F. (2020). Conceptualizing soil organic matter into particulate and mineral-associated forms to address global change in the 21st century. *Glob. Change Biol.* 26, 261–273. doi:10.1111/gcb.14859

Lei, L., Zhang, K., Zhang, X., Wang, Y. P., Xia, J., Piao, S., et al. (2019). Plant feedback aggravates soil organic carbon loss associated with wind erosion in northwest China. *J. Geophys. Res. Biogeosci.* 124, 825–839. doi:10.1029/2018jg004804

Li, D., Wang, X. M., Li, k. Y., and Gu, Y. P. (2024). Estimation of soil organic carbon content in the bohu basin based on synthetic images and multi-variables. *Environ. Sci*. doi:10.13227/j.hjkx.202406088

Li, J. W., Li, M. Y., Dong, L. B., Wang, K., Liu, Y., Hai, X., et al. (2020). Plant productivity and microbial composition drive soil carbon and nitrogen sequestrations foll owing cropland abandonment. *Sci. Total Environ.* 744, 140802. doi:10.1016/j.scitotenv.2020.140802

Liu, J., Su, Y., Li, Y., and Huang, G. (2021a). Shrub colonization regulates δ13C enrichment between soil and vegetation in deserts by affecting edaphic variables. *Catena* 203, 105365. doi:10.1016/j.catena.2021.105365

Liu, Z., Sun, H., Lin, K., Zhou, C., and Huang, W. (2021b). Occurrence regularity of silt–clay minerals in wind eroded deserts of northwest China. *Sustainability* 13, 2998. doi:10.3390/su13052998

Lopez, B. R., and Bacilio, M. (2020). Weathering and soil formation in hot, dry environments mediated by plant–microbe interactions. *Biol. Fertil. Soils* 56, 447–459. doi:10.1007/s00374-020-01456-x

Lützow, M. V., Kögel-knabner, I., Ekschmitt, K., Matzner, E., Guggenberger, G., Marschner, B., et al. (2006). Stabilization of organic matter in temperate soils: mechanisms and their relevance under different soil conditions – a review. *Eur. J. Soil Sci.* 57, 426–445. doi:10.1111/j.1365-2389.2006.00809.x

Mendes, I. C., Bandick, A. K., Dick, R. P., and Bottomley, P. J. (1999). Microbial biomass and activities in soil aggregates affected by winter cover crops. *Soil Sci. Soc. Am. J.* 63, 873–881. doi:10.2136/sssaj1999.634873x

Midwood, A. J., and Boutton, T. W. (1998). Soil carbonate decomposition by acid has littleeffect on δ13C of organic matter. *Soil Biol. biochem.* 30, 1301–1307. doi:10.1016/s0038-0717(98)00030-3

Moni, C., Derrien, D., Hatton, P. J., Zeller, Z., and Kleber, M. (2012). Density fractions versus size separates: does physical fractionation isolate functional soil compartments? *Biogeosciences* 9, 5181–5197. doi:10.5194/bg-9-5181-2012

Ni, H. B., Zhang, L. P., Zhang, D. R., Wu, X. Y., and Fu, X. T. (2018). Weathering of pisha-sandstones in the wind-water erosion crisscrossregion on the Loess Plateau. *J. Mt. Sci.* 5, 340–349. doi:10.1007/s11629-008-0218-5

Poulter, B., Frank, D., Ciais, P., Myneni, R. B., Andela, N., Bi, J., et al. (2014). Contribution of semi-arid ecosystems to interannual variability of the global carbon cycle. *Nature* 509 (7502), 600–603. doi:10.1038/nature13376

Pratt, R. N., and Kopp, G. A. (2013). Velocity measurements around low-profile, tilted, solar arrays mounted on large flat-roofs, for wall normal wind directions. *J. Wind Eng. Industrial Aerodynamics* 123, 226–238. doi:10.1016/j.jweia.2013.09.001

Qu, Q., Deng, L., Gunina, A., Hai, X., Deng, J., Shangguan, Z., et al. (2024). Grazing exclusion increases soil organic C through microbial necromass of root-derived C as traced by 13C labelling photosynthate. *Biol. Fertil. Soil* 60, 407–420. doi:10.1007/s00374-024-01807-y

Qu, Q., Zhang, J., Hai, X. Y., Wu, J., Fan, J., Wang, D., et al. (2022). Long-term fencing alters the vertical distribution of soil δ13C and SOC turnover rate: revealed by MBC- δ13C. *Agric. Ecosyst. Environ.* 339, 108119. doi:10.1016/j.agee.2022.108119

Schutter, M. E., and Dick, R. P. (2002). Microbial community profiles and activities among aggregates of winter fallow and cover-cropped soil. *Soil Sci. Soc. Am. J.* 66, 142–153. doi:10.2136/sssaj2002.1420

Slessarev, E. W., Chadwick, O. A., Sokol, N. W., Nuccio, E. E., and Pett-Ridge, J. (2022). Rock weathering controls the potential for soil carbon storage at a continental scale. *Biogeochemistry* 157, 1–13. doi:10.1007/s10533-021-00859-8

Smith, K. R., and Waring, B. G. (2019). Broad-scale patterns of soil carbon (C) pools and fluxes across semiarid ecosystems are linked to climate and soil texture. *Ecosystems* 22, 742–753. doi:10.1007/s10021-018-0299-0

Sokol, N. W., and Bradford, M. A. (2019). Microbial formation of stable soil carbon is more efficient from belowground than aboveground input. *Nat. Geosci.* 12, 46–53. doi:10.1038/s41561-018-0258-6

Sokol, N. W., Whalen, E. D., Jilling, A., Kallenbach, C., Pett-Ridge, J., and Georgiou, K. (2022). Global distribution, formation and fate of mineral-associated soil organic matter under a changing climate: a trait-based perspective. *Funct. Ecol.* 36, 1411–1429. doi:10.1111/1365-2435.14040

Srivastava, P., Singh, R., Bhadouria, R., Tripathi, S., and Raghubanshi, A. S. (2020). Temporal change in soil physicochemical, microbial, aggregate and available C characteristic in dry tropical ecosystem. *Catena* 190, 104553. doi:10.1016/j.catena.2020.104553

Tang, G. D., Meng, Z. J., Gao, Y., and Dang, X. (2021). Impact of utilityscale solar photovoltaic array on the aeolian sediment transport in Hobq Desert, China. *J. Arid Land* 13, 274–289. doi:10.1007/s40333-021-0096-y

Tanner, K. E., Moore-O′Leary, K. A., Parker, I. M., Pavlik, B. M., and Hernandez, R. R. (2020). Simulated solar panels create altered microhabitats in desert landforms. *Ecosphere* 211, e03089. doi:10.1002/ecs2.3089

Williams, C. A., Hanan, N., Scholes, R. J., and Kutsch, W. (2009). Complexity in water and carbondioxide fluxes following rain pulses in an African savanna. *Oecologia* 161 (3), 469–480. doi:10.1007/s00442-009-1405-y

Xu, S., Silveira, M. L., Ngatia, L. W., Normand, A. E., Sollenberger, L. E., and Ramesh Reddy, K. (2017). Carbon and nitrogen pools in aggregate size fractions as affected by sieving method and land use intensification. *Geofis. Int.* 305, 70–79. doi:10.1016/j.geoderma.2017.05.044

Zhang, J. M., Chi, F. Q., Han, J. Z., Zhou, B. K., and Kuang, E. J. (2017). SOC distribution characteristics of mollisols aggregates in different long-term fertilization systems. *Soils Crops* 6, 49–54. doi:10.11689/j.issn.2095-2961.2017.01.008

Zhang, L. am., Xu, M. G., Lou, Y. H., Xiao-li, WANG, and Zhong-fang, L. I. (2014). Soil organic carbon fractionation methods. *Acta Pedol. Sin.* (4), 1–6. doi:10.11838/sfsc.20140401

Zhang, Y. F., Chen, L., Zhang, B. B., and Li, X. B. (2023). Characteristics of organic carbon particle size composition and carbon pool management index in surface soil of desert grassland. *J. Soil Water Conservation* 37, 283–290. doi:10.13870/j.cnki.stbcxb

Zhao, W., Liu, L., Chen, J., and Ji, J. (2019). Geochemical characterization of major elements in desert sediments and implications for the Chinese loess source. *Sci. China Earth Sci.* 62, 1428–1440. doi:10.1007/s11430-018-9354-y

Zhao, Y. Y., Ying, J., Li, Z. C., Gao, X. G., and Luo, Y. (2022). Characteristics of meteorological elements of photovoltaic PowerPlants in gobi. *Plateau Meteorol.* 41, 977–987. doi:10.7522/j.issn.1000-0534.2022.00073

frontiers | Frontiers in Environmental Science

TYPE Original Research
PUBLISHED 08 July 2025
DOI 10.3389/fenvs.2025.1599278

OPEN ACCESS

EDITED BY
Tianjiao Feng,
Beijing Forestry University, China

REVIEWED BY
Yi Wang,
Chinese Academy of Sciences (CAS), China
Yuan Li,
Natural Resources Institute Finland (Luke), Finland

*CORRESPONDENCE
Yunxia Ma,
1572666975@qq.com

RECEIVED 24 March 2025
ACCEPTED 23 June 2025
PUBLISHED 08 July 2025

CITATION
Shao Y, Ma Y, Li G and Ma X (2025) Analysis of changes in soil chemical stoichiometric ratios under different cultivation durations of *Pennisetum giganteum* in inner Mongolia, China.
Front. Environ. Sci. 13:1599278.
doi: 10.3389/fenvs.2025.1599278

Analysis of changes in soil chemical stoichiometric ratios under different cultivation durations of *Pennisetum giganteum* in inner Mongolia, China

Yazhou Shao[1,2], Yunxia Ma[1,2]*, Gangtie Li[1] and Xiaolu Ma[1]

[1]College of Desert Control Science and Engineering, Inner Mongolia Agricultural University, Hohhot, China, [2]State Key Laboratory of Water Engineering Ecology and Environment in Arid Area, Inner Mongolia Agricultural University, Hohhot, China

This study aims to investigate the impact of *Pennisetum giganteum* cultivation on soil stoichiometric ratios in different regions of Inner Mongolia (Naiman Banner, Ulan Buh Desert, and Tumd Left Banner), clarifying the relationship between years of cultivation and changes in soil nutrient contents as well as stoichiometric ratios, thereby providing a scientific basis for regional ecological restoration. The experimental design used *Pennisetum giganteum* as the research subject, establishing experimental plots in three regions. Soil samples from 0 to 100 cm at different depths were collected before planting (CK), after the first-year harvest (YK), and after the second-year harvest (EK). The contents of soil SOC, TN, and TP were measured, and the ratios of C/N, C/P, and N/P were calculated. Through one-way ANOVA and Pearson correlation analysis, the relationships among cultivation years, soil depth, and soil nutrients as well as stoichiometric ratios were evaluated. The results indicate that *Pennisetum giganteum* cultivation significantly increased soil nutrient contents. For example, in Naiman Banner, the soil layer of 0–10 cm showed an increase in C from 1.41 g/kg to 2.06 g/kg, N from 1.47 g/kg to 1.74 g/kg, and P from 1.27 g/kg to 1.85 g/kg. Changes in soil stoichiometric ratios varied with region and soil depth: in Tumd Left Banner, the C/N ratio generally decreased (e.g., from 1.48 to 0.77 in the 0–10 cm soil layer), indicating an accelerated rate of N accumulation; whereas in the Ulan Buh Desert, the C/N ratio exhibited an increasing trend, possibly due to more pronounced C accumulation under arid conditions. The C/P and N/P ratios decreased in most regions, reflecting an improvement in P availability. Correlation analysis revealed that cultivation years were significantly positively correlated with soil C, N, and P contents, while they were mostly negatively correlated with the C/P and N/P ratios.

KEYWORDS

Pennisetum giganteum, soil elements, stoichiometric ratio, planting year, soil depth

1 Introduction

China's land desertification problem is extremely severe, manifesting in multiple ways such as a decline in productivity, reduced surface vegetation cover, and diminished biodiversity (Lu et al., 2024). Desertification not only leads to a reduction in available land area but also triggers a series of disasters—including frequent sandstorms and widespread flooding—that have profound impacts on the economy, society, and ecological environment (Li et al., 2024). The deterioration of the ecosystem accompanied by economic impoverishment has become one of the major factors hindering China's sustainable development. Inner Mongolia is among the provinces with the most concentrated and severe desertification; its desertified area ranks second in the country, only trailing Xinjiang, and its trend of desertification is particularly notable nationwide, making it a key region for national desertification monitoring and remediation (Zhao et al., 2022; Liao et al., 2020; Ren et al., 2023). Based on this, the present study selected three experimental sites: Ulan Buh Desert, Tumd Left Banner in Hohhot, and Naiman Banner in Tongliao. The causes of land desertification in Inner Mongolia are mainly attributed to both natural and anthropogenic factors. Among the natural factors, insufficient precipitation is one of the key reasons for desertification; the combination of scarce rainfall and high evaporation accelerates vegetation degradation and land desertification processes (Li and Narisu, 2011; Yao, 2018). As for anthropogenic factors, the combined effects of overgrazing, excessive logging, and other human activities, together with climatic changes, have disrupted the ecological balance of grasslands, leading to increasingly severe grassland and land desertification that significantly constrain regional economic and social development (Li, 2001; Wang et al., 2006; Nie et al., 2008). Therefore, it is particularly urgent to introduce a plant species that can not only effectively stabilize the wind and fix the sand but also yield certain economic benefits.

Pennisetum giganteum, a member of the genus *Pennisetum* within the Poaceae family, is a perennial, erect, clump-forming plant whose distribution extends from Hainan in southern China to the northern region of Inner Mongolia (Zhou et al., 2020). This plant primarily relies on asexual reproduction, with its root system being exceptionally well-developed; it possesses a large number of adventitious and lateral roots that enable it to maintain robust vitality even in deep soil layers (Ma et al., 2023). These characteristics make *Pennisetum giganteum* an optimal choice for combating soil erosion. It not only enhances soil quality by optimizing soil structure, increasing organic matter content, and activating microbial activity, but also effectively prevents land degradation and desertification (Li et al., 2020; Sheng, 2023). In addition to its tall stature, *Pennisetum giganteum* yields impressive biomass that is rich in crude protein and crude fiber, allowing for multiple harvests annually. Its nutritional value is particularly high during the seedling stage, and its palatable taste renders it a superior forage resource. The three primary nutrients essential for plant growth—carbon (C), nitrogen (N), and phosphorus (P)—play crucial roles in plant physiological processes and are closely interrelated [15–16]. The ratios of C/N, C/P, and N/P in soil are key indicators of the composition and quality of soil organic matter, revealing the efficiency of nutrient utilization by plants and the extent of nutrient limitations(Cheng et al., 2010). Specifically, the soil C/N ratio reflects the mineralization rate of organic matter (Wang and Yu, 2008): a ratio exceeding 25 indicates that the accumulation of organic matter surpasses its decomposition rate, while a ratio between 12 and 16 suggests active decomposition of organic matter (Bui and Henderson, 2013). The soil C/P ratio demonstrates the capacity of soil microorganisms to mineralize organic matter and release phosphorus(Tao et al., 2017), whereas the soil N/P ratio serves as a diagnostic indicator for nitrogen saturation, helping to determine the critical point of nutrient limitation (Huang and Yuan, 2020).

Based on the aforementioned background, this study poses the following specific research questions: First, under varying planting durations, how does *Pennisetum giganteum* affect the contents of C, N, and P in soils at different vertical depths (0–100 cm) across Ulan Buh Desert, Tumd Left Banner, and Naiman Banner? Second, what changes occur in the stoichiometric ratios (C/N, C/P, and N/P) of soils in these three regions as a result of *Pennisetum giganteum* plantation over different planting years? Third, what is the relationship between soil nutrient contents, their stoichiometric ratios, and the duration of planting?

This study focuses on *Pennisetum giganteum* and conducted planting experiments in the Ulan Buh Desert, Tumd Left Banner, and Naiman Banner. Soil samples were collected at various vertical depths (0–10 cm, 10–20 cm, 20–40 cm, 40–60 cm, 60–80 cm, and 80–100 cm) to determine the content of C, N, and P in the soil after 2 years of cultivation. Subsequently, the soil C/N, C/P, and N/P ratios were calculated to analyze the influence of different planting durations on the stoichiometric characteristics of soils at varying depths. The results are intended to provide data support for the formulation of scientifically sound ecological restoration strategies and to serve as a reference for preventing land desertification in Inner Mongolia and maintaining regional ecological security.

2 Materials and methods

2.1 Overview of the study area

This experiment selected the Ulan Buh Desert, Tumd Left Banner, and Naiman Banner in Inner Mongolia as the research areas.

The Ulan Buh Desert study area is located in the northeastern part, with geographic coordinates ranging from 106°35′ to 106°59′ in longitude and 40°17′ to 40°29′ in latitude. This region is adjacent to the Yellow River and lies in a transitional zone between desert and desert grassland, characterized by an Asian temperate desert climate. The climate is notably arid with limited rainfall, a significant diurnal temperature range, an annual mean temperature of 7.5°C, and a frost-free period of approximately 160–170 days.

The Tumd Left Banner is situated between 110°46′ and 112°10′ in longitude and 40°51′ and 41°8′ in latitude, positioned on the Inner Mongolian Plateau within the middle section of the Yinshan Mountains, specifically in the central area of the Daqing Mountains. This area features a temperate continental climate, characterized by dryness, scarce precipitation, a short frost-free period, and an annual mean temperature of 7.3°C.

The Naiman Banner study area is located in the southeastern part of the Horqin Sandy Land, with geographic coordinates ranging

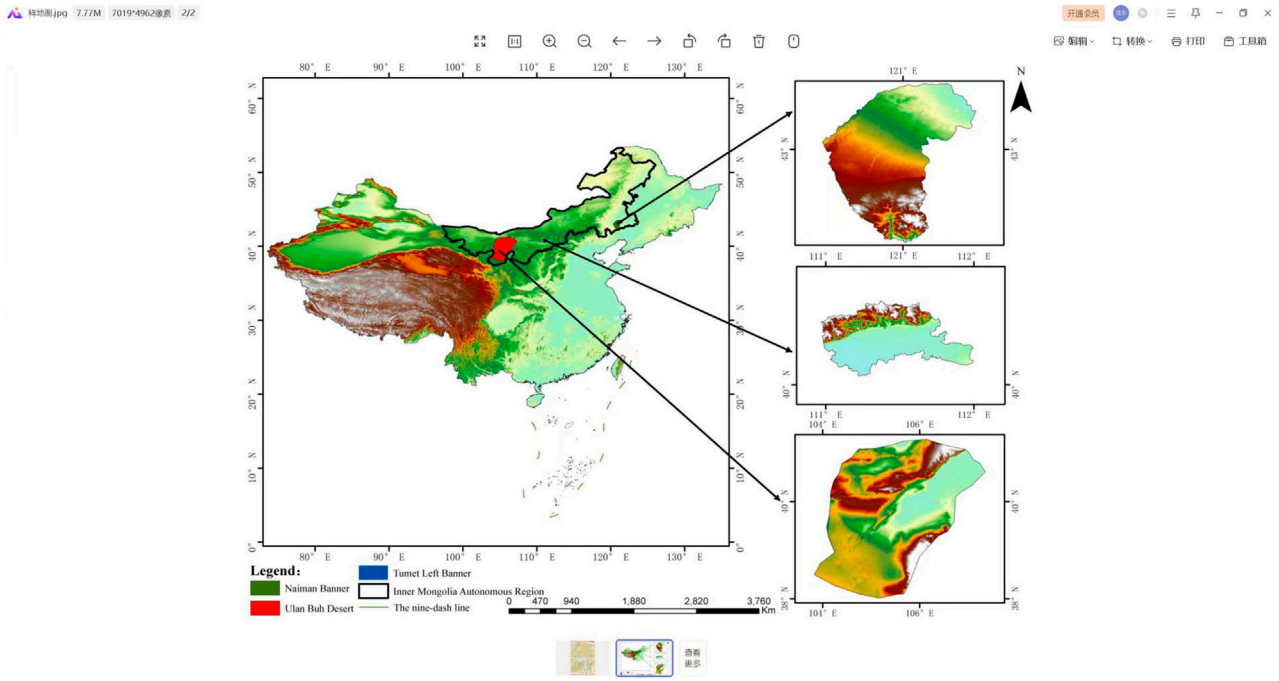

FIGURE 1
Overview of the study area.

from 120°19′ to 121°35′ in longitude and 42°14′ to 43°32′ in latitude (Figure 1). This region exhibits a temperate semi-arid climate, with a pronounced diurnal temperature variation, extreme low temperatures reaching as low as −29.3°C, extreme high temperatures up to 39°C, and a frost-free period of 135–140 days.

2.2 Experimental design

This study selected experimental sites in the eastern Ulan Buh Desert *Pennisetum giganteum* plantation area, the Hailutuo plantation area in Tumd Left Banner, and the *Pennisetum giganteum* plantation area in the western Khorchin sandy land of Naiman Banner, Inner Mongolia. All three sites began the introduction trials in 2018. Due to the relatively weak cold tolerance of *Pennisetum giganteum*, which makes natural overwintering in northern regions difficult, the harvest was scheduled during the autumn and winter seasons while retaining the root systems in the soil. In the following spring, the land was tilled and *Pennisetum giganteum* was replanted in the original plots. During the experiment, soil samples were collected at three stages: before planting (CK), after the first year's harvest (YK), and after the second year's harvest (EK), with the specific sampling times occurring in mid-October of 2018, 2019, and 2020, respectively.

Each study plot was a rectangle measuring 40 × 50 m. In terms of irrigation, water was applied during the growing season based on local climatic conditions and soil moisture status. During the experimental period from 2018 to 2020, the irrigation period each year commenced after the spring planting of *Pennisetum giganteum* and concluded before the autumn harvest. In 2018, during the vigorous growth phase of *Pennisetum giganteum* (June to August), irrigation was conducted three times per month, with an application rate of approximately 0.06 m^3 per square meter per event; during the other months, irrigation was applied one to two times per month at approximately 0.03 m^3 per square meter per event, resulting in a total annual irrigation of about 0.78 m^3 per square meter. The irrigation patterns in 2019 and 2020 were essentially the same as in 2018; however, due to slight climatic variations, the total annual irrigation was approximately 0.75 m^3 per square meter in 2019 and 0.80 m^3 per square meter in 2020. In terms of fertilization, a compound fertilizer containing nitrogen, phosphorus, and potassium (N:P:K = 15:15:15) was used. Prior to spring planting each year, 0.075 kg of base fertilizer was applied per square meter, and during the growth of *Pennisetum giganteum*, top-dressing was carried out in June and August, with 0.03 kg applied per square meter at each occasion. Additionally, for comparative analysis, soil samples were collected from adjacent bare sandy areas to serve as controls. In each study plot, soil samples were collected three times using an S-shaped sampling design. For sampling, soil profiles were first excavated, and then soil samples were collected in layers along the vertical profile (0–100 cm). Nutrient analyses conducted on the collected soil samples further evaluated the ameliorative effect of *Pennisetum giganteum* on the spatial distribution of soil nutrients and its ecological restoration function.

2.3 Determination of indicators and calculation of stoichiometric ratios

After natural air-drying and sieving through a 0.25 mm mesh, the soil samples were first subjected to the determination of C, N, and P contents. Carbon was measured using the potassium

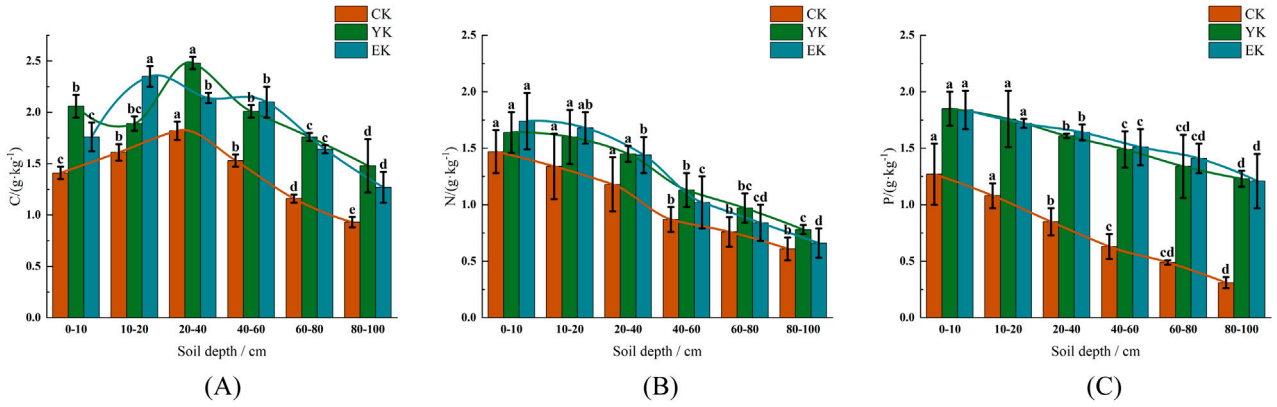

FIGURE 2
Contents of C, N and P in soil under different planting years of Naiman Banner Pennisetum giganteum. **(A)** C; **(B)** N; **(C)** P.Note: Different letters indicate significant differences at $P < 0.05$.

dichromate oxidation method with heating, nitrogen by the Kjeldahl method, and phosphorus by the molybdenum-antimony colorimetric method (Li, 2000). Based on the measured contents of C, N, and P, the ratios of C/N, C/P, and N/P were subsequently calculated (Dong et al., 2019). The determination and calculation of these indices provide an important basis for assessing soil nutrient status and its stoichiometric characteristics.

2.4 Data processing

2.4.1 Data organization and preliminary statistics

The original data were organized using Excel 2019, including the computation of the mean, standard deviation, and 95% confidence interval (CI) for soil C, N, and P contents. Data were standardized to ensure the accuracy of subsequent analyses.

2.4.2 One-way analysis of variance (ANOVA)

One-way ANOVA was conducted using SPSS 26.0 to compare the significant differences in soil C, N, and P contents and stoichiometric ratios (C/N, C/P, N/P) under different planting durations (CK, YK, EK) and soil layer depths (0–100 cm stratification). The significance level was set at $p < 0.05$. If the results were significant, further multiple comparisons (e.g., Tukey HSD test) were performed to clarify specific differences among the groups.

2.4.3 Correlation analysis

Pearson correlation coefficients were used to analyze the relationships between planting duration, soil layer depth, and soil C, N, and P contents as well as stoichiometric ratios. The strength of the correlations was assessed based on significance levels ($p \leq 0.05$, $p \leq 0.01$, $p \leq 0.001$), and a heatmap (e.g., Figures 5–7) was generated to visually illustrate the trends in correlation.

2.4.4 Data visualization

Charts were created using Origin 2021, including bar charts (Figures 2–4) that display the variations in C, N, and P contents across different soil layers and planting durations, as well as tables (Tables 1–3) summarizing the patterns in stoichiometric ratios. The charts were annotated with Mean ± SD and the 95% CI to ensure the completeness of data representation.

3 Results

3.1 Changes in C, N, and P contents in soil under different planting years of *Pennisetum giganteum* in inner Mongolia

3.1.1 Changes in soil C, N, and P contents under different planting years of *Pennisetum giganteum* in Naiman Banner

In the Naiman Banner experimental area, *Pennisetum giganteum* planting significantly increased soil C content (Figure 2A). Before planting (CK), the C content in 0–10 cm soil layer was 1.41 ± 0.06 g/kg (95% CI: 1.31–1.51 g/kg), which decreased significantly with the deepening of soil layer ($P < 0.05$), and it was only 0.93 ± 0.05 g/kg (95% CI: 0.84–1.02 g/kg) in 80–100 cm soil layer. After harvest in the first year (YK), the C content in 0–10 cm soil layer increased significantly to 2.06 ± 0.11 g/kg (95% CI: 1.87–2.25 g/kg, $P < 0.05$), and reached the peak of 2.48 ± 0.06 g/kg (95% CI: 2.39–2.58 g/kg) in 20–40 cm soil layer. After harvest in the second year (EK), the surface C content decreased slightly (1.76 ± 0.14 g/kg, 95% CI: 1.53–2.00 g/kg), but the 10–20 cm soil layer increased significantly to 2.35 ± 0.10 g/kg (95% CI: 2.19–2.52 g/kg, $P < 0.05$), indicating that *Pennisetum giganteum* had a more lasting effect on the improvement of middle soil.

Soil N content increased significantly with the increase of planting years (Figure 2B). In the CK stage, the N content in the 0–10 cm soil layer was 1.47 ± 0.19 g/kg (95% CI: 1.17–1.78 g/kg), and the deep layer (80–100 cm) decreased to 0.61 ± 0.10 g/kg (95% CI: 0.44–0.78 g/kg). In the YK stage, the surface N content increased to 1.64 ± 0.18 g/kg (95% CI: 1.35–1.93 g/kg, $P < 0.05$), and the 20–40 cm soil layer maintained a high level (1.45 ± 0.07 g/kg). At the EK stage, the N content in the 0–10 cm soil layer further

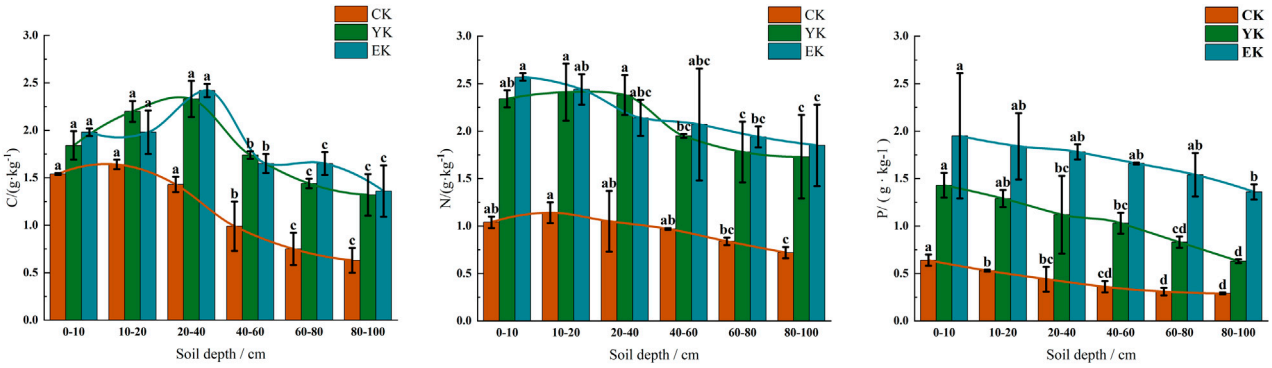

FIGURE 3
The contents of C, N and P in soil under different planting years of Tumd Left Banner *Pennisetum giganteum*. **(A)** C; **(B)** N; **(C)** P. Note: Different letters indicate significant differences at $P < 0.05$.

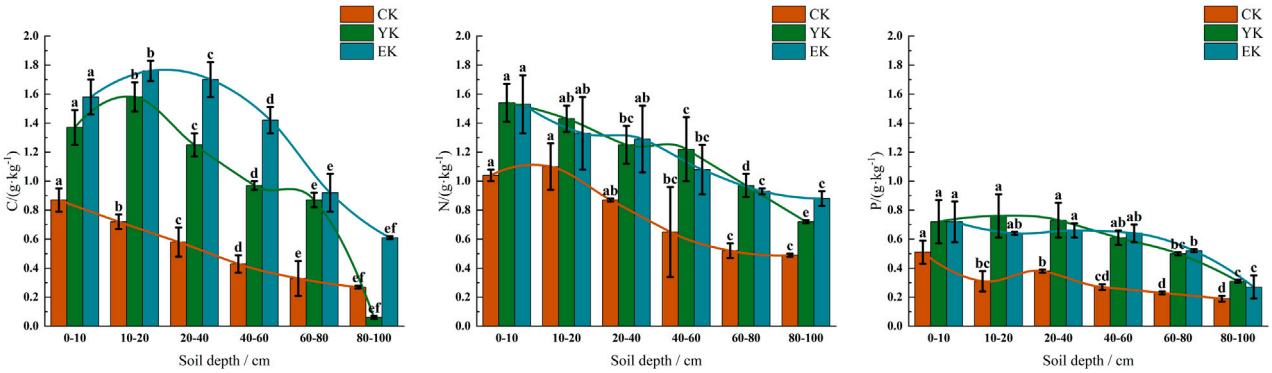

FIGURE 4
Contents of C, N and P in soil under different planting years of Ulan Buh Desert *Pennisetum giganteum*. **(A)** C; **(B)** N; **(C)** P. Note: Different letters indicate significant differences at $P < 0.05$.

increased to 1.74 ± 0.25 g/kg (95% CI: 1.35–2.15 g/kg), but the increase in the deep layer (80–100 cm) was small (0.66 ± 0.13 g/kg), indicating that N accumulation was mainly concentrated in the surface layer.

Pennisetum giganteum planting significantly increased soil P content (Figure 2C). In the CK stage, the P content in the 0–10 cm soil layer was 1.27 ± 0.27 g/kg (95% CI: 0.84–1.70 g/kg), and the deep layer (80–100 cm) was significantly reduced to 0.31 ± 0.05 g/kg ($P <$ 0.05). In the YK stage, the P content in the surface layer reached 1.85 ± 0.15 g/kg (95% CI: 1.62–2.09 g/kg, $P < 0.05$), and the P content in each soil layer increased significantly. In the EK stage, P content remained stable, 1.84 ± 0.17 g/kg (95% CI: 1.57–2.12 g/kg) in the 0–10 cm soil layer, but the increase in the deep layer (80–100 cm) slowed down (1.21 ± 0.24 g/kg), indicating that the improvement effect of P decreased with depth.

3.1.2 Changes in soil C, N, and P contents under *Pennisetum giganteum* of different planting years in Tumed Left Banner

In the Tumd Left Banner test area, *Pennisetum giganteum* planting significantly affected the content of soil C, N and P, and the response of different soil depths was different. As shown in Figure 3A, before planting (CK), soil C content decreased significantly with the increase of soil depth ($P < 0.05$), which was 1.54 ± 0.01 g/kg (95% CI: 1.53–1.57 g/kg) in 0–10 cm soil layer and 0.63 ± 0.13 g/kg (95% CI: 0.42–0.85 g/kg) in 80–100 cm soil layer. After the first year of harvest (YK), the C content of each soil layer increased significantly ($P < 0.05$), the 0–10 cm soil layer increased to 1.84 ± 0.15 g/kg (95% CI: 1.59–2.09 g/kg), and the 20–40 cm soil layer reached the peak (2.33 ± 0.19 g/kg, 95% CI: 2.01–2.65 g/kg). After harvest in the second year (EK), the C content in the surface layer (0–10 cm) further increased to 1.98 ± 0.04 g/kg (95% CI: 1.91–2.05 g/kg), while that in the deep layer (80–100 cm) decreased slightly (1.36 ± 0.27 g/kg, 95% CI: 0.93–1.79 g/kg), but was still significantly higher than that of CK ($P < 0.05$).

It can be seen from Figure 3B that in CK stage, N content decreased with depth (0–10 cm: 1.04 ± 0.06 g/kg, 95% CI: 0.94–1.14 g/kg; 80–100 cm: 0.72 ± 0.06 g/kg, 95% CI: 0.61–0.83 g/kg). In the YK stage, N content increased significantly ($P < 0.05$), reaching 2.34 ± 0.09 g/kg (95% CI: 2.18–2.50 g/kg) in the 0–10 cm soil layer and 2.41 ± 0.30 g/kg (95% CI: 1.93–2.90 g/kg) in the 10–20 cm soil layer. In the EK stage,

TABLE 1 Soil stoichiometry under different planting years of *Pennisetum giganteum* in Naiman Banner.

Soil stoichiometric ratio	Soil depth/cm	CK	YK	EK
C/N	0–10	0.97 ± 0.17c	1.27 ± 0.18b	1.02 ± 0.11c
	10–20	1.25 ± 0.28bc	1.19 ± 0.12b	1.40 ± 0.05c
	20–40	1.59 ± 0.32ab	1.71 ± 0.06a	1.49 ± 0.17bc
	40–60	1.79 ± 0.28a	1.80 ± 0.30a	2.12 ± 0.51a
	60–80	1.56 ± 0.34ab	1.83 ± 0.24a	2.00 ± 0.37ab
	80–100	1.56 ± 0.35ab	1.88 ± 0.27a	1.99 ± 0.52ab
C/P	0–10	1.14 ± 0.22c	1.11 ± 0.08b	0.97 ± 0.16c
	10–20	1.49 ± 0.11c	1.09 ± 0.18b	1.37 ± 0.09ab
	20–40	2.19 ± 0.44b	1.54 ± 0.04a	1.30 ± 0.04ab
	40–60	2.47 ± 0.50ab	1.36 ± 0.19ab	1.40 ± 0.22a
	60–80	2.34 ± 0.17b	1.36 ± 0.31ab	1.17 ± 0.09bc
	80–100	3.03 ± 0.62a	1.20 ± 0.23b	1.06 ± 0.12c
N/P	0–10	1.22 ± 0.43b	0.88 ± 0.07a	0.95 ± 0.16ab
	10–20	1.22 ± 0.21b	0.92 ± 0.18a	0.98 ± 0.11a
	20–40	1.44 ± 0.44b	0.90 ± 0.05a	0.87 ± 0.08ab
	40–60	1.39 ± 0.28b	0.76 ± 0.077ab	0.69 ± 0.24bc
	60–80	1.53 ± 0.20ab	0.77 ± 0.29ab	0.59 ± 0.09c
	80–100	1.96 ± 0.29a	0.63 ± 0.03b	0.58 ± 0.25c

the surface N content continued to increase to 2.57 ± 0.04 g/kg (95% CI: 2.51–2.63 g/kg), but the content of some deep layers (80–100 cm) fluctuated slightly (1.85 ± 0.43 g/kg, 95% CI: 1.15–2.55 g/kg), which was still significantly higher than that of CK ($P < 0.05$).

As shown in Figure 3C, in the CK stage, P content decreased significantly from the surface layer (0–10 cm: 0.64 ± 0.06 g/kg, 95% CI: 0.55–0.75 g/kg) to the deep layer (80–100 cm: 0.29 ± 0.01 g/kg, 95% CI: 0.27–0.32 g/kg) ($P < 0.05$). In the YK stage, the P content increased significantly ($P < 0.05$), reaching 1.43 ± 0.13 g/kg (95% CI: 1.23–1.64 g/kg) in the 0–10 cm soil layer. In the EK stage, the P content increased further, with 1.95 ± 0.66 g/kg (95% CI: 0.90–3.01 g/kg) in the 0–10 cm soil layer, but the increase in the deep layer (80–100 cm) slowed down (1.36 ± 0.08 g/kg, 95% CI: 1.24–1.50 g/kg).

3.1.3 Changes in C, N, and P contents in soil under different planting years of *Pennisetum giganteum* in Ulan Buh Desert

In the Ulan Buh Desert experimental area, *Pennisetum giganteum* planting significantly affected the content of soil C, N and P, and the response of different soil depths was significantly different. As shown in Figure 4A, before planting (CK), soil C content decreased significantly with the increase of soil depth ($P < 0.05$), 0.87 ± 0.08 g/kg (95% CI: 0.74–1.01 g/kg) in 0–10 cm soil layer and 0.27 ± 0.01 g/kg (95% CI: 0.26–0.28 g/kg) in 80–100 cm soil layer. After the first year of harvest (YK), the C content in each soil layer increased significantly ($P < 0.05$), and the 10–20 cm soil layer reached the peak (1.58 ± 0.10 g/kg, 95% CI: 1.42–1.76 g/kg), while the 80–100 cm soil layer had the lowest content due to weak root activity (0.06 ± 0.017 g/kg, 95% CI: 0.04–0.09 g/kg). After the second year of harvest (EK), the C content in the surface layer (0–10 cm) further increased to 1.58 ± 0.12 g/kg (95% CI: 1.39–1.78 g/kg), and the deep layer (80–100 cm) significantly recovered to 0.61 ± 0.01 g/kg (95% CI: 0.58–0.64 g/kg), but it was still lower than the shallow level ($P < 0.05$).

As shown in Figure 4B, in the CK stage, the N content was the highest in the 0–10 cm soil layer (1.04 ± 0.04 g/kg, 95% CI: 0.96–1.12 g/kg), and decreased with depth to 80–100 cm (0.49 ± 0.01 g/kg, 95% CI: 0.47–0.51 g/kg). In the YK stage, N content increased significantly ($P < 0.05$), reaching 1.54 ± 0.13 g/kg (95% CI: 1.33–1.75 g/kg) in the 0–10 cm soil layer, but the increase in the deep layer (80–100 cm) was small (0.72 ± 0.01 g/kg, 95% CI: 0.70–0.75 g/kg). At the EK stage, the surface N content remained stable (1.53 ± 0.20 g/kg, 95% CI: 1.21–1.85 g/kg), while the deep layer (80–100 cm) increased significantly to 0.88 ± 0.05 g/kg (95% CI: 0.79–0.97 g/kg), indicating that the improvement of *Pennisetum giganteum* on deep soil was lagging.

As shown in Figure 4C, in the CK stage, P content decreased significantly from the surface layer (0–10 cm: 0.51 ± 0.08 g/kg, 95% CI: 0.38–0.64 g/kg) to the deep layer (80–100 cm: 0.19 ± 0.02 g/kg, 95% CI: 0.16–0.23 g/kg) ($P < 0.05$). At YK stage, P content increased significantly in 0–40 cm soil layer ($P < 0.05$), and reached 0.76 ± 0.15 g/kg (95% CI: 0.53–1.01 g/kg) in 10–20 cm soil layer. In the EK stage, P content remained stable in the surface layer (0–10 cm) (0.72 ± 0.14 g/kg, 95% CI: 0.49–0.96 g/kg), but decreased to 0.27 ± 0.08 g/kg (95% CI: 0.13–0.41 g/kg) in the deep layer (80–100 cm).

TABLE 2 Soil stoichiometric ratio of *Pennisetum giganteum* under different planting years in Tumed Left Banner.

Soil stoichiometric ratio	Soil depth/cm	CK	YK	EK
C:N	0–10	1.48 ± 0.08a	0.78 ± 0.06b	0.77 ± 0.02b
	10–20	1.45 ± 0.16a	0.92 ± 0.16ab	0.82 ± 0.12b
	20–40	1.45 ± 0.43a	0.98 ± 0.10a	1.14 ± 0.08a
	40–60	1.02 ± 0.28b	0.88 ± 0.03ab	0.85 ± 0.28b
	60–80	0.88 ± 0.15b	0.83 ± 0.15ab	0.85 ± 0.12b
	80–100	0.88 ± 0.17b	0.77 ± 0.07b	0.75 ± 0.14b
C:P	0–10	2.40 ± 0.20ab	1.28 ± 0.12c	1.10 ± 0.35a
	10–20	3.09 ± 0.12ab	1.71 ± 0.16abc	1.12 ± 0.32a
	20–40	3.37 ± 0.73a	2.22 ± 0.57a	1.36 ± 0.10a
	40–60	2.84 ± 1.17ab	1.69 ± 0.15bc	0.99 ± 0.06a
	60–80	2.43 ± 0.63ab	1.75 ± 0.19abc	1.10 ± 0.27a
	80–100	2.16 ± 0.51b	2.10 ± 0.43ab	1.00 ± 0.25a
N:P	0–10	1.62 ± 0.18b	1.64 ± 0.22b	1.44 ± 0.50a
	10–20	2.15 ± 0.27ab	1.87 ± 0.15b	1.35 ± 0.22a
	20–40	2.53 ± 1.21ab	2.31 ± 0.70ab	1.20 ± 0.16a
	40–60	2.74 ± 0.50a	1.91 ± 0.23b	1.24 ± 0.36a
	60–80	2.72 ± 0.45a	2.14 ± 0.36ab	1.27 ± 0.13a
	80–100	2.44 ± 0.34ab	2.76 ± 0.79a	1.36 ± 0.34a

3.2 Soil stoichiometric ratio of *Pennisetum giganteum* under different planting years in inner Mongolia

3.2.1 Changes in soil stoichiometric ratio under different planting years of *Pennisetum giganteum* in Naiman Banner

As shown in Table 1, there are differences in the variation of C/N ratio across each soil layer. Some soil layers showed an upward trend after harvest in the first year, but decreased after harvest in the second year, while others showed continuous growth. Specifically, the C/N ratio in the 0–10 cm soil layer increased from the initial 0.97 to 1.27 (an increase of 0.30) after the first year of harvest, but fell back to 1.02 (a decrease of 0.25) after the second year of harvest. The C/N ratio of the 10–20 cm soil layer decreased slightly from 1.25 to 1.19 (a decrease of 0.06), and then increased to 1.40 (an increase of 0.21) in the second year. The C/N ratio of the 20–40 cm soil layer increased from 1.59 to 1.71 (an increase of 0.12), but decreased to 1.49 (a decrease of 0.22) in the second year. The C/N ratio of the 40–60 cm soil layer increased slightly from 1.79 to 1.80 (an increase of 0.01), and further increased to 2.12 (an increase of 0.32) in the second year. The C/N ratio of the 60–80 cm soil layer increased from 1.56 to 1.83 (an increase of 0.27) in the first year, and continued to increase to 2.00 (an increase of 0.17) in the second year. The C/N ratio of the 80–100 cm soil layer increased from 1.56 to 1.88 (an increase of 0.32) in the first year, and further increased to 1.99 (an increase of 0.11) in the second year.

The C/P ratio generally showed a downward trend in each soil layer, particularly in the deep soil. The C/P ratio in the 0–10 cm soil layer decreased from 1.14 at the beginning to 1.11 after the first year of harvest (a decrease of 0.03), and further decreased to 0.97 (a decrease of 0.14) in the second year. The C/P ratio of the 10–20 cm soil layer decreased from 1.49 to 1.09 (a decrease of 0.40), and increased to 1.37 (an increase of 0.28) in the second year. The C/P ratio of the 20–40 cm soil layer decreased from 2.19 to 1.54 (a decrease of 0.65) in the first year, and continued to decrease to 1.30 (a decrease of 0.24) in the second year. The C/P ratio of the 40–60 cm soil layer decreased significantly from 2.47 to 1.36 (a decrease of 1.11), and increased slightly to 1.40 (an increase of 0.04) in the second year. The C/P ratio of the 60–80 cm soil layer decreased from 2.34 to 1.36 (a decrease of 0.98) in the first year, and continued to decrease to 1.17 (a decrease of 0.19) in the second year. The C/P ratio of the 80–100 cm soil layer decreased significantly from 3.03 to 1.20 (1.83), and further decreased to 1.06 (0.14) in the second year.

The N/P ratio generally showed a downward trend in each soil layer. The N/P ratio of the 0–10 cm soil layer decreased from 1.22 at the beginning to 0.88 after the first year of harvest (a decrease of 0.34), and increased slightly to 0.95 in the second year (an increase of 0.07). The N/P ratio in the 10–20 cm soil layer decreased from 1.22 to 0.92 (a decrease of 0.30), and increased to 0.98 (an increase of 0.06) in the second year. The N/P ratio in the 20–40 cm soil layer decreased from 1.44 to 0.90 (a decrease of 0.54), and continued to decrease to 0.87 (a decrease of 0.03) in the second year. The N/P ratio of the 40–60 cm soil layer decreased significantly from 1.39 to 0.76 (a decrease of 0.63), and further decreased to 0.69 (a decrease of

TABLE 3 Soil stoichiometric ratio under different planting years of *Pennisetum giganteum* in Ulan Buh Desert.

Soil stoichiometric ratio	Soil depth/cm	CK	YK	EK
C:N	0–10	0.84 ± 0.08a	0.89 ± 0.13bc	1.04 ± 0.11b
	10–20	0.67 ± 0.10a	1.11 ± 0.09a	1.35 ± 0.18a
	20–40	0.66 ± 0.11a	1.01 ± 0.14ab	1.34 ± 0.23a
	40–60	0.79 ± 0.44a	0.82 ± 0.15c	1.33 ± 0.18a
	60–80	0.64 ± 0.30a	0.90 ± 0.10bc	0.99 ± 0.14b
	80–100	0.55 ± 0.02a	0.08 ± 0.02d	0.69 ± 0.05c
C:P	0–10	1.73 ± 0.36b	1.98 ± 0.53ab	2.24 ± 0.37ab
	10–20	2.36 ± 0.53a	2.12 ± 0.39a	2.73 ± 0.14a
	20–40	1.52 ± 0.28b	1.73 ± 0.25ab	2.57 ± 0.28a
	40–60	1.62 ± 0.35b	1.59 ± 0.16b	2.22 ± 0.19ab
	60–80	1.40 ± 0.49b	1.73 ± 0.12ab	1.77 ± 0.28b
	80–100	1.40 ± 0.17b	0.20 ± 0.05c	2.46 ± 0.96ab
N:P	0–10	2.05 ± 0.24b	2.25 ± 0.78a	2.14 ± 0.23b
	10–20	3.65 ± 1.13a	1.92 ± 0.41a	2.06 ± 0.38b
	20–40	2.30 ± 0.08b	1.76 ± 0.53a	1.94 ± 0.31b
	40–60	2.45 ± 1.24b	2.00 ± 0.41a	1.67 ± 0.10b
	60–80	2.28 ± 0.38b	1.93 ± 0.10a	1.77 ± 0.09b
	80–100	2.55 ± 0.19b	2.32 ± 0.13a	3.60 ± 1.52a

0.07) in the second year. The N/P ratio in the 60–80 cm soil layer decreased from 1.53 to 0.77 (a decrease of 0.76) in the first year, and continued to decrease to 0.59 (a decrease of 0.18) in the second year. The N/P ratio in the 80–100 cm soil layer decreased significantly from 1.96 to 0.63 (1.33) in the first year, and decreased slightly to 0.58 (0.05) in the second year.

3.2.2 Soil stoichiometric ratio changes under different planting years of *Pennisetum giganteum* in Tumd Left Banner

Table 2 reveals that the C/N generally decreases with depth in different soil layers. In the 0–10 cm soil layer, the C/N ratio decreased significantly from 1.48 before planting to 0.78 (a decrease of 0.70) after the first year of harvest, and slightly decreased to 0.77 (a decrease of 0.01) in the second year. In the 10–20 cm soil layer, the C/N ratio decreased from 1.45 to 0.92 (a decrease of 0.53), and continued to decrease to 0.82 (a further decrease of 0.10) in the second year. In the 20–40 cm soil layer, the C/N ratio decreased from 1.45 to 0.98 (a decrease of 0.47), and increased to 1.14 (an increase of 0.16) in the second year. In the 40–60 cm soil layer, the C/N ratio decreased from 1.02 to 0.88, a 0.14 decrease, and continued to decrease to 0.85, a further 0.03 decrease, in the second year. In the 60–80 cm soil layer, the C/N ratio decreased from 0.88 to 0.83 (a decrease of 0.05), and increased slightly to 0.85 (an increase of 0.02) in the second year. In the 80–100 cm soil layer, the C/N ratio decreased from 0.88 to 0.77 (a decrease of 0.11), and continued to decrease to 0.75 (a further decrease of 0.02) in the second year.

The C/P generally exhibited a downward trend across different soil layers. In the 0–10 cm soil layer, the C/P ratio decreased from 2.40 before planting to 1.28 (a decrease of 1.12) after harvest in the first year, and continued to decrease to 1.10 (a further decrease of 0.18) in the second year. In the 10–20 cm soil layer, the C/P ratio decreased from 3.09 to 1.71 (a decrease of 1.38), and further decreased to 1.12 (a decrease of 0.59) in the second year. In the 20–40 cm soil layer, the C/P ratio decreased from 3.37 to 2.22 (a decrease of 1.15), and continued to decrease to 1.36 (a decrease of 0.86) in the second year. In the 40–60 cm soil layer, the C/P ratio decreased from 2.84 to 1.69 (a decrease of 1.15), and further decreased to 0.99 (a decrease of 0.70) in the second year. In the 60–80 cm soil layer, the C/P ratio decreased from 2.43 to 1.75 (a decrease of 0.68), and continued to decrease to 1.10 (a further decrease of 0.65) in the second year. In the 80–100 cm soil layer, the C/P ratio decreased slightly from 2.16 to 2.10 (a decrease of 0.06), and decreased significantly to 1.00 (a decrease of 1.10) in the second year.

The change trend of nitrogen and phosphorus ratio (N/P) in different soil layers is more complex. In the 0–10 cm soil layer, the N/P ratio increased slightly from 1.62 before planting to 1.64 after harvest in the first year (an increase of 0.02), and decreased to 1.44 in the second year (a decrease of 0.20). In the 10–20 cm soil layer, the N/P ratio decreased from 2.15 to 1.87 (a decrease of 0.28), and continued to decrease to 1.35 (a further decrease of 0.52) in the second year. In the 20–40 cm soil layer, the N/P ratio decreased from 2.53 to 2.31 (a decrease of 0.22), and decreased significantly to 1.20 (a decrease of 1.11) in the second year. In the 40–60 cm soil layer, the

N/P ratio decreased from 2.74 to 1.91 (a decrease of 0.83), and continued to decrease to 1.24 (a further decrease of 0.67) in the second year. In the 60–80 cm soil layer, the N/P ratio decreased from 2.72 to 2.14 (a decrease of 0.58), and further decreased to 1.27 (a decrease of 0.87) in the second year. In the 80–100 cm soil layer, the N/P ratio increased from 2.44 to 2.76 (an increase of 0.32), and decreased significantly to 1.36 (a decrease of 1.40) in the second year.

3.2.3 Changes in soil stoichiometric ratio under different planting years of *Pennisetum giganteum* in Ulan Buh Desert

As shown in Table 3, the C/N generally exhibited an increasing trend across different soil layers. In the 0–10 cm soil layer, the C/N ratio increased from 0.84 before planting to 0.89 after the first year of harvest (an increase of 0.05), and continued to increase to 1.04 (an increase of 0.15) in the second year. In the 10–20 cm soil layer, the C/N ratio significantly increased from 0.67 to 1.11 (a 0.44 increase), and further increased to 1.35 (a 0.24 increase) in the second year. In the 20–40 cm soil layer, the C/N ratio increased from 0.66 to 1.01 (an increase of 0.35), and continued to increase to 1.34 (a further increase of 0.33) in the second year. In the 40–60 cm soil layer, the C/N ratio increased slightly from 0.79 to 0.82 (an increase of 0.03), and increased significantly to 1.33 (an increase of 0.51) in the second year. In the 60–80 cm soil layer, the C/N ratio increased from 0.64 to 0.90 (an increase of 0.26), and continued to increase to 0.99 (an additional increase of 0.09) in the second year. In the 80–100 cm soil layer, the C/N ratio decreased significantly from 0.55 to 0.08 (a decrease of 0.47), and increased to 0.69 (an increase of 0.61) in the second year.

The C/P fluctuated across different soil layers. In the 0–10 cm soil layer, the C/P ratio increased from 1.73 before planting to 1.98 after harvest in the first year (an increase of 0.25), and continued to increase to 2.24 in the second year (an increase of 0.26). In the 10–20 cm soil layer, the C/P ratio decreased from 2.36 to 2.12 (a decrease of 0.24), and increased to 2.73 (an increase of 0.61) in the second year. In the 20–40 cm soil layer, the C/P ratio increased from 1.52 to 1.73 (an increase of 0.21), and significantly increased to 2.57 (an increase of 0.84) in the second year. In the 40–60 cm soil layer, the C/P ratio decreased slightly from 1.62 to 1.59 (a decrease of 0.03), and increased significantly to 2.22 (an increase of 0.63) in the second year. In the 60–80 cm soil layer, the C/P ratio increased from 1.40 to 1.73, an increase of 0.33, and continued to increase to 1.77, a further increase of 0.04, in the second year. In the 80–100 cm soil layer, the C/P ratio decreased significantly from 1.40 to 0.20 (a decrease of 1.20), and increased significantly to 2.46 (an increase of 2.26) in the second year.

The N/P ratio fluctuated in different soil layers. In the 0–10 cm soil layer, the N/P ratio increased from 2.05 before planting to 2.25 after harvest in the first year (an increase of 0.20), and decreased to 2.14 in the second year (a decrease of 0.11). In the 10–20 cm soil layer, the N/P ratio decreased significantly from 3.65 to 1.92 (a 1.73 decrease), and increased to 2.06 (+0.14) in the second year. In the 20–40 cm soil layer, the N/P ratio decreased from 2.30 to 1.76 (a 0.54 decrease), and increased to 1.94 (a 0.18 increase) in the second year. In the 40–60 cm soil layer, the N/P ratio decreased from 2.45 to 2.00 (a decrease of 0.45), and continued to decrease to 1.67 (a further decrease of 0.33) in the second year. In the 60–80 cm soil layer, the N/P ratio decreased from 2.28 to 1.93 (a decrease of 0.35), and continued to decrease to 1.77 (a further decrease of 0.16) in the second year. In the 80–100 cm soil layer, the N/P ratio decreased from 2.55 to 2.32 (a decrease of 0.23), and increased significantly to 3.60 (an increase of 1.28) in the second year.

3.3 Correlation of *Pennisetum giganteum* planting years with soil C, N, P and their stoichiometric ratios

3.3.1 Correlation between planting years of Naiman Banner *Pennisetum giganteum* and soil C, N, P and their stoichiometric ratios

Figure 5 illustrates that there is a positive correlation between the number of cultivation years and the contents of soil carbon (C), nitrogen (N), and phosphorus (P), with these correlations reaching statistical significance at various levels. This indicates that as the cultivation period of *Pennisetum giganteum* increases, the contents of C, N, and P in the soil also increase. The extensive root system of *Pennisetum giganteum* continuously grows and decomposes in the soil, supplying additional organic matter that promotes the accumulation of soil nutrients, thereby progressively enhancing the contents of C, N, and P. The relationship between the C/N ratio and cultivation age is more complex. In some cases, the C/N ratio initially increases and then decreases, reflecting that during the early stages of cultivation, the growth of *Pennisetum giganteum* leads to a relative accumulation of C in the soil, which elevates the C/N ratio; however, as cultivation years increase, enhanced microbial decomposition of C or a faster rate of N accumulation causes the C/N ratio to decline. In contrast, the C/P and N/P ratios exhibit a negative correlation with cultivation years. This suggests that as the years of cultivation increase, the relative proportions of C to P and N to P in the soil undergo continuous changes, with either an increase in the relative content of P or a decrease in the relative contents of C and N. This may be due to shifts in the absorption and utilization patterns of P by *Pennisetum giganteum* over time, or alterations in the release and migration processes of P in the soil, ultimately leading to decreases in both the C/P and N/P ratios.

3.3.2 Correlation between Tumd Left Banner *Pennisetum giganteum* planting years and soil C, N, P and their stoichiometric ratios

It can be seen from Figure 6 that there is an extremely significant positive correlation between the duration of cultivation and soil C content ($p \leq 0.001$). As the cultivation period increases, the soil C content rises, indicating that the cultivation of *Pennisetum giganteum* has a marked facilitative effect on soil C accumulation. For instance, in the 0–10 cm soil layer, the C content increased from 1.54 ± 0.01 g/kg before cultivation (CK) to 1.98 ± 0.04 g/kg after the second-year harvest (EK). This increase is attributed to the continuous input of organic substances into the soil via root exudates and plant residues from *Pennisetum giganteum*, which are decomposed and transformed by microorganisms, thereby enhancing the soil's C reserves. Furthermore, there is a significant positive correlation between the cultivation period and soil N content ($^{*}p \leq 0.01$, $p \leq 0.05$). The longer *Pennisetum giganteum* is grown, the higher the soil N content becomes. For example, in the 0–10 cm soil layer, the soil N

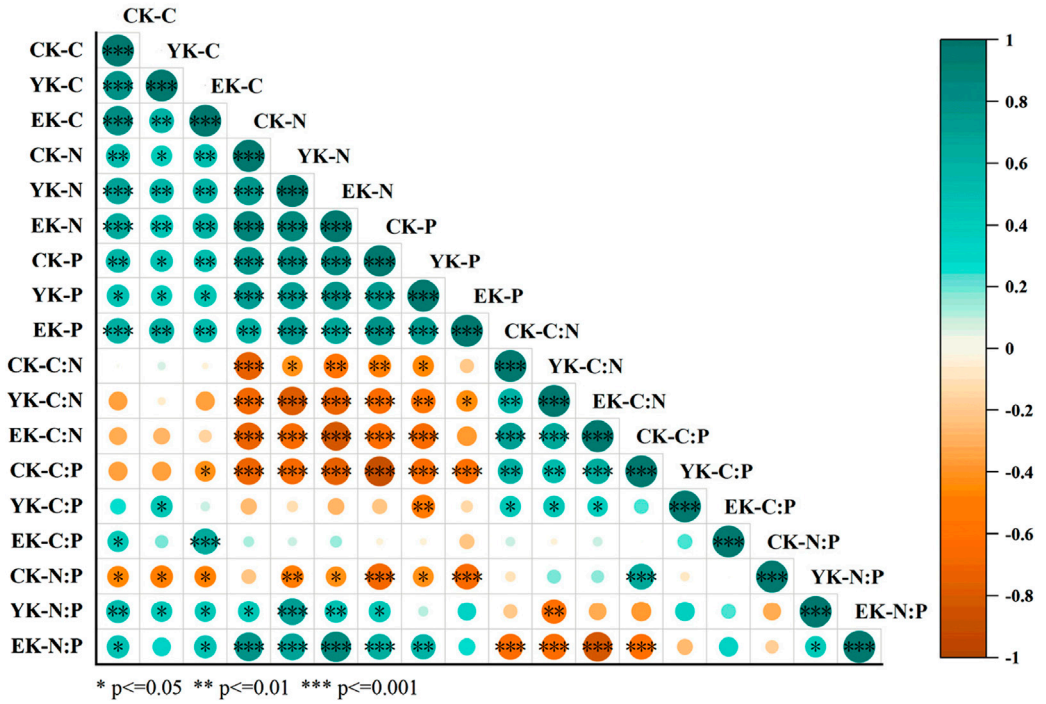

FIGURE 5
Correlation of Naiman Banner *Pennisetum giganteum* planting years-soil depth-soil C, N, P and their stoichiometric ratios.

content increased from 1.04 ± 0.06 g/kg in the CK stage to 2.57 ± 0.04 g/kg in the EK stage. This increase may be due to the nitrogen-fixing ability of *Pennisetum giganteum* and its capacity to improve the soil environment, thereby promoting the activity of nitrogen-fixing microorganisms in the soil. Additionally, there is a positive correlation between the duration of cultivation and soil P content ($p \leq 0.05$). With the passage of time, the soil P content gradually increases. For instance, in the 0–10 cm soil layer, the soil P content rose from 0.64 ± 0.06 g/kg in the CK stage to 1.95 ± 0.66 g/kg in the EK stage. This is because *Pennisetum giganteum* absorbs and accumulates P during its growth, and after its death and decomposition, the P is returned to the soil, thereby enhancing the soil P content.

The planting duration is significantly negatively correlated with the C/N ratio ($p \leq 0.05$). As the planting duration increases, the C/N ratio decreases, indicating that the accumulation rate of nitrogen in the soil is relatively faster than that of organic carbon, thereby enhancing the decomposition of soil organic matter. For example, in the 0–10 cm soil layer, the C/N ratio declined from 1.48 before planting to 0.77 after the second-year harvest, demonstrating that the cultivation of *Pennisetum giganteum* improved the nitrogen supply in the soil. This improvement favorably facilitates microbial decomposition and transformation of organic matter, thereby increasing the effectiveness of soil nutrients.

Additionally, the planting duration is extremely significantly negatively correlated with the C/P ratio ($p \leq 0.001$). With increased planting time, the C/P ratio sharply decreases, indicating a relatively more pronounced accumulation of phosphorus in the soil compared to organic carbon. In the 10–20 cm soil layer, the C/P ratio dropped from 3.09 before planting to 1.12 after the second-year harvest, reflecting that the cultivation of *Pennisetum giganteum* markedly increased soil phosphorus content. This alteration in the relative proportions of carbon and phosphorus in the soil has important implications for the soil phosphorus cycle and plant phosphorus utilization.

Moreover, the planting duration is also significantly negatively correlated with the N/P ratio ($^{*}p \leq 0.01$). As the planting duration increases, the N/P ratio decreases, indicating a shift in the relative contents of nitrogen and phosphorus in the soil, with phosphorus accumulating at a faster rate than nitrogen. In the 20–40 cm soil layer, the N/P ratio declined from 2.53 before planting to 1.20 after the second-year harvest, thereby affecting the balance of nitrogen and phosphorus uptake by plants and ultimately influencing plant growth and the functioning of the soil ecosystem.

3.3.3 Correlation between planting years of Ulan Buh Desert *Pennisetum giganteum* and soil C, N, P and their stoichiometric ratios

As shown in Figure 7, soil carbon content is highly significantly and positively correlated with the duration of *Pennisetum giganteum* cultivation ($p \leq 0.001$), indicating that soil carbon accumulates substantially as cultivation time increases. For example, the carbon content in the 0–10 cm soil layer increased from 0.87 ± 0.08 g/kg before planting to 1.58 ± 0.12 g/kg after the second harvest. Moreover, soil nitrogen content demonstrated a significant positive correlation with cultivation duration ($p \leq 0.01$), suggesting that longer cultivation periods lead to greater nitrogen accumulation; for instance, nitrogen content in deeper soil layers gradually increased during the cultivation process. In contrast, soil phosphorus content showed a weak correlation with cultivation duration, with variations

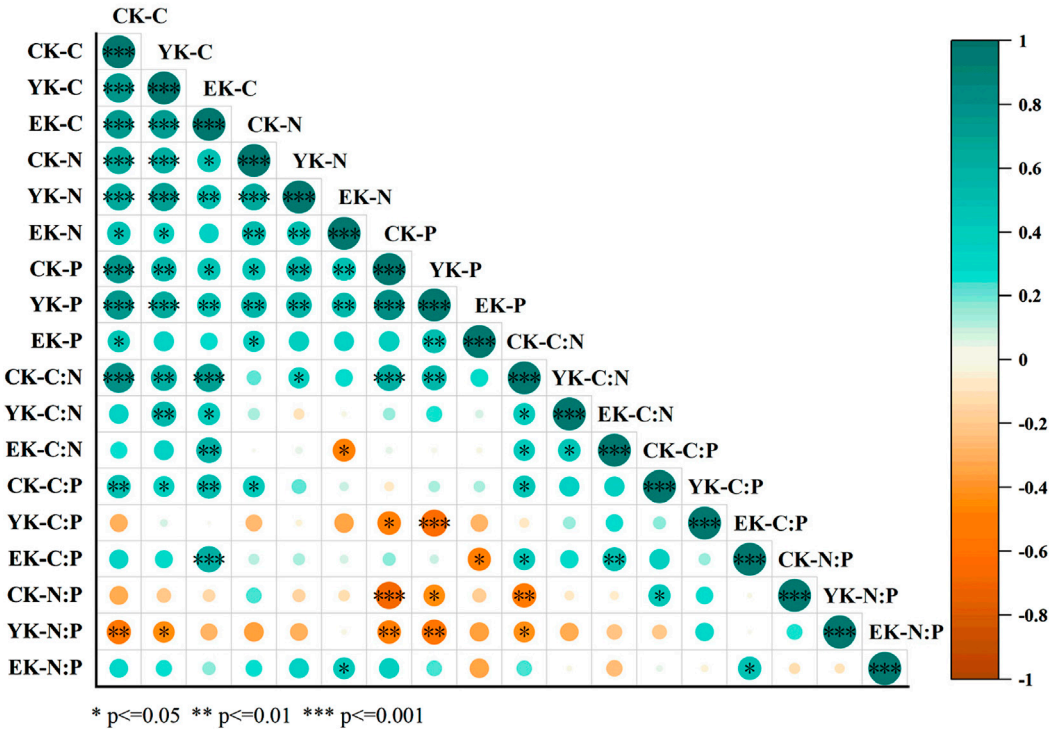

FIGURE 6
Tumd Left Banner *Pennisetum giganteum* planting years-soil depth-soil C, N, P and their stoichiometric correlations.

observed in the topsoil and at certain stages, yet overall the association remained tenuous—exemplified by fluctuations in topsoil phosphorus content across different cultivation stages and complex changes at greater depths.

The C/N ratio was significantly and positively correlated with cultivation duration ($p \leq 0.05$), reflecting that as cultivation time increases, the rate of carbon accumulation in the soil exceeds that of nitrogen, thereby altering soil organic matter mineralization and nutrient cycling, with a general increase in the C/N ratio across different soil layers. The correlation between the C/P ratio and cultivation duration was complex; although no clear unified trend emerged, variations across different stages and soil depths were evident. This suggests that the capacity of soil microorganisms to mineralize organic matter and release phosphorus is influenced by the duration of cultivation, with responses varying across soil depths. Similarly, the N/P ratio exhibited a relatively complex correlation with cultivation duration, fluctuating across different soil layers, which indicates that the relative abundances of nitrogen and phosphorus in the soil are affected by cultivation duration, thereby altering the nutrient supply to plants and the conditions of growth limitation.

4 Discussion

Studies on soil element dynamics have revealed that, following the cultivation of *Pennisetum giganteum* in the experimental areas of Naiman Banner, Tumd Left Banner, and Ulan Buh Desert, the overall contents of soil carbon (C), nitrogen (N), and phosphorus (P) tend to increase (Liu, 2019). This trend is primarily attributable to the well-developed root system of *Pennisetum giganteum*, whose root exudates and litter provide an abundant source of organic matter, thereby promoting the growth and activity of soil microorganisms and consequently accelerating the accumulation of soil nutrients (Zhou, 2019). In certain soil layers, nutrient content fluctuations observed after the second-year harvest may result from substantial nutrient uptake during the later growth stages of *Pennisetum giganteum*, as well as seasonal influences on soil microbial activity that alter the dynamic balance between nutrient release and immobilization (Yang, 2019).

Soil stoichiometric ratios reflect the relative proportions and interrelationships of elements in the soil and serve as critical indicators of soil ecosystem functions. In Naiman Banner, the C/N ratio in some soil layers initially increased and then decreased, while in others it continuously rose. This pattern suggests that the early stages of *Pennisetum giganteu*m cultivation may have promoted the accumulation of soil organic matter, followed by an enhancement of decomposition processes in later stages; meanwhile, both the C/P and N/P ratios generally declined, indicating an enhanced mineralization of phosphorus by soil microorganisms and an increased availability of soil phosphorus (Bi, 2019). In Tumd Left Banner, the C/N and C/P ratios generally decreased, and the N/P ratio exhibited complex variations, reflecting that soil nutrient cycling was significantly influenced by the cultivation of *Pennisetum giganteum*, with the transformation relationships among C, N, and P changing over the years of cultivation (Mei, 2018). In the Ulan Buh Desert, the C/N ratio generally increased while the C/P and N/P ratios fluctuated, a

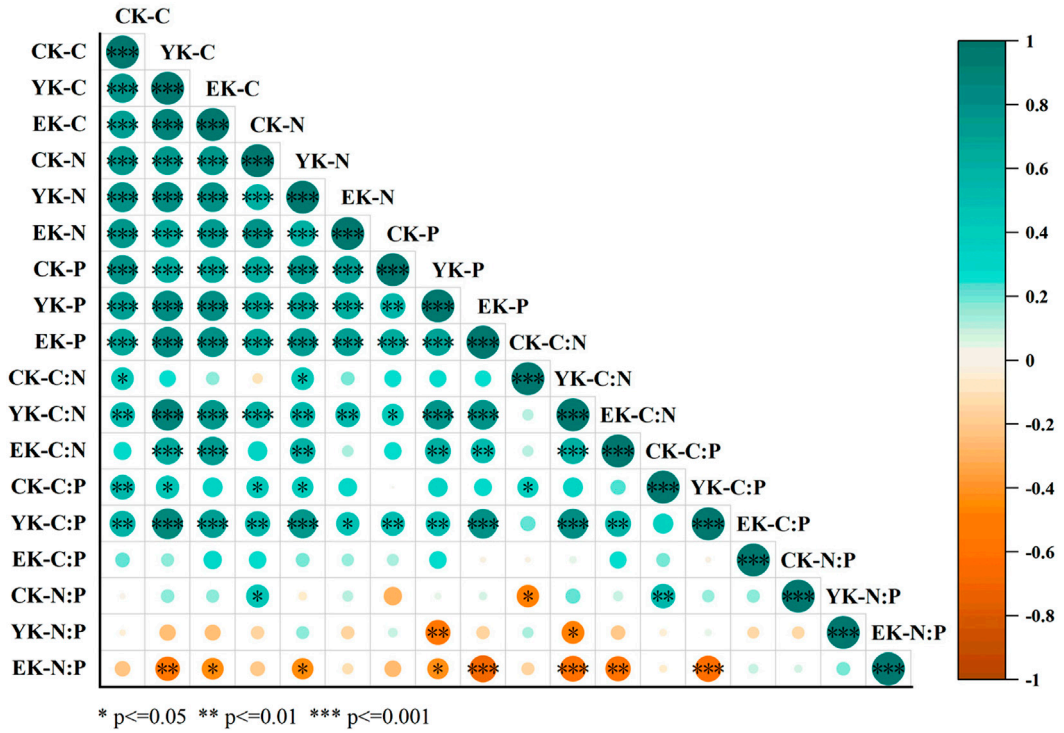

FIGURE 7
Correlation of Ulan Buh Desert *Pennisetum giganteum* planting years-soil depth-soil C, N, P and their stoichiometric ratios.

pattern closely related to the unique soil texture and moisture conditions characteristic of desert regions. The cultivation of *Pennisetum giganteum* improved soil structure, thereby affecting the retention and release of soil nutrients (Wu, 2018).

Regional distribution differences have had a significant impact on the soil chemical stoichiometry under the cultivation of *Pennisetum giganteum*. Naiman Banner experiences a temperate semi-arid climate, Tumd Left Banner a temperate continental climate, and Ulan Buh Desert a temperate desert climate; these varying hydrological conditions directly affect the growth rate, biomass, and the structure and activity of soil microbial communities associated with *Pennisetum giganteum* (Huang, 2011). For instance, under the arid and low-precipitation conditions in Ulan Buh Desert, the growth of *Pennisetum giganteum* may rely more on deep soil moisture and nutrients, thereby exerting a greater influence on the chemical stoichiometry of deeper soil layers; in contrast, the relatively milder climatic conditions in Tumd Left Banner may be more conducive to soil microbial activity, promoting the transformation and cycling of soil nutrients (Song et al., 2023).

From the perspective of spatial distribution, as soil depth increases, soil nutrient content and stoichiometric ratios exhibit various trends. The surface soil is strongly influenced by the exudates and litter of *Pennisetum giganteum* roots, resulting in more dynamic nutrient changes and notable fluctuations in stoichiometric ratios; whereas the nutrient variations in deeper soils are relatively minor. However, in the long term, the extension of *Pennisetum giganteum* roots can gradually improve the quality of the deeper soil layers (Wang et al., 2023). This suggests that in ecological restoration practices, it is important to fully consider the characteristics of different soil layers and develop targeted planting and management strategies in order to achieve overall optimization of the soil ecosystem.

5 Conclusion

(1) *Pennisetum giganteum* planting significantly increased soil nutrient content: *Pennisetum giganteum* planting significantly increased soil C, N and P content, especially in the surface soil (0–20 cm), nutrient accumulation was more significant. For example, Naiman Banner increased C from 1.41 g/kg to 2.06 g/kg, N from 1.47 g/kg to 1.74 g/kg, and P from 1.27 g/kg to 1.85 g/kg in the 0–10 cm soil layer.

(2) The change of soil stoichiometric ratio reflects the dynamics of nutrient cycling: After *Pennisetum giganteum* was planted, the soil C/N, C/P and N/P changed significantly. The change of C/N ratio indicates that the decomposition rate of soil organic matter is accelerated, and the decrease of C/P ratio and N/P ratio indicates that the mineralization of phosphorus by soil microorganisms is enhanced, and the effectiveness of soil P is improved.

(3) Regional differences significantly affected soil nutrient transformation: The climatic conditions and soil texture in different regions affected the growth of *Pennisetum giganteum* and the transformation of soil nutrients. The drought conditions of Ulan Buh Desert make *Pennisetum giganteum* more dependent on the nutrient absorption of deep soil, while the mild climate of Tumd Left Banner is more

conducive to the activity of soil microorganisms and promotes the rapid transformation of nutrients.

Data availability statement

The original contributions presented in the study are included in the article/supplementary material, further inquiries can be directed to the corresponding author.

Author contributions

YS: Data curation, Formal Analysis, Investigation, Software, Writing – original draft. YM: Writing – review and editing, Project administration, Methodology. GL: Funding acquisition, Supervision, Writing – review and editing. XM: Investigation, Data curation, Writing – original draft.

Funding

The author(s) declare that financial support was received for the research and/or publication of this article. This work was financially supported by the Inner Mongolia Autonomous Region "Unveiling the List and Leading the Way" Project (2024JBGS0023), Technology Special Project of Erdos City (2022EEDSKJZDZX012) and the High-level/excellent Doctor Introduction Project of Inner Mongolia Agricultural University (NDYB 2021-9).

Conflict of interest

The authors declare that the research was conducted in the absence of any commercial or financial relationships that could be construed as a potential conflict of interest.

Generative AI statement

The author(s) declare that no Generative AI was used in the creation of this manuscript.

Publisher's note

All claims expressed in this article are solely those of the authors and do not necessarily represent those of their affiliated organizations, or those of the publisher, the editors and the reviewers. Any product that may be evaluated in this article, or claim that may be made by its manufacturer, is not guaranteed or endorsed by the publisher.

References

Bi, L. L. (2019). *Preliminary study on the remediation of cadmium - contaminated soil by modified* Pennisetum giganteum *biochar*. Guangdong University of Technology.

Bui, E. N., and Henderson, B. L. (2013). C:N:P stoichiometry in Australian soils with respect to vegetation and environmental factors. *Plant Soil* 373 (1), 553–568. doi:10.1007/s11104-013-1823-9

Cheng, B., Zhao, Y. J., and Zhang, W. G. (2010). Research progress of ecological stoichiometry. *Acta Ecol. Sin.* 30 (06), 1628–1637.

Dong, X., Hao, Y. G., and Xin, Z. M. (2019). Stoichiometric characteristics of soil carbon, nitrogen and phosphorus under four typical shrubs in horqin sandy land. *Acta Bot. Boreali - Occident. Sin.* 39 (1), 164–172.

Gou, B. W., Wei, B., and Ma, S. M. (2020). Study on the distribution characteristics of soil nutrients in the root zone of Haloxylon ammodendron on the Southern edge of the gurbantunggut desert. *Southwest China J. Agric. Sci.* 33 (6), 1229–1234.

Huang, G. Y. (2011). Research and prospect on the application of Juncao Technology in the treatment of desertified land in Ningxia. *Prot. For. Sci. Technol.* (2), 46–48.

Huang, J., and Yuan, Z. N. (2020). Overview of ecological stoichiometric characteristics and influencing factors of soil carbon, nitrogen and phosphorus. *Mod. Agric. Res.* 49 (01), 73–76.

Li, W. C. (2001). The situation, causes and countermeasures of land desertification in Inner Mongolia. *North. Econ.* (10), 4–8.

Li, Y., Li, Y., Zhang, Q., Xu, G., Liang, G., and Kim, D. G. (2024). Enhancing soil carbon and nitrogen through grassland conversion from degraded croplands in China: assessing magnitudes and identifying key drivers of phosphorus reduction. *Soil Tillage Res.* 236, 105943. doi:10.1016/j.still.2023.105943

Li, Y. K. (2000). Correct expression of calculation formulas for soil agrochemical analysis results. *Chin. J. Soil Sci.* (06), 275–272.

Li, Y. P., and Narisu, W. (2011). Remote sensing monitoring and analysis of grassland desertification in Inner Mongolia. *Chin. J. Grassl.* 33 (3), 79–86.

Li, Y. S., Zhao, X. D., and Chen, T. D. (2020). Application of *Pennisetum giganteum* in ecological restoration and governance. *Rural. Sci. Exp.* (4), 63–64.

Liao, X. L., Zhang, T., and Xu, Y. (2020). Research on the evolution trend of desertification in semi - arid areas: a case study of horqin left rear banner. *Chin. J. Agric. Resour. Regional Planning* 41 (4), 299–307.

Liu, Z. G. (2019). *Characteristics of soil microbial community structure of* Pennisetum giganteum *in the dry - hot valley of Panzhihua*. Sichuan Agricultural University.

Lu, Z. Q., Dou, Y. Y., and Wang, J. Z. (2024). Impact of ecosystem type conversion on soil wind erosion in key ecological function areas of Inner Mongolia autonomous region. *Bull. Soil Water Conservation* 44 (04), 247–256.

Ma, Y. J., Yang, G. Z., and Duan, R. J. (2023). *Biological characteristics and application of artificial cultivation techniques of* Pennisetum giganteum. Hebei Agricultural Machinery, 85–87.

Mei, L. (2018). *Dynamic changes of soil enzyme activity and microorganisms of* Pennisetum giganteum *at different stages in the Pisha sandstone area*. Fujian Agriculture and Forestry University.

Nie, H. G., Li, Z. P., and Yue, L. P. (2008). Development trend and causes of land desertification in the ejina basin, Western Inner Mongolia. *Geol. Bull. China* (08), 1335–1343.

Ren, Y., Zhang, B., and Chen, X. D. (2023). Assessment of land desertification sensitivity in horqin sandy land. *J. Desert Res.* 43 (02), 159–169.

Sheng, L. (2023). Discussion on the application of *Pennisetum giganteum* in the ecological governance of the Ulan Buh desert. *Inn. Mong. For.* (05), 34–35.

Song, S. M., Lin, D. M., and Zhou, H. Y. (2023). Effects of planting *Pennisetum giganteum* on plant species diversity and soil physical and chemical properties in the Ulan Buh desert. *Ecol. Environ. Sci.* 32 (09), 1595–1605.

Tao, Y., Wu, G. L., and Liu, Y. B. (2017). Soil stoichiometric characteristics and their influencing factors of typical shrub communities in the gurbantunggut desert. *J. Desert Res.* 37 (02), 305–314.

Wang, L., Liu, W. C., and He, H. X. (2006). Remote sensing investigation of land desertification and environmental quality assessment in central Inner Mongolia. *Geoscience* (03), 505–512.

Wang, L. M., Li, G. T., and Zhang, B. (2023). Effects of *Pennisetum giganteum* on soil physical and chemical properties in the introduction area of Inner Mongolia. *J. Anhui Agric. Sci.* 51 (04), 58–60+67.

Wang, S. Q., and Yu, G. R. (2008). Ecological stoichiometric characteristics of carbon, nitrogen and phosphorus elements in ecosystems. *Acta Ecol. Sin.* (08), 3937–3947.

Wu, Q. (2018). *Study on the growth characteristics and wind - proof and sand - fixing effects of* Pennisetum giganteum *in the yellow River section of the Ulan Buh Desert*. Inner Mongolia Agricultural University.

Yang, S. L. (2019). *Root growth and nutrient dynamics of* Pennisetum giganteum *in the dry - hot Valley of panxi*. Sichuan Agricultural University.

Yao, Y. Z. (2018). Research on the driving forces of desertification and soil and water conservation in Inner Mongolia. *Chin. J. Agric. Resour. Regional Planning* 39 (02), 13–17+87.

Zhao, K., Yue, Y. J., and He, R. (2022). Research on the spatial distribution of land desertification sensitivity in naiman banner. *For. Resour. Manag.* (01), 52–60.

Zhou, J., Lin, X. S., and Lin, H. (2020). Research and application progress of Juncao. *J. Fujian Agric. For. Univ. Nat. Sci. Ed.* 49 (02), 145–152.

Zhou, Y. (2019). *Study on the improvement effect of* Pennisetum giganteum *on soil physical and chemical properties in the dry - hot Valley of panxi*. Sichuan Agricultural University.

Zhou, Y., Boutton, T. W., and Wu, X. B. (2018). Soil phosphorus does not keep pace with soil carbon and nitrogen accumulation following woody encroachment. *Glob. Change Biol.* 24 (5), 1992–2007. doi:10.1111/gcb.14048

frontiers | Frontiers in Environmental Science

TYPE Original Research
PUBLISHED 15 July 2025
DOI 10.3389/fenvs.2025.1617210

OPEN ACCESS

EDITED BY
Pengcheng Hu,
Commonwealth Scientific and Industrial Research Organisation (CSIRO), Australia

REVIEWED BY
Kun Zhang,
Nanjing Institute of Environment Science, China
Chuan Yuan,
Southwest University, China

*CORRESPONDENCE
Jian Hou,
houjian@bifu.edu.cn

RECEIVED 24 April 2025
ACCEPTED 30 June 2025
PUBLISHED 15 July 2025

CITATION
Jiang J, Hou J, Zeng C, Feng H and Zhu Y (2025) Research on the driving mechanisms of ecosystem services in the alpine canyon areas of Southwest China.
Front. Environ. Sci. 13:1617210.
doi: 10.3389/fenvs.2025.1617210

Research on the driving mechanisms of ecosystem services in the alpine canyon areas of Southwest China

Jiahui Jiang[1], Jian Hou[1]*, Chen Zeng[2], Haobo Feng[1] and Yufan Zhu[1]

[1]School of Soil and Water Conservation, Beijing Forestry University, Beijing, China, [2]Institute of Tibetan Plateau Research, Chinese Academy of Sciences, Beijing, China

The Alpine Canyon Area of Southwest China represents a region of ecological and cultural significance, where multi-ethnic communities rely heavily on ecosystem services for sustenance, including food, water, and other vital resources. To systematically evaluate these dependencies, this study utilized multi-source datasets to quantify the spatiotemporal patterns of four key ecosystem services in the region: carbon sequestration food supply (FS), water yield (WY), and soil conservation (SR). Spearman correlation analysis, geographically weighted regression, and the geographic detector method were employed to analyze trade-offs and synergies among these ecosystem services and explore their driving mechanisms. The results indicated: (1) The four ecosystem services in the study area exhibited significant spatiotemporal heterogeneity. (2) During the study period, the synergies were observed between CS-WY, CS-SR, and WY-SR, highlighting a particularly strong synergy for WY-SR. Conversely, trade-offs were observed for CS-FS, FS-WY, and FS-SR, with the strongest trade-off occurring between food supply and water yield. (3) The trade-offs and synergies among ecosystem services in the region were significantly influenced by a combination of natural and socio-economic factors, with elevation, slope degree, temperature, and population density playing pivotal roles. Among all ecosystem services pairs, the interaction between elevation and other influencing factors represented the most critical driver combination. This study highlights the importance of ecosystem services in multi-ethnic regions, provides insights into ecosystem services trade-offs and synergies, and offers scientific support for regional ecological management.

KEYWORDS

southwest alpine canyon, ecosystem services, spatiotemporal patterns, trade-offs and synergies, geographically weighted regression model, driving mechanisms

1 Introduction

Ecosystem services (ESs), derived from ecosystem structures, processes, and functions, bridge ecological and social systems, ensuring ecological security, human safety, and quality of life (Fu and Yu, 2016; Reid et al., 2005; Costanza et al., 1998). Addressing the challenge of meeting humanity's growing demand for natural resources while maintaining fundamental ecosystem functions and resilience require an in-depth understanding of the complex relationships between ESs, understanding trade-offs - where enhancing one ESs diminish

another - and synergies, where multiple ESs change concurrently (Tomscha and Gergel, 2016; Tomscha et al., 2016). Optimizing the management of conflicts between multiple objectives in ecosystem services management and alleviating trade-offs between ESs are essential for ensuring the diversification of ecosystem services and high-quality regional development (Cord et al., 2017).

According to the United Nations Millennium Ecosystem Assessment, most of the global ecosystem services have experienced degradation or unsustainable use over the past half-century, posing significant threats to regional and global ecological security (Pereira et al., 2024; Tomscha et al., 2016; Reid et al., 2005). To address challenges and conflicts arising from the impacts of ecosystem services on sustainable development, interdisciplinary research in geography, ecology, and economics have increasingly focused on ESs trade-offs and synergies (Boithias et al., 2014; Peng et al., 2017). Recent studies have employed diverse methodologies to explore ESs spatial-temporal patterns and capture trade-offs/synergies across diverse regions and scales (Wang et al., 2022; Yang et al., 2024). For instance, Shifaw et al. (2024) mapped the spatial-temporal distribution of four ESs (water production, carbon-fixation, habitat quality, and soil conservation) in the Upper Qing Nile River Basin in northwestern Ethiopia to evaluate the trade-offs and synergies. Similarly, Feng et al. (2021) utilized a Bayesian probability network to analyze trade-offs and synergies in the Beijing-Tianjin-Hebei region. These studies underscored the importance of understanding trade-offs and synergies in ESs for effective regional ecological management (Hao et al., 2023). Based on this, this study aims to examine these dynamics in ESs trade-offs/synergies and identify the underlying mechanisms driving these patterns, offering actionable insights to support sustainable ecological decision-making.

The Southwest Alpine Canyon are situated in southwestern China. Over 40 snow-capped mountains exceeding 6,000 m in elevation dominate the landscape, providing freshwater for China major rivers, such as the Yangtze and Pearl Rivers. Water vapor and river runoff influenced by the Qinghai-Tibet Plateau and the Himalayas (Li, 2010; Da-ming and Xuan-juan, 2001; Daming et al., 2004). It is also a multi-ethnic settlement area, where diverse ethnic groups have developed unique cultural, religious, and customary practices, fostering ecosystem protection through traditional beliefs like “nature worship” and sacred ancestral lands (Wang et al., 2019; Lin and Gui, 2024). Settlements are concentrated in lowland areas, where water and soil cultivation, combined with natural barriers, enhance production and living spaces (Guo et al., 2023). However, rapid economic development has led to significant anthropogenic interference, resulting in resource overconsumption and ecosystem degradation (Ramyar et al., 2020; Zhang et al., 2020). Despite its ecological and cultural significance, the region remains understudied, with previous research primarily focusing on low and medium altitude areas, which differ markedly from the alpine canyon environment. Systematic evaluations of ESs are urgently needed to understand their overall characteristics, complex interactions, and the mechanisms driving trade-offs and synergies. Addressing these gaps are critical for advancing regional research, enhancing ESs value, and informing sustainable management in this unique alpine canyon area.

The Southwest Alpine Canyon exhibit significant ecological vulnerability due to its complex geological landforms, which create intricate ecosystems with low stability, poor recovery capacity, and high sensitivity to external disturbances (Ding et al., 2021; Tan et al., 2024). Key ecological challenges include degradation from soil erosion, bedrock exposure, and stone desertification (Guo et al., 2023), making water yield and soil retention particularly crucial for ecosystem management (Yahdjian et al., 2015). These processes are further exacerbated by land use changes that affect carbon sequestration services (Hall et al., 2012) and alter food supply systems, ultimately impacting regional governance and the livelihoods of ethnic minority communities dependent on these ecosystems. Based on the above, this study utilized multi-source datasets in the Southwest Alpine Canyon Area to analyze ESs. (1) The InVEST model was employed to evaluate four key ESs: carbon sequestration (CS), food supply (FS), water yield (WY), and soil conservation (SR). (2) Spearman correlation analysis and geographically weighted regression were used to reveal trade-offs, synergies, and spatial heterogeneity among these ESs. (3) The geographic detector model was applied to explore the mechanisms driving variations in ESs trade-offs and synergies. Our findings provide valuable insights for rational land use, ecological management, and the formulation of targeted strategies to ensure ecological safety in ethnic minority areas, offering guidance for the sustainable utilization of alpine canyon resources.

2 Study area and data

2.1 Study area

The Southwest Alpine Canyon Area, located in southwestern China (Figure 1), spans geographic coordinates from 24°56′N–33°09′N latitude and 91°24′E–104°15′E longitude. It encompasses three major topographic steps of China: The Transverse Mountains on the first topographic step, the Sichuan Basin on the second topographic step, and the plains in the middle and lower reaches of the Yangtze River on the third topographic step (Wang et al., 2019). The region exhibits a complex geological structure shaped by extensive tectonic movements, with landscapes ranging from mountains, hills, and plateaus to basins, canyons, river valleys, and dams, characterized by significant elevation variations (Li, 2010). The climate is diverse and vertically stratified, encompassing subtropical, temperate and cool-temperate (Lin and Gui, 2024). The water system is dense, with major rivers such as the Yarlung Zangbo, Lancang, and Jinsha Rivers flowing from northwest to southeast, forming extensive river networks (Daming et al., 2004). The region is home to a wide distribution of ethnic minorities, with nearly 30 groups, including the Yi, Pumi, Lisu, Hani, Lahu, Tibetan, and Hui, accounting for approximately 80% of the total population. This cultural diversity adds to the socio-environmental complexity of the area.

2.2 Data sources

Estimation of ESs relies on multi-source datasets (Table 1). Spatial data were primarily sourced from public databases, with additional data derived using conversion tools and formulas. Land

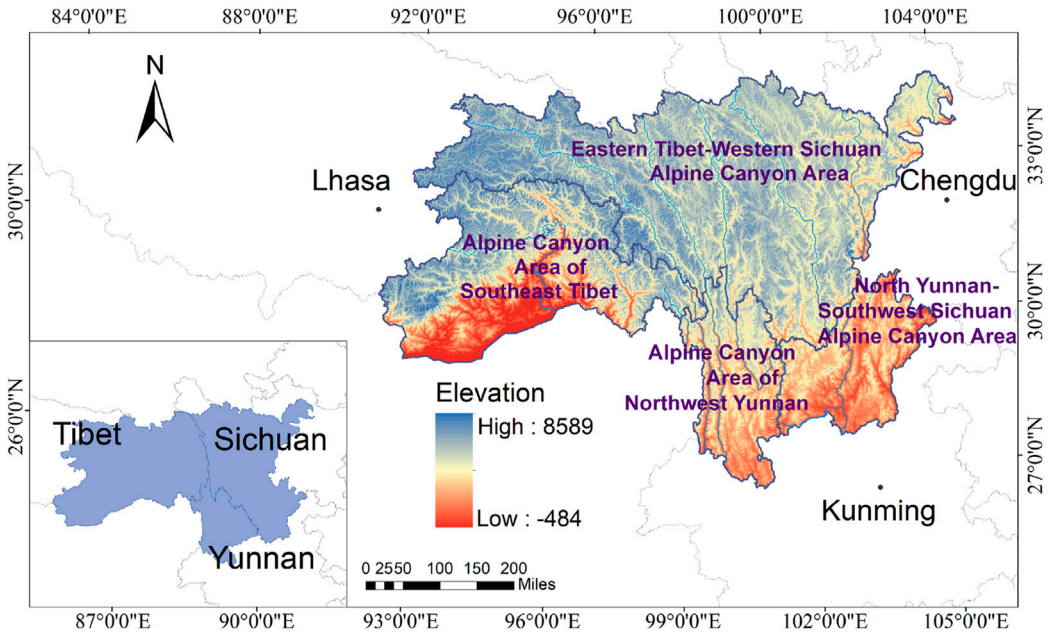

FIGURE 1
Location of the study area.

TABLE 1 Data required for the InVEST model.

Data requirements	Data sources
Land use	https://zenodo.org/
DEM	https://www.gscloud.cn/
Temperature, precipitation, evapotranspiration	https://www.geodata.cn/data/
Plant Available Water Content	https://www.fao.org/soils-portal/data-hub/
Fractional Vegetation Cover	http://www.gis5g.com/
Harmonized World Soil Database	https://gaez.fao.org/pages/hwsd
Population density, GDP, primary sector, secondary sector, tertiary sector	https://www.stats.gov.cn/

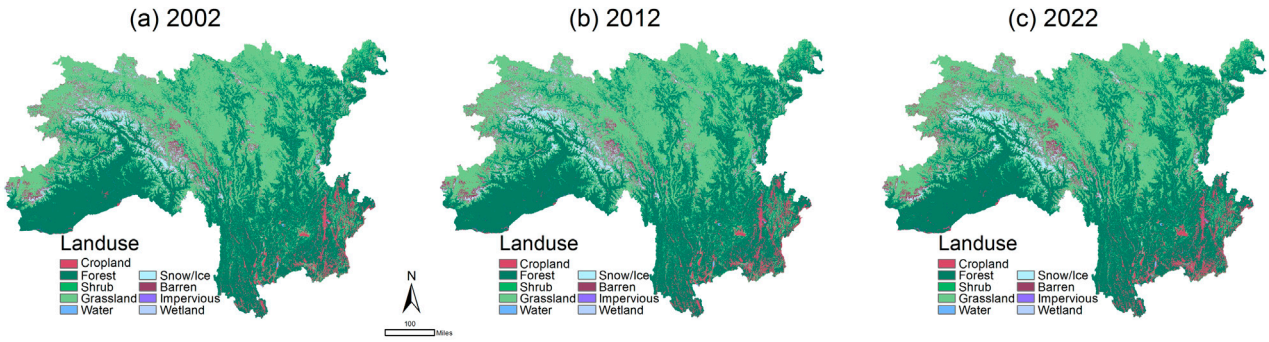

FIGURE 2
Land use in the Southwest Alpine Canyon, **(a)** 2002; **(b)** 2012; **(c)** 2022.

TABLE 2 Methods for evaluating ecosystem services.

Ecosystem services	Principles and methods	Calculation process
Carbon sequestration	Carbon Storage and Sequestration module of the InVEST model: summarizing the amount of carbon stored based on the land use data provided. The amount of carbon stored in the study area depends strongly on the size of four carbon reservoirs: aboveground biomass, underground biomass, soil and dead organic matter	$C_{tot} = C_{above} + C_{below} + C_{soil} + C_{dead}$ (1) Where, C_{tot} denotes the total carbon stock, C_{above} denotes the aboveground biogenic carbon stock, C_{below} denotes the belowground biogenic carbon stock, C_{soil} denotes the soil carbon stock, and C_{dead} denotes the dead organic carbon stock
Food supply	InVEST model Crop Production module: based on regression models. Crop production regression models can provide yield estimates for a given fertilizer input (Mueller et al., 2016)	
Water yield	The InVEST model Annual Water Yield module: runs on a rasterized map and evaluates the amount of water in each sub-basin of a given watershed (Donohue et al., 2012)	$Y(x) = (1 - \frac{AET(x)}{P(x)}) \cdot P(x)$ (2) Where, $AET(x)$ is the annual actual evapotranspiration of the x grid and $P(x)$ is the annual precipitation of the x grid
Soil conservation	InVEST model Sediment Delivery Ratio module: it can overcome the limitations of traditional soil erosion models, analyze the soil loss and sediment output of each land use type. Quantifying the amount of sediment in rivers, reservoirs and other water bodies, thus enabling the characterization of hydrological connectivity in watersheds	$SR = RKLS - USLE = R \times K \times LS \times (1 - C \times P)$ (3) Where, SR is the annual soil conservation (t/hm^2), RKLS is the maximum possible soil loss (t/hm^2), USLE is the actual soil loss (t/hm^2)

use data for 2002, 2012, and 2022, with a spatial resolution of 30 m × 30 m, were obtained from the CLCD dataset, updated by Prof. Jie Yang and Xin Huang of Wuhan University. The dataset includes land use types such as cropland, forests, shrubs, grasslands, watersheds, snow and ice, bare ground, impervious surfaces, and wetlands (Figure 2). Meteorological data (temperature, precipitation, and evapotranspiration) were acquired from the National Earth System Science Data Center at a 1 km resolution. Elevation data, derived from a DEM, were sourced from the Geospatial Data Cloud Platform at a 30 m resolution. Plant-available water content data were obtained from the World Soil Database, jointly developed by the Food and Agriculture Organization (FAO) and the International Institute for Applied Systems Analysis (IIASA). Vegetation cover data, with a resolution of 250 m, were downloaded from the Earth Resources Data Cloud Platform. Soil data were extracted from the Harmonized World Soil Database (HWSD), with soil erodibility calculated from soil texture using the EPIC model. Socio-economic data, including population density, GDP, and primary, secondary, and tertiary industry data, were sourced from the China County Statistical Yearbook of the National Bureau of Statistics.

2.3 Methods

2.3.1 Quantification of ecosystem services

The assessment methodology employs the InVEST model, a spatially explicit tool developed by Stanford University and collaborators to evaluate how ecosystem changes influence the provision of benefits to human societies. Based on a production function approach, the InVEST model quantifies ecosystem services and supports decision-making in natural resource management by identifying priority areas for investment to enhance both human wellbeing and ecological sustainability. The specific assessment procedures and computational frameworks for four key ecosystem services, carbon sequestration, food supply, water yield, and soil conservation, are detailed in Table 2.

2.3.2 Correlation analysis

Correlation analysis can effectively reflect the direction and intensity of ESs trade-offs and synergies (Agudelo et al., 2020). Spearman correlation analysis was used to quantify variation and relationships between ESs trade-offs and synergies on the three temporal scales in 2002, 2012, and 2022. Positive correlations between ESs correspond to synergies, and negative correlations correspond to trade-offs. The formula was as follows:

$$\rho_{X,Y} = \frac{cov(X,Y)}{\sigma_x \sigma_y} = \frac{E\left((X-\mu_x)\left(Y-\mu_y\right)\right)}{\sigma_x \sigma_y} = E(XY) - \frac{E(X)E(Y)}{\sqrt{E(X^2)-E^2(X)}\sqrt{E(Y^2)-E^2(Y)}} r_g = \rho_{rg_X, rg_Y} = \frac{cov(rg_X, rg_Y)}{\rho_{rg_X}\rho_{rg_Y}} \quad (4)$$

$\rho_{X,Y}$ denotes the Pearson correlation coefficient of variables X and Y, cov denotes covariance, σ denotes standard deviation, and ρ_{rg_X} and ρ_{rg_Y} denote the Spearman's correlation coefficient applied to the rank order of the original variables.

2.3.3 Geographically weighted regression (GWR) model

While correlation analysis offers a general understanding of overall trade-offs and synergies, it fails to capture the spatial heterogeneity of these effects. The GWR model, a robust spatial data analysis method, addresses this limitation by accounting for the heterogeneity and non-stationarity of spatial data, surpassing traditional regression models (Kupfer and Farris, 2007). To gain deeper insights into the spatial distribution of trade-offs and synergies among ESs, the GWR model was employed to reveal their spatial variations. The calculation formula was as follows:

$$y_i = \beta_o(u_i, v_i) + \sum_{k=1}^{p} \beta_k(u_i, v_i) x_{ik} + \varepsilon_i \quad (5)$$

In the formula, y_i is the explanatory variable, x_{ik} is the independent variable, (u_i, v_i) is the spatial location of point I, $\beta_o(u_i, v_i)$ is the intercept at point I, $\beta_k(u_i, v_i)$ is the regression

TABLE 3 Factors affecting ESs trade-offs and synergies.

Type	Nature	Socio-economic
Driving factors	Elevations	Population density
	Precipitation	GDP
	Evapotranspiration	primary industry
	Temperature	secondary industry
	Slope degree	tertiary industry
	Slope aspect	
	Forest vegetation cover	

coefficient, K is the ordinal number of the independent variable, P is the number of the independent variable, and $\beta > 0$ is the positive correlation between explanatory and independent variables, and *vice versa* for the negative correlation. ε_i is a random disturbance term.

2.3.4 Geographic detector model

Geographic detector is a new statistical method for revealing the underlying mechanism driving it. Its q-statistics, which detect explanatory factors, and analyze interactions between variables, have been widely applied across natural and social sciences (Zhao et al., 2020). In this study, factor detection within the geographic detector framework was employed to explore the influence of individual factors on trade-offs and synergies among ESs, while interaction detection was used to further elucidate the interplay among these driving factors.

Factor detection quantifies the extent to which a single driver explains spatial divergence in ESs trade-offs and synergies, measured using the q-value metric. The formula was calculated as follows:

$$q = 1 - \frac{\sum_{k=1}^{n} N_k \sigma_k^2}{N\sigma^2} \quad (6)$$

where q is the effect of the driving factor on ESs trade-offs and synergies. K = 1, . . . , n is the classification of this influencing factor. N_K and N are the number of cells in the sub-region and the whole region, respectively. σ^2_K and σ^2 are the variance in the Y-values in the sub-region and the whole region, respectively.

Interaction detection was conducted to assess the relationships among different factors, specifically whether their combined interactions enhance or diminish the explanatory power of trade-offs and synergies among ESs, or whether their effects operate independently. The following five types of relationships were included:

If $q(A\cap B)<\mathrm{Min}(q(A), q(B))$, the two factors are nonlinearly weakened.

If $\mathrm{Min}(q(A), q(B))<q(A\cap B)<\mathrm{Max}(q(A), q(B))$, the one-factor nonlinearity is weakened.

If $q(A\cap B)>\mathrm{Max}(q(A), q(B))$, then the two factors are enhanced.

If $q(A\cap B) = q(A)+q(B)$, the two factors are independent of each other.

If $q(A\cap B)>q(A)+q(B)$, then the two factors are nonlinearly enhanced.

Building on the primary factors identified in previous studies as drivers of variation in ESs trade-offs and synergies, and considering the distinctive landscape patterns of the Southwest Alpine Canyon Area, 12 influencing factors, encompassing both natural and socio-economic dimensions, were selected for analysis (Table 3).

3 Results

3.1 Spatial and temporal patterns of ecosystem services

The four ESs of CS, FS, WY, and SR in study area exhibit distinct spatial distribution patterns (Figure 3). During the study period, low-value areas of CS were predominantly concentrated in the high-altitude alpine canyon regions of southeastern Tibet and the alpine canyon areas of eastern Tibet-western Sichuan (Figure 1). High-value areas of FS were mainly located in the southern part of the study area, particularly in the high mountain canyon regions of southeastern Yunnan-southwestern Sichuan. WY exhibited high-value areas primarily in the high-altitude alpine canyon region of southeastern Tibet, while SR high-value areas were concentrated along the edges of the high-altitude alpine canyon region in southeastern Tibet and the alpine canyon region of northwestern Yunnan. Severe soil erosion and low soil conservation efficiency are prevalent in this region. High-value areas of soil retention and water yield were primarily located in the forested regions of the southern high-altitude alpine canyon area in southeastern Tibet, where extensive vegetation coverage, effective artificial protection measures, and high water and soil retention capacities prevail. These areas experience minimal human interference and exhibit elevated levels of ESs. In contrast, low-value zones were mainly found in the high mountain canyon regions of northern Yunnan-southwestern Sichuan and northwestern Yunnan, where intensive human activities have reduced naturalness and ESs levels. Arable lands in the high mountain valley areas of northern Yunnan-western Sichuan and northwestern Yunnan were significantly influenced by anthropogenic activities, leading to enhanced crop production capacity. The study area exhibited superior carbon storage services due to the widespread distribution of forest, which enhance carbon sequestration capabilities. Conversely, low-value areas of carbon storage were primarily located in the ice and snow-covered regions of the western part of the study area.

From 2002 to 2022, the degree of change in ESs is illustrated in Figure 4, with distinct patterns observed across different services. Carbon sequestration initially decreased and then increased, while both water yield and soil conservation showed a declining trend, with more pronounced changes in water production. Among all ESs, food supply demonstrated the most significant increase, showing a continuous upward trend. For the periods 2002–2012 and 2012–2022, water yield decreased by 1.14% and 6.75%, respectively, while soil conservation decreased by 1.72% and 1.63%, respectively. In contrast, food supply experienced an overall improvement, increasing by 8.46% and 10.04% during the same periods. Carbon sequestration decreased by 0.11% from 2002 to 2012 but showed a slight increase of 0.25% from 2012 to 2022.

3.2 Ecosystem services trade-offs and synergies

3.2.1 Trade-offs and synergies between ecosystem services

From 2002 to 2022, the study identified trade-offs and synergistic relationships among four ecosystem services: CS, FS,

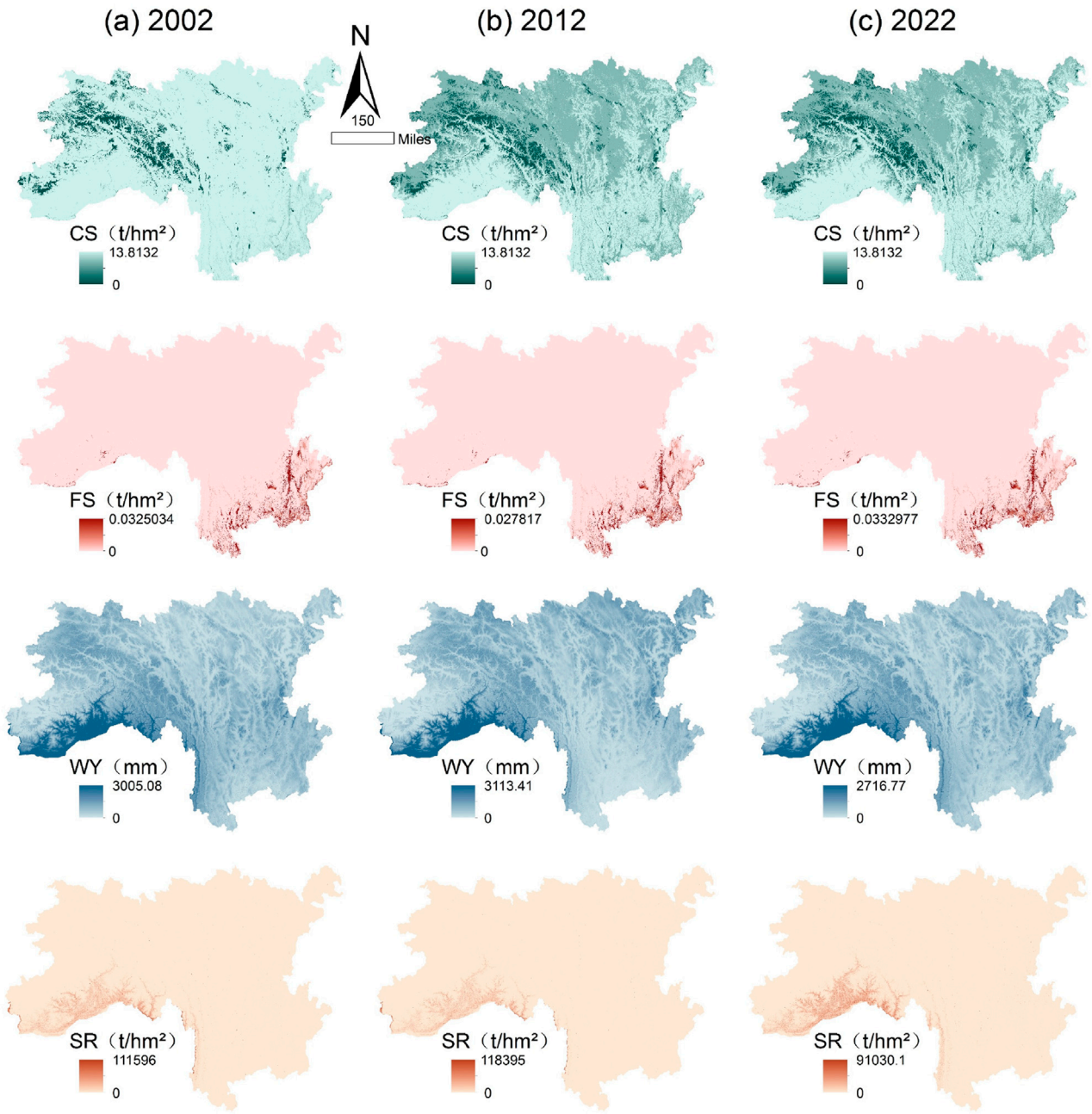

FIGURE 3
Spatial and temporal characteristics of ESs in the Southwest Alpine Canyon Area listed left to right as follows: **(a)** 2002, **(b)** 2012 and **(c)** 2022, and from top to bottom: CS, carbon sequestration; FS, food supply; WY, water yield; SR, soil conservation.

WY, and SR (Figure 5). Six pairs of relationships were found, revealing significant synergistic effects for CS-WY, CS-SR, and WY-SR, highlighting a particularly strong synergy for WY-SR. Conversely, trade-off effects were observed for CS-FS, FS-WY, and FS-SR, with FS consistently exhibiting trade-offs with other ESs. The most pronounced trade-off was between FS and WY. Over the three time periods, the trade-offs between FS-WY and FS-SR initially intensified and subsequently weakened. The weakest trade-offs were recorded in 2002 (−0.44 and −0.38, respectively), while the strongest trade-offs occurred in 2012 (−0.66 and −0.56, respectively).

3.2.2 Spatial heterogeneity in ecosystem services trade-offs and synergies

The study revealed significant spatial heterogeneity of trade-offs and synergies among ecosystem services (Figure 6). The spatial synergies of between FS and WY as well as between FS and SR exhibited a broad distribution, predominantly concentrated in the high-altitude alpine canyon regions of southeastern Tibet and the alpine canyon areas of eastern Tibet-western Sichuan within the western part of the study area (Figure 1). Conversely, the spatial trade-offs of between WY and SR were widely distributed across most regions in study area, excluding the northern edge of the study

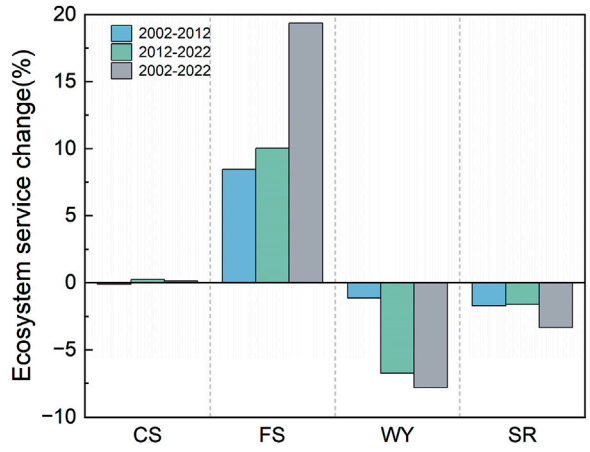

FIGURE 4
Changes in ESs in the southwestern alpine canyon area, 2002–2022. Note: CS, carbon sequestration; FS, food supply; WY, water yield; SR, soil conservation.

area, with particularly pronounced strong trade-offs observed in the alpine canyon regions of northern Yunnan-southwestern Sichuan and northwestern Yunnan. Furthermore, during the study period, a pronounced increasing trend in the spatial strong trade-offs between CS and WY, as well as between WY and SR, was consistently observed over time.

3.3 Mechanisms driving ecosystem services trade-offs and synergies

3.3.1 Explanatory power of natural factors and socio-economic factors

The study assessed the explanatory power of drivers affecting trade-offs and synergies among ecosystem services, and used q-statistic to identify dominant drivers (Figure 7). In 2002, elevation was the primary driver for the vast majority ESs trade-offs and synergistic pairs, while slope degree dominated CS-SR. Temperature ranked second for CS-FS and WY-SR. GDP was the second most influential factor for CS-WY, and population density was the second most important for FS-WY and FS-SR. In 2012, elevation remained the primary factor for CS-FS, while temperature emerged as the dominant driver for CS-WY and WY-SR. Slope degree continued to lead CS-SR, and population density became the primary factor for FS-WY and FS-SR. In 2022, elevation retained its dominance for most ESs trade-offs and synergistic pairs. Secondary industry became the primary factor for CS-SR, and temperature was the most influential for WY-SR. Temperature ranked second for CS-FS, population density was the second most important for CS-WY, FS-WY, and FS-SR, slope degree was the second most significant for CS-SR, and elevation was the second most important for WY-SR.

In summary, elevation consistently drove CS-FS dynamics, other ESs pairs exhibited temporal shifts in dominant factors, such as slope degree (2002–2012) and secondary industry (2022) for CS-SR. Furthermore, the trade-offs and synergies among ESs in the region are significantly influenced by a combination of natural and socio-economic factors, with elevation, slope degree, temperature, and population density playing pivotal roles.

3.3.2 Combination of interactions between natural factors and socio-economic factors

The results showed that the interactions between any two factors significantly enhanced explanatory power (Figure 8). During the study period, FS-WY and FS-SR interactions exhibited the highest sensitivity. In 2002, the interactions between elevation and slope degree, forest vegetation cover, tertiary industry exhibited the strongest explanatory power for CS-FS. For CS-WY, the interaction between slope degree and elevation, secondary industry, had significant influence. Forest vegetation cover and slope degree dominated CS-SR. The interactions between elevation and precipitation, evapotranspiration, and forest

FIGURE 5
Trade-offs and synergies among ESs in the southwestern alpine canyon area: spearman correlation between different ecosystem services, in **(a)** 2002, **(b)** 2012, and **(c)** 2022. (Green indicate trade-offs, purple indicate synergies and the size of the circle indicate the strength of the correlation) Note: CS, carbon sequestration; FS, food supply; WY, water yield; SR, soil conservation.

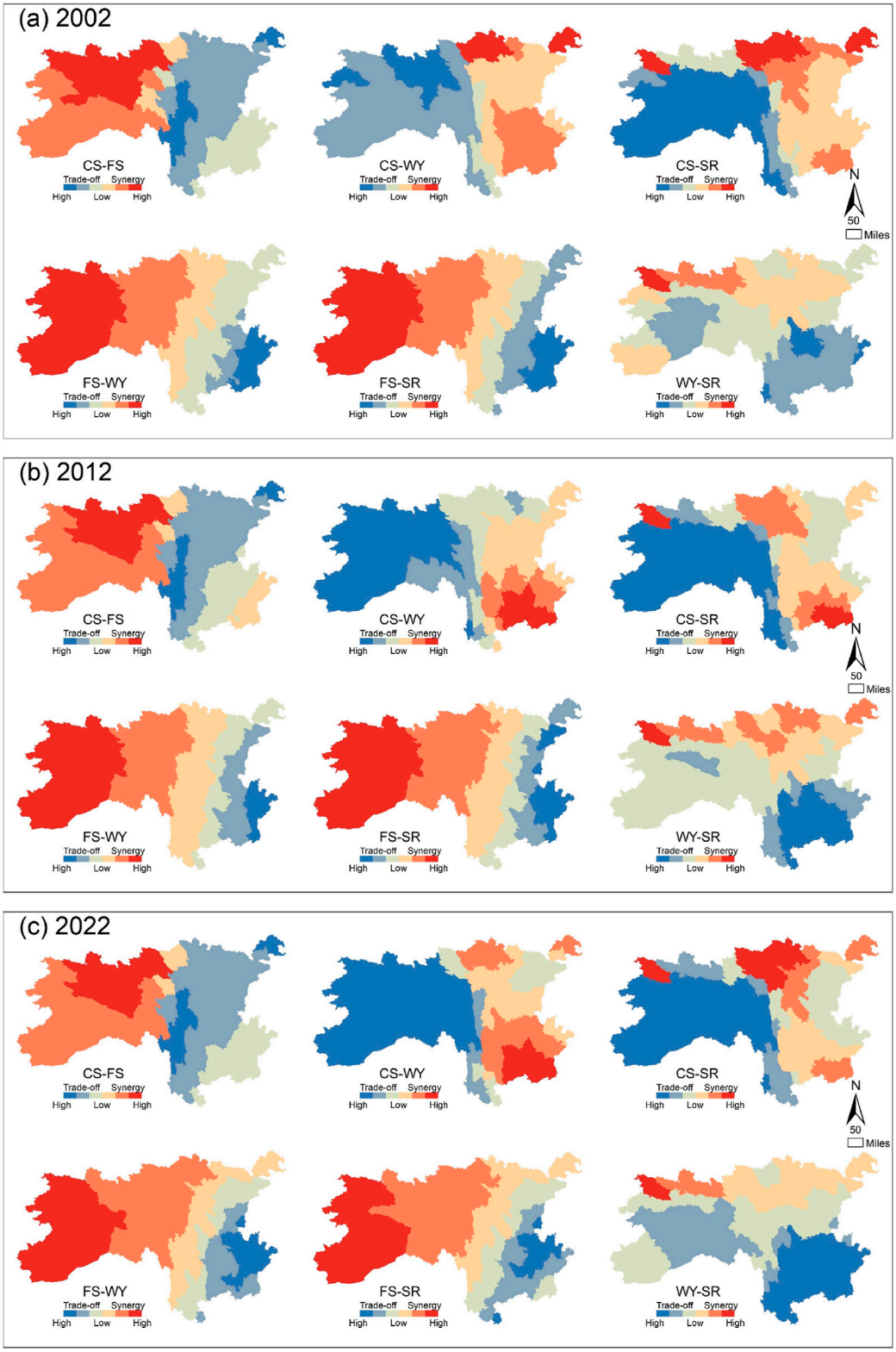

FIGURE 6
Spatial patterns of trade-offs and synergies among ESs in the Southwest Alpine Canyon Area from top to bottom: **(a)** 2002, **(b)** 2012 and **(c)** 2022. Note: CS-FS, carbon sequestration and food supply; CS-WY, carbon sequestration and water yield; CS-SR, carbon sequestration and soil conservation; FS-WY, food supply and water yield; FS-SR, food supply and soil conservation; WY-SR, water yield and soil conservation.

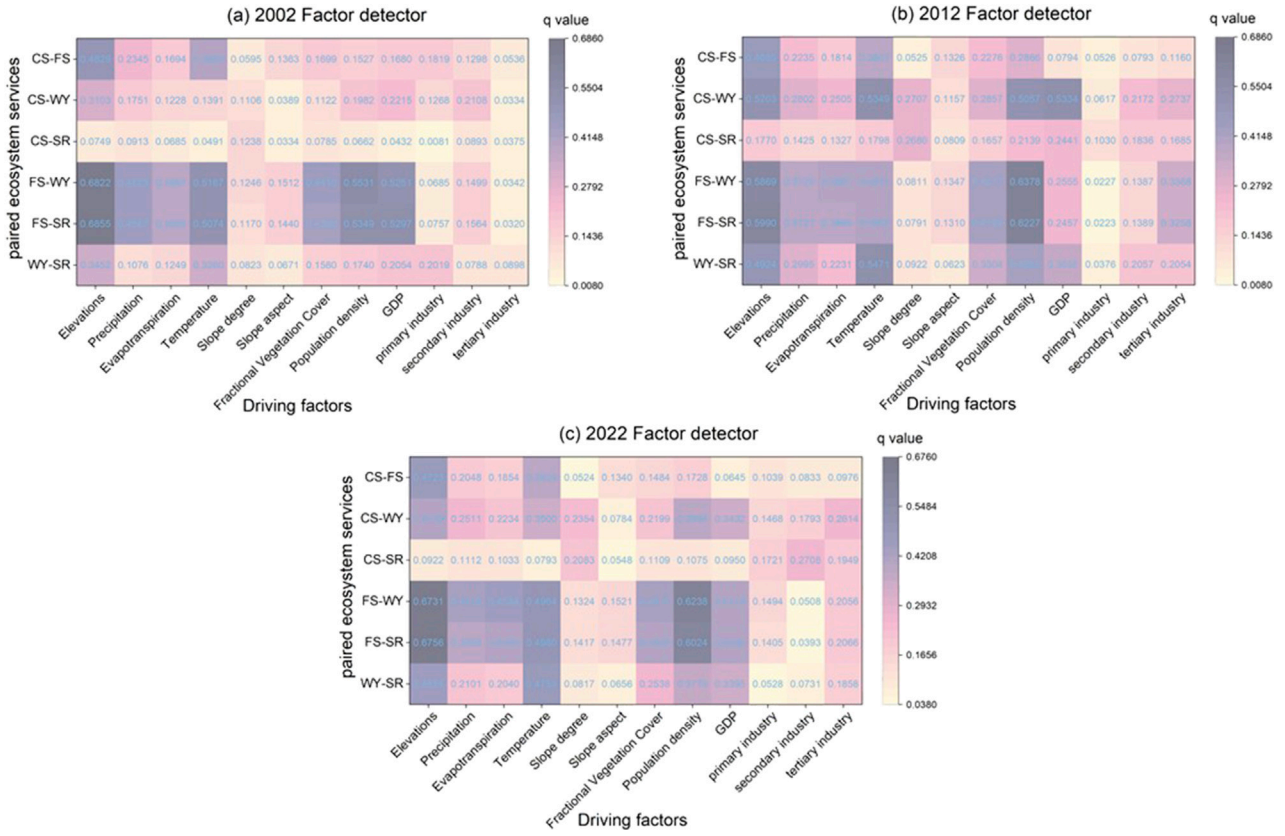

FIGURE 7
Factor detection results revealing the effects of factors on trade-offs and synergies between ESs. From top to bottom, respectively: **(a)** 2002 Factor detector, **(b)** 2012 Factor detector and **(c)** 2022 Factor detector. Note: CS-FS, carbon sequestration and food supply; CS-WY, carbon sequestration and water yield; CS-SR, carbon sequestration and soil conservation; FS-WY, food supply and water yield; FS-SR, food supply and soil conservation; WY-SR, water yield and soil conservation.

vegetation cover were the primary driver combinations for FS-WY and FS-SR. Regarding WY-SR, the interaction between temperature and primary industry, tertiary industry was the most significant explanatory power. In 2012, elevation and slope degree, primary industry, and tertiary industry were the main interaction combinations for CS-FS. For CS-WY, slope degree and elevation, GDP and evapotranspiration, and temperature and precipitation were the primary combinations of explanatory power. Tertiary industry and slope degree exerted the most significant influence on CS-SR, while the interactions between elevation and population density, primary industry had the largest effect on FS-WY and FS-SR. The interactions between temperature and evapotranspiration, slope degree, primary industry, and tertiary industry were the primary driver combinations for WY-SR. In 2022, secondary industry and elevation were the most significant for CS-FS and CS-WY. Primary industry and elevation dominated CS-SR. The interaction between elevation and other factors constitutes the primary driver combination for FS-WY and FS-SR. Primary industry and temperature were the most influential for WY-SR.

In summary, interactions were primarily characterized by two-factor enhancement or nonlinear enhancement, with no independent effects. In all ESs pairs, the interaction between elevation and other influencing factors represents the most critical driver combination.

4 Discussion

4.1 Ecosystem services in alpine canyon areas of Southwest China

Human survival is fundamentally dependent on the continuous provision of ecosystem services, and this dependence intensifies over time (Bennett et al., 2009). In the alpine canyon area of southwest China, carbon sequestration services provide the most significant ESs benefits. Areas with high carbon sequestration capacity are predominantly located in mountainous and hilly regions, where extensive natural and semi-natural forest landscapes serve as critical carbon sinks (Shen et al., 2020). Furthermore, the region's high elevation and rugged terrain enhance humid airflow, resulting in abundant precipitation, while the elevated altitude reduces evaporation rates (Tan et al., 2024). These topographic and climatic characteristics collectively enhance the carbon sequestration potential and protective capacity of the Southwest Alpine Canyon. However, soil conservation and water yield services in this region have exhibited a decline, undermining their ecological functions (Aneseyee et al., 2020). Previous studies have indicated that water yield and soil conservation services tend to diminish when the forest area ratio exceeds a certain threshold (Pergams and Zaradic, 2008). To meet growing service demands, ecosystems

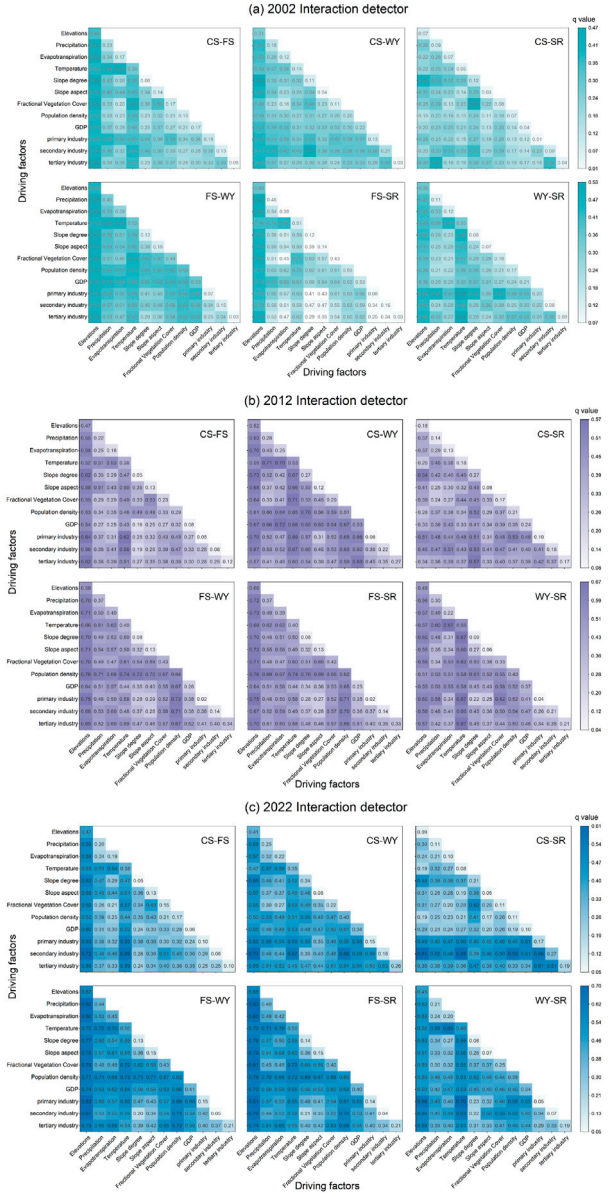

FIGURE 8
Interaction detection results of factors driving trade-offs and synergies between ESs from top to bottom: **(a)** 2002 Interaction detector, **(b)** 2012 Interaction detector and **(c)** 2022 Interaction detector. Note: CS-FS, carbon sequestration and food supply; CS-WY, carbon sequestration and water yield; CS-SR, carbon sequestration and soil conservation; FS-WY, food supply and water yield; FS-SR, food supply and soil conservation; WY-SR, water yield and soil conservation.

are often transformed, either by reducing natural ecosystem areas or intensifying human energy inputs (Zhou et al., 2022). For instance, converting mountains and slopes for crop cultivation increases food supply but exacerbates soil erosion. Similarly, deforestation for agricultural expansion boosts food production but reduces biodiversity, water production, and soil retention capacity. To address these challenges, ecological protection must be prioritized during development, ensuring a balance between progress and conservation.

4.2 Dynamics of ecosystem service trade-offs and synergies

The relationships between ESs in the study area have changed over time. These changes are characterized by trade-offs and synergies, influenced by the diversity of ESs types, their uneven spatial distribution, and selective human utilization (Wang et al., 2024). These interactions are inherently complex (Schirpke et al., 2019), necessitating systematic analysis to clarify their dynamics and optimize ecosystem structure. In this study, trade-offs were observed between food supply and carbon sequestration, water yield, and soil conservation, consistent with findings from other regions. For instance, Raudsepp-Hearne and Peterson (2016) highlighted the importance of scale in ESs evaluation in the Richelieu and Yamaska basins of Canada, while Hao et al. (2023) identified similar trade-offs in the Qiantang River Basin in southeastern China. Additionally, significant synergies were observed for CS-WY, CS-SR, and WY-SR. These findings align with studies in the Beijing-Tianjin-Hebei region (Feng et al., 2021) and the Nile River Basin (Shifaw et al., 2024), which also reported synergies between CS, SR, and WY. The spatial heterogeneity of ESs trade-offs and synergies further underscores their complexity. For example, in the eastern part of the study area where precipitation is abundant, precipitation enhances wind erosion resistance and carbon fixation by regulating soil moisture and increasing vegetation coverage, fostering synergies between water production and carbon fixation services (Abera et al., 2021). However, arid and semi-arid areas in the western part of the study area, increased precipitation and soil moisture elevate evaporation rates, reducing surface temperatures and limiting vegetation photosynthesis in high-altitude cold areas (Xu et al., 2017; Tallis et al., 2008), resulting in a trade-off between water production and carbon fixation services. Understanding these dynamics provide a scientific foundation for regional land planning, biodiversity conservation, and ecological compensation.

4.3 Factors influencing ecosystem services trade-offs and synergies

The study explore the intrinsic mechanisms underlying changes in ESs trade-offs and synergies, and identify the natural and socio-economic factors influencing ESs trade-offs and synergies (Li et al., 2022; Liang et al., 2024; Yang et al., 2024). The results reveal that the trade-offs and synergies among ESs in the region are significantly influenced by a combination of natural and socio-economic factors, with elevation, slope degree, temperature, and population density playing pivotal roles. These factors are intricately interconnected, shaping the dynamics of ESs interactions in the region. Notably, in all ESs pairs, the interaction between elevation and other influencing factors represent the most critical driver combination. Mountainous areas, characterized by more complex topographic conditions than plains (Li et al., 2013), the effect of elevation is amplified by carrying greater elevation change per unit of horizontal distance and by the mountain range orientation interfering with atmospheric circulation. Widely varying elevation differences are common in the study area, leading to reorganization of hydrothermal conditions that directly determine vegetation types, soil development, and species distribution (Wang and Dai, 2020). These findings

corroborate the conclusion that elevation are primary drivers of ESs trade-offs and synergies. Population density and GDP significantly explained ESs interactions, underscoring the regulatory role of human activities. Furthermore, the results indicate that two-factor enhancement and nonlinear enhancement dominated, emphasizing the critical role of factor interactions in shaping ESs dynamics (Bennett et al., 2009).

4.4 Sustainable development and research prospects

Ethnic minority communities in Southwest China have long inhabited the high-altitude alpine canyon areas, where limited production and construction land coexist with fragile ecosystems. These communities have accumulated substantial ecological wisdom, integrated into their traditional culture, which is crucial for the region's sustainable development. This study conducted an in-depth analysis of ESs trade-offs and synergies in the alpine canyon, elucidating the mechanisms by which natural and human factors interact to shape ESs dynamics. This approach addresses the limitations of quantitative analyses in highly vulnerable and complex ecosystems, providing novel insights into ESs research in alpine canyons. By emphasizing the importance of individual factors and their interactions, as well as analyzing the spatial heterogeneity of ESs trade-offs and synergies, establishing development and protection priorities can inform optimal land use planning and policy measures. These measures support sustainable development, environmental protection, and regional planning in the Alpine Canyon area. Furthermore, this study offers scientific and technological support for ecological civilization policies and economic development in ethnic minority gathering areas of the China Southwest Alpine Canyon.

5 Conclusion

This study, utilizing multi-source datasets from the Southwest Alpine Canyon Area, quantitatively evaluate the spatiotemporal dynamics of key ESs - including carbon sequestration, food supply, water yield, and soil conservation - from 2002 to 2022. The trade-offs and synergies among ESs were quantified, and their spatial heterogeneity was systematically analyzed. Furthermore, the primary driving factors of ESs trade-offs and synergies, as well as the explanatory power of interactions among these factors, were identified. For the whole study area, carbon sequestration initially decreased and then increased. Water yield and soil conservation generally declined, with water yield showing more significant changes. Among all services, food supply exhibited the most significant increase, continuing to rise over the study period. A trade-off was observed between food supply and other ESs, with the most pronounced trade-off occurring between food supply and water yield. Spatially, this trade-off was predominantly distributed in the environmentally favorable alpine canyon regions of North Yunnan-Southwest Sichuan and Northwest Yunnan. In all ESs pairs, the interaction between elevation and other influencing factors represent the most critical driver combination. The trade-offs and synergies among ESs in the region are significantly influenced by a combination of natural and socio-economic factors, with elevation, slope degree, temperature, and population density playing pivotal roles. These factors are intricately interconnected, shaping the dynamics of ESs interactions in the region. These findings provide both valuable insights and theoretical foundations for the scientific management of ESs in the Southwest Alpine Canyon Area. By analyzing the trade-offs and synergies among ESs, this research identifies strategies to optimize resource utilization intensity, thereby reducing the vulnerability of both the environment and society to emergencies. Additionally, the study offers practical value for land use management in multi-ethnic gathering areas, as well as for enhancing ecological construction and environmental protection in key watersheds within the region.

Data availability statement

The original contributions presented in the study are included in the article/supplementary material, further inquiries can be directed to the corresponding author.

Author contributions

JJ: Investigation, Writing – review and editing, Conceptualization, Validation, Software, Methodology, Formal Analysis, Writing – original draft, Data curation, Visualization. JH: Funding acquisition, Project administration, Resources, Formal Analysis, Validation, Writing – review and editing, Conceptualization, Supervision. CZ: Funding acquisition, Project administration, Resources, Writing – review and editing. HF: Writing – review and editing, Resources, Data curation, Project administration, Investigation. YZ: Data curation, Investigation, Writing – review and editing.

Funding

The author(s) declare that financial support was received for the research and/or publication of this article. This research was supported by the National Key Research and Development Program of China (2022YFF1302905).

Conflict of interest

The authors declare that the research was conducted in the absence of any commercial or financial relationships that could be construed as a potential conflict of interest.

Generative AI statement

The author(s) declare that no Generative AI was used in the creation of this manuscript.

Publisher's note

References

Abera, W., Tamene, L., Kassawmar, T., Mulatu, K., Kassa, H., Verchot, L., et al. (2021). Impacts of land use and land cover dynamics on ecosystem services in the yayo coffee forest biosphere reserve, Southwestern Ethiopia. *Ecosyst. Serv.* 50, 101338. doi:10.1016/j.ecoser.2021.101338

Agudelo, C. A. R., Bustos, S. L. H., and Moreno, C. A. P. (2020). Modeling interactions among multiple ecosystem services. A critical review. *Ecol. Modell.* 429, 109103. doi:10.1016/j.ecolmodel.2020.109103

Aneseyee, A. B., Elias, E., Soromessa, T., and Feyisa, G. L. (2020). Land use/land cover change effect on soil erosion and sediment delivery in the winike watershed, omo gibe basin, Ethiopia. *Sci. Total Environ.* 728, 138776. doi:10.1016/j.scitotenv.2020.138776

Bennett, E. M., Peterson, G. D., and Gordon, L. J. (2009). Understanding relationships among multiple ecosystem services. *Ecol. Lett.* 12, 1394–1404. doi:10.1111/j.1461-0248.2009.01387x

Boithias, L., Acuña, V., Vergoñós, L., Ziv, G., Marcé, R., and Sabater, S. (2014). Assessment of the water supply: demand ratios in a Mediterranean Basin under different global change scenarios and mitigation alternatives. *Sci. Total Environ.* 470, 567–577. doi:10.1016/j.scitotenv.2013.10.003

Cord, A. F., Bartkowski, B., Beckmann, M., Dittrich, A., Hermans-Neumann, K., Kaim, A., et al. (2017). Towards systematic analyses of ecosystem service trade-offs and synergies: main concepts, methods and the road ahead. *Ecosyst. Serv.* 28, 264–272. doi:10.1016/j.ecoser.2017.07.012

Costanza, R., d'Arge, R., De Groot, R., Farber, S., Grasso, M., Hannon, B., et al. (1998). The value of the world's ecosystem services and natural capital. *Ecol. Econ.* 25, 3–15. doi:10.1016/S0921-8009(98)00020-2

Daming, H., Wenjuan, Z., and Yan, F. (2004). Research progress of international Rivers in China. *J. Geogr. Sci.* 14, 21–28. doi:10.1007/BF02841103

Da-ming, H., and Xuan-juan, L. (2001). Equitable utilisation and effective protection of sharing transboundary water resources: international Rivers of Western China. *J. Geogr. Sci.* 11, 490–500. doi:10.1007/BF02837978

Ding, Z., Jichun, T., Wenyong, T., Wang, K., Zhao, S., Song, W., et al. (2021). A graph theory into street network characteristics of the plain-type and the slope-type historical blocks: based on China's Southwestern regions. *Fundam. Res., ISUF 2020 Virtual Conf. Proc.* 104, 110. doi:10.1016/j.fmre.2021.02.002

Donohue, R. J., Roderick, M. L., and McVicar, T. R. (2012). Roots, storms and soil pores: incorporating key ecohydrological processes into Budyko's hydrological model. *J. Hydrol.* 436, 35–50. doi:10.1016/j.jhydrol.2012.02.033

Feng, Z., Chen, T., and Wu, J. (2021). Understanding trade-offs and synergies of ecosystem services to support the decision-making in the beig-tian-hebei region. *Land Use Policy* 106, 105446. doi:10.1016/j.landusepol.2021.105446

Fu, B. J., and Yu, D. D. (2016). Trade-off analyses and synthetic integrated method of multiple ecosystem services. *Resour. Sci.* 38, 1–9. doi:10.18402/resci.2016.01.01

Guo, B., Yang, F., Fan, Y., and Zang, W. (2023). The dominant driving factors of rocky desertification and their variations in typical mountainous karst areas of southwest China in the context of global change. *Catena* 220, 106674. doi:10.1016/j.catena.2022.106674

Hall, G. L., Thompson, B. R., Stanojevic, S., Abramson, M. J., Beasley, R., Coates, A., et al. (2012). The global lung initiative 2012 reference values reflect contemporary Australasian spirometry. *Respirology* 17, 1150–1151. doi:10.1111/j.1440-1843.2012.02232x

Hao, X., Yuan, S., and Prishchepov, A. V. (2023). Spatial-temporal heterogeneity of ecosystem service interactions and their social-ecological drivers: implications for spatial planning and management. *Resour. Conserv. Recy.* 189, 106767. doi:10.1016/j.resconrec.2022.106767

Kupfer, J. A., and Farris, C. A. (2007). Incorporating spatial non-stationarity of regression coefficients into predictive vegetation models. *Landsc. Ecol.* 22, 837–852. doi:10.1007/s10980-006-9058-2

Li, J. H. (2010). *The cultural interpretation of southwest settlement patterns*. Chongqing: Chongqing University.

Li, S. C., Zhang, C. Y., Liu, J. L., Zhu, W. B., Ma, C., and Wang, J. (2013). The tradeoffs and synergies of ecosystem services: research progress, development trend, and themes of geography. *Geogr. Res.* 32, 1379–1390. doi:10.1111/geor.12016

Li, Y., Zeng, C., Liu, Z., Cai, B., and Zhang, Y. (2022). Integrating landscape pattern into characterising and optimising ecosystem services for regional sustainable development. *Land* 11, 140. doi:10.3390/land11010140

Liang, S., Yang, F., Zhang, J., Xiong, S., and Xu, Z. (2024). Assessment and management zoning of ecosystem service trade-Off/Synergy based on the social-ecological balance: a case of the chang-zhu-tan metropolitan area. *Land* 13, 127. doi:10.3390/land13020127

Lin, L., and Gui, Y. (2024). Traditional culture of settlements associated with the natural environment: the case of yi minority southwest China. *J. Asian Archit. Build. Eng.* 24, 2411–2429. doi:10.1080/13467581.2024.2373822

Mueller, A. H., Szymanowski, L., Wallon, S., Gao, B. W., and Yuan, F. (2016). Sudakov resummations in mueller-navelet dijet production. *J. High. Energy Phys.* 2016, 96–24. doi:10.1007/JHEP03(2016)096

Peng, J., Hu, X. X., Zhao, M. Y., Liu, Y., and Tian, L. (2017). Research progress on ecosystem service trade-offs: from cognition to decision-making. *Acta Geogr. Sin.* 72, 960–973. doi:10.11821/dlxb201706002

Pereira, H. M., Martins, I. S., Rosa, I. M., Kim, H., Leadley, P., Popp, A., et al. (2024). Global trends and scenarios for terrestrial biodiversity and ecosystem services from 1900 to 2050. *Science* 384, 458–465. doi:10.1126/science.adn3441

Pergams, O. R., and Zaradic, P. A. (2008). Evidence for a fundamental and pervasive shift away from nature-based recreation. *Proc. Natl. Acad. Sci. U. S. A.* 105, 2295–2300. doi:10.1073/pnas.0709893105

Ramyar, R., Saeedi, S., Bryant, M., Davatgar, A., and Hedjri, G. M. (2020). Ecosystem services mapping for green infrastructure planning–the case of Tehran. *Sci. Total Environ.* 703, 135466. doi:10.1016/j.scitotenv.2019.135466

Raudsepp-Hearne, C., and Peterson, G. D. (2016). Scale and ecosystem services: how do observation, management, and analysis shift with scale-lessons from Québec. *Ecol. Soc.* 21, art16. doi:10.5751/es-08605-210316

Reid, W. V., Mooney, H. A., Cropper, A., Capistrano, D., Carpenter, S. R., and Chopra, K. (2005). *Ecosystems and human well-being-Synthesis: a report of the millennium ecosystem assessment*. Island Press. Available online at: https://research.wur.nl/en/publications/ecosystems-and-human-well-being-synthesis-a-report-of-the-millenn

Schirpke, U., Candiago, S., Vigl, L. E., Jäger, H., Labadini, A., Marsoner, T., et al. (2019). Integrating supply, flow and demand to enhance the understanding of interactions among multiple ecosystem services. *Sci. Total Environ.* 651, 928–941. doi:10.1016/j.scitotenv.2018.09.235

Shen, J., Tang, P., and Zeng, H. (2020). Does China's carbon emission trading reduce carbon emissions? Evidence from listed firms. *Energy sustain. Dev.* 59, 120–129. doi:10.1016/j.esd.2020.09.007

Shifaw, E., Sha, J., Li, X., Bao, Z., Ji, J., Ji, Z., et al. (2024). Ecosystem services dynamics and their influencing factors: synergies/tradeoffs interactions and implications, the case of upper Blue Nile basin, Ethiopia. *Sci. Total Environ.* 938. doi:10.1016/j.scitotenv.2024.173524

Tallis, H., Kareiva, P., Marvier, M., and Chang, A. (2008). An ecosystem services framework to support both practical conservation and economic development. *Proc. Natl. Acad. Sci. U. S. A.* 105, 9457–9464. doi:10.1073/pnas.0705797105

Tan, F., Lu, Z., and Zeng, F. (2024). Study on the trade-off/synergy spatiotemporal benefits of ecosystem services and its influencing factors in hilly areas of southern China. *Front. Ecol. Evol.* 11, 1342766. doi:10.3389/fevo.2023.1342766

Tomscha, S. A., and Gergel, S. E. (2016). Ecosystem service trade-offs and synergies misunderstood without landscape history. *Ecol. Soc.* 21, art43. doi:10.5751/ES-08345-210143

Tomscha, S. A., Sutherland, I. J., Renard, D., Gergel, S. E., Rhemtulla, J. M., Bennett, E. M., et al. (2016). A guide to historical data sets for reconstructing ecosystem service change over time. *BioScience* 66, 747–762. doi:10.1093/biosci/biw086

Wang, C., Ma, L., Zhang, Y., Chen, N., and Wang, W. (2022). Spatiotemporal dynamics of wetlands and their driving factors based on PLS-SEM: a case study in wuhan. *Sci. Total Environ.* 806, 151310. doi:10.1016/j.scitotenv.2021.151310

Wang, J., Wu, W., Yang, M., Gao, Y., Shao, J., Yang, W., et al. (2024). Exploring the complex trade-offs and synergies of global ecosystem services. *Environ. Sci. Ecotech.* 21, 100391. doi:10.1016/j.ese.2024.100391

Wang, Y., and Dai, E. (2020). Spatial-temporal changes in ecosystem services and the trade-off relationship in Mountain regions: a case study of hengduan Mountain region in southwest China. *J. Clean. Prod.* 264, 121573. doi:10.1016/j.jclepro.2020.121573

Wang, Z., Jiang, Q., and Jiao, Y. (2019). Traditional ecological wisdom in modern society: perspectives from terraced fields in honghe and chongqing, southwest China. *Ecol. Wis. Theory Pract.*, 125–148. doi:10.1007/978-981-13-0571-9_8

Xu, S., Liu, Y., Wang, X., and Zhang, G. (2017). Scale effect on spatial patterns of ecosystem services and associations among them in semi-arid area: a case study in Ningxia hui autonomous region, China. *China.* Sci. Total Environ. 598, 297–306. doi:10.1016/j.scitotenv.2017.04.009

Yahdjian, L., Sala, O. E., and Havstad, K. M. (2015). Rangeland ecosystem services: shifting focus from supply to reconciling supply and demand. *Front. Ecol. Environ.* 13, 44–51. doi:10.1890/140156

Yang, Y., Yuan, X., An, J., Su, Q., and Chen, B. (2024). Drivers of ecosystem services and their trade-offs and synergies in different land use policy zones of Shaanxi Province, China. *J. Clean. Prod.* 452, 142077. doi:10.1016/j.jclepro.2024.142077

Zhang, L., Guo, X., Li, J., Chen, Q., Wei, Y., and Zhao, X. (2020). Urbanization and its impact on ecosystem services: a review. *Sustainability* 12, 4725. doi:10.3390/s12114725

Zhao, R., Zhan, L., Yao, M., and Yang, L. (2020). A geographically weighted regression model augmented by geodetector analysis and principal component analysis for the spatial distribution of PM2.5. *Sustain. Cities Soc.* 56, 102106. doi:10.1016/j.scs.2020.102106

Zhou, M., Ma, Y., Wu, T., Zhang, S., and Chen, W. (2022). Modeling the impacts of land use changes on ecosystem services in a rapidly urbanizing.

frontiers | Frontiers in Environmental Science

TYPE Review
PUBLISHED 18 July 2025
DOI 10.3389/fenvs.2025.1610193

OPEN ACCESS

EDITED BY
Can Wang,
Southwest Jiaotong University, China

REVIEWED BY
Chen Zhang,
Institute of Loess Plateau, Shanxi University, China
Qiming Mao,
Central South University, China

*CORRESPONDENCE
Wei Zhou,
46752711@qq.com
Longzao Luo,
luolongzao@sru.edu.cn

†These authors have contributed equally to this work and share first authorship

RECEIVED 11 April 2025
ACCEPTED 09 July 2025
PUBLISHED 18 July 2025

CITATION
Qiao Z, Lin X, Zhang T, Luo S, Wang C, Zhou W and Luo L (2025) A review of research progress on the application of bryophytes in the ecological restoration of mining areas of China. *Front. Environ. Sci.* 13:1610193. doi: 10.3389/fenvs.2025.1610193

A review of research progress on the application of bryophytes in the ecological restoration of mining areas of China

Zhanrui Qiao[1,2†], Xiaoai Lin[3†], Tao Zhang[1,4], Shuigen Luo[5], Cunbao Wang[1,4], Wei Zhou[1,4*] and Longzao Luo[5*]

[1]Technology Innovation Center for Land Spatial Ecological Protection and Restoration in Great Lakes Basin, Ministry of Natural Resources of the People's Republic of China, Nanchang, Jiangxi, China, [2]The Eight Geological Team of Jiangxi Geological Bureau Shangrao, Shangrao, Jiangxi, China, [3]College of Life Science, Shangrao Normal University, Shangrao, China, [4]Jiangxi Provincial Institute of Land and Space Survey and Planning, Nanchang, Jiangxi, China, [5]School of Chemistry and Environmental Science, Shangrao Normal University, Shangrao, Jiangxi, China

The process of mining is invariably associated with ecological and environmental challenges within the mining region, making ecological restoration efforts in these areas especially crucial. Bryophytes, acting as key pioneer species, exhibit distinctive advantages and potential for application in the ecological restoration of mining sites. This study offered a concise overview of the fundamental traits of bryophytes, as well as their classification and distribution in mining regions across China using literature synthesis and field surveys. It primarily explored the role bryophytes played in the ecological restoration of such areas, the selection of appropriate bryophyte species, and cultivation techniques through systematic analysis. Additionally, the case studies of bryophytes' applications in ecological restoration within mining regions were analyzed. Results indicated that bryophytes in China's mining areas were diverse and widely distributed. Notably, bryophytes contributed to soil improvement, vegetation recovery, and the monitoring and indication of heavy metal pollution, with most demonstrating a robust tolerance to these contaminants. Future research should focus on screening suitable bryophytes, refining cultivation methods, and investigating their interactions with soil microorganisms.

KEYWORDS

bryophyte, mining area, ecological restoration, bryophyte ecological restoration, rapid cultivation

1 Introduction

Mining activities have significantly contributed to the economic development of mining regions and adjacent areas, but the detrimental impacts on the ecological environment cannot be underestimated. Prolonged mineral extraction has led to the destruction of surface vegetation, exacserbating soil erosion and degradation (Figure 1). These processes have reduced soil fertility and hinder vegetation recovery and growth (Chen et al., 2023). Furthermore, waste residues and effluents generated during mining operations have caused severe contamination of soil and water resources, posing threats to both the local ecosystem and public health (Feng et al., 2025). The resulting environmental degradation has also triggered a decline in biodiversity, disrupted ecological equilibrium, and destabilized the

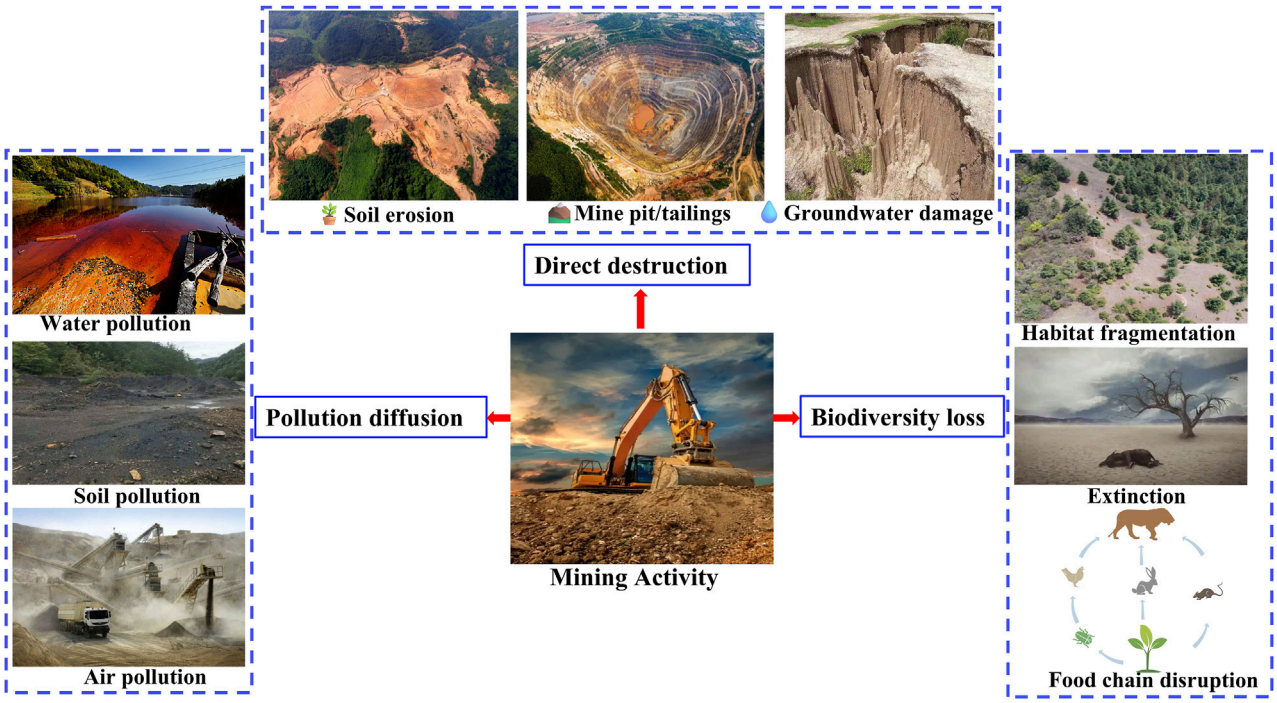

FIGURE 1
Impacts of mining activities on the ecological environment.

broader ecosystem (Chen et al., 2023). To mitigate these challenges, ecological restoration in mining areas is imperative. Effective strategies include vegetation rehabilitation, soil amelioration, water resource conservation, and heavy metal pollution remediation. These measures enhance environmental quality, conserve biodiversity, create sustainable economic opportunities, and ultimately advance the goals of ecological civilization and long-term sustainability (Feng et al., 2025). Given the severe ecological damage caused by mining activities, exploring effective ecological restoration strategies is imperative. Among these strategies, bryophytes offer unique advantages and potential, as detailed in the following sections.

Bryophytes act as pioneer species in ecological restoration, contributing to soil improvement and vegetation recovery through strong adaptability and tolerance to harsh environments. Although bryophytes possess a simple structure without true roots, stems, or leaves, these organisms thrive in harsh environments and are therefore regarded as pioneer species in vegetation restoration. Bryophytes demonstrate extraordinary vitality, capable of surviving in extreme environments such as barrenness, drought, and acidity. Additionally, these plants exhibit excellent soil-binding and water-retaining abilities, which effectively control soil erosion and improve soil structure (Cao et al., 2020). Unlike conventional methods (e.g., vascular plant seeding, chemical stabilization), bryophytes establish on degraded slopes without soil replacement/amendment, reducing long-term maintenance costs through minimized reseeding or chemical applications. Furthermore, bryophytes can absorb carbon dioxide and release oxygen through photosynthesis, improving air quality and creating favorable conditions for the growth of other organisms. Bryophytes assimilate atmospheric carbon dioxide via photosynthesis and convert it into organic carbon stored within biomass, thereby contributing to long-term carbon sequestration. This process holds substantial relevance for advancing China's "dual carbon" goals. Bryophytes regulate net carbon dioxide emissions via litter input, photosynthesis, and respiration (Elbert et al., 2012). For example, *Sphagnum* contributes more than half of the world's peat, accounting for 10%–15% of terrestrial carbon storage (Zhu, 2022). Therefore, bryophytes are ideal materials for ecological restoration and have shown great potential in the ecological restoration of mining areas.

In recent years, extensive research has been conducted globally on the application of bryophytes in ecological restoration of mining areas. Internationally, universities and research institutions have validated the efficacy of bryophytes under diverse environmental conditions through experimental studies. Notable examples include investigations in Ukraine (Lobachevska et al., 2019), Canada (Liu et al., 2024), Slovakia (Širka et al., 2018), the United States (Stern et al., 2016), Turkey (Karakaya et al., 2015), Portugal (Anawar et al., 2013), Poland (Rola and Osyczka, 2018), and Japan (Suzuki et al., 2016), which collectively highlight the adaptability of bryophytes in varying mining contexts. In China, significant advancements have also been achieved. For example, researchers from Sichuan University showed that bryophyte mats not only significantly reduced rainfall-induced heavy metal migration (particularly Cd and Cu) but also improved critical soil characteristics including pH regulation, cation exchange capacity, and bulk density optimization. These improvements further stimulated microbial community diversity and abundance in pyritic tailings (Lin K. K. et al., 2024). Investigations by research groups from Wuhan City and Guizhou Province characterized bryophyte assemblages in mining

TABLE 1 Morphological and structural characteristics of bryophytes.

Characteristic	Specific manifestation	Ecological significance
Morphological structure	Absence of vascular tissues, rhizoids composed of uniseriate cells (not unicellular)	Reduced metabolic consumption; adaptation to nutrient-poor substrates
Water metabolism	Direct water absorption through leaves, low transpiration rate (0.5–2.0 mmol m^{-2} s^{-1})	Drought tolerance, maintenance of microhabitat humidity
Reproductive strategy	High spore production (>10^6 per plant), regenerative capacity of vegetative propagules (<2 mm)	Rapid colonization, facilitation of community succession

areas through community architecture (Pengpeng et al., 2023; Han et al., 2022; Huang and Zhang, 2017; Ji and Zhang, 2015; Jiang and Zhang, 2012; Pan and Zhang, 2011), metallophyte adaptation (Pengpeng et al., 2023; Ma et al., 2023), life history strategies (Liao et al., 2024), and restoration ecology applications (Ren et al., 2021). Furthermore, scholars explored bryophyte community dynamics and artificial cultivation techniques in rare earth mining regions of southern Jiangxi Province, providing critical insights for region-specific restoration practices (Kong et al., 2023; Shen et al., 2022).

Despite the significant potential of bryophytes in ecological restoration of mining areas, practical application of bryophytes in ecological restoration faces persistent challenges. Key issues include the selection of species adapted to site-specific environmental conditions, optimization of planting techniques and management protocols, and the development of robust evaluation frameworks to assess restoration efficacy. These challenges demand immediate attention, as unresolved limitations may hinder the scalability and long-term success of bryophyte-based restoration strategies. Consequently, advancing research on the mechanistic roles of bryophytes and refining technical methodologies is critical for enhancing restoration technologies and accelerating ecological recovery. Through a systematic review and meta-analysis of global case studies, this work evaluated the practical viability of bryophytes in mining area restoration, aiming to bridge knowledge gaps and inform future scientific and engineering endeavors.

2 Biological characteristics and ecological functions of bryophytes

2.1 Morphological characteristics and adaptive traits

Bryophytes, classified as non-vascular plants, lack true roots and vascular tissues. The morphology is typically characterized by small stature, green leaf-like structures, and simple thalloid or foliose gametophytes, accompanied by distinct reproductive organs (Table 1). Reproduction occurs through sexual (spore dispersal) and asexual strategies (vegetative fragmentation, stem segment regeneration, and clonal colonization via specialized structures like gemmae) (Wang et al., 2022). Notably, bryophytes exhibit exceptional environmental adaptability, thriving under extreme conditions such as drought, low temperatures, nutrient-poor substrates, and limited light availability (Wang et al., 2022). Additionally, bryophytes demonstrate remarkable tolerance to abiotic stressors, including high salinity, acidic pH, and elevated heavy metal concentrations (Lin X. et al., 2024; Guan and Zhang, 2020). These adaptive traits underpin their ecological resilience in mining areas, where harsh environments (e.g., metal-contaminated soils, unstable substrates) necessitate robust survival mechanisms. Consequently, bryophytes serve as pivotal agents in mining area restoration by stabilizing substrates, enhancing microhabitat conditions, and facilitating secondary succession.

2.2 Role of bryophytes in ecological restoration in mining areas

Bryophytes play a pivotal role in ecological restoration within mining areas, particularly through capacity to rehabilitate degraded soils (Figure 2). During growth, bryophytes accumulate substantial organic matter, which enhances soil structure and fertility, thereby establishing a nutrient-rich foundation for subsequent vegetation recovery (Chun et al., 2021). The water absorption capability of bryophytes reduce soil moisture evaporation, improving water-holding capacity and creating optimal hydration conditions for plant regeneration (Chun et al., 2021). Furthermore, bryophytes secrete organic acids that chelate mineral ions, forming insoluble complexes. These complexes, combined with bryophyte detritus, facilitate the accumulation of soil organic matter, ultimately elevating nutrient availability and promoting vascular plant establishment (Feng et al., 2022). Empirical validation from the Shengli Coal Mine reclamation project in Inner Mongolia confirmed fundamental bryophyte-soil synergies, with statistical analyses demonstrating significant positive correlations between bryophyte colonization density and critical soil nutrient parameters including total nitrogen content and phosphorus availability across rehabilitation chrono sequences. Bryophyte distribution patterns further aligned with microscale improvements in organic matter stabilization and biogeochemical cycling efficiency, establishing these non-vascular plants as both biomarkers and active mediators of pedogenic recovery in post-mining ecosystems (Chun et al., 2021). Similarly, long-term studies on a potassium-magnesium salt tailings pond in Sweden revealed that natural succession over decades led to the formation of resilient biological soil crusts dominated by bryophytes, lichens, and cyanobacteria. These crusts demonstrated high tolerance to heavy metals (e.g., Cd, Pb) and effectively restored soil functionality by stabilizing substrates and enhancing microbial activity (Lobachevska et al., 2019). Complementary research by Ren et al. in manganese slag areas further highlighted the role of bryophytes in enriching bioavailable nutrients and diversifying soil microbial communities, which collectively primed the environment for vascular plant

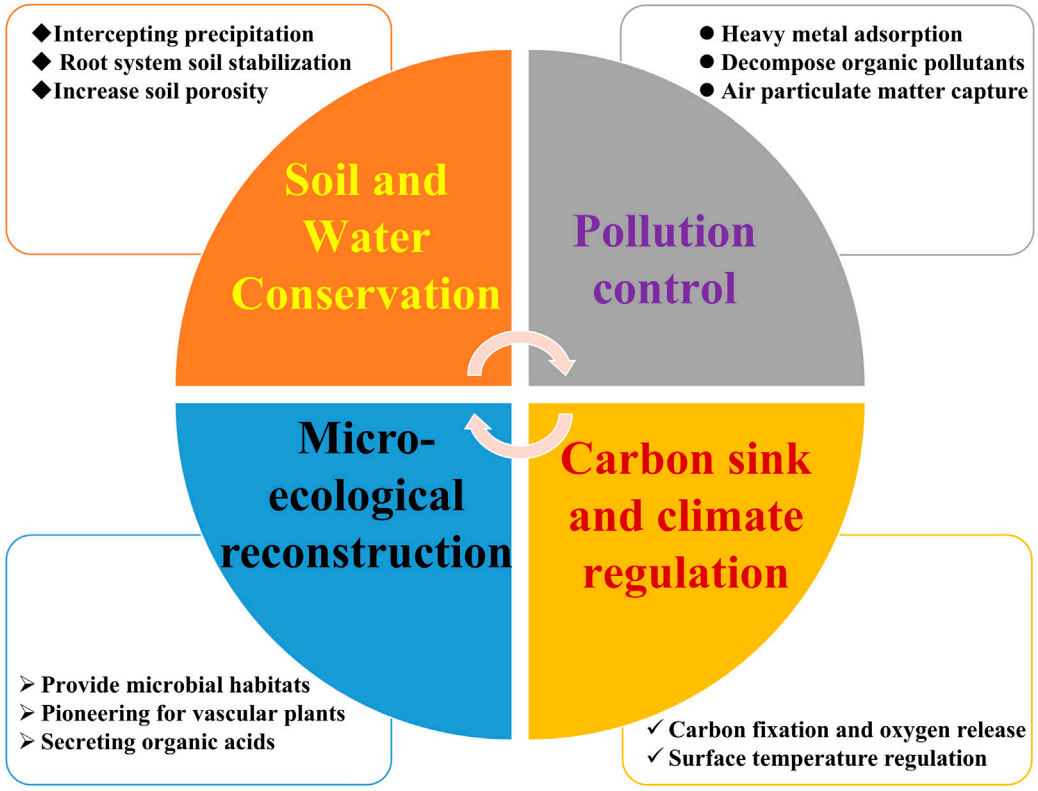

FIGURE 2
Ecological functions of bryophytes.

colonization (Ren et al., 2021). These findings underscore the pivotal role of bryophytes in initiating ecological succession, which is further explored in the following section on species screening.

As pioneer species in mining area restoration, bryophytes colonize exposed slag surfaces, creating foundational soil and moisture conditions for subsequent vegetation establishment (Chun et al., 2021). The collaborative interactions with algae, lichens, bacteria, and fungi drive the formation of biological soil crusts (BSCs). BSCs stabilize substrates, mitigate erosion, and shield emerging plant communities during early succession (Song et al., 2018). Beyond physical protection, bryophytes regulate soil microenvironments by modulating temperature fluctuations and enhancing moisture retention, thereby optimizing conditions for vascular plant recruitment (Gao et al., 2017). Field investigations in rare earth tailing ecosystems revealed the crucial ecological functions of bryophytes. Shen et al. recognized T*richostomum brachydontium*, *T. involutum*, *Anoectangium stracheyanum*, and *Brachymenium exile* as stress-adapted bryophyte species that can expedite revegetation via rapid substrate stabilization (Shen et al., 2022). Similarly, Širka et al. measured the contributions of bryophytes to biodiversity restoration in Central Slovakian mercury and copper slag heaps. Total of 83 and 76 bryophyte taxa were reported respectively. These bryophytes together increased species richness and promoted successional paths (Širka et al., 2018).

Bryophytes act as potent bioindicators in mining areas due to high heavy metal capability. Quantifying metal concentrations in bryophyte tissues (e.g., Cu, Pb, Cd) provides a reliable proxy for assessing soil pollution levels, with elevated values directly correlating to anthropogenic mining impacts (Ren et al., 2020). Moreover, changes in bryophyte communities, particularly increases in the number of species and their diversity, can be used to measure the success of ecological restoration. This is because a greater variety of species often indicates better habitat conditions (Feng et al., 2022). Field investigations in Wanshan mercury mining district in Guizhou Province demonstrated that mercury speciation analysis (total Hg and methyl-Hg concentrations) in seven bryophyte species effectively tracked atmospheric Hg pollution sources and quantified spatiotemporal dispersion gradients. This biomonitoring approach revealed distinct species-specific accumulation patterns correlated with industrial emission profiles and microclimatic deposition dynamics (Cao et al., 2016). Although lichens and bryophytes are well-known for indicating air quality, their potential for diagnosing soil pollution is not fully used. Notably, Rola and Osyczka documented that lichen-bryophyte consortia in southern Poland's Zn-Pb mining zones exhibited high sensitivity to soil metal gradients, enabling quantitative estimation of contamination severity (Rola and Osyczka, 2018). Similarly, in Turkey's Giresun sulfide deposits, *Rhabdoweisia crispata*, *Pohlia nutans*, and *Pohlia elongata* showed remarkable metal accumulation capabilities, which could be ascribed to the absence of cuticles and cation-exchangeable cell walls (Karakaya et al., 2015). Japanese researchers further identified *Scopelophila cataractae* as a dual Cu-As hyperaccumulator in aquatic systems

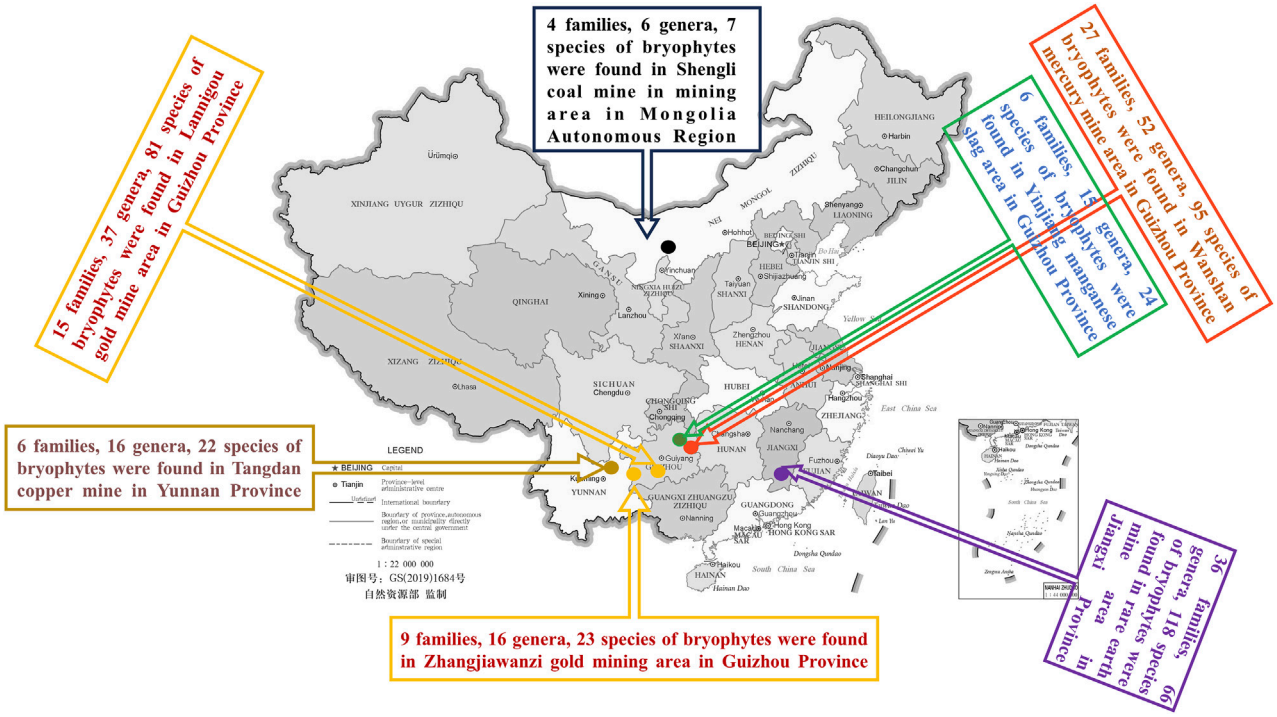

FIGURE 3
Distribution of bryophyte species in different types of mines in China.

TABLE 2 Comparison of species diversity and heavy metal enrichment characteristics of bryophytes in Chinese mining areas.

Mine type	Representative mine	Number of moss species	Dominant families	Heavy metal enrichment ability	Typical data source
Copper mine	Tangdan Copper Mine in Yunnan Province	22 species	*Pottiaceae*	68% of species inhabited patinated cupreous rocks and 32% cupreous soil	Zhou and Zhang (2007)
Gold mine	Guizhou Zhangjiawanzi Gold Mine	23 species	*Pottiaceae* and *Bryaceae*	Gymnostomum subrigidulum has a strong ability to enrich Cd, with an enrichment coefficient of 5.58 for Cd	Bing and Zhaohui (2008)
Mercury Mine	Guizhou Wanshan Mercury Mining Area	95 species	*Hypnaceae*, *Thuidiaceae* and *Brachytheciaceae*	With total mercury contents of 120–450 mg kg^{-1}, methylmercury contents of 0.8–3.2 mg kg^{-1}	(Pan and Zhang (2011), Cao et al. (2016)
Manganese Mine	Guizhou Yinjiang Manganese Slag Area	24 species	*Pottiaceae* and *Bryaceae*	Mn enrichment coefficient of 0.009–0.212, Cd enrichment coefficient of 0.754–5.360	Ren et al. (2021)
Rare Earth Mine	Jiangxi South rare earth ion-type mine	118 species	*Polytrichaceae, Dicranales, Fissidentales* and *Pottiales*	—	Kong et al. (2023), Cai et al. (2023)
Coal Mine	Inner Mongolia Shengli Coal Mine	7 species	*Ditrichaceae*, *Bryaceae*, *Funariaceae* and *Pottiaceae*	—	Feng et al. (2022)

near copper tailings, demonstrating bryophytes' niche-specific adaptation to polymetallic stress (Suzuki et al., 2016).

2.3 Distribution characteristics of bryophytes in mining areas of China

There are approximately 3,108 bryophyte species spanning 160 families and 632 genera in mining areas of China, demonstrating exceptional diversity and stress adaptation (Zhu et al., 2022). Recent research prioritizes the spatial heterogeneity and metal hyperaccumulation capacities, particularly regarding bioremediation mechanisms in post-mining ecosystems. Figure 3; Table 2 systematically presented the bryophyte species and the heavy metal enrichment characteristics in copper, gold, manganese, rare earth, and coal mining areas in China.

2.3.1 Copper mines

The Tangdan Copper Mine in Yunnan Province's metallogenic belt exemplified extreme edaphic constraints on bryophyte

colonization, sustaining merely six families (e.g., *Pottiaceae*, *Mniaceae*) with 68% of observed species selectively inhabiting Cu-oxide encrustations rather than Cu-saturated soils. This niche partitioning showed specialized substrate optimization. Protonemal attachment and exocellular metal exclusion strategies allowed survival in Cu-rich environments (Zhou and Zhang, 2007).

2.3.2 Gold mines

The Zhangjiawanzi and Lanni Gou gold mines in Guizhou Province exhibited striking bryophyte community contrasts driven by microenvironmental heterogeneity. At Zhangjiawanzi, 23 species (16 genera, 9 families) demonstrated extreme oligotrophic adaptation. The families *Polytrichaceae* and *Bryaceae* were particularly dominant, indicating a preference for the nutrient-poor, acidic soils often found in gold mine environments. In contrast, the nearby Lanni Gou Gold Mine boasted a richer bryophyte community, with 81 species spread across 37 genera and 15 families, pointing to a greater ecological complexity and a higher level of biodiversity in this area (Bing and Zhaohui, 2008).

2.3.3 Mercury mines

The Wanshan Mercury Mine in Guizhou Province presented a striking contrast to typical mining environments, with a notable diversity of 95 bryophyte species spanning 52 genera and 27 families. This remarkable biodiversity might stem from the unique ecological niches formed by mercury extraction activities, which created heterogeneous microhabitats. A parallel example from Yunchangping Town, also in Guizhou Province, documented 62 bryophyte species over a 1-year period. These findings underscored the resilience and adaptability of bryophyte communities in heavily contaminated environments, suggesting high dynamic capacity to colonize and thrive under persistent heavy metal stress (Pan and Zhang, 2011).

2.3.4 Manganese mines

A 50-year-old manganese slag heap in Guizhou Province has developed into a distinct bryophyte refuge, supporting 20 taxa dominated by the structurally resilient families *Bryaceae* and *Polytrichaceae*. In the manganese slag area of Yinjiang County, 24 bryophyte species were found. *Gymnostomum subrigidulum*, *Pohlia gedeana*, and *Bryum atrovirens* were the most common, probably because they can tolerate high levels of metals. By contrast, the electrolytic manganese slag area in Songtao County hosted a depauperate bryophyte community of just six species, reflecting harsher edaphic or microclimatic conditions. Strikingly, *B. atrovirens* populations in both regions exhibit dual hyperaccumulation of manganese and cadmium. This remarkable ability of *B. atrovirens* to bind metals makes it a prime candidate for phytostabilization efforts in ecosystems contaminated with heavy metals (Ren et al., 2021).

2.3.5 Rare earth mines

In Jiangxi Province, ion-adsorption rare earth mines presented a unique ecological scenario where bryophyte biocrusts played a crucial role in shaping microbial community diversity and structure. Land-use intensity and anthropogenic disturbances strongly mediated bryophyte distribution patterns, with soil moisture regimes and substrate stability identified as key determinants of habitat suitability. Erect-growing forms were the most common in these groups, a trait that likely helps them retain moisture and stabilize soil in damaged areas. This ecological specialization positioned bryophytes as pivotal agents for post-mining revegetation, offering a natural template for restoring biogeochemical cycles in leached soils (Kong et al., 2023). Building on this, Cai et al. demonstrated that targeted bryophyte cultivation could accelerate ecosystem recovery pathways, leveraging dual role in microbial habitat provisioning and physical substrate rehabilitation (Cai et al., 2023).

2.3.6 Coal mines

In the semi-arid steppes of Inner Mongolia Autonomous Region, the Shengli Coal Mine was a key test site for studying how bryophytes adapt to post-industrial environments. Bryophyte assemblages here were tightly mediated by soil edaphic filters, particularly pH gradients and silt content, which served as deterministic forces structuring community composition. Only 7 bryophyte species were observed in the Shengli Coal Mine, likely due to aridity and alkaline soils limiting diversity. These findings revealed that the physical and chemical characteristics of the soil play a pivotal role in determining the species composition and distribution of bryophytes in coal mine environments (Feng et al., 2022).

Together, these studies delineated bryophytes as biodiversity hotspots within China's mining regions, showcasing not only wide biogeographic range but also evolutionarily refined heavy metal detoxification pathways. The capacity to dominate oligotrophic, metal-laden substrates underscored the dual ecological role as pioneers in primary succession and engineers of microhabitat amelioration. This dominance is further underpinned by critical interactions with soil microbiomes, including the secretion of organic acids (e.g., oxalate) for nutrient solubilization and metal bioavailability control, as well as stress-alleviating fungal symbioses that form nutrient-sharing networks analogous to mycorrhizae. Crucially, this functional resilience positioned bryophytes as keystone species for phytostabilization protocols and bioindicator frameworks. These distribution patterns further exemplify niche partitioning theory, with species like *B. atrovirens* (Mn-Cd hyperaccumulator) and *G. subrigidulum* occupying distinct ecological niches. Metal toxicity and edaphic filters shape these niches, driving community assembly through resource-use differentiation (Table 2).

3 Mine-adapted bryophytes screening

Screening aimed to identify bryophyte species with high adaptability to the harsh environmental conditions of mining areas, such as heavy metal contamination, soil erosion, and extreme pH levels. The selection of bryophyte species suitable for mining ecosystem rehabilitation was guided by a multi-criteria screening framework that integrates environmental tolerance, functional performance, and ecological benefits (Figure 4). The screening criteria encompassed five key parameters: (1) Tolerance to Heavy Metals, defined as the ability to survive and proliferate in soils contaminated with elevated concentrations of toxic elements, (2) Soil Adaptation, reflecting the capacity to establish in nutrient-poor substrates characterized by low organic matter and extreme pH ranges, (3) Drought Resistance, quantified through survival rates under prolonged water scarcity and post-dehydration recovery

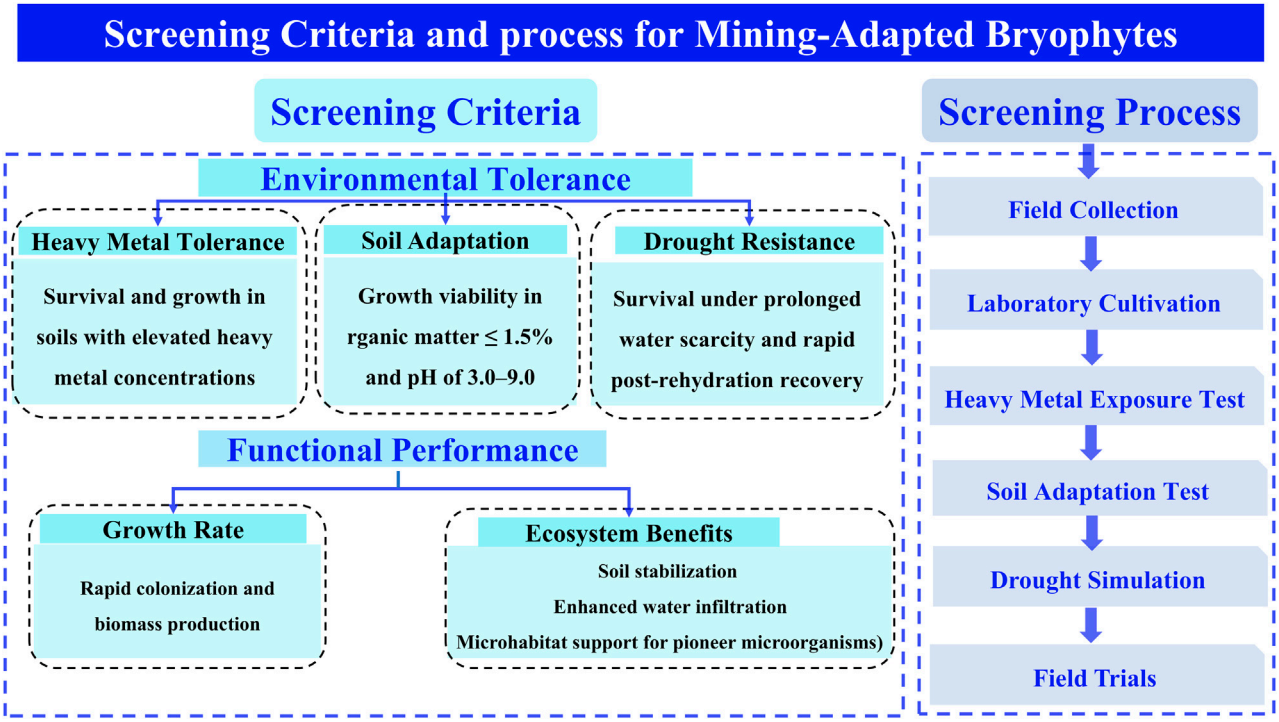

FIGURE 4
screening criteria and process for mining-adapted.

efficiency, (4) Growth Rate, prioritizing species with rapid colonization and high biomass accumulation, and (5) Ecosystem Benefits, including soil stabilization via rhizoid networks, enhanced water infiltration capacity, and facilitation of microbial symbionts.

The screening process followed a sequential experimental protocol (Figure 4). Initially, bryophyte samples were collected from naturally occurring populations in mining-impacted zones or analogous degraded ecosystems. These specimens underwent laboratory cultivation under controlled light, temperature, and humidity to assess baseline growth dynamics and stress resilience. Subsequent heavy metal exposure tests employed dose-response assays to evaluate metal tolerance thresholds and bioaccumulation potential. Concurrently, soil adaptation tests measure establishment successed in mining-derived substrates, with performance metrics including shoot elongation rate and biomass partitioning. Drought simulation experiments utilized osmotic stress gradients to quantify desiccation tolerance and rehydration recovery kinetics. Finally, candidate species demonstrating robust laboratory performance were subjected to field trials involving transplantation to target mining sites, where long-term viability, ecological integration, and functional efficacy were monitored over ≥2 growing seasons. This systematic approach ensured the identification of bryophyte species that align with site-specific rehabilitation goals while minimizing ecological risks.

Researchers systematically evaluated bryophyte species to identify candidates with high adaptability, rapid growth rates, and multifunctional ecological benefits for mining area restoration. Selected species exhibited exceptional survival rates and restoration efficacy under harsh mining conditions. Early research emphasized the pioneering role of bryophytes in ecological restoration, particularly the drought tolerance (xerophytic adaptation), resilience to nutrient-poor substrates, and prolific reproductive strategies, which collectively prime degraded sites for subsequent vegetation recovery (Sun et al., 2004; Zuo et al., 2006). For instance, Sun et al. assessed the feasibility of bryophyte-mediated restoration in Jiuzhaigou Valley's post-disaster landscapes, identifying key constraints (e.g., substrate instability) requiring mitigation in practical applications (Sun et al., 2004). Subsequent studies shifted focus to drought resistance screening. Through controlled drought simulations, Li et al. identified three hyper-tolerant bryophyte species (e.g., *Bryum argenteum*) in northern Hebei Province and optimized the cultivation protocols for slope stabilization (Li, 2017). Following the Jiuzhaigou earthquake, Xia et al. developed an Analytic Hierarchy Process (AHP)-based evaluation framework to prioritize bryophyte species for revegetating exposed slopes. Criteria included stress tolerance, propagule availability, ecological functionality, reproductive capacity, biomass yield, and aesthetic value. This approach selected five species—*Racomitrium japonicum*, *Hypnum plumaeforme*, *Eurohypnum leptothallum*, *Plagiomnium acutum*, and *Brachythecium rutabulum*—for targeted slope greening (Xia et al., 2023).

4 Cultivation of bryophytes

Figure 5 outlined a standardized *in vitro* protocol for bryophyte rapid propagation, integrating surface sterilization, hormone-

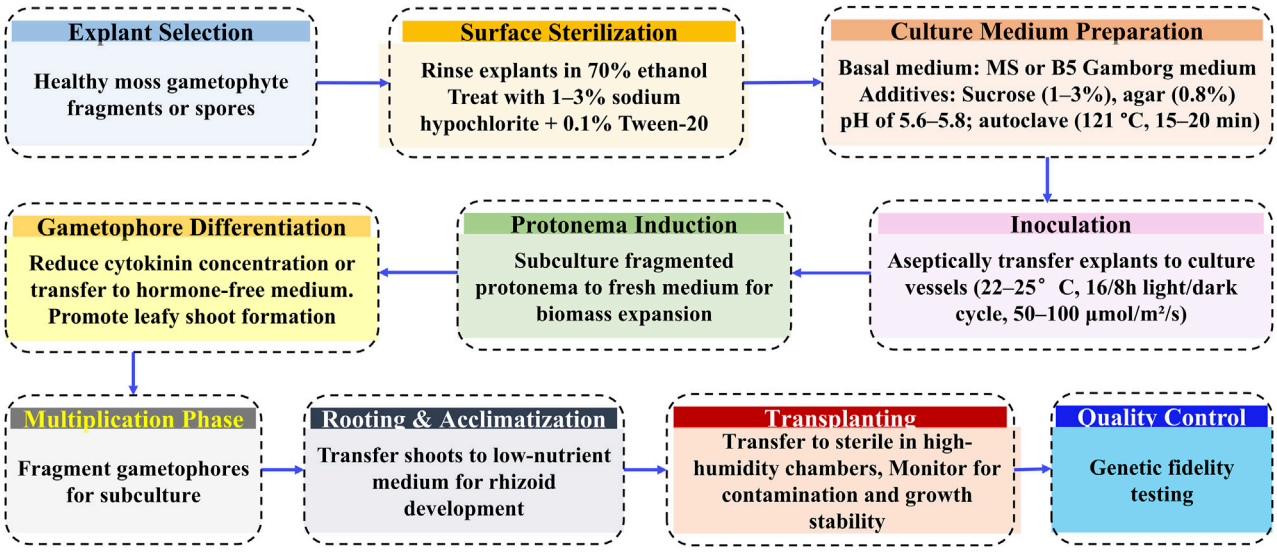

FIGURE 5
Rapid propagation scheme for bryophytes.

regulated differentiation, and cyclic subcultures to achieve high-efficiency biomass production while maintaining genetic uniformity and pathogen-free status. This optimized protocol enabled rapid clonal propagation of bryophyte species (e.g., *Physcomitrium* patens) through surface-sterilized gametophyte explants cultured on hormone-supplemented media (MS/B5) under controlled light and temperature. Protonema induction, cytokinin-mediated gametophore differentiation, and cyclic subcultures ensured scalable biomass production, followed by acclimatization on low-nutrient substrates. Genetic fidelity and contamination-free status were validated via molecular assays, supporting applications in research and ecological restoration.

Common methods for bryophyte cultivation include stem cutting propagation and tissue culture rapid propagation. Stem cutting propagation technology can rapidly propagate certain bryophyte species and adapt to artificial environmental control. For example, Chen et al. successfully identified the suitable environmental conditions and propagation factors for the feather bryophyte in artificial culture through stem cutting propagation experiments, providing an efficient rapid propagation method for stone slope greening and ecological restoration (Chen et al., 2022). Additionally, the application of tissue culture technology has made rapid propagation of bryophytes possible while ensuring the genetic stability of the seed sources (Zhang X. et al., 2023). Taking Yue's research as an example, rapid propagation of bryophytes was achieved by inducing callus formation, adventitious buds, and adventitious roots (Huanli, 2009). Huang et al. used four wild bryophyte species from a uranium tailings area as materials to explore the effects of different pH, temperature, cultivation substrates, and plant growth regulators on bryophyte growth and established the rapid propagation techniques for the grey bryophyte, large grey bryophyte, sharp-leafed creeping light bryophyte, and scale bryophyte (Huang et al., 2019). Although bryophyte cultivation techniques have made some progress, there are still some challenges. The application scalability of bryophytes is compromised by poikilohydric constraints, particularly slow biomass accrual rates and multi-year reproductive maturation periods, requiring targeted culturing innovations to overcome these physiological barriers. Spore propagation is greatly influenced by environmental factors, and its germination rate and survival rate are usually low. Moreover, bryophytes have strict requirements for the growth environment, necessitating precise control of light, water, temperature, and other conditions, which can lead to relatively high cultivation costs.

In recent years, important research achievements have been made in the field of bryophyte cultivation techniques. Studies indicate that bryophyte species possess different preferences for cultivation substrates. Common cultivation substrates like peat, perlite, and vermiculite demonstrate high compatibility with multiple bryophyte species. This was exemplified by a Canadian case study on lithium mine waste rock revegetation in Quebec, where bryophyte regeneration success rates showed significant variation depending on substrate composition and microenvironmental conditions (Liu et al., 2024). Meanwhile, special substrates such as volcanic rock and forest humus have a significant promotional effect on the growth of certain bryophyte species (Shi et al., 2022). Through proportional experiments with different substrates, researchers can select the most suitable ratio for the growth of specific bryophytes. For example, a volume ratio of peat to vermiculite of 2:1 is most beneficial for the growth of short-toothed bryophyte (Yu et al., 2024). In terms of environmental factors, light intensity is a key factor affecting bryophyte growth. Studies have shown that moderate shading helps the growth of certain bryophyte species (Fazan et al., 2022). Water and temperature are also limiting factors for bryophyte growth. Appropriate watering and a suitable temperature range can promote bryophyte growth, while excessive watering or extreme temperatures can inhibit bryophyte growth (Slate et al., 2024; Zhang Y. et al., 2023).

5 Application cases of bryophytes in mine ecological restoration

5.1 Application of bryophytes in ecological restoration of limestone mine slopes in northern Guangxi Province

Guangxi Province is one of China's representative regions for karst landscapes, rich in limestone resources. In the past, simple open-pit mining methods severely damaged the landforms and vegetation in mining areas, making ecological restoration research critical. Li conducted a case study at the Tieshan Quarry (Qixing District, Guilin City, Guangxi Province) to investigate bryophyte-based ecological restoration on limestone mine slopes. The mining area located in a subtropical monsoon climate zone with brown-gray limestone soil. Open-pit mining has damaged the land, vegetation, mountain structures, and rock and soil exposures. By integrating drone surveys with ground-based observations, a 3D terrain model was developed and six bryophyte species across five families and six genera were identified, with *Barbula unguiculata* as the dominant taxon. The study revealed that climatic temperature-humidity fluctuations critically regulate bryophyte colonization, while an optimized protocol combining crushed bark inoculation, Hoagland solution application, and intermittent misting achieved a coverage of 7.18% within 20 days, which was much higher than the control treatment (0.17%) (Li, 2023).

5.2 Application of bryophytes in semi-underground space ecological restoration of a 100-m deep mining pit

In karst areas, abandoned mining pits often have complex geological conditions due to post-mining changes like increased karstification and more fissures in rock walls. This makes it hard for plants to grow and difficult to redevelop the land. In the ecological restoration of Xinsheng Cement Plant's abandoned mining pit (Changsha City, Hunan Province), a novel rapid greening technology was developed using cold-tolerant bryophytes and biodegradable bio-glue for concrete and rock wall stabilization (Li et al., 2021). Through rigorous species screening, xerophytic mosses with 99.5% survival rates under high solar irradiance and drought stress were selected. This approach significantly accelerated plant community succession, transforming the degraded site into the "Joyful Paradise" landscape within 12 months. This ecological engineering approach created synergistic value chains where bryophyte-mediated slope stabilization enhanced biodiversity, which in turn attracted nature-based tourism while empowering local stakeholders through hands-on restoration workshops.

These applications operationalize ecological succession theory. Bryophytes act as early-successional engineers that accelerate trajectory shifts from degraded to functional states. Bryophyte restoration helps achieve UN Sustainable Development Goals by naturally repairing damaged land. Bryophytes act as pioneer species that form erosion-proof living crusts on degraded sites like mines, supporting SDG 15 for terrestrial ecosystems. These organisms capture carbon three to five times more effectively than regular plants, directly advancing climate action under SDG 13, with peat mosses alone locking away 10%–15% of the world's land-based carbon. Dense mats of bryophytes also filter toxic metals from runoff, protecting water quality for SDG 6. Unlike traditional methods that often need chemicals or repeated planting, bryophyte solutions eliminate pollution while cutting long-term costs. By creating self-sustaining microhabitats that boost biodiversity, bryophytes offer a practical nature-based path to meet global sustainability targets in challenging environments.

6 Conclusion

Bryophytes are emerging as pivotal agents in mining ecosystem restoration, bridging applied remediation needs with fundamental ecological research due to strong adaptability, soil-binding ability, and heavy metal enrichment capacity. While substantial progress has been made in laboratory settings, field implementation challenges persist, particularly regarding scaling propagation protocols and ensuring survivability in oligotrophic substrates or metal-contaminated environments. Notably, tolerant species immobilize contaminants through exclusion/detoxification mechanisms, enabling phytostabilization, whereas hyperaccumulators actively concentrate metals in harvestable tissues for phytoextraction, which requires distinct deployment strategies to avoid ecological risks. Moreover, overcoming key practical barriers, notably high propagation costs, slow growth rates, and the logistical complexity of large-scale deployment, remains critical for enhancing the scalability and economic feasibility of bryophyte-based restoration as a transformative ecological strategy. Future research should prioritize three interconnected fronts: 1) conducting long-term monitoring studies on bryophyte-based restoration projects, 2) exploring the combined use of bryophytes with other plant species for enhanced restoration outcomes, and 3) refining species-specific cultivation matrices through machine learning optimization, deciphering bryophyte-microbiome synergies governing metal (loid) sequestration, and mapping epigenetic adaptation pathways under climate fluctuation scenarios. These investigations will catalyze next-generation phytostabilization technologies while advancing ecological theory on pioneer species' roles in anthropogenic landscape rehabilitation.

Author contributions

ZQ: Conceptualization, Writing – original draft, Data curation, Methodology. XL: Formal Analysis, Writing – original draft. TZ: Writing – original draft, Methodology, Validation, Investigation. SL: Writing – review and editing, Conceptualization, Resources. CW: Writing – review and editing, Writing – original draft, Formal Analysis. WZ: Formal Analysis, Writing – review and editing. LL: Supervision, Writing – review and editing, Investigation, Project administration.

Funding

The author(s) declare that financial support was received for the research and/or publication of this article. This work was funded by the Open Project of Technology Innovation Center for Land Spatial Ecological Protection and Restoration in Great Lakes Basin, MNR, grant number No. JXCXZX2024007.

Conflict of interest

The authors declare that the research was conducted in the absence of any commercial or financial relationships that could be construed as a potential conflict of interest.

Generative AI statement

The author(s) declare that Generative AI was used in the creation of this manuscript. Generative AI was used to grammar, spelling errors, etc.

Publisher's note

All claims expressed in this article are solely those of the authors and do not necessarily represent those of their affiliated organizations, or those of the publisher, the editors and the reviewers. Any product that may be evaluated in this article, or claim that may be made by its manufacturer, is not guaranteed or endorsed by the publisher.

References

Anawar, H. M., Canha, N., Santa-Regina, I., and Freitas, M. C. (2013). Adaptation, tolerance, and evolution of plant species in a pyrite mine in response to contamination level and properties of mine tailings: sustainable rehabilitation. *J. Soils Sediments* 13, 730–741. doi:10.1007/s11368-012-0641-7

Bing, L., and Zhaohui, Z. (2008). Studies on the bryophytes and analysis of ecological restore potential in the lannigou gold deposit, Guizhou province. *J. Trop. Subtropical Bot.* 16, 511–515. doi:10.3969/j.issn.1005-3395.2008.6.2047

Cai, Q. Y., Li, B., Cai, M. T., Liu, Y. Z., Wu, L., and Ge, G. (2023). Diversity and distribution of bryophytes in ion-type rare Earth mines in southern Jiangxi province, southeast China, and the implications for vegetation restoration. *Plant Soil* 484, 79–94. doi:10.1007/s11104-022-05771-0

Cao, A., Ao, M., Liang, L., Xu, X., Qiu, G., and Chen, Z. (2016). Mercury concentration in epilithic mosses and its bio-indication of atmospheric Mercury pollution. *Huanjing Huaxue-Environmental Chem.* 35, 2204–2210. doi:10.7524/j.issn.0254-6108.2016.10.2016022505

Cao, W., Xiong, Y. X., Zhao, D. G., Tan, H. Y., and Qu, J. J. (2020). Bryophytes and the symbiotic microorganisms, the pioneers of vegetation restoration in karst rocky desertification areas in Southwestern China. *Appl. Microbiol. Biotechnol.* 104, 873–891. doi:10.1007/s00253-019-10235-0

Chen, J., Jiskani, I. M., and Li, G. (2023). Ecological restoration of coalmine-degraded lands: influence of plant species and revegetation on soil development. *Sustainability* 15, 13772. doi:10.3390/su151813772

Chen, X., Bu, C., Wang, C., Mo, Q., and Wang, H. (2022). Propagation by cutting stems of Brachythecium plumosum and its growth factors. *J. Central South Univ. For.* 42, 117–126. doi:10.14067/j.cnki.1673-923x.2022.06.013

Chun, F., Yu, S., Zhang, W., and Sai, X. (2021). Variability of aboveground biomass and interspecific compensatory effect of grassland communities in baiyinhua mining Area,Inner Mogolia,China. *Acta Agrestia Sin.* 29, 1533–1539. doi:10.11733/j.issn.1007-0435.2021.07.020

Elbert, W., Weber, B., Burrows, S., Steinkamp, J., Büdel, B., Andreae, M. O., et al. (2012). Contribution of cryptogamic covers to the global cycles of carbon and nitrogen. *Nat. Geosci.* 5, 459–462. doi:10.1038/ngeo1486

Fazan, L., Gwiazdowicz, D. J., Fragniere, Y., Faltynowicz, W., Ghosn, D., Remoundou, I., et al. (2022). Factors influencing the diversity and distribution of epiphytic lichens and bryophytes on the relict tree *Zelkova abelicea* (lam.) boiss. (*ulmaceae*). *Lichenologist* 54, 195–212. doi:10.1017/s0024282922000159

Feng, C., Gan, Y., He, X., Lei, S., Cheng, W., Huang, J., et al. (2022). Bryophyte diversity of a grassland mining area and its relationship with soil physical and chemical properties. *J. East China Normal Univ. Nat. Sci.*, 76–84. doi:10.3969/j.issn.1000-5641.2022.01.010

Feng, S., Li, Z., Zhang, C., Qi, R., and Yang, L. (2025). Ecological restoration in high-altitude mining areas: evaluation soil reconstruction and vegetation recovery in the jiangcang coal mining area on the Qinghai-Tibet Plateau. *Front. Environ. Sci.* 12, 1538243. doi:10.3389/fenvs.2024.1538243

Gao, Y., Ding, C., Ren, D., and Bai, X. (2017). Impacts of ree's enrichment on growth and anatomy of eight common mosses from baiyun obo. *Acta Bot. Boreali-Occidentalia Sin.* 37, 23–31. doi:10.7606/j.issn.1000-4025.2017.01.0023

Guan, Q., and Zhang, R. (2020). Study on the arsenic release characteristics of bryophytes in acid high-arsenic coal mine. *Environ. Sci. Technol.* 43, 6–10. doi:10.19672/j.cnki.1003-6504.2020.04.002

Han, J.-H., Wang, Z.-H., and Zhang, Z.-H. (2022). Moss biomonitors for heavy metal pollution in soils of manganese carbonate mine across ecological succession stages. 67, 83–92.

Huang, H., and Zhang, Z.-H. (2017). Diversity characteristics of bryophytes in different succession stages on the karst bauxite tailing piles. *Plant Sci. J.* 35, 807–814. doi:10.11913/psj.2095-0837.2017.60807

Huang, Q., Luo, X., Tang, W., Zhao, J., and Liang, Z. (2019). Effects of different cultivation substrates on the growth of three bryophytes. *Guangdong Agric. Sci.* 46, 56–62. doi:10.16768/j.issn.1004-874X.2019.09.008

Huanli, Y. (2009). *The investigation in application and selection of bryophyte to roadside ecological restoration*. Beijing: Beijing Forestry University.

Ji, Y., and Zhang, Z. (2015). Biodiversity of bryophytes and their characteristics of ecological distribution in the second lindai karst bauxite area. *Carsologica Sin.* 34, 599–606. doi:10.11932/karst20150609

Jiang, H., and Zhang, Z. (2012). Comparative study on bryophytes between laterite gold deposit southwest Guizhou and Tuobuka-boka gold mine in Yunnan province. *Guangdong Agric. Sci.* 39, 179–182. doi:10.16768/j.issn.1004-874x.2012.23.003

Karakaya, M. Ç., Karakaya, N., Küpeli, Ş., Karadağ, M. M., and Kırmacı, M. (2015). Potential bioaccumulator mosses around massive sulfide deposits in the vicinity of the Giresun area. *Northeast Turk.* 43, 27–37. doi:10.1002/clen.201200651

Kong, Z., Zhong, H., Jin, X., Cai, Q., Zou, Z., Ge, G., et al. (2023). Linking microbial community structure to function underneath moss-dominated biocrusts in rare Earth elements mine areas under a subtropical climate. *Land Degrad. and Dev.* 34, 4057–4069. doi:10.1002/ldr.4737

Li, J., He, C., and Zeng, B. (2021). Research on ecological restoration and utilization technology of semi-underground space in 100-meter mine pit. *Constr. Technol.* 50, 20–22. doi:10.7672/sgjs2021020020

Li, S. (2023). *Application of bryophytes in the ecological restoration of limestone mine slopes in northern guilin-tie Shan quarry in guilin as an example*. Guilin City: Guilin University of Technology.

Li, T. (2017). *Study on the selection of bryophytes for side-slope rehabilitation in northern Hebei Province*. Beijing: Beijing Forestry University.

Liao, K., Tao, Y., Zeng, Y., Tu, J., She, S., Fu, Y., et al. (2024). A feasible method of induced biological soil crust propagation through the inoculation of moss and addition of soil amendments in a Pb-Zn tailing pond. *Sci. Total Environ.* 910, 168569. doi:10.1016/j.scitotenv.2023.168569

Lin, K. K., Jian, J. N., Zhang, Y. M., Liu, Y. K., Li, S. Y., Zhao, Y., et al. (2024a). Study on plant-blanket to reduce heavy metal migration caused by precipitation and to improve the soil environment of pyritic tailings. *Sci. Total Environ.* 939, 173376. doi:10.1016/j.scitotenv.2024.173376

Lin, X., Zhuo, Y., Liu, L., Shi, X., and Zhuo, L. (2024b). Membrane stability of the desert moss Syntrichia caninervis mitt. During NaCl stress. *Acta Ecol. Sin.* 44, 3483–3491. doi:10.20103/j.stxb.202306161284

Liu, C., Pouliot, K., Roy, S., and Rochefort, L. (2024). Moss regeneration for lithium mine waste rock revegetation in Québec, Canada. *Botany* 102, 26–40. doi:10.1139/cjb-2023-0110

Lobachevska, O. V., Kyyak, N. Y., and Rabyk, I. V. (2019). Ecological and physiological peculiarities of bryophytes on a post-technogenic salinized territory. *Biosyst. Divers.* 27, 342–348. doi:10.15421/011945

Ma, Y., Zhang, Z., and Wang, Z. (2023). Response of mosses and their rhizobial bacterial communities to heavy metal pollution in manganese mining areas of south China. *Water, Air, and Soil Pollut.* 235, 28. doi:10.1007/s11270-023-06834-3

Pan, S., and Zhang, Z.-H. (2011). Bryophyte communities from abandoned mercury mine in eastern Guizhou province. *Bull. Botanical Res.* 31, 241–248. doi:10.7525/j.issn.1673-5102.2011.02.020

Pengpeng, C., Zhihui, W., and Zhaohui, Z. (2023). Dynamic characteristics of soil heavy metals and microbial communities under moss cover at different successional stages in a manganese mining area. *Environ. Geochem. Health* 45, 7711–7726. doi:10.1007/s10653-023-01681-x

Ren, J., Liu, F., Luo, Y., Zhu, J., Luo, X., and Liu, R. (2021). The pioneering role of bryophytes in ecological restoration of manganese waste residue areas. *Southwest. China* 2021, 9969253. doi:10.1155/2021/9969253

Ren, J., Liu, F., Zhu, J., Luo, Y., Li, S., and Zhong, X. (2020). Diversity of the bryophytes and heavy metal pollution monitoring in manganese ore waste area. *J. Saf. Environ.* 20, 2398–2407. doi:10.13637/j.issn.1009-6094.2019.1335

Rola, K., and Osyczka, P. (2018). Cryptogamic communities as a useful bioindication tool for estimating the degree of soil pollution with heavy metals. *Ecol. Indic.* 88, 454–464. doi:10.1016/j.ecolind.2018.01.013

Shen, F., Zheng, T., Duan, J., Hu, R., and Yu, R. (2022). Feasibility on artificial cultivation of bryophytes in rare Earth tailings in southern Jiangxi. *Sci. Soil Water Conservation* 20, 136–144. doi:10.16843/j.sswc.2022.04.017

Shi, B., Wang, X., Chen, H., and Yang, S. (2022). Growth and physiological responses of Plagiomnium acutum to different cultivation substrates. *Acta Bot. Boreali-Occidentalia Sin.* 42, 1208–1218. doi:10.7606/j.issn.1000-4025.2022.07.1208

Širka, P., Bittnerová, S., and Turisová, I. (2018). Succession pattern at two mineralogically different spoil heaps in central Slovakia. *Biologia* 73, 809–820. doi:10.2478/s11756-018-0095-5

Slate, M. L., Antoninka, A., Bailey, L., Berdugo, M. B., Callaghan, D. A., Cárdenas, M., et al. (2024). Impact of changing climate on bryophyte contributions to terrestrial water, carbon, and nitrogen cycles. *New Phytol.* 242, 2411–2429. doi:10.1111/nph.19772

Song, L., Bai, Z., Fan, X., Sun, P., and Wei, Y. (2018). Effect of biological soil crust on photographically measured value of vegetation coverage. *Acta Ecol. Sin.* 38, 1272–1283. doi:10.5846/stxb201612312723

Stern, M., Medeiros, I. D., Negoita, L., and Rajakaruna, N. (2016). Limestone flora of the simonton corner quarry preserve, rockport, Maine, USA. *Rhodora* 118, 206–226. doi:10.3119/15-23

Sun, J., Chen, Q., Wang, Y., and Yang, J. (2004). Application of bryophytes in vegetation restoration project of jiuzhaigou valley scenic and historic interest area scenic spot.

Suzuki, Y., Takenaka, C., Tomioka, R., Tsubota, H., Takasaki, Y., and Umemura, T. (2016). Accumulation of arsenic and copper by bryophytes growing in an aquatic environment near copper mine tailings. *Mine Water Environ.* 35, 265–272. doi:10.1007/s10230-015-0335-7

Wang, Y., Zheng, J., and Peng, X. (2022). A review on ecological functions of bryophytes in extreme environments. *Plant Physiology J.* 58, 101–108. doi:10.13592/j.cnki.ppj.2021.0223

Xia, H., Liu, L., Zhou, X., Chen, K., Li, Y., Kuang, P., et al. (2023). Selection of suitable mosses for bare rock and steep slope greening after jiuzhaigou earthquake based on the analytic hierarchy process. *Bull. Botanical Res.* 43, 540–549. doi:10.7525/j.issn.1673-5102.2023.04.007

Yu, W., He, X., Lei, S., Kou, J., and Feng, C. (2024). Effects of different substrate compositions and concentrations on the growth of didymodon tectorus. *J. Nanjing For. Univ. Nat. Sci. Ed.* 48, 184–190. doi:10.12302/j.issn.1000-2006.202207003

Zhang, X., Yu, W., Xue, Y., Hu, D., and Feng, C. (2023a). Tissue culture of seven typical xerophytic mosses. *J. North-East For. Univ.* 51, 23–28. doi:10.13759/j.cnki.dlxb.2023.08.008

Zhang, Y., He, N., and Liu, Y. (2023b). Temperature factors are a primary driver of the forest bryophyte diversity and distribution in the southeast Qinghai-Tibet Plateau. *For. Ecol. Manag.* 527, 120610. doi:10.1016/j.foreco.2022.120610

Zhou, L., and Zhang, Z. (2007). Bryophytes in tangdan copper mine site in Yunnan province. *J. Trop. Subtropical Bot.* 15, 82–85. doi:10.3969/j.issn.1005-3395.2007.01.014

Zhu, R. (2022). Peat mosses (sphagnum): ecologically, economically, and scientifically important group of carbon sequestration plants. *Chin. Bull. Bot.* 57, 559–578. doi:10.11983/CBB22031

Zhu, R., Ma, X., Cao, C., and Cao, Z. (2022). Advances in research on bryophyte diversity in China. *Biodivers. Sci.* 30, 22378. doi:10.17520/biods.2022378

Zuo, Y., Gu, B., and Ai, Y. (2006). Investigation of application of bryophyte to road side ecological restoration. *Sci. Soil Water Conservation* 4, 122–125. doi:10.16843/j.sswc.2006.s1.028

frontiers | Frontiers in Environmental Science

TYPE Brief Research Report
PUBLISHED 06 August 2025
DOI 10.3389/fenvs.2025.1560323

OPEN ACCESS

EDITED BY
Tianjiao Feng,
Beijing Forestry University, China

REVIEWED BY
Zhi-Cong Dai,
Jiangsu University, China
Pervaiz Dar,
University of Kashmir, India

*CORRESPONDENCE
Chun-Jing Wang,
wangchunjing00@163.com
De-Chao Chen,
chendechao519@163.com

RECEIVED 14 January 2025
ACCEPTED 25 June 2025
PUBLISHED 06 August 2025

CITATION
Ma Y-Q, Wang C-J, Chen D-C, Deng D-Z, Yan W-X, Yang J-Y and Wan J-Z (2025) Impacts of grazing on species diversity among different plant communities on the Qinghai–Tibet Plateau.
Front. Environ. Sci. 13:1560323.
doi: 10.3389/fenvs.2025.1560323

Impacts of grazing on species diversity among different plant communities on the Qinghai–Tibet Plateau

Yu-Qi Ma[1,2], Chun-Jing Wang[1,3]*, De-Chao Chen[1,3]*, Dong-Zhou Deng[1,3], Wu-Xian Yan[1,3], Jing-Yu Yang[1,3] and Ji-Zhong Wan[4]

[1]Sichuan Academy of Forestry, Chengdu, China, [2]College of Life Science, Qinghai Normal University, Xining, China, [3]Sichuan Provincial Forestry and Grassland Key Laboratory of Combating Desertilicatlon, Chengdu, China, [4]Key Laboratory of Mountain Surface Processes and Ecological Regulation, Institute of Mountain Hazards and Environment, Chinese Academy of Sciences, Chengdu, China

The Qinghai–Tibet Plateau is a region with rich biodiversity and fragile ecosystems, and its plant species diversity is greatly affected by grazing activities. In this study, we aimed to explore the impact of grazing on the diversity of different plant communities on the Qinghai–Tibet Plateau. To this end, we collected grazing and vegetation data for the period of 1982–2015; calculated the grazing, Shannon–Wiener diversity, inverse Simpson's, and Pielou's evenness indices along with species richness; and conducted correlation and regression analyses. The results show that the grazing index was positively correlated with the richness of grassland plant communities, and in particular, there were significant relationships between the variance and maximum value of the grazing data and plant species richness. However, no significant correlations were found between the grazing index and diversity indices in shrub land and desert plant communities. Moderate grazing promotes the renewal and growth of grassland vegetation and increases plant species diversity. Therefore, grazing management plans should be developed based on specific ecological environments to achieve sustainable ecosystem development and to protect species diversity.

KEYWORDS

China, grazing, plant communities, Qinghai-Tibet Plateau, species diversity, vegetation type

1 Introduction

The Qinghai–Tibet Plateau is the highest and largest plateau on Earth and is a key ecological functional area for water conservation, windbreaks, and sand fixation in Asia (Sun et al., 2012; Wang et al., 2022). It is also an important ecological security barrier in China, with rich ecosystems and unique biodiversity (Li et al., 2024). Biodiversity is crucial for maintaining ecosystem stability and plays an important role in water-source protection, climate regulation, and soil conservation (Li et al., 2022; Lee et al., 2015; Sun et al., 2023). The biodiversity of the Qinghai–Tibet Plateau also has a profound impact on the lives and cultures of local residents, especially pastoral communities that rely on natural resources as an indispensable foundation for their livelihood (Zhou et al., 2019). With the increase in human activities, especially overgrazing and infrastructure construction, the ecological

environment of the Qinghai–Tibet Plateau is facing unprecedented pressure (Yang et al., 2024). Therefore, protecting the biodiversity of the Qinghai–Tibet Plateau is of great importance for maintaining regional ecological security and promoting sustainable development. Additional research is required to identify effective protective measures to preserve the biodiversity of the Qinghai–Tibet Plateau.

The high elevation and extreme climate of the Qinghai–Tibet Plateau region limit the growth and reproduction of many plant species, increasing their vulnerability and influencing plant species diversity (Mu et al., 2021; Chen et al., 2021; Bhattarai et al., 2021). Additionally, the intensification of climate change and human activity in this region has increased the survival pressure on plant species (Tilman and Lehman, 2001). With increases in temperature and changes in precipitation patterns caused by global warming, many plant species may experience habitat loss and display inadequate adaptability (Theodoridis et al., 2024). This lack of adaptability hinders the ability of plant species to cope effectively with rapidly changing environments, thereby increasing their risk of extinction (Losapio and Schöb, 2017). Temperature changes have led to an increase in forest and shrub land areas and a decrease in alpine meadows on the Qinghai–Tibet Plateau, whereas the intensification of drought has resulted in vegetation degradation in some areas of the southern Qinghai–Tibet Plateau (Gao et al., 2016; Wang et al., 2021). Protecting the plant species diversity of the Qinghai–Tibet Plateau is not only an urgent need for ecological protection but also an important measure to mitigate the impacts of climate change and maintain the ecological balance (Wang et al., 2022).

Animal husbandry is a crucial part of the Qinghai–Tibet Plateau economy, and grasslands are the main locations where local herders engage in grazing activities. Grazing is a traditional agricultural activity that has potential impacts on biodiversity. Moderate grazing can promote the growth and renewal of grasslands (Luo et al., 2012; Zhang et al., 2018); however, a large number of livestock foraging and trampling on grasslands can damage vegetation and lead to soil erosion, which in turn affects biodiversity (Wang Q. X. et al., 2023; Barros and Pickering, 2014). In particular, concentrated grazing may lead to the excessive consumption of vegetation or overgrazing (Hao et al., 2018). With an increase in grazing intensity, the diversity and richness of herbaceous plants, shrubs, and other plant communities on the Qinghai–Tibet Plateau markedly increased and then decreased (Wang et al., 2022). Studies have also reported that high-intensity grazing reduced plant diversity on the Qinghai–Tibet Plateau, whereas both non-grazing and low-intensity grazing alleviated plant biomass loss (Wang Q. X. et al., 2023). Furthermore, community resistance was optimal under low-intensity grazing conditions (Wang Q. X. et al., 2023). However, livestock manure and urine add nutrients and organic matter to the soil, affecting nutrient cycling and organic matter decomposition, thereby influencing the accumulation and distribution of soil organic carbon (Du et al., 2022). Grazing also affects the soil biota and functions, which are important components of material cycling and energy flow in underground ecosystems (Zhou et al., 2023). Thus, rational grazing can help maintain plant diversity and enhance ecosystem productivity and stability, whereas overgrazing can lead to the degradation of grassland vegetation, thereby reducing the richness and diversity of plant species, which in turn affects the quality of animal habitats and ultimately causes ecosystem imbalances (Li et al., 2023; Hao et al., 2018). With human population growth and economic development, the scale and intensity of grazing activities have gradually increased, and grazing has become a major contributing factor to grassland degradation on the Qinghai–Tibet Plateau in recent years (Fayiah et al., 2020). Therefore, grazing management is crucial for protecting plants and animals, and the adoption of effective grazing management strategies can effectively maintain ecosystem health (Zhao et al., 2022).

With the intensification of global climate change and human activity, the stability of ecosystems and biodiversity is facing unprecedented challenges (Liu et al., 2024). The Qinghai–Tibet Plateau is a unique and fragile ecosystem, and changes in its biodiversity are influenced by various factors, with grazing activities playing a dominant role. Although previous studies have explored the impacts of different degrees of grazing on grassland ecosystems, the specific mechanisms of and differences in the effect of grazing on different vegetation types remain unclear. Therefore, in this study, we aimed to explore: (1) the effects of grazing on the species diversity of plant communities on the Qinghai–Tibet Plateau and (2) the differences in this effect among different plant communities. The results of this study provide a scientific basis for the ecological protection and sustainable management of the Qinghai–Tibet Plateau.

2 Materials and methods

2.1 Vegetation data

The plant-plot data used in this study were extracted from datasets published by Wang Q. et al. (2023) and Jin et al. (2022). The datasets include quadrat sampling data from 455 herb quadrats in the Huangshui River Basin, Qinghai Province, including Haiyan County in Haibei Tibetan Autonomous Prefecture; the main urban area of Xining City, Huangyuan County, Huangzhong District; and Datong Hui and Tu Autonomous County, as well as Ledu District, Ping'an District, Minhe Hui and Tu Autonomous County, Huzhu Tu Autonomous County, and Hehuang New District in Haidong City. The quadrats of grassland communities are dominated by plant species belonging to Leguminosae, Rosaceae, Ranunculaceaem Cyperaceae and Poaceae. Shrub species are included, but their abundances are low, and individual sizes are small in the herb quadrats (Wang Q. et al., 2023; Supplementary Figure S1). In shrub plots, the abundances of shrub species were relatively low due to grazing effects and human disturbance. The plots of shrubland communities are dominated by shrub species belonging to Dasiphora.

The sampling locations of the plot-based dataset of plant communities on the Qinghai–Tibet Plateau included the Three River source region, southern Tibetan mountains, Ali region, and Qaidam Basin, as well as high mountains, oases, and desert areas, such as the Qilian, Altun, and Kunlun mountains. These two datasets report detailed information on the species present in the survey plots, including species name, number of plants, and coverage of each species. Additionally, the datasets report information on each plot, such as the plot number, longitude, latitude, elevation, degree of human interference, and total coverage of the plot.

These two datasets contain 1,213 sample plots, and we merged the data into one table. After removing forest sample plots based on vegetation type data, 880 sample plots remained. Each plot retained the plot number, plant name, coverage, and vegetation type information. The study area encompasses three principal vegetation types: grassland, shrubland, and desert. Sampling protocols employed vegetation-specific plot dimensions: grassland quadrats were established at 0.5 m × 0.5 m or 1 m × 1 m scales, while shrubland communities were surveyed using nested plots of 2 m × 2 m, 5 m × 5 m, and 10 m × 10 m. The maps of shrub species richness, individual and relative abundance of plant communities were shown on Supplementary Figure S1, showing that shrub species were distributed in many plots of our study. It is certainly determined to identify grassland, shrubland, and desert based on vegetation classification ranges. Vegetation classification for Qinghai-Tibet Plateau plant communities was predominantly guided by the phytosociological framework delineated in the Revised Scheme of the Vegetation Classification System of China (Guo et al., 2020), with additional reference to biogeographic zonation descriptors in the Vegetation and Its Geographical Pattern in China: Specifications for the Vegetation Map of the People's Republic of China (1:1,000,000) (Editorial Committee of Vegetation Map of China, the Chinese Academy of Sciences, 2007).

2.2 Grazing data

Grazing data were obtained from a dataset published by Meng et al. (2023). This dataset was constructed using a methodological framework that combined the cross-scale feature extraction method and a random forest model to produce a high-resolution gridded grazing dataset for the Qinghai–Tibet Plateau from 1982 to 2015. This framework included the following steps: identifying features that affect grazing, extracting theoretically suitable grazing areas, building a grazing spatialization model, and correcting the grazing spatialization dataset. When building the grazing spatialization model, combining a random forest model with partition and cross-scale features increased the model accuracy by 35.59% compared to that of traditional random forest models. Furthermore, Meng et al. (2023) compared this dataset with three other datasets (the actual livestock carrying capacity dataset, Gridded Livestock of the World 2.01, and Gridded Livestock of the World 3) and concluded that its time resolution was higher, making it more suitable for long-term research. Hence, we selected grazing data from Meng et al. (2023) for analysis. All grazing data is presented as sheep units/pixel/year, which was calculated based on the number of livestock (e.g., cattle, sheep, and horses), according to national standards. Livestock had strong accessibility to the study plots under grazing pressure. The sample plots were overlaid with the grazing data pixels.

2.3 Data analysis

We used ArcGIS 10.7 to extract grazing grid data from 1982 to 2015 and obtained the grazing status of each plot in each year through multi-value point extraction. We calculated the Shannon–Wiener diversity, inverse Simpson's diversity, and Pielou's evenness indices, along with species richness, for 880 plots; merged these indices with the grazing data; and removed invalid data. There were no correlations between diversity indices and plot size, which did not affect our results ($P > 0.1$). We used R 4.4.1 for data analysis and visualization and employed a generalized linear model to evaluate the differences in the impact of the grazing index on diversity among different vegetation types. We employed an analysis of variance (ANOVA) model to identify significant interactions and perform multiple comparisons of significant combinations, grouping them by vegetation type to establish a linear regression model.

3 Results

3.1 Relationships between grazing index and plant diversity indices

In grassland plant communities, the variance (SD) of the grazing data from 1981 to 2015 was directly proportional to plant species richness, and the fitting formula was: richness = 7.6860785 + 0.0012608 × SD ($P < 0.1$, $R^2 > 0.1$; Figure 1). The maximum value (Max) of the grazing index was directly proportional to plant species richness, and the fitting formula was: richness = 8.0253677 + 0.0001065 × Max ($P < 0.1$, $R^2 > 0.1$; Figure 1). There were no significant correlations between other grazing data and the grassland plant community diversity indices ($P < 0.1$; Figure 1). We calculated the following mean values for grassland plant diversity: Shannon–Wiener index, 1.54; inverse Simpson's index, 3.99; richness, 9.08; and Pielou's evenness index, 0.73. The Shannon–Wiener index ranged from 0.07 to 2.75, the inverse Simpson's index ranged from 1.03 to 11.28, the richness ranged from two to 26, and Pielou's evenness index ranged from 0.11 to 1 (Figure 2).

3.2 Comparison of relationships between grazing index and plant diversity indices among vegetation types

When comparing the models with and without interaction terms through ANOVA, $P < 0.05$ was considered significant, indicating a significant interaction effect. The impacts of the SD of the grazing data on the Shannon–Wiener index and species richness differed significantly between grassland and shrub land, with the slope of the grassland regression line being significantly steeper than that of the shrub land regression line. The diversity index of desert vegetation had no significant interaction with either the grazing index or other vegetation types (Figure 3).

4 Discussion

4.1 Impact of grazing on plant diversity

Grazing had different effects on the species diversity of different vegetation types. The results indicate that the Max from 1981 to 2015 was directly proportional to the grassland plant community richness, whereas grazing did not have a substantial impact on plant

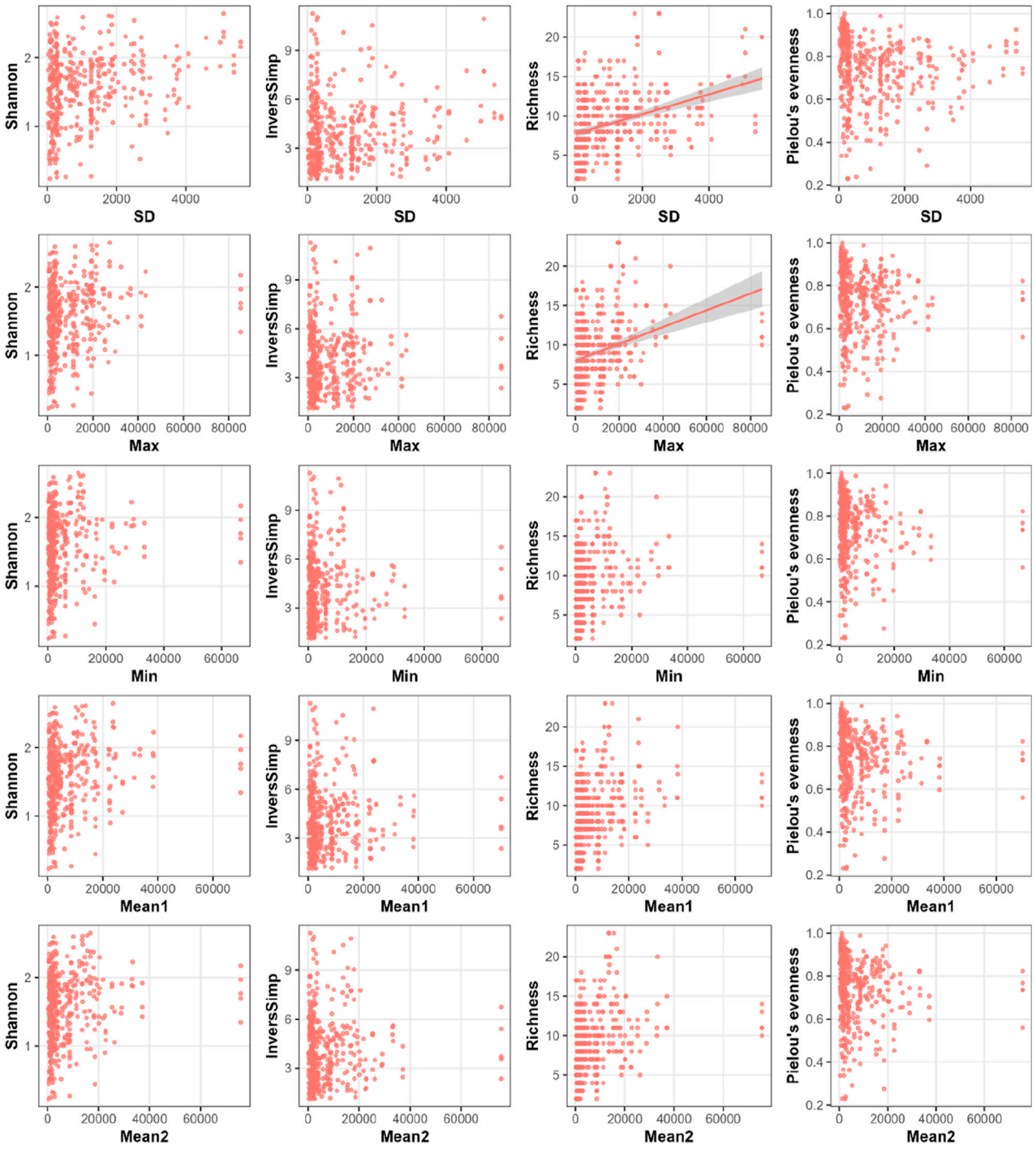

FIGURE 1
Scatter plots of grazing values and diversity indices of grassland communities. SD: variance of grazing data from 1981 to 2015; Max: maximum value of grazing data from 1981 to 2015; Min: minimum value of grazing data from 1981 to 2015; Mean1: mean of grazing data from 1981 to 2000; Mean2: mean of grazing data from 2001 to 2015. The red line represents the fitting line.

community diversity in shrub land and deserts. The Max reflects an extreme level of grazing, and its correlation with plant richness suggests that the grassland received high nutrient inputs from livestock manure and urine, which provided favorable growth conditions for the plants. Meanwhile, the SD reflects the differences in the grazing index at different temporal and spatial scales. Heterogeneity can create diverse habitat conditions and promote plant species coexistence. In addition, neither shrub land nor desert vegetation showed significant correlations in their responses to grazing. This difference from grassland may have arisen from the inherent life strategies of the vegetation. Shrubs typically possess deep root systems and lignified stems, enabling them to tolerate trampling and browsing by livestock. Jafarian et al. (2013) compared the soil physicochemical properties (organic carbon, total

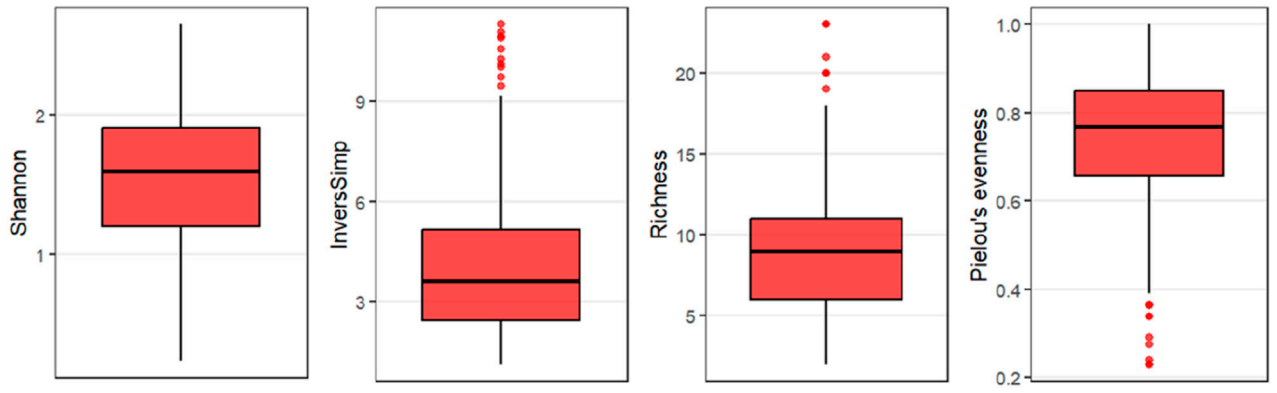

FIGURE 2
Boxplots of four species diversity indices of grassland communities. Boxplots show the medium values (black lines), 25% and 75% quartiles (boxes), and 5% minima and 95% maxima (bars) of four species diversity indices.

nitrogen, and electrical conductivity) of grasslands and shrub lands in Iran and found that the soil conditions in shrub lands were more suitable for plant growth than those in grasslands. Meanwhile, desert vegetation adapts to arid environments through physiological mechanisms such as succulent tissue and reduced transpiration. The conservative ecological niche of desert vegetation makes it less sensitive to grazing disturbance. In addition, by comparing the correlations between the grazing and species diversity indices among different vegetation types, we found that the correlations were stronger for grassland vegetation than for other vegetation types. Similar to the findings of this study, desert and dry grasslands in Mongolia have shown significant negative responses to severe grazing (Munkhzul et al., 2021). However, the increase in species richness in meadow steppes may be attributed to reduced competitive pressure from dominant species due to grazing, which aligns with the "intermediate disturbance hypothesis." These regional differences highlight the moderating effects of vegetation type and climatic context on grazing impacts. Due to the lack of recent data from 2016 to 2025, the current study was based on long-term observational data from 1982 to 2015, covering multiple climatic fluctuation cycles and grazing management phases. This study systematically revealed the response patterns of different vegetation types to grazing disturbance, providing a reference for future research.

4.2 Mechanisms of the impact of grazing on plant diversity

Grazing is an essential component of animal husbandry on the Qinghai–Tibet Plateau and can directly or indirectly affect vegetation. Direct impacts are typically manifested when herbivores directly feed on plants, which can lead to a reduction in species biodiversity and vegetation biomass (Zhu et al., 2012). Selective grazing by livestock may reduce high-nutrient species and increase low-nutrient ones (Török et al., 2018), thus altering plant community structure and function. Indirect impacts arise in several ways. Livestock excreta release nutrients into the soil, changing its properties (e.g., nutrient levels and water content) and affecting plant growth (Du et al., 2022). Moreover, grazing can indirectly influence plant productivity and ecosystem services by altering the soil microbial community composition and functions. A global meta-analysis by Zhou et al. (2023) demonstrated that moderate grazing boosts soil nematode diversity and organic matter decomposition efficiency.

The grazing index, which is based on the number of grazing animals, grazing time, and grazing frequency, is used to evaluate the pressure and impact of grazing on grassland ecosystems (Zhang et al., 2018). Many studies have been conducted on the effects of the grazing index. Different grazing intensities and durations were found to have different effects on the species diversity of grassland plant communities (Deng et al., 2014). Moderate grazing increased grassland species diversity, whereas heavy and long-term grazing reduced it. Along with the grazing intensity, different grazing practices have been found to impact grassland ecosystems. Liu et al. (2015) found that for grasslands with high plant diversity, mixed grazing by cattle and sheep significantly improved plant diversity; however, grazing by either cattle or sheep alone had no effect. Meanwhile, for grasslands with low plant diversity, both individual and mixed grazing significantly increased plant diversity but significantly reduced plant biomass (Liu et al., 2015). Additionally, the impacts of grazing on vegetation can become more complex through interactions with other ecological factors. For instance, climate change may alter vegetation growth conditions and herbivore behavior, thereby amplifying or mitigating grazing effects (Qiqige et al., 2023).

4.3 Recommendations

Based on our findings regarding the impact of grazing on plant diversity and its mechanisms on the Qinghai–Tibet Plateau, we propose the following grazing management practices. First, grazing strategies that are tailored to different vegetation types should be developed. Our results indicate that grassland vegetation is highly responsive to grazing, and moderate grazing can enhance species coexistence and community stability. Thus, a dynamic moderate grazing strategy should be implemented in grasslands to prevent biodiversity loss and ecological degradation from long-term high-intensity grazing. For

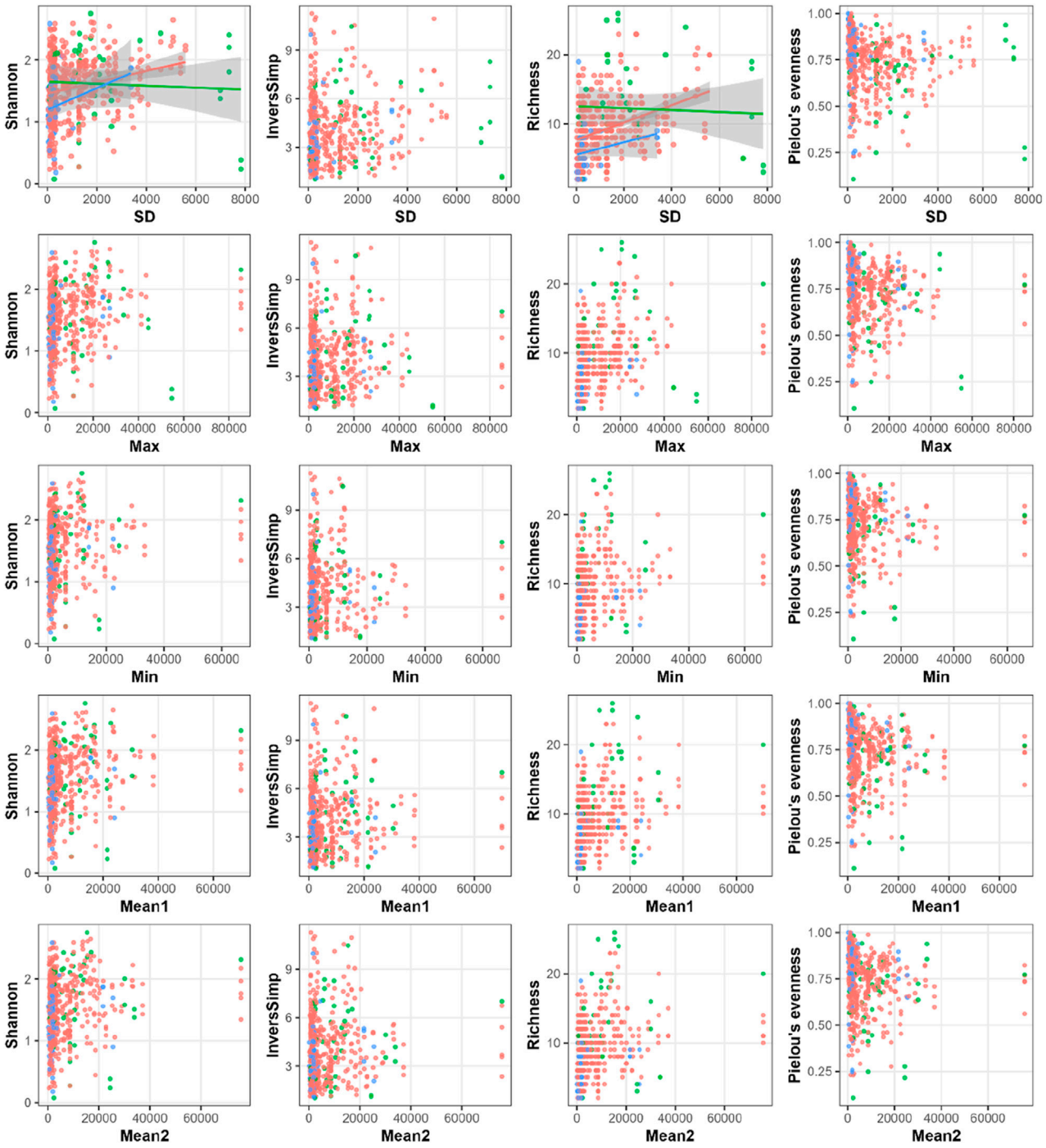

FIGURE 3
Correlations between grazing index and plant species diversity across different vegetation types. Red, green, and blue lines represent fitted lines for relationships between grazing index and plant species diversity in three vegetation types, namely, grassland, shrub land, and desert, respectively. SD: variance of grazing data from 1981 to 2015; Max: maximum value of grazing data from 1981 to 2015; Min: minimum value of grazing data from 1981 to 2015; Mean1: mean of grazing data from 1981 to 2000; Mean2: mean of grazing data from 2001 to 2015.

shrub lands and deserts, which show weak or complex responses to grazing, more conservative and observation-driven grazing measures are recommended. Second, the monitoring and management of grazing intensity and timing should be strengthened. For example, remote sensing and ground observations could be integrated to establish a grazing index monitoring and early warning system. Continuous monitoring and assessment of the risks of extreme grazing events will help to avert irreversible grassland degradation beyond the ecological carrying capacity. Additionally, the ecological role of a fluctuating grazing index should be recognized by adjusting grazing rhythms to create diverse microhabitat conditions, which can boost species coexistence and plant diversity (Du et al., 2022). Moreover, mixed cattle and sheep grazing should be promoted as an effective approach to enhance grassland plant diversity. Liu et al. (2015) reported

that mixed grazing regulates interspecific competition among different plant functional groups, optimizes the vegetation structure, and improves resource-use efficiency, particularly in high-diversity grasslands. Therefore, multi-species livestock combination grazing should be prioritized, and the types and ratios of cattle, sheep, and other livestock should be scientifically allocated based on local ecological conditions and forage composition to achieve the dual goals of biodiversity conservation and improved forage-use efficiency.

5 Conclusion

Grazing activities have varying effects on the species diversity of different vegetation types on the Qinghai–Tibet Plateau. For grassland vegetation, the grazing index was positively correlated with plant community richness. Among the shrub land and desert vegetation types, grazing activity had no significant effect on plant community diversity. In addition, there were differences in the correlations between the grazing and diversity indices among the different vegetation types, with stronger correlations for grassland vegetation. These results indicate that the impact of vegetation type and grazing activity on plant community diversity on the Qinghai–Tibet Plateau is complex and diverse. Moderate grazing can promote vegetation renewal and growth and improve plant species diversity. Rational grazing plans should be developed based on specific ecological environments and biological community characteristics to achieve sustainable ecosystem development and to preserve species diversity.

Data availability statement

The original contributions presented in the study are included in the article/Supplementary Material, further inquiries can be directed to the corresponding author.

Author contributions

Y-QM: Conceptualization, Data curation, Formal Analysis, Investigation, Methodology, Resources, Software, Writing – original draft. C-JW: Conceptualization, Project administration, Supervision, Writing – original draft, Writing – review and editing. D-CC: Funding acquisition, Validation, Visualization, Writing – review and editing. D-ZD: Funding acquisition, Project administration, Supervision, Writing – review and editing. W-XY: Funding acquisition, Project administration, Supervision, Validation, Visualization, Writing – review and editing. J-ZW: Conceptualization, Supervision, Visualization, Writing – review and editing.

Funding

The Project of Sichuan Forestry and Grassland Technology Innovation Team from C-JW. Sichuan Provincial Science and Technology Planning Project (No. 2024YFNH0005) from D-CC, Central Financial Forest and Grass Science and Technology Promotion Demonstration Project - Promotion and Demonstration of Technology for Consolidating and Enhancing Ecological Effects of Severe Desertification Land Management in the High-Altitude Cold Region of the Upper Reaches of the Yellow River and Forestry Ecological Construction and Industrial Development Scientific Research Project - 2021 Annual Monitoring Project on the Effectiveness of Governance in Vulnerable Regions form Wu-Xian Yan.

Conflict of interest

The authors declare that the research was conducted in the absence of any commercial or financial relationships that could be construed as a potential conflict of interest.

Generative AI statement

The author(s) declare that no Generative AI was used in the creation of this manuscript.

Publisher's note

Supplementary material

The Supplementary Material for this article can be found online at: https://www.frontiersin.org/articles/10.3389/fenvs.2025.1560323/full#supplementary-material

SUPPLEMENTARY FIGURE S1
Maps of shrub species richness **(a)**, individual **(b)** and relative abundance **(c)** of plant communities. The circle size represents the increasing values of shrub species richness, individual and relative abundance. The color from light blue to red indicates the higher attitude of the Qinghai–Tibet Plateau.

References

Barros, A., and Pickering, C. M. (2014). Impacts of experimental trampling by hikers and pack animals on a high-altitude alpine sedge meadow in the andes. *Plant Ecol. and Divers.* 8 (2), 265–276. doi:10.1080/17550874.2014.893592

Bhattarai, P., Zheng, Z., Bhatta, K. P., Adhikari, Y. P., and Zhang, Y. (2021). Climate-driven plant response and resilience on the Tibetan Plateau in space and time: a review. *Plants* 10, 480. doi:10.3390/plants10030480

Chen, C., Li, T., Sivakumar, B., Sharma, A., Albertson, J., Zhang, L., et al. (2021). Combined effects of warming and grazing on rangeland vegetation on the Qinghai-Tibet Plateau. *Front. Environ. Sci.* 9, 797971. doi:10.3389/fenvs.2021.797971

Deng, L., Sweeney, S., and Shangguan, Z. P. (2014). Grassland responses to grazing disturbance: plant diversity changes with grazing intensity in a desert steppe. *Grass Forage Sci.* 69, 524–533. doi:10.1111/gfs.12065

Du, Z. Y., Wang, X. D., and Cai, Y. J. (2022). Short-term effects of yak and Tibetan sheep urine deposition on soil carbon and nitrogen concentrations in an alpine steppe of the northern Tibetan Plateau, China. *J. Mt. Sci.* 19, 1156–1167. doi:10.1007/s11629-021-7026-6

Editorial Committee of Vegetation Map of China, the Chinese Academy of Sciences (2007). *Vegetation map of the people's Republic of China (1:1 000 000)*. Beijing: Geology Press.

Fayiah, M., Dong, S., Khomera, S. W., Rehman, S. A., Yang, M., and Xiao, J. (2020). Status and challenges of Qinghai-Tibet plateau's grasslands: an analysis of causes, mitigation measures, and way forward. *Sustainability* 12, 1099. doi:10.3390/su12031099

Gao, Q. Z., Guo, Y. Q., Xu, H. M., Ganjurjav, H., Li, Y., Wan, Y. F., et al. (2016). Climate change and its impacts on vegetation distribution and net primary productivity of the alpine ecosystem in the Qinghai-Tibetan Plateau. *Sci. Total Environ.* 554-555, 34–41. doi:10.1016/j.scitotenv.2016.02.131

Guo, K., Fang, J. Y., Wang, G. H., Tang, Z. Y., Xie, Z. Q., Shen, Z. H., et al. (2020). A revised scheme of vegetation classification system of China. *Chin. J. Plant Ecol.* 44, 111–127. doi:10.17521/cjpe.2019.0271

Hao, L., Pan, C., Fang, D., Zhang, X., Zhou, D., Liu, P., et al. (2018). Quantifying the effects of overgrazing on mountainous watershed vegetation dynamics under a changing climate. *Sci. Total Environ.* 639, 1408–1420. doi:10.1016/j.scitotenv.2018.05.224

Jafarian, Z., Kargar, M., and Ghorbani, J. (2013). Comparison of soil physical and chemical properties in grassland and shrub land communities, Iran. *Commun. Soil Sci. Plant Analysis* 44, 331–338. doi:10.1080/00103624.2013.741944

Jin, Y. L., Wang, H. Y., Wei, L. F., Hou, Y., Hu, J., Wu, K., et al. (2022). A plot-based dataset of plant community on the Qingzang Plateau. *Chin. J. Plant Ecol.* 46, 846–854. doi:10.17521/cjpe.2022.0174

Lee, J. H., Lee, M. J., and Lee, G. G. (2015). National level assessment of biodiversity importance-focusing on South Korea. *KSCE J. Civ. Eng.* 19, 46–62. doi:10.1007/s12205-013-0678-1

Li, H., Tan, L., Li, X., and Cai, Q. (2024). Aquatic protected area system in the Qinghai-Tibet Plateau: establishment, challenges and prospects. *Front. Ecol. Evol.* 12, 1204494. doi:10.3389/fevo.2024.1204494

Li, S., Zhu, Y. P., Cao, M., and Li, J. S. (2022). Current status, issues, and suggestions for the standard system of biodiversity conservation in China. *Biodivers. Sci.* 30, 192–200.

Li, W., Su, T., Shen, Y., Ma, H., Zhou, Y., Lu, Q., et al. (2023). Effects of warming seasonal rotational grazing on plant communities' structure and diversity in desert steppe. *Ecol. Evol.* 13, e9748. doi:10.1002/ece3.9748

Liu, J., Feng, C., Wang, D. L., Wang, L., Wilsey, B. J., and Zhong, Z. W. (2015). Impacts of grazing by different large herbivores in grassland depend on plant species diversity. *J. Appl. Ecol.* 52, 1053–1062. doi:10.1111/1365-2664.12456

Liu, L., Zhang, S., Liu, W., Qu, H., and Guo, L. (2024). Spatiotemporal changes and simulation prediction of ecological security pattern on the Qinghai-Tibet Plateau based on deep learning. *Land* 13, 1073. doi:10.3390/land13071073

Losapio, G., and Schöb, C. (2017). Resistance of plant-plant networks to biodiversity loss and secondary extinctions following simulated environmental changes. *Funct. Ecol.* 31, 1145–1152. doi:10.1111/1365-2435.12839

Luo, G. P., Han, Q. F., Zhou, D. C., Li, L., Chen, X., Li, Y., et al. (2012). Moderate grazing can promote aboveground primary production of grassland under water stress. *Ecol. Complex.* 11, 126–136. doi:10.1016/j.ecocom.2012.04.004

Meng, N., Wang, L. J., Qi, W. C., Dai, X. H., Li, Z. Z., Yang, Y. Z., et al. (2023). A high-resolution gridded grazing dataset of grassland ecosystem on the Qinghai-Tibet Plateau in 1982-2015. *Sci. Data* 10, 68. doi:10.1038/s41597-023-01970-1

Mu, X., Jia, K., Zhao, W., Liu, S., Wei, X., and Wang, B. (2021). Spatio-temporal changes of ecological vulnerability across the Qinghai-Tibetan Plateau. *Ecol. Indic.* 123, 107274. doi:10.1016/j.ecolind.2020.107274

Munkhzul, O., Oyundelger, K., Narantuya, N., Tuvshintogtokh, I., Oyuntsetseg, B., Wesche, K., et al. (2021). Grazing effects on Mongolian steppe Vegetation-A systematic review of local literature. *Front. Ecol. Evol.* 9, 703220. doi:10.3389/fevo.2021.703220

Qiqige, B., Wei, B., Wei, Y., Liu, M., Bi, Y., Xu, R., et al. (2023). Climate, not grazing, influences soil microbial diversity through changes in vegetation and abiotic factors on geographical patterns in the Eurasian steppe. *Front. Plant Sci.* 14, 1238077. doi:10.3389/fpls.2023.1238077

Sun, H. L., Zheng, D., Yao, T. D., and Zhang, Y. L. (2012). Conservation and construction of the national ecological security barrier on the Qinghai-Tibet Plateau. *Acta Geogr. Sin.* 67, 3–12.

Sun, Y., Liu, S., Liu, C., Sun, J., Liu, Y., and Wang, F. (2023). Interactive response and spatial heterogeneity of alpine grassland biodiversity to soil, topography, climate, and human factors on the Qinghai-Tibet Plateau. *Land Degrad. and Dev.* 34, 4488–4502. doi:10.1002/ldr.4735

Theodoridis, S., Hickler, T., and Thines, M. (2024). Mountain greening and rising temperatures erode habitats of ironwort (sideritis), an important natural medicinal resource. *Plants, People, Planet* 6, 862–874. doi:10.1002/ppp3.10497

Tilman, D., and Lehman, C. (2001). Human-caused environmental change: impacts on plant diversity and evolution. *Proc. Natl. Acad. Sci.* 98, 5433–5440. doi:10.1073/pnas.091093198

Török, P., Penksza, K., Tóth, E., Kelemen, A., Sonkoly, J., and Tóthmérész, B. (2018). Vegetation type and grazing intensity jointly shape grazing effects on grassland biodiversity. *Ecol. Evol.* 8, 10326–10335. doi:10.1002/ece3.4508

Wang, Q., Shang, C., Wang, C. J., and Wan, J. Z. (2023). A dataset of quadrat sampling of 455 herb quadrats in Huangshui River Basin, Qinghai Province. *China Sci. Data* 8 (1), 328–336. doi:10.57760/sciencedb.03329

Wang, Q. X., Cao, W., and Huang, L. (2023). Evolutionary characteristics and zoning of ecosystem functional stability on the Qinghai-Tibet Plateau. *Acta Geogr. Sin.* 78, 1104–1118.

Wang, X., Zhu, J. L., Peng, S. T., Zheng, T. L., Qi, Z. Y., Hu, J. B., et al. (2022). Patterns of grassland community composition and structure along an elevational gradient on the Qinghai-Tibet Plateau. *J. Plant Ecol.* 15, 808–817. doi:10.1093/jpe/rtab119

Yang, Y., Yu, C., Liu, M., and Wei, H. (2024). Uncovering the coupling relationships and key factors linking ecosystem services to human well-being through system dynamics: a case study in the Qinghai-Tibet Plateau. *Ecol. Indic.* 166, 112408. doi:10.1016/j.ecolind.2024.112408

Zhang, C., Dong, Q., Chu, H., Shi, J., Li, S., Wang, Y., et al. (2018). Grassland community composition response to grazing intensity under different grazing regimes. *Rangel. Ecol. and Manag.* 71, 196–204. doi:10.1016/j.rama.2017.09.007

Zhao, L., Liu, Z., Hu, Y., Zhou, W., Peng, Y., Ma, T., et al. (2022). Evaluation of reasonable stocking rate based on the relative contribution of climate change and grazing activities to the productivity of alpine grasslands in Qinghai Province. *Remote Sens.* 14, 1455. doi:10.3390/rs14061455

Zhou, J., Xiang, Y., Sheng, X., and Wu, J. (2023). Effects of grazing on soil nematodes in grasslands: a global meta-analysis. *J. Appl. Ecol.* 60, 814–824. doi:10.1111/1365-2664.14374

Zhou, Q. R., Shuai, L. L., Hu, J., Tian, L. H., Chen, Y. J., Wang, H., et al. (2019). The connotation of agricultural ethics in the Qinghai-Tibet Plateau grassland civilization and its reference to grassland ecological protection. *Pratacultural Sci.* 36 (11), 2997–3006.

Zhu, H., Wang, D., Wang, L., Bai, Y., Fang, J., and Liu, J. (2012). The effects of large herbivore grazing on meadow steppe plant and insect diversity. *J. Appl. Ecol.* 49, 1075–1083. doi:10.1111/j.1365-2664.2012.02195.x

frontiers | Frontiers in Environmental Science

TYPE Original Research
PUBLISHED 07 October 2025
DOI 10.3389/fenvs.2025.1673993

OPEN ACCESS

EDITED BY
Qiang Li,
University of Houston–Downtown,
United States

REVIEWED BY
Jianhua Xiao,
Chinese Academy of Sciences (CAS), China
Pankaj Kumar Sharma,
Birla Institute of Technology and Science, India
Ferdinand J. Dina Ebouel,
Botswana International University of Science and Technology, Botswana

*CORRESPONDENCE
Mengjing Guo,
guomengjing263@163.com

RECEIVED 27 July 2025
ACCEPTED 17 September 2025
PUBLISHED 07 October 2025

CITATION
Yue S, Guo M, Yuan B, Ye D, Ma H and Bai W (2025) Spatial variability characteristics of soil physicochemical properties in fixed-axis and tracking tilted single-axis photovoltaic panels in qinghai desert areas.
Front. Environ. Sci. 13:1673993.
doi: 10.3389/fenvs.2025.1673993

Spatial variability characteristics of soil physicochemical properties in fixed-axis and tracking tilted single-axis photovoltaic panels in qinghai desert areas

Shengjuan Yue[1,2,3], Mengjing Guo[4]*, Bo Yuan[5], Deli Ye[6], Hongyuan Ma[6] and Wenwen Bai[1,2,3]

[1]School of Civil Engineering and Water Resources, Qinghai University, Xining, China, [2]Laboratory of Ecological Protection and High Quality Development in the Upper Yellow River, Qinghai University, Xining, China, [3]Key Laboratory of Water Ecology Remediation and Protection at Headwater Regions of Big Rivers, Ministry of Water Resources, Qinghai University, Xining, China, [4]State Key Laboratory of Eco-hydraulics in Northwest Arid Region of China, Xi'an University of Technology, Xi'an, China, [5]College of Geology and Environment, Xi'an University of Science and Technology, Xi'an, China, [6]Qinghai Huanghe Hydropower Development Co.,LTD., Xining, China

To clarify the influence of photovoltaic (PV) panels on the spatial distribution characteristics of soil properties in desert areas, the soil of fixed-axis (FIX) PV panels and tracking tilted single-axis (TTS) PV panels in the Gonghe large-scale PV power plant in the Qinghai desert was taken as the research object. The PV panels were divided into the south edge, the north edge, under and between panels. The soil in the undisturbed area outside the PV power plant was taken as the control area. The results showed that, except between the PV panels, the soil bulk density (BD) increased significantly at other locations of the TTS PV panels ($p < 0.001$), soil organic carbon (SOC), total carbon (TC) and total nitrogen (TN), and available nitrogen (AN) decreased significantly (−35.07%, −29.62%, −38.25%, and −32.86% under the panels, respectively), and the total phosphorus (TP) content was significantly decreased only in the north edge and between the panels ($p < 0.01$). Soil water content (SWC) of FIX PV panels increased significantly (+74.74% under the panels, $p < 0.001$), and pH decreased. Comparing the two types of PV panels, except the north edge, SWC, SOC, TN, SOC: TP, TN: TP, and AN were significantly higher in the FIX PV panels than in the TTS PV panels, and BD, total potassium (TK), and SOC: TN were considerably lower than in the TTS PV panels. There was no significant difference ($p > 0.05$) in soil quality and multifunctionality index in the PV panel area. The research results can provide theoretical support for soil restoration of PV power plants in desert grassland.

KEYWORDS

desert area, large-scale PV power plant, soil properties, soil quality index, multifunctionality index

1 Introduction

In order to cope with energy needs and reduce carbon emissions, renewable energy has become an essential choice, and photovoltaic (PV) has become the dominant force in the growth of renewable energy. According to an estimate by the International Renewable Energy Agency (IRENA), global renewable energy capacity additions will exceed 5,500 GW from 2024 to 2030, almost tripling the increase from 2017 to 2023. From 2024 to 2030, the global average annual increase in PV installed capacity will exceed 600 GW (IEA, 2024). By the end of 2024, China's total installed power generation capacity reached approximately 3,350 GW, with PV capacity accounting for about 890 GW (National Energy, 2024). Large-scale deployment of ground-mounted PVs requires vast land. Consequently, China's northwestern deserts and Gobi desert regions have become the main development areas of PV power generation.

The installation of PV power plants has consistently been regarded as a "win-win" strategy, as it reduces carbon emissions and prevents desertification in arid regions (Xia et al., 2023; Xia et al., 2022; Lu et al., 2021). However, the leveling of the site during the construction of the PV power plant will destroy the soil structure and make the soil more susceptible to wind and water erosion. The removal of topsoil during construction reduces soil carbon (Choi et al., 2020), nitrogen, and phosphorus (Geissen et al., 2013) and reduces the stability of soil aggregates, which has a negative impact on the environment. During the operational stage, the physical presence of the PV panels changes the local climatic conditions (Bai et al., 2022). At the same time, the PV panels will concentrate water on their lower edge, which increases the local heterogeneity of the soil moisture distribution and produces more lasting water storage under the PV panels (Adeh et al., 2018). In addition, due to the reduction in solar radiation directly under the PV panels, the potential evaporation is reduced, which reduces drought, increases soil moisture availability, and helps to reduce water loss in arid climates (Choi et al., 2020). Wu et al. (2023) showed that different positions of PV panels have little effect on SOC and available phosphorus (AP). The contents of nitrate nitrogen (NO_3-N), TN, and TC under the PV panel are slightly higher than those between the PV panels, and the content of available potassium (AK) is significantly increased. Wang et al. (2016) showed that the soil SWC, organic matter, AK, and AP in the PV panel area increased compared with the non-PV control area. The soil BD increased in the shaded area and decreased in the unshaded area. Andrew et al. (2024) found that soil organic matter in the PV plant in the northeastern United States increased, and the pH increased significantly. Sheep grazing in the PV plant may improve the pasture quality of the solar site over time. In contrast, Moscatelli et al. (2022) showed that soil nutrients, soil moisture, and soil temperature under PV panels were significantly reduced. Furthermore, the heterogeneous light intensity under PV panels results in significant differences in soil microbial community composition (Li et al., 2023), decreased microbial activity (Moscatelli et al., 2022) and microbial biomass (Lambert et al., 2021b), whereas increased alpha diversity of the fungal community (Li et al., 2023). These studies found that the influence of PV plants on soil properties is still uncertain, and may be affected by local climate, soil conditions, PV panel operation mode and other factors (Yavari et al., 2022).

Tracking PV panels can adjust the solar incident angle in real time to obtain maximum power generation efficiency (Li et al., 2025). Compared to fixed systems, their annual electricity output can increase by up to 29% (Lubitz, 2011), and the gap between adjacent PV module strings receives up to 84% of solar radiation (Graham et al., 2021). Tracking PV panels optimise ventilation, light and humidity through elevated panels and dynamic shading, creating a more uniform microenvironment conducive to positive changes in soil properties (Liu et al., 2025). This enhances vegetation photosynthesis and SOC inputs, thereby improving soil quality (Ramos-Fuentes et al., 2023; Zhang B. et al., 2024). In contrast, FIX PV panels are mounted at a fixed angle; they reconfigure precipitation and solar radiation differently than tracking PV panels. Static shading in FIX PV panels may limit photosynthesis and SOC accumulation (Zhang et al., 2025).

In view of this, the goal of this research is to assess the effects of TTS PV panels and FIX PV panels on soil physicochemical properties and whether the PV panels induced spatial heterogeneity of soils in desert areas. The specific goals were to: (1) compare soil physicochemical properties of TTS PV panels, FIX PV panels, and undisturbed control areas (CK), and (2) compare soil physicochemical properties of PV panels at different shading locations.

2 Study area and methods

2.1 Overview of the study area

The study area is located in the Longyangxia Hydro-PV Park in Talatan, Qinghai Province (100°22′E–100°39′E, 35°56′N-36°13′N). The PV power plant was built in 2012 and completed in 2015, with a total installed capacity of 850 MW. It is characterized by 'PV + ecological management + ecological pastoralism'. We collected soil samples at a FIX and a TTS PV array (Figure 1). FIX PV mounting system that does not track the rotation of the sun. The lower eaves of the PV panels are 0.5 m from the ground, the inclination angle of the PV panels is 39°, and the spacing between the PV panels is 6.87 m (Figure 2c). TTS PV mounting system rotates at a fixed inclination to track the sun's trajectory from east to west, with the lower eave of the PV panels 1.2 m above the ground (Figure 2d).

The ground elevation of the PV plant is 2,900–2,950 m. The overall terrain is high in the west and low in the east, and the slope is not large. The climate in the region is predominantly a highland continental climate, with an annual rainfall of 246.3 mm and an average annual temperature of 4 °C. Local soil types mainly include calcic brown soil and calcite chestnut soil (Zhao and Na, 1996).

2.2 Soil sample collection

In July 2019, 6 years after the construction of the PV power plant, soil samples were collected. Five samples were taken from five rows of 20 m intervals along the east-west direction in the FIX and TTS PV arrays (Figure 2a). The sampling points were located on the south edge, north edge, under, and between PV panels (Figures 2c,d). Therefore, there were 100 sampling positions in the FIX and TTS PV arrays, respectively. The non-PV panel area at 400 m east of

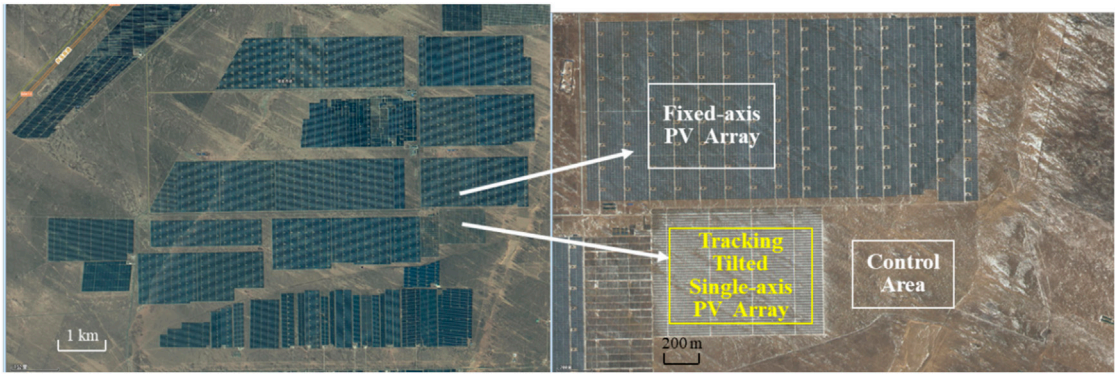

FIGURE 1
The position of the FIX PV array, the TTS PV array and the CK. FIX, fixed-axis. TTS, tracking tilted Single-axis. CK, control area.

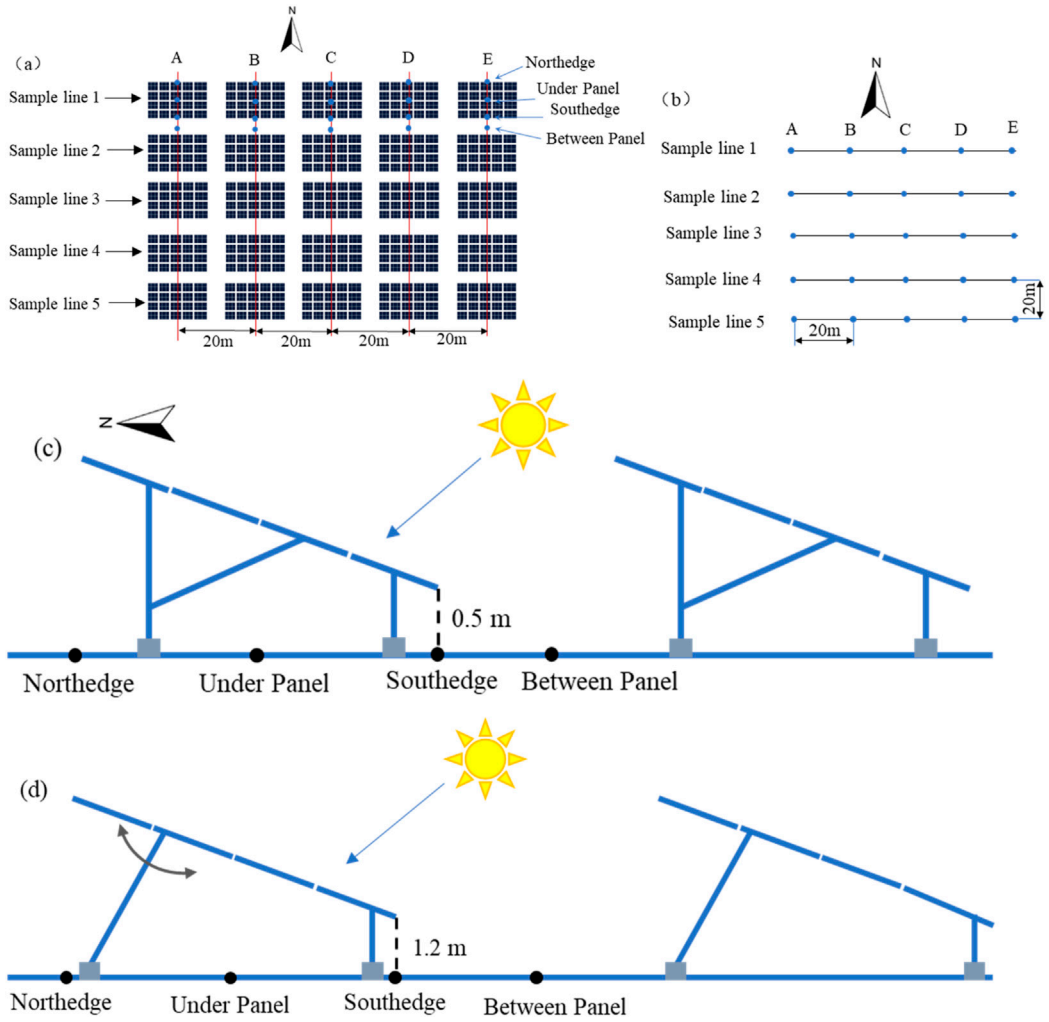

FIGURE 2
Soil sampling point layout diagram. **(a)** PV arrays. **(b)** CK. **(c)** Schematic detailing the sampling locations relative to the FIX PV panels. **(d)** Schematic detailing the sampling locations relative to the TTS PV panels.

the TTS PV array area was used as the control area. The spacing of the east-west and north-south sampling points in the control area was 20 m (Figure 2b). There were 25 sampling points in the control area. Soil samples were collected from the 0–20 cm top soil layer mixed and bagged, air-dried, and brought back to the laboratory for physical and chemical properties. A total of 225 soil samples were collected.

2.3 Measurement of soil physicochemical properties

A total of 14 soil physicochemical indicators were measured. The indicators were monitored referencing the "analytical method of soil agriculture chemistry" (Lu, 2000). Bulk density was measured by ring knife method, and pH was measured by potentiometric method. TN was measured by the concentrated sulfuric acid-catalyst-flow analyzer method. TP was measured based on the sodium hydroxide melting-molybdenum antimony colorimetric method. TK was measured by the sodium hydroxide melting-flame photometric method. TC was measured by the combustion method. SOC was measured using potassium dichromate combined with the heating method. AK was measured by the ammonium acetate-flame photometric method. AP was measured by the molybdenum antimony anti-colorimetric method. AN was measured by the alkaline hydrolysis diffusion method. Mechanical composition was measured using a laser particle sizer (Malvern, model 2000), and SWC was measured *in situ* with a WET instrument (Delta-T, WET-2).

2.4 Calculation of the soil quality index (SQI)

The data of the 14 soil physicochemical indicators measured were standardised and the indicators were converted to values between 0 and 1 using the linear scoring function method. Indicators were categorized into two types based on the sensitivity of soil quality. If the indicator is positively correlated with soil quality, the "more is better" scoring model applies, i.e., Equation 1. Conversely, the "less is better" scoring model, Equation 2, applies.

$$S_L = \begin{cases} 0.1 & (x \le x_{\min}) \\ 0.9 \times \dfrac{x - x_{\min}}{x_{\max} - x_{\min}} + 0.1 & (x_{\min} < x < x_{\max}) \\ 1 & (x \ge x_{\max}) \end{cases} \text{Positive} \quad (1)$$

$$S_L = \begin{cases} 1 & (x \le x_{\min}) \\ 1 - 0.9 \times \dfrac{x - x_{\min}}{x_{\max} - x_{\min}} & (x_{\min} < x < x_{\max}) \\ 0.1 & (x \ge x_{\max}) \end{cases} \text{Negative} \quad (2)$$

Where S_L is the linear score of each indicator between 0 and 1; x is the measured value; $x_{\max}$ and $x_{\min}$ are the maximum and minimum values of the indicator, respectively.

The weight of each indicator is calculated by principal component analysis. The calculation method is detailed in Yue et al. (2024). The results were shown in Supplementary Tables 1–9. The SQI is calculated according to Equation 3:

$$SQI = \sum_{i=1}^{n} W_i \times S_i \quad (3)$$

Where W_i is the weight value of each quality factor, n is the total number of indicators, S_i is a linear score. The SQI ranges from 0 to 1, with higher SQI indicating higher soil quality.

2.5 Calculation of the soil multifunctionality index (MFI)

The multifunctionality of soils reflects the cycling of carbon, nitrogen, and phosphorus, as well as the supply capacity of the resources available to the soil (Manning et al., 2018). MFI was calculated based on the measured 14 soil physicochemical indicators. MFI was calculated by the mean value method, and the measured values of different functions were transformed and averaged. Finally, the representative index of functional average level, namely, the soil multifunctional index, was obtained. The MFI calculation formula is as shown in Equation 4:

$$MFI = \frac{1}{F}\sum_{i=1}^{F} g\left(r_i\left(f_i\right)\right) \quad (4)$$

Where F is the number of functions measured, f_i is the measured value of function i, r_i is the mathematical function that transforms f_i into a positive function, and g is the normalization function.

2.6 Statistical analysis

SPSS 25.0 software was used to perform one-way ANOVA, principal component analysis, and significance tests. Origin 2021 software was used for graphing.

3 Results

3.1 Characteristics of soil basic physicochemical properties

The soil BD in the south edge, north edge, under, and between panels of TTS PV panels was significantly ($p < 0.001$) higher than that in the control area. They were 3.14%, 3.11%, 3.38% and 2.90% higher, respectively. Whereas, the BD of the FIX PV panels was not significantly different ($p > 0.05$) from the control area. The soil BD of the two PV panels was significantly ($p < 0.05$) different only at the southern edge, under and between the panels, whereas there was no significant difference ($p > 0.05$) at the northern edge (Figure 3a).

SWC of the FIX PV panels was significantly ($p < 0.001$) higher than that of the TTS PV panels and the control area. SWC of the FIX PV panels increased by 64.81%, 64.12%, 74.74%, and 48.49% at the south edge, north edge, under, and between PV panels, respectively, compared with the control area (Figure 3b).

There was no significant difference ($p > 0.05$) in soil clay, silt, and sand content among FIX PV, TTS PV panels, and control area (Figures 3c–e).

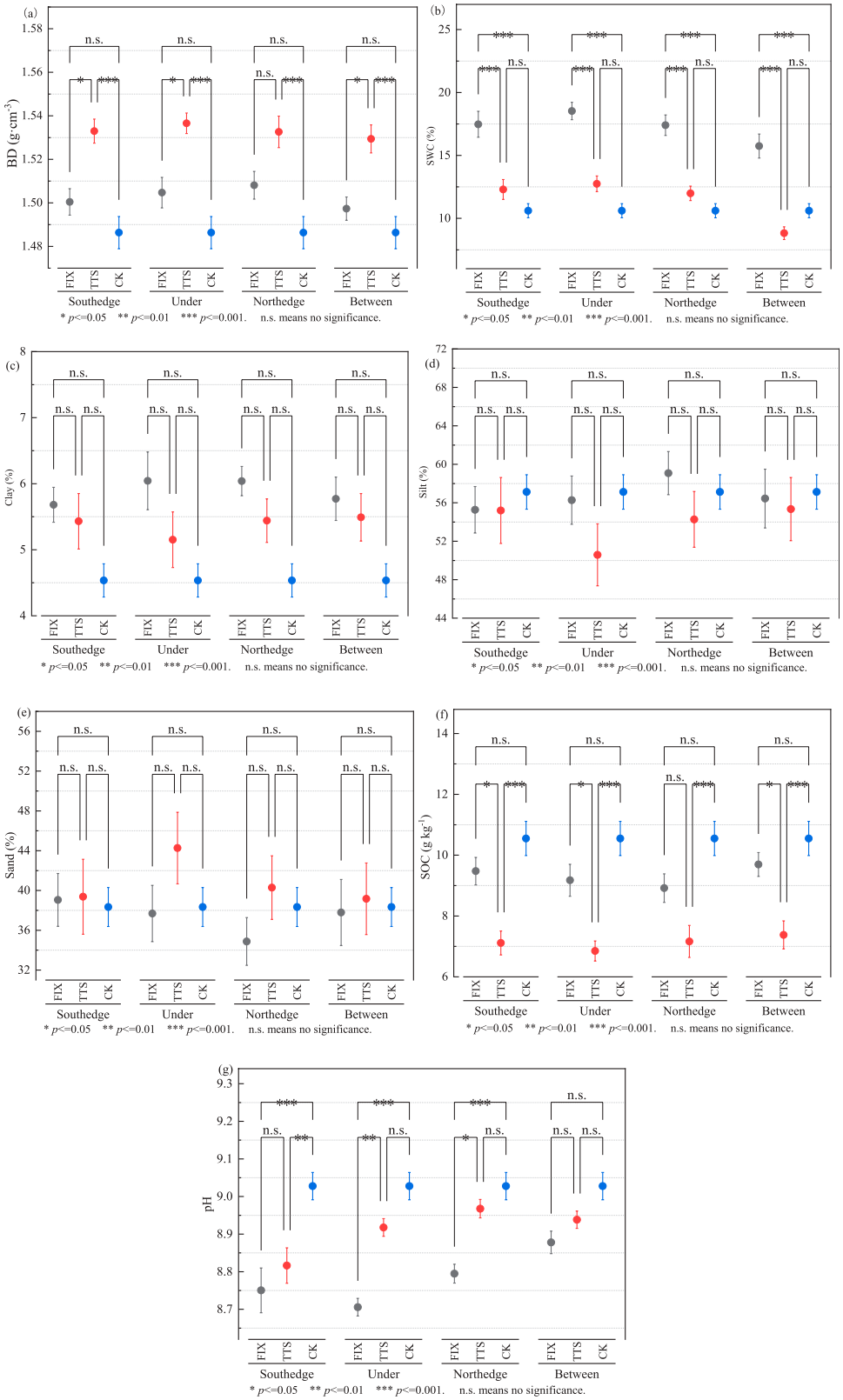

FIGURE 3
Results of analyses of soil basic physicochemical properties at different locations of PV panels. **(a)** Bulk density (BD), **(b)** soil water content (SWC), **(c)** clay, **(d)** silt, **(e)** sand, **(f)** soil organic carbon (SOC). **(g)** pH. FIX, fixed-axis PV panels. TTS, tracking tilted Single-axis PV panels. CK, control area.

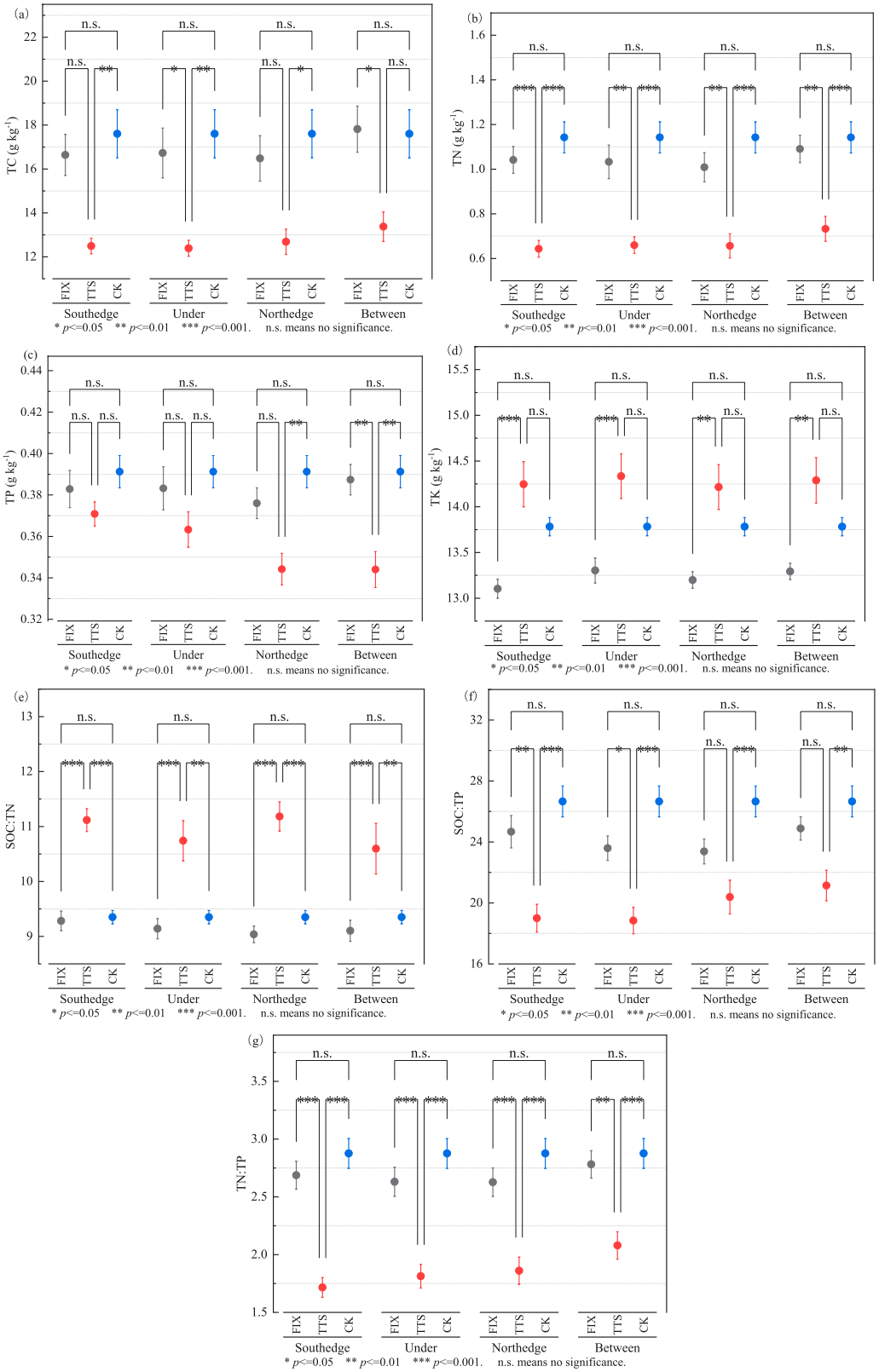

FIGURE 4
Results of analyses of soil total nutrient properties at different locations of PV panels. **(a)** Total carbon (TC), **(b)** total nitrogen (TN), **(c)** total phosphorus (TP), **(d)** total potassium (TK), **(e)** C: N ratio (SOC: TN), **(f)** C: P ratio (SOC: TP), **(g)** N:P ratio (TN: TP).

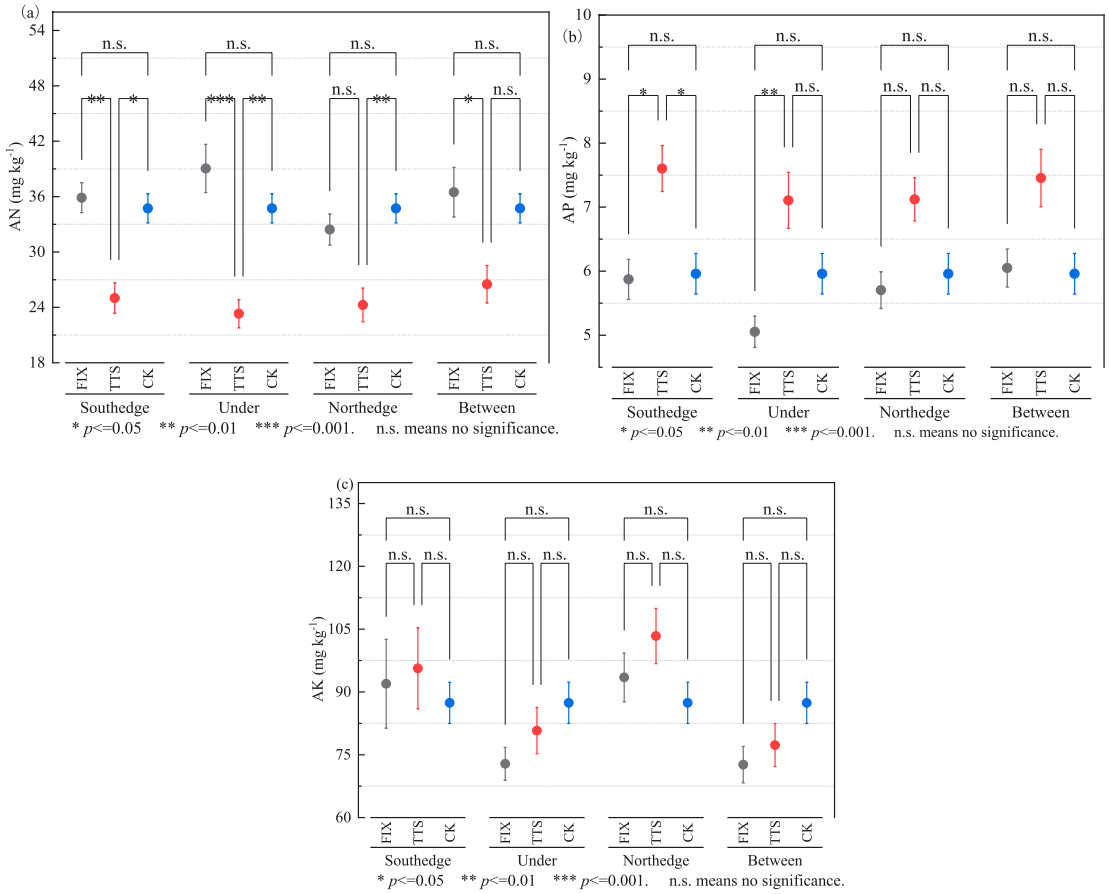

FIGURE 5
Results of analyses of soil available nutrient properties at different locations of PV panels. **(a)** Available nitrogen (AN), **(b)** available phosphorus (AP) and **(c)** available potassium (AK).

SOC at the south edge, north edge, under and between TTS PV panels was significantly ($p < 0.001$) lower than that of the control area by 32.57%, 32.10%, 35.07% and 30.06%, respectively. While the SOC of FIX PV panels was not significantly different ($p > 0.05$) from the control area. SOC at the southern edge, under and between TTS PV panels was significantly ($p < 0.05$) decreased by 24.93%, 25.35%, and 23.88% compared to the FIX PV panels (Figure 3f).

Soil pH at the south edge, north edge, and under FIX PV panels was significantly ($p < 0.05$) decreased by 3.07%, 2.58% and 3.57% compared to the control area. Soil pH between panels with FIX and TTS PV was not significantly different ($p > 0.05$) from the control area (Figure 3g).

3.2 Soil total nutrient properties

TC content in the south edge and under the TTS PV panel was significantly ($p < 0.01$) decreased by 29.03% and 29.62% compared to the control area, and the north edge was significantly ($p < 0.05$) decreased by 27.94%. There was no significant ($p > 0.05$) difference in FIX PV panels (Figure 4a).

TN content of the south edge, north edge, under and between TTS PV panels was significantly lower ($p < 0.001$) than that in the control area, which was reduced by 43.71%, 42.56%, 42.27%and 35.86%, respectively. Whereas, there was no significant difference ($p > 0.05$) in the FIX PV panels. TN content of TTS PV panels was significantly decreased by 38.25% ($p < 0.001$) in the south edge, and by 34.93%, 36.14%, and 32.80% ($p < 0.01$) in the north edge, under and between panels, respectively, compared to that of the FIX PV (Figure 4b).

TP content was significantly reduced by 12.02% and 12.06% only in the north edge and between TTS PV panels compared with the control area. There was no significant difference ($p > 0.05$) between the FIX PV panels (Figure 4c).

TK content in FIX PV and TTS PV panels was not significantly different ($p > 0.05$) from that of the control area, whereas TK content in the south edge and under the FIX PV panels was significantly lower ($p < 0.001$) than that of TTS PV, and in the north edge and between the panels was significantly lower ($p < 0.01$) by 7.15%, and by 6.97%, respectively (Figure 4d).

SOC: TN of the TTS PV panels was significantly increased ($p < 0.001$) than that in the control area (Figure 4e), SOC: TP (except between panels), and TN: TP was significantly decreased ($p < 0.001$), while the FIX PV panel had no significant difference ($p > 0.05$) (Figures 4f,g).

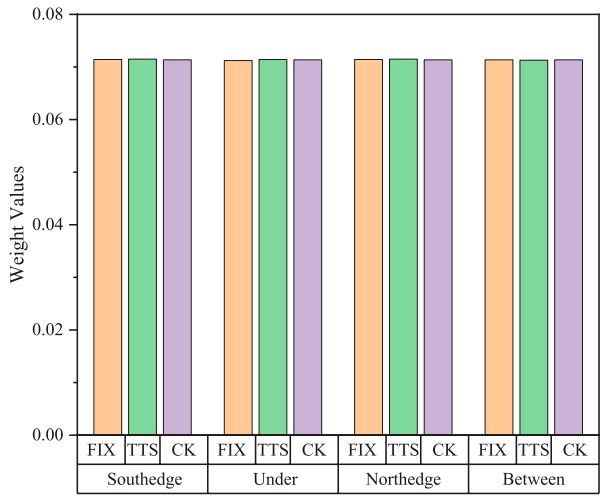

FIGURE 6
The average weight value of soil quality evaluation index at different locations.

3.3 Soil available nutrient properties

Compared with the control area, the south edge of the TTS PV panel significantly increased AP ($p < 0.05$, +27.56%), and AN was significantly reduced ($p < 0.05$, −27.97%). AN under the panel and the north edge were significantly reduced ($p < 0.01$) by 32.86% and 30.12%, and there was no significant difference ($p > 0.05$) in AK. There was no significant difference ($p > 0.05$) in AP, AK, and AN between the FIX PV panels and the control area (Figure 5).

3.4 Soil quality and multifunctionality assessment

3.4.1 Principal component analysis

Principal component analysis (PCA) was conducted on 14 indicators (S1-S9). The results indicate that three principal components can be extracted for soil indicators at the north edge of the TTS panels (S6), between FIX panels (S7), and between TTS PV panels (S8), with cumulative contribution rates of 76.864%, 74.421%, and 74.771% respectively. Meanwhile, soil indicators from the remaining locations can be extracted into four principal components, with cumulative contribution rates exceeding 80.342%, effectively representing the variation information of the indicator variables. This demonstrates that the extracted components effectively represent the variation in the indicator variables. In the first principal component, BD at the southern edge of the TTS PV panel (S2) and under TTS PV panels (S4) has a higher weight, whereas TN at other locations has a higher weight. In the second principal component, the sand indicator demonstrates higher weighting at the following locations: under TTS PV panels (S4), north edge of the TTS PV (S6), between TTS PV (S8), and control area (S9).

The weights of soil quality evaluation indexes at different locations were obtained by PCA (Figure 6), and the weights were between 0.0712 and 0.0715, with little difference.

3.4.2 Soil quality and multifunctionality index

Changes in soil physicochemical properties directly affect soil fertility and plant growth. There was no significant difference ($p > 0.05$) in SQI and MFI between the FIX PV panel, the TTS PV panel, and the control area (Figure 7). The SQI of FIX PV panels was higher in the south edge than in the control area, and the MFI was higher in the control area than in other locations. The SQI of the TTS PV panel was higher in the south edge and under the panel than in the control area, and the MFI was higher under the panel than in the control area.

Regression analysis of SQI and MFI showed a significant positive correlation ($R^2 > 0.89$) (Figure 8).

4 Discussion

4.1 Effect of PV panels on soil physicochemical properties

In this study, soil BD of TTS PV panels increased significantly, while there was no significant difference in FIX PV panels (Figure 3A). This may be due to the shading effect of PV panels will reduce soil moisture evaporation, enhance soil water retention capacity, reduce porosity, and increase BD (Zhang et al., 2021). In addition, PV panels cause uneven distribution of precipitation, and uneven precipitation affects BD differently, as concentrated precipitation causes soil erosion and increases bulk density (Wang Y. et al., 2021; Zhang et al., 2020; Dvoráčková et al., 2024). If the soil is located in arid regions, the addition of water can lead to a decrease in BD, as moisture helps to loosen the bond between soil particles, thereby increasing the gaps between them. This decrease in soil density enhances water and air permeability, positively impacting plant growth and other biological processes within the soil (Pan et al., 2020).

In this study, SWC of the FIX PV panel was significantly higher than that of the control area and the TTS PV panel (Figure 3b). The main reason was that the FIX PV panel had a relatively large shading area and reduced soil water evaporation. In contrast, tracking PV systems were found to increase SWC in the Zhangjiakou PV power plant at the southern edge of the typical temperate grassland in Inner Mongolia, China, but the increase was not significant for fixed PV systems (Zhang S. et al., 2024). The presence of PV panels concentrates water along their lower edges, resulting in great heterogeneity in the spatial distribution of soil moisture (Choi et al., 2023), and soil moisture heterogeneity may have an important effect on plant growth, especially in arid regions where small changes in water availability may have a large impact on plant growth (D'Odorico et al., 2007). Compared with the fixed PV system, the east/west (E/W) agricultural PV design for vertical bifacial solar panels provides better spatial uniformity in the daily crop shading distribution of crops, providing higher crop yield and greater energy production (Riaz et al., 2021).

The pH of the FIX PV panels in this study was generally reduced (Figure 3g). Shading by PV panels lowers soil temperatures and slows down the rate of biological processes in the soil, such as organic matter decomposition and nutrient mineralization. With the slow decomposition of organic matter, humic and fulvic acid, and other acidic substances are released, which can reduce soil

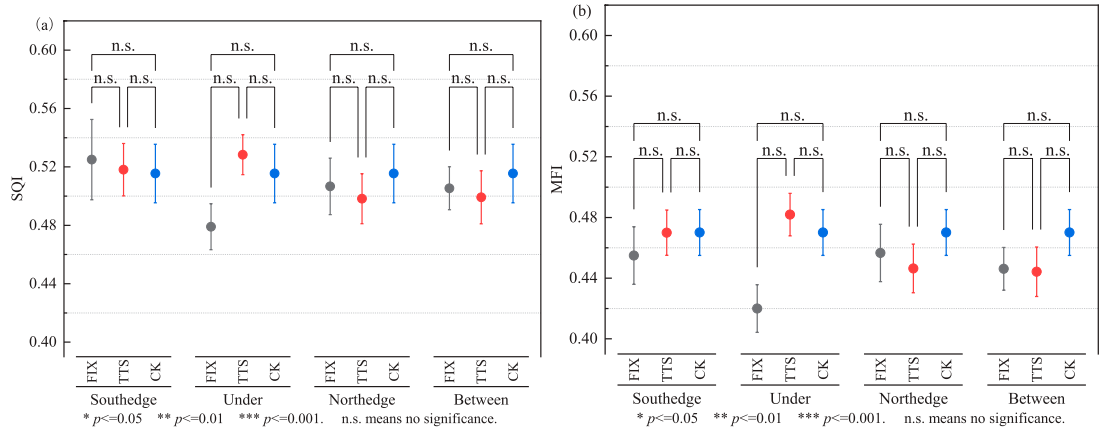

FIGURE 7
Soil quality and multifunctionality index. **(a)** Soil quality index (SQI) at different locations of PV panels. **(b)** Soil multifunctionality index (MFI) at different locations of PV panels.

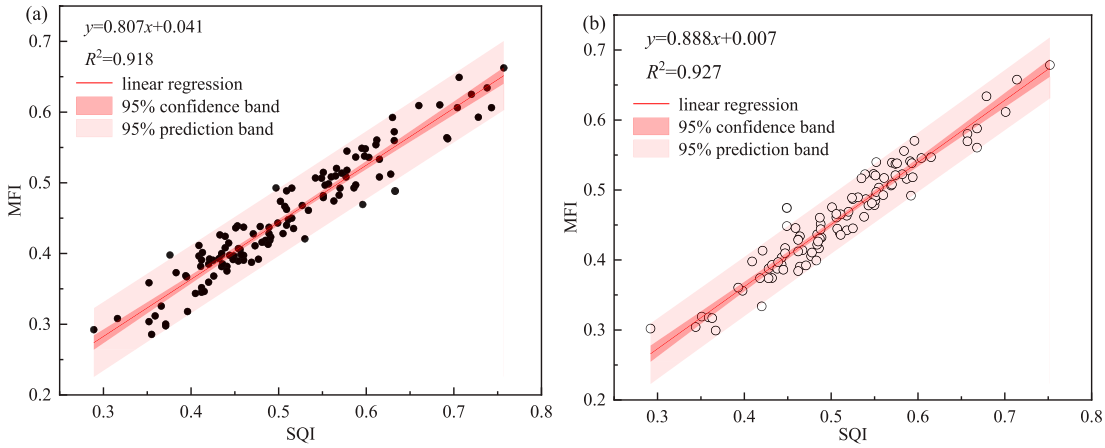

FIGURE 8
The linear model of SQI and MFI. **(a)** FIX PV panels. **(b)** TTS PV panels.

pH (Wang C. et al., 2021). Soil pH decreased by 13.93% at the Datong saline-alkali PV power plant in China (Yi, 2020).

The TN, TC, and SOC contents of FIX PV panels were higher than those of TTS PV panels at all locations in this study (Figures 4a,b,e). While soil TN and TC content in Zhangjiakou PV power plant at the southern edge of the typical temperate grassland in Inner Mongolia, China was significantly higher in the tracking tilted PV system. And soil TN, TC, and SOC contents were significantly lower in the fixed system (Zhang S. et al., 2024). The rotation of the tracking tilted PV system allows plants to capture more light and increase litter, thereby further increasing biomass accumulation and improving soil nutrients. In the desert grassland PV power plant on the southern margin of the Mu Us Sandy Land, it was also found that SOC under the flat single-axis tracking PV panel was significantly higher than that under the fixed adjustable tracking PV panel (Tong et al., 2024). In the Hongsibu PV power plant in Ningxia, it was found that the SOC under and in front of the PV panel increased, and the PV panel had a positive impact on the carbon sink of arid and semi-arid ecosystems (Liu et al., 2023). Since the topsoil was removed during the PV construction process, the carbon and nitrogen contents in the PV soil were still lower than those in the control area after 7 years of vegetation restoration in a non-vegetated PV power plant in Colorado, United States (Choi et al., 2023). In addition, studies on PV power plants in Malaysia have shown that significant changes in microclimate characteristics cannot affect the physical and chemical properties of the soil (Noor and Reeza, 2022).

In this study, SOC: TP and TN: TP were significantly reduced at all positions of the TTS PV panel (Figures 4f,g), which may be due to the improvement of soil moisture conditions promoting plant growth and increasing biomass and litter input, which further altered the soil C/N and N/P ratios (Hume et al., 2016). On the other hand, if precipitation infiltration is too intensive, it may lead to soil nutrient leaching and loss of organic matter, which may also lead to changes in soil C/N ratios (Brust, 2019).

In this study, soil AP significantly increased in the south edge of TTS PV panels, AN significantly decreased under and between panels, and

there was no significant difference in AK (Figure 5). PV panels change the distribution of precipitation and affect soil moisture, nitrogen, and phosphorus availability (Uldrijan et al., 2023). TTS PV panels promoted biomass accumulation and grassland restoration (Zhang S. et al., 2024), potentially reducing AN. In contrast, the desert grassland PV plant at the southern edge of the Mu Us Sandy Land showed that soil NO_3-N, AP and AK content did not change significantly under panels, between panels and at the control site (Tong et al., 2024), The reason may be that in the aeolian sandy soil, the content of these available nutrients is very low, and the degree of disturbance under and between the panels is not enough to have an impact on the content of these available nutrients, and also because the time for natural restoration is only 2 years, so the content of the soil available nutrients changes have not yet been observed.

4.2 Soil quality in PV power plant

There is no significant difference in SQI and MFI between FIX PV panels and TTS PV panels in this study (Figure 7). It may be due to the fact that the mean value method was used to calculate the MFI in this study. While this method is straightforward to calculate and widely used, it fails to reflect the differing weightings of each individual function. SQI is greater than the control area for the south edge of FIX PV panels, and greater than the control area for the south edge and under panels of TTS PV. MFI is less than the control area for the FIX PV panels at all locations, and TTS PV with the south edge and under the panels is higher than the control area. MFI is lower than the control area for FIX PV panels at all locations, and higher than the control area for the under and south edge of the panels with TTS PV. This may be due to the fact that the tracking PV panel has a dynamic change in the precipitation redistribution at the southern edge of the PV panel, and there are also differences in the light and heat distribution. The influence of TTS PV panels on microclimate and soil is more complicated than that of FIX PV panels (Suuronen et al., 2017). Soil quality of tracking flat single-axis PV panels in a typical sandy PV plant in western Inner Mongolia was higher than that of the control area, with higher soil quality between PV panels, before and after the panels, and lower soil quality under the panels (Yuan and Gao, 2024). The soil quality between and under the flat single-axis tracking PV panels in the desert grassland on the southern edge of the Mu Us Sandy Land is better than that of the fixed PV panel (Tong et al., 2024). Yunnan agro-PV plant showed that planting crops significantly improved the soil quality and versatility index (Luo et al., 2024). In rocky desertification PV power plants, different degrees of shading by PV panels had no significant effect on the SQI (Wu et al., 2023). Similarly, agricultural PV systems in the Mediterranean environment of the Puglia region (Italy), the land equivalence ratio was improved and without negative impacts on biological soil quality (Riaz et al., 2021). The SQI in Mediterranean PV power plants is about three times lower than that of semi-natural land (Lambert et al., 2021a), and the main reason for the decrease in soil quality is the increase in soil erosion due to the disturbance of the soil during the construction period, the decrease in soil compaction (Quinton et al., 2010) and organic matter content, and consequently the decrease in the soil's water-holding capacity (Mujdeci et al., 2017) and stability (Šimansk'y et al., 2013).

5 Conclusion

The environmental heterogeneity of different shading positions of PV panels affected soil physicochemical properties to different degrees. FIX PV panels showed a significant increase in SWC, which was very beneficial to vegetation restoration in the desert area. There was no significant difference in soil quality and soil multifunctionality index between the two types of PV panels. The high efficiency of tracking PV arrays in electricity generation also contributes to a more uniform distribution of sunlight and moisture. In the future, as we face arid climates and increasing land scarcity, the combination of tracking PV technology and agriculture holds great potential.

Data availability statement

The original contributions presented in the study are included in the article/Supplementary Material, further inquiries can be directed to the corresponding author.

Author contributions

SY: Conceptualization, Writing – original draft. MG: Conceptualization, Writing – review and editing. BY: Conceptualization, Writing – review and editing. DY: Supervision, Writing – review and editing. HM: Supervision, Writing – review and editing. WB: Data curation, Writing – review and editing.

Funding

The author(s) declare that financial support was received for the research and/or publication of this article. This research was supported by the Kunlun Talent, High-end Innovation and Entrepreneurship Talents Program of Qinghai Province, Qinghai University Youth Fund (2024-QGY-9), the Natural Science Foundation of Technology Department of Qinghai Province (Grant No. 2025-ZJ-976Q), the Qinghai University Research Ability Enhancement Project (2025KTST07), and SPIC Huanghe Hydropower Development Co.,LTD. Scientific Research Project (KY-C-2024-GF04, KY-C-2025-HB05).

Conflict of interest

Authors DY and HM were employed by Qinghai Huanghe Hydropower Development Co.,LTD.

The remaining authors declare that the research was conducted in the absence of any commercial or financial relationships that could be construed as a potential conflict of interest.

Generative AI statement

The author(s) declare that no Generative AI was used in the creation of this manuscript.

Any alternative text (alt text) provided alongside figures in this article has been generated by Frontiers with the support of artificial intelligence and reasonable efforts have been made to ensure accuracy, including review by the authors wherever possible. If you identify any issues, please contact us.

Publisher's note

All claims expressed in this article are solely those of the authors and do not necessarily represent those of their affiliated organizations, or those of the publisher, the editors and the reviewers. Any product that may be evaluated in this article, or claim that may be made by its manufacturer, is not guaranteed or endorsed by the publisher.

Supplementary material

The Supplementary Material for this article can be found online at: https://www.frontiersin.org/articles/10.3389/fenvs.2025.1673993/full#supplementary-material

References

Adeh, E. H., Selker, J. S., and Higgins, C. W. (2018). Remarkable agrivoltaic influence on soil moisture, micrometeorology and water-use efficiency. *PLoS One* 13, e0203256. doi:10.1371/journal.pone.0203256

Andrew, A., Hain, L., Barter, J., Goldberg, Z., Desario, A., Antoszewski, K., et al. (2024). "Sheep grazing impacts on soil health and pasture quality at commercial solar sites in northeastern USA: solar sheep grazing and site conditions", in *AgriVoltaics conference proceedings*.

Bai, Z., Jia, A., Bai, Z., Qu, S., Zhang, M., Kong, L., et al. (2022). Photovoltaic panels have altered grassland plant biodiversity and soil microbial diversity. *Front. Microbiol.* 13, 1065899. doi:10.3389/fmicb.2022.1065899

Brust, G. E. (2019). "Management strategies for organic vegetable fertility", in *Safety and practice for organic food* (Elsevier), 193–212.

Choi, C. S., Cagle, A. E., Macknick, J., Bloom, D. E., Caplan, J. S., and Ravi, S. (2020). Effects of revegetation on soil physical and chemical properties in solar photovoltaic infrastructure. *Front. Environ. Sci.* 8, 140. doi:10.3389/fenvs.2020.00140

Choi, C. S., Macknick, J., Li, Y., Bloom, D., McCall, J., and Ravi, S. (2023). Environmental Co-benefits of maintaining native vegetation with solar photovoltaic infrastructure. *Earth's Futur* 11, e2023EF003542. doi:10.1029/2023EF003542

Dvo\vráčková, H., Dvo\vráček, J., Vlček, V., and R\uužička, D. (2024). Are the soils degraded by the photovoltaic power plant? *Cogent Food \& Agric.* 10, 2294542. doi:10.1080/23311932.2023.2294542

D'Odorico, P., Caylor, K., Okin, G. S., and Scanlon, T. M. (2007). On soil moisture--vegetation feedbacks and their possible effects on the dynamics of dryland ecosystems. *J. Geophys. Res. Biogeosciences* 112, G4. doi:10.1029/2006jg000379

Geissen, V., Wang, S., Oostindie, K., Huerta, E., Zwart, K. B., Smit, A., et al. (2013). Effects of topsoil removal as a nature management technique on soil functions. *Catena* 101, 50–55. doi:10.1016/j.catena.2012.10.002

Graham, M., Ates, S., Melathopoulos, A. P., Moldenke, A. R., DeBano, S. J., Best, L. R., et al. (2021). Partial shading by solar panels delays bloom, increases floral abundance during the late-season for pollinators in a dryland, agrivoltaic ecosystem. *Sci. Rep.* 11, 7452. doi:10.1038/s41598-021-86756-4

Hume, A., Chen, H. Y. H., Taylor, A. R., Kayahara, G. J., and Man, R. (2016). Soil C: N: P dynamics during secondary succession following fire in the boreal forest of central Canada. *For. Ecol. Manage.* 369, 1–9. doi:10.1016/j.foreco.2016.03.033

IEA (2024). "Renewables 2023",. Paris. Available online at: https://www.iea.org/reports/renewables-2023.

Lambert, Q., Bischoff, A., Cluchier, A., Cueff, S., and Gros, R. (2021a). Effects of solar parks on soil quality, CO2 effluxes and vegetation under Mediterranean climate. *Authorea Prepr.* doi:10.22541/au.162300877.73953918/v1

Lambert, Q., Bischoff, A., Cueff, S., Cluchier, A., and Gros, R. (2021b). Effects of solar park construction and solar panels on soil quality, microclimate, $_{CO2}$ effluxes, and vegetation under a Mediterranean climate. *L. Degrad. \and Dev.* 32, 5190–5202. doi:10.1002/ldr.4101

Li, C., Liu, J., Bao, J., Wu, T., and Chai, B. (2023). Effect of light heterogeneity caused by photovoltaic panels on the plant--soil--microbial system in solar park. *Land* 12, 367. doi:10.3390/land12020367

Li, Y., Armstrong, A., Simmons, C., Krasner, N. Z., and Hernandez, R. R. (2025). Ecological impacts of single-axis photovoltaic solar energy with periodic mowing on microclimate and vegetation. *Front. Sustain* 6, 1497256. doi:10.3389/frsus.2025.1497256

Liu, Z., Peng, T., Ma, S., Qi, C., Song, Y., Zhang, C., et al. (2023). Potential benefits and risks of solar photovoltaic power plants on arid and semi-arid ecosystems: an assessment of soil microbial and plant communities. *Front. Microbiol.* 14, 1190650. doi:10.3389/fmicb.2023.1190650

Liu, Y., Ma, S., Miao, Y., Liu, Y., Wei, S., Su, J., et al. (2025). Comparison of tracking and fixed photovoltaic systems for soil quality improvement in desert: a 5-year field study. *Sci. Total Environ.* 997, 180221. doi:10.1016/j.scitotenv.2025.180221

Lu, R. (2000). *Analytical method of soil agriculture chemistry*. Beijing, China: China Agricultural Science and Technology Press.

Lu, Z., Zhang, Q., Miller, P. A., Zhang, Q., Berntell, E., and Smith, B. (2021). Impacts of large-scale Sahara solar farms on global climate and vegetation cover. *Geophys. Res. Lett.* 48, e2020GL090789. doi:10.1029/2020gl090789

Lubitz, W. D. (2011). Effect of manual tilt adjustments on incident irradiance on fixed and tracking solar panels. *Appl. Energy* 88, 1710–1719. doi:10.1016/j.apenergy.2010.11.008

Luo, J., Luo, Z., Li, W., Shi, W., and Sui, X. (2024). The early effects of an agrivoltaic system within a different crop cultivation on soil quality in dry--hot valley eco-fragile areas. *Agronomy* 14, 584. doi:10.3390/agronomy14030584

Manning, P., Van Der Plas, F., Soliveres, S., Allan, E., Maestre, F. T., Mace, G., et al. (2018). Redefining ecosystem multifunctionality. *Nat. Ecol. \and Evol.* 2, 427–436. doi:10.1038/s41559-017-0461-7

Moscatelli, M. C., Marabottini, R., Massaccesi, L., and Marinari, S. (2022). Soil properties changes after seven years of ground mounted photovoltaic panels in Central Italy coastal area. *Geoderma Reg.* 29, e00500. doi:10.1016/j.geodrs.2022.e00500

Mujdeci, M., Simsek, S., and Uygur, V. (2017). The effects of organic amendments on soil water retention characteristics under conventional tillage system. *Fresenius Environ. Bull.* 26, 4075–4081.

National Energy, A. (2024). NEA releases national power industry statistics for 2024.

Noor, N. F. M., and Reeza, A. A. (2022). Effects of solar photovoltaic installation on microclimate and soil properties in UiTM 50MWac Solar Park, Malaysia. *IOP Conf. Ser. Earth Environ. Sci.* 12031. doi:10.1088/1755-1315/1059/1/012031

Pan, H., Chen, M., Feng, H., Wei, M., Song, F., Lou, Y., et al. (2020). Organic and inorganic fertilizers respectively drive bacterial and fungal community compositions in a fluvo-aquic soil in northern China. *Soil Tillage Res.* 198, 104540. doi:10.1016/j.still.2019.104540

Quinton, J. N., Govers, G., Van Oost, K., and Bardgett, R. D. (2010). The impact of agricultural soil erosion on biogeochemical cycling. *Nat. Geosci.* 3, 311–314. doi:10.1038/ngeo838

Ramos-Fuentes, I. A., Elamri, Y., Cheviron, B., Dejean, C., Belaud, G., and Fumey, D. (2023). Effects of shade and deficit irrigation on maize growth and development in fixed and dynamic AgriVoltaic systems. *Agric. Water Manag.* 280, 108187. doi:10.1016/j.agwat.2023.108187

Riaz, M. H., Imran, H., Younas, R., and Butt, N. Z. (2021). The optimization of vertical bifacial photovoltaic farms for efficient agrivoltaic systems. *Sol. Energy* 230, 1004–1012. doi:10.1016/j.solener.2021.10.051

Šimansk'y, V., Bajčan, D., and Ducsay, L. (2013). The effect of organic matter on aggregation under different soil management practices in a vineyard in an extremely humid year. *Catena* 101, 108–113. doi:10.1016/j.catena.2012.10.011

Suuronen, A., Muñoz-Escobar, C., Lensu, A., Kuitunen, M., Guajardo Celis, N., Espinoza Astudillo, P., et al. (2017). The influence of solar power plants on microclimatic conditions and the biotic community in Chilean desert environments. *Environ. Manage.* 60, 630–642. doi:10.1007/s00267-017-0906-4

Tong, W., Yuanyuan, D., Jie, L., Jiena, L., Xiaozheng, W., and Zhenggang, G. (2024). Effects of different photovoltaic array construction on natural restoration of plant community and soil physicochemical properties in desert grassland. *Pratacultural Sci.*, 1–13.

Uldrijan, D., Winkler, J., and Vaverková, M. D. (2023). Bioindication of environmental conditions using solar park vegetation. *Environments* 10, 86. doi:10.3390/environments10050086

Wang, T., Wang, D., Guo, T., Zhang, G., Zhao, S., Niu, H., et al. (2016). The impact of photovoltaic power construction on soil and vegetation. *Res. Soil Water Conserv.* 23, 90–94. doi:10.13869/j.cnki.rswc.2016.03.016

Wang, C., Morrissey, E. M., Mau, R. L., Hayer, M., Piñeiro, J., Mack, M. C., et al. (2021). The temperature sensitivity of soil: microbial biodiversity, growth, and carbon mineralization. *ISME J.* 15, 2738–2747. doi:10.1038/s41396-021-00959-1

Wang, Y., Zhang, Q., Majidzadeh, H., He, C., Shi, Q., Kong, S., et al. (2021). Depletion of soil water-extractable organic matter with long-term coverage by impervious surfaces. *Front. Environ. Sci.* 9, 714311. doi:10.3389/fenvs.2021.714311

Wu, C., Liu, H., Yu, Y., Zhao, W., Liu, J., Yu, H., et al. (2022). Ecohydrological effects of photovoltaic solar farms on soil microclimates and moisture regimes in arid Northwest China: a modeling study. *Sci. Total Environ.* 802, 149946. doi:10.1016/j.scitotenv.2021.149946

Wu, Z., Luo, Z., Luo, J., Sui, X., Wu, S., and Luo, X. (2023). Spatial differentiation of soil fertility in a photovoltaic power station in rocky desertification zone. *Chin. J. Ecol.* 42, 2597–2603. doi:10.11829/j.issn.1001-0629.2024-0089

Xia, Z., Li, Y., Zhang, W., Chen, R., Guo, S., Zhang, P., et al. (2022). Solar photovoltaic program helps turn deserts green in China: evidence from satellite monitoring. *J. Environ. Manage.* 324, 116338. doi:10.1016/j.jenvman.2022.116338

Xia, Z., Li, Y., Zhang, W., Guo, S., Zheng, L., Jia, N., et al. (2023). Quantitatively distinguishing the impact of solar photovoltaics programs on vegetation in dryland using satellite imagery. *L. Degrad. \and Dev.* 34, 4373–4385. doi:10.1002/ldr.4783

Yavari, R., Zaliwciw, D., Cibin, R., and McPhillips, L. (2022). Minimizing environmental impacts of solar farms: a review of current science on landscape hydrology and guidance on stormwater management. *Environ. Res. Infrastruct. Sustain.* 2, 032002. doi:10.1088/2634-4505/ac76dd

Yi, L. (2020). *Effects of photovoltaic power station on two typical degraded ecosystems in northern Shanxi Province*. Shanxi: Shanxi University of Finance and Economics.

Yuan, J., and Gao, Y. (2024). Spatial differentiation characteristics of soil nutrients in sand area tracking photovoltaic array area. *J. Agric. Sci. Technol.*, 1–10.

Yue, S., Guo, M., Yuan, B., and Zhao, Q. (2024). Large-scale photovoltaic farms in the Qinghai desert: soil quality assessment methods. *Environ. Eng. Sci.* 41, 251–259. doi:10.1089/ees.2023.0290

Zhang, Z., Teng, C., Zhou, K., Peng, C., and Chen, W. (2020). Degradation characteristics of dissolved organic matter in nanofiltration concentrated landfill leachate during electrocatalytic oxidation. *Chemosphere* 255, 127055. doi:10.1016/j.chemosphere.2020.127055

Zhang, D., Gong, C., Zhang, W., Zhang, H., Zhang, J., and Song, C. (2021). Labile carbon addition alters soil organic carbon mineralization but not its temperature sensitivity in a freshwater marsh of Northeast China. *Appl. Soil Ecol.* 160, 103844. doi:10.1016/j.apsoil.2020.103844

Zhang, B., Zhang, R., Li, Y., Wang, S., Zhang, M., and Xing, F. (2024). Deploying photovoltaic arrays in degraded grasslands is a promising win-win strategy for promoting grassland restoration and resolving land use conflicts. *J. Environ. Manage.* 349, 119495. doi:10.1016/j.jenvman.2023.119495

Zhang, S., Gong, J., Zhang, W., Dong, X., Hu, Y., Yang, G., et al. (2024). Photovoltaic systems promote grassland restoration by coordinating water and nutrient uptake, transport and utilization. *J. Clean. Prod.* 447, 141437. doi:10.1016/j.jclepro.2024.141437

Zhang, S., Gong, J., Wang, R., Zheng, K., Zhang, W., Dong, X., et al. (2025). Improving the microenvironment of tracking photovoltaic systems promotes soil organic carbon accumulation by mediating plant carbon inputs and microbial necromass retention. *J. Environ. Manage.* 388, 125937. doi:10.1016/j.jenvman.2025.125937

Zhao, X., and Na, W. (1996). A study on the utilization direction of the Tala Shoal grassland,Qinghai. *J. Nat. Resour.* 11, 272–279.

Frontiers in Environmental Science

Explores the anthropogenic impact on our natural world

An innovative journal that advances knowledge of the natural world and its intersections with human society. It supports the formulation of policies that lead to a more inhabitable and sustainable world.

Discover the latest Research Topics

See more →

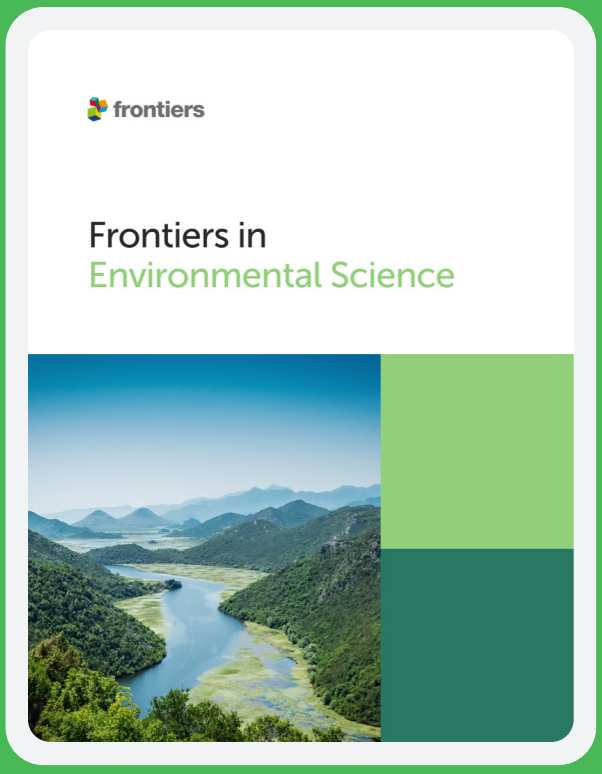

Frontiers

Avenue du Tribunal-Fédéral 34
1005 Lausanne, Switzerland
frontiersin.org

Contact us

+41 (0)21 510 17 00
frontiersin.org/about/contact